

Hyper-velocity Stars -
a spectroscopic and kinematic study
of blue stars

Der Naturwissenschaftlichen Fakultät
der Friedrich-Alexander-Universität
Erlangen-Nürnberg

zur

Erlangung des Doktorgrades Dr. rer. nat.

vorgelegt von

Franz Alfred Tillich

aus Arad/Rumänien

**Als Dissertation genehmigt
von der Naturwissenschaftlichen Fakultät
der Friedrich-Alexander-Universität Erlangen-Nürnberg**

Tag der mündlichen Prüfung: 27. April 2010

Vorsitzender der
Promotionskommission: Prof. Dr. Eberhard Bänsch

Erstberichterstatte: Prof. Dr. Ulrich Heber

Zweitberichterstatte: Prof. Dr. Dave Kilkenny

Contents

Zusammenfassung

Summary

1	Introduction	1
2	The fast and the (UV-)luminous	5
2.1	Blue star group	6
2.1.1	B-type stars on the main sequence	7
2.1.2	Red giants and horizontal branch stars	8
2.1.3	Blue stragglers	10
2.1.4	Hot subdwarfs	12
2.2	Stars beyond the speed limit	15
2.2.1	Runaway stars	16
2.2.2	Hills scenario and the super-massive black hole	18
2.2.3	The first hyper-velocity stars	19
2.2.4	Blue stars near the Galactic centre	20
2.2.5	The Multiple Mirror Telescope survey for hyper-velocity stars	21
2.2.6	A hyper-velocity star from the Large Magellanic Cloud	23
2.2.7	Further scenarios	25
3	Quantitative spectral analysis	28
4	Advanced Kinematics	33
4.1	Distance determination	34
4.2	Evolutionary tracks and errors	35
4.3	Proper motion measurement	37
4.4	Integrating in the Galactic Potential	42
4.5	Error propagation	44
5	Analysis of known Hyper-velocity stars	46
5.1	HVS 7	47
5.2	HVS 8,9,10	51
5.3	Further candidates	53

6	Wanted - A sample of A-type Hyper-velocity star candidates	57
6.1	Just an A-type sample	57
6.2	J0136+2425 - the first late B-type HVS from the Galactic rim	60
6.2.1	Spectroscopy	60
6.2.2	Kinematics	63
6.2.3	Conclusion	64
6.3	J1300+0422 - A halo blue straggler on a highly eccentric retrograde orbit	68
6.3.1	Spectroscopy	70
6.3.2	Kinematics	71
6.3.3	Conclusion	73
6.4	J1539+0239 - weighing the Galactic dark matter halo: a lower mass limit from the fastest halo star known	77
6.4.1	Spectroscopy	77
6.4.2	Kinematics	80
6.4.3	Conclusion	82
7	The Hyper-MUCHFUSS project	85
7.1	Aims	86
7.2	Survey	87
7.3	Kinematics	87
7.4	Results	89
7.5	Conclusion	96
8	Outlook	103
A	Appendix	106

List of Figures

1.1	Rotation curve for NGC 3198	3
2.1	Hertzsprung-Russell diagram for different stellar types	6
2.2	Hertzsprung-Russell diagram including MK- and Harvard classes	7
2.3	Colour-magnitude diagram for M3	8
2.4	Comparison of the colour-magnitude diagrams for M3 and M13	10
2.5	Colour-magnitude diagram for NGC 1851	11
2.6	Colour-magnitude diagram with components for M3	13
2.7	UV upturn in the spectrum of NGC 4552	14
2.8	Schematic Disruption of a massive binary	18
2.9	Spectrum of the subdwarf O star US 708	20
2.10	Velocity histogram of the Brown et al. (2007a) sample	23
2.11	Example of evolutionary tracks	24
2.12	Metal abundances for HE 04375439	25
3.1	Spectral fit for the subdwarf B star J1211+1437	29
3.2	Spectral synthesis for HVS 8 and BCAND371	30
3.3	Comparison between observed and synthetic spectra for J1300+0422	32
4.1	Equatorial versus Galactic coordinates	34
4.2	T_{eff} -log g -diagram for the candidates from W.Brown	36
4.3	POSS-E and POSS-O plate for J1644+4523	38
4.4	POSS II-R and <i>SDSS</i> plates for J1644+4523	40
4.5	Proper motion fit for the subdwarf B star J2156+0036	41
4.6	Cylindrical coordinates	42
4.7	Sample distribution of the Galactic rest-frame velocities	45
5.1	Colour target selection in the MMT HVS survey	47
5.2	Spectrum synthesis for HVS 7 in selected regions	49
5.3	Spectral synthesis for HVS 9 from a new model grid	53
5.4	Classification of HVS 7, 8, 9, 10 into evolutionary models	54
5.5	Spectral synthesis for BCAND364 from a new model grid	55
5.6	Classification of the further candidates into evolutionary models	56
6.1	Proper motion fits for J0136+2425	61
6.2	Spectrum synthesis for J0136+2425 and J1539+0239 in selected regions	62

6.3	Comparison of J0136+2425 with evolutionary models in a T_{eff} -log g diagram	64
6.4	Distribution of the GRF velocity distribution for J0136+2425	65
6.5	Trajectories for J0136+2425 including its origin	66
6.6	Linear fit of the position measurements for J1300+0422, where 1978.84 is the zero epoch.	69
6.7	Comparison of J1300+0422 with evolutionary models in a T_{eff} -log g diagram	72
6.8	Distribution of the Galactic restframe velocity for J1300+0422	72
6.9	$V - U$ and $e-J_Z$ diagram for J1300+0422 in different halos with reference sample	74
6.10	Trajectories for the blue straggler J1300+0422	75
6.11	Proper motion measurement for J1539+0239	78
6.12	Spectrum synthesis for J1539+0239 in selected regions	79
6.13	Comparison of J1539+0239 with evolutionary models in a T_{eff} -log g diagram	80
6.14	Distribution of the GRF velocity distribution for J1539+0239	82
6.15	Trajectories for J1539+0239 applying different Galactic halos	83
7.1	Flow of the target selection method	88
7.2	T_{eff} -log g -diagram for the HMF subdwarf B stars	91
7.3	$V - U$ and $e-J_Z$ diagram for our 12 Hyper-MUCHFUSS targets with reference sample	93
7.4	Spectral synthesis for the sdBs J1644+4523 and J0948+5516	95
7.5	Distribution of the Galactic restframe velocity for J1211+1437	96
7.6	Spectral synthesis for the sdB J1211+1437 and the post-EHB star J1556+4708	97
7.7	Positions for all analysed stars and trajectory for J1644+4523 in a 3D plot	98
7.8	Positions for all analysed stars and trajectory for J1211+1437 in a 3D plot	99
7.9	Past intersection with the Galactic disk, Part 1	101
7.10	Past intersection with the Galactic disk, Part 2	102
A.1	Spectral synthesis for HVS 10 and BCAND485	108
A.2	Spectral synthesis for BCAND563 and BHVS462	109
A.3	Proper motion measurement for J1553+0030	110
A.4	Proper motion measurement for J0758+1158 and J0844+1139	111
A.5	Proper motion measurement for J0845+1352 and J0849+1455	112
A.6	Proper motion measurement for J0948+5516 and J1020+0137	113
A.7	Proper motion measurement for J1125+0333 and J1211+1437	114
A.8	Proper motion measurement for J1358+4729 and J1556+4708	115
A.9	Proper motion measurement for J1629+1307 and J1632+2051	116
A.10	Proper motion measurement for J1644+4523 and J2244+0106	117
A.11	Spectral synthesis for the sdBs J0844+1139 and J0845+1352	118
A.12	Spectral synthesis for the DA J0849+1455 and the sdB J1020+0137	119
A.13	Spectral synthesis for the DA J1358+4729 and the sdB J1632+2051	120
A.14	Spectral synthesis for the sdBs J2156+0036 and J2244+0106	121

List of Tables

2.1	Currently known hyper-velocity stars	21
4.1	Constants for the used Galactic potential	43
5.1	Stellar parameters & elemental abundances of HVS 7	48
5.2	Results of the quantitative spectroscopic analysis for HVS 8, 9 and 10. . .	52
5.3	Result of the quantitative spectroscopic analysis for further candidates. . .	55
6.1	Proper motion measurements for the positive detections. We found signif- icant proper motions only for the four brightest stars.	58
6.2	Details on the obtained data for the sample of Xue et al. (2008)	59
6.3	Results of the quantitative spectroscopic and kinematic analysis of J0136+2425	63
6.4	Results of the quantitative spectroscopic and kinematic analysis of J1300+0422	71
6.5	Results of the quantitative spectroscopic and kinematic analysis of J1539+0239	81
7.1	Table of significant proper motions	89
7.2	Stellar parameters for the stars with full phase space information	90
7.3	Table of velocities and distances	92
A.1	Preliminary stellar parameters for the 29 subdwarf stars with constant RV	106
A.2	Table of radial velocities for the 12 Hyper-MUCHFUSS stars	107

Zusammenfassung

Die Entdeckung der “Hyper-velocity” Sterne im Jahr 2005 erregte viel Aufsehen, nicht zuletzt weil die Entstehung dieser Sterne in enger Verbindung zum super-massiven schwarzen Loch im galaktischen Zentrum stehen könnte.

Die Fachwelt erinnerte sich, dass bereits in den 1980er Jahren ein Schleudermechanismus aufgrund numerischer Experimente vorhergesagt worden war. Dabei wird ein Doppelstern von einem massereichen schwarzen Loch zerrissen - einer der Sterne kreist weiter um das massereiche schwarze Loch, während der andere mit einer Geschwindigkeit ausgeworfen wird, die sogar höher als die Fluchtgeschwindigkeit aus der Galaxie sein kann. Diese Sterne wurden “Hyper-velocity” Sterne (HVS) genannt und können bis zu 4000 km s^{-1} schnell werden. Zu diesem Zeitpunkt gab es noch keinen Beweis für die Existenz eines massereichen schwarzen Lochs im Zentrum unserer Galaxie. Gleichwohl war die kompakte Radioquelle Sagittarius A* schon seit Jahrzehnten bekannt. Schließlich, im Jahr 2002 wurde die Existenz eines supermassiven schwarzen Lochs mit einer Masse von ca. $3 \times 10^6 M_{\odot}$ im galaktischen Zentrum nachgewiesen. Dies geschah durch die Beobachtung der Bewegung der Sterne in der direkten Umgebung des massereichen schwarzen Lochs mit Hilfe exakter astrometrischer Messungen. Es sollten jedoch noch einige Jahre bis zur Entdeckung des ersten HVS vergehen. Bis dahin waren die einzigen bekannten Sterne mit einer beträchtlichen Geschwindigkeit die Hochgeschwindigkeitssterne des Typs O und B, die man bereits in den 1960er Jahren in hohen galaktischen Breiten gefunden hatte. Diese Sterne wurden “Runaway” Sterne genannt, da ihre hohe Raumgeschwindigkeit und ihre Nachbarschaft zu gasreichen OB-Assoziationen den Schluss nahelegten, dass sie dort entstanden sind. Die Identifikation solcher Objekte und ihre Abgrenzung zu anderen schnellen Sternen, ist jedoch bis heute schwierig geblieben.

Als schließlich im Jahr 2005 die ersten drei HVS entdeckt wurden, erzeugte dies viel Aufmerksamkeit, und trieb die Forschung, sowohl von theoretischer als auch von experimenteller Seite erneut an. Die Harvard Universität begann sofort mit einer systematischen Suche nach weiteren HVS am Multiple Mirror Telescope in Arizona. Am Ende waren insgesamt 16 solcher Objekte entdeckt. Viele davon sind einander sehr ähnlich; es sind Hauptreihensterne des späten B-Typs. Obwohl ein wirklicher Beweis dafür fehlt, dass diese Sterne aus dem galaktischen Zentrum kommen, stützen statistische Argumente diese These. Jedoch bereits im Jahr 2005 wurde nachgewiesen, dass der Hauptreihenstern HE 0437–5439 zu jung ist, um im galaktischen Zentrum entstanden zu sein. Sowohl die beobachteten Metallhäufigkeiten als auch die Entwicklungszeitskalen sprechen eindeutig für eine Entstehung in der Großen Magellanschen Wolke.

Speziell für Sterne des späten B-Typs, zu denen die allermeisten HVS zählen, ergibt sich eine grundlegende Schwierigkeit: die Bestimmung des Entwicklungszustands als jung und massereich (Hauptreihe) oder alt und massearm (Horizontalast). Das Fehlen dieser Information führt unvermeidlich zu verschiedenen Lösungen für die Entfernung und die Transversalgeschwindigkeit eines Sterns. Besonders wichtig ist dies in dem Bereich des charakteristischen $T_{\text{eff}}\text{-log } g$ -Diagramms, in dem sich Horizontalast und Hauptreihe überschneiden. Aus diesem Grund entschlossen wir uns einen genaueren Blick auf die bereits bekannten HVS 7 bis 10 zu werfen. Um mehr über ihre Beschaffenheit herauszufinden, untersuchten wir sie unter Zuhilfenahme eines neuen synthetischen Gitters aus Modellspektren für verschiedene Wasserstoff-zu-Helium Anteile. Die schnelle Rotation schließt den Horizontalast aus. Es muss sich also um Hauptreihensterne von $2 - 3 M_{\odot}$ handeln. Da es uns außerdem gelang die Fehlerbalken zu minimieren, konnten wir ermitteln, dass HVS 8 und HVS 10 gar nicht im eben erwähnten problematischen Bereich liegen. Wir analysierten ebenfalls einige neue HVS Kandidaten, die aus der Durchmusterung von W. Brown stammen. Für diese Kandidaten konnte eine Horizontalastzugehörigkeit leider nicht in allen Fällen ausgeschlossen werden.

Im Fall von HVS 7 gelang es uns hochaufgelöste Daten mit Hilfe des UVES Spektrographen am Very Large Telescope zu erhalten, mit denen wir eine detaillierte quantitative Spektralanalyse durchführen konnten. Dazu benutzen wir Methoden zur Modellierung von synthetischen Sternspektren, die dem aktuellen Stand der Technik (Programmpakete Atlas9, Detail und Surface) entsprechen. Auf diese Weise fanden wir heraus, dass HVS 7 ein außergewöhnlicher, chemisch pekulärer Stern des späten B-Typs ist und eine moderate projizierte Rotationsgeschwindigkeit besitzt. Dieses Ergebnis war jedoch nicht völlig unerwartet, da der Anteil an solch besonderen Objekten unter den Hauptreihensternen des späten B-Typs besonders hoch ist. Gerade diese Tatsache erschwert die Identifikation solcher Sterne.

Ein fundamentales Problem bei der Interpretation von HVS ist das Fehlen von Messungen der Eigenbewegung. Alle bisher publizierten Untersuchungen stützen sich ausschließlich auf die Radialgeschwindigkeit. Dadurch wird eine genauere kinematische Auswertung unmöglich. Aus diesem Grund riefen wir ein Projekt ins Leben, das sich mit der Analyse von HVS Kandidaten im 6-dimensionalen Phasenraum befasst. Da die bekannten HVS zu dunkel dafür sind, waren wir gezwungen uns hellere Kandidaten zu suchen.

Dabei fiel uns sofort die Auswahl von mehr als 10 000 A-Typ Sternen von Xue et al. (2008) ins Auge. Die Autoren publizierten eine Liste heliozentrisch korrigierter Radialgeschwindigkeiten, die wir ins galaktische Ruhesystem umrechneten und zur gezielten Suche nach HVS benutzten. Wir beschränkten uns dabei ausschließlich auf die schnellsten Objekte und bestimmten erstmals erfolgreich deren Eigenbewegung. Dazu benutzten wir alle photographischen Platten der verfügbaren Epochen und kombinierten sie mit Positionsbestimmungen aus modernen Durchmusterungen. Auf diese Weise erhielten wir die größtmögliche Zeitbasis (über 50 Jahre). Da wir ebenfalls noch die spektroskopische Entfernung bestimmten, konnten wir die Flugbahn der Sterne vollständig rekonstruieren und analysieren. Zur detaillierten Auswertung benutzten wir das galaktische Potential von Allen & Santillan (1991) und die Methode nach Odenkirchen & Brosche (1992). Eine

signifikante Eigenbewegung konnte für 4 Sterne gemessen werden. J1553+0030 stellte sich als spektroskopischer Doppelstern heraus und konnte deshalb nicht weiter analysiert werden. J0136+2425 ist ein Hauptreihenstern des A-Typs der mit $\approx 590 \text{ km s}^{-1}$ durch die Galaxie fliegt und wahrscheinlich ungebunden ist. Aufgrund seiner Ähnlichkeit zu den bereits bekannten HVS, kann er als ausgezeichnete HVS Kandidat bezeichnet werden. Von viel größerer Bedeutung ist jedoch die Tatsache, dass er anscheinend vom Rand der galaktischen Scheibe und nicht wie erwartet aus dem galaktischen Zentrum stammt. Das sollte aber der Fall sein, falls er von dort durch das super-massive schwarze Loch herausgeschleudert worden wäre. Daher können wir folgern, dass ein anderer Entstehungsmechanismus existieren muss.

J1300+0422 ist ein metallarmer “Blue Straggler” aus der Population II und wurde auf einem weiten retrograden Halo Orbit entdeckt. Zum ersten Mal wurde eine genaue NLTE Analyse durchgeführt und mit dem Standard LTE Ansatz verglichen. Wir charakterisierten seine Kinematik mit Hilfe einer Gruppe weißer Zwerge, die als Kalibratoren dienten. Unter Annahme eines Standard Potentials für unsere Galaxie ist J1300+0422 nur geringfügig gravitativ gebunden.

Die wohl interessanteste unserer Entdeckungen ist J1539+0239, der eine sehr große negative Radialgeschwindigkeit besitzt und daher auf uns zu kommt. Dieser blaue Horizontalaststern der Population II bewegt sich mit der höchsten bekannten Raumgeschwindigkeit auf uns zu, die je unter Halo Sternen gemessen wurde. Seine außergewöhnliche Kinematik erlaubte uns eine signifikante untere Grenze für die Masse des dunklen Halos zu bestimmen. Indem wir eine gebundene Trajektorie annahmen und die durchschnittliche Dichte erhöhten, konnten wir die Gesamtmasse des galaktischen Halo zu $M_{\text{halo}} \geq 1,7_{-1,1}^{+2,3} \times 10^{12} M_{\odot}$ bestimmen. Dieser Wert ist zwar um 80% höher als der von Xue et al. (2008) ermittelte Wert, jedoch durchaus konsistent mit anderen Arbeiten. Eine solche Annahme hat sogar direkte Auswirkungen auf die HVS, da in diesem Fall die galaktische Fluchtgeschwindigkeit viel höher sein muss als bisher angenommen.

Bis zum heutigen Tag kennen wir nur einen HVS, der zur alten Sternpopulation II gehört: den unterleuchtkräftigen (Subdwarf) O-Typ Stern US 708. Solche heißen unterleuchtkräftigen Sterne kommen in zwei Varianten (Subdwarfs des O-, und B-Typs) vor und sind aufgrund ihres Entwicklungszustands eher ungewöhnliche Objekte. Sie fusionieren Helium im Kern und haben sich bereits von der Hauptreihe weg entwickelt. Der Kern dieser Sterne ist von einer sehr dünnen ($<0,02 M_{\odot}$) inaktiven Hülle aus Wasserstoff umgeben. Bei Subdwarf Sternen des O-Typs ist beinahe kein Wasserstoff mehr in der Hülle zu finden. Deshalb besitzen sie sehr einzigartige Spektren, die von Helium Absorptionslinien dominiert werden. Subdwarf Sterne des B-Typs haben Massen von ungefähr $0,5 M_{\odot}$ und überspringen in ihrer weiteren Entwicklung die zweite Phase als Riesenstern. Sie wandern direkt auf die Abkühlsequenz der weißen Zwerge. Die Entdeckung des Subdwarfs US 708 war einem Zufall zu verdanken. Aufgrund der Existenz dieses Prototyps entschieden wir uns eine systematische Suche nach solch außergewöhnlichen Subdwarf HVS zu starten, da wir eine größere Population dieser Objekte erwarteten. Das HyperMUCHFUSS (Hyper-velocity stars or Massive Unseen Companions of Hot Faint Underluminous Stars from *SDSS*) Projekt zielt deshalb direkt auf die Entdeckung einer alten Halo

Population von Subdwarf Sternen mit hohen Geschwindigkeiten ab. Unsere Beobachtungen wurden unter anderem am Very Large Telescope der ESO in Chile durchgeführt. Alle Sterne, die wir analysierten gehören zwangsläufig zu einer von zwei Kategorien. Entweder es sind Doppelsterne mit kompakten schweren Begleitern, bei denen man hohe Variationen der Radialgeschwindigkeit erwartet. Oder es sind Einzelsterne mit konstant hoher Geschwindigkeit im galaktischen Ruhesystem. Wir benutzten eine ausgeklügelte Auswahlmethode um alte Sterne mit solch hohen Geschwindigkeiten zu selektieren. Sie basiert auf der riesigen spektralen Datenbank des Sloan Digital Sky Survey (Data Release 6). Diese Sternspektren wurden zur Messung der Radialgeschwindigkeit für eine erste Epoche benutzt. Wir konnten etwa ein Drittel der ausgewählten Sterne erneut beobachten und fanden bei 39 keine Änderung der Radialgeschwindigkeit. Auf diese Weise konnten wir ausschließen, dass es sich um Doppelsterne handelt. Bei 15 dieser Sterne gelang es uns zusätzlich eine signifikante Eigenbewegung zu messen. Zehn Sterne erwiesen sich nach detaillierter Spektralanalyse als Subdwarf Sterne, zwei als weiße Zwerge. Mit Hilfe der kinematischen Analyse versuchten wir mehr über den Entstehungsort dieser Sterne zu erfahren. Wir fanden unter anderem, den ungebundenen Subdwarf J1211+1437 und verfolgten die Bahn von zwei weiteren Subdwarfs (J1644+4523 und J0948+5516) bis zu ihrer letzten Passage der galaktischen Scheibe zurück. Dabei entdeckten wir, dass beide aus dem galaktischen Bulge zu kommen scheinen. Insgesamt könnten bis zu 40% unserer Subdwarfs einen solchen Ursprung haben. Dagegen haben 30% bei ihrer letzten Passage der galaktischen Scheibe nur den Rand der Galaxie gekreuzt.

Daraus wird klar ersichtlich, dass die gesuchte Population von Subdwarf Sternen mit hoher Geschwindigkeit existiert und von uns nachgewiesen wurde. Wir fanden dabei auch den ersten ungebundenen Subdwarf des B-Typs. Mindestens zwei der untersuchten Subdwarfs könnten im galaktischen Bulge durch den sogenannten Hills Mechanismus beschleunigt worden sein. Dagegen können sechs unserer Sterne nicht aus dem galaktischen Zentrum kommen; zumindest nicht während ihrer letzten Passage der galaktischen Scheibe. Deshalb vermuten wir, dass ein relativ hoher Prozentsatz (bis zu 60%) unserer Hochgeschwindigkeits-Population durch andere Mechanismen (z.B. des "Runaway"-Typs, siehe Kapitel 7) beschleunigt wurde.

Die hier verwendeten Techniken sind hervorragend dazu geeignet um die Suche nach HVS erfolgreich auszudehnen. Die endgültige Veröffentlichung der Daten des Sloan Digital Sky Survey (Data Release 7) wäre ein perfekter Grundstein dafür. Aber auch jede andere Auswahl von Sternen mit gemessenen Radialgeschwindigkeiten kann dazu benutzt werden. Ein Ausblick auf die zukünftige Global Astrometric Interferometer for Astrophysics (GAIA) Satelliten Mission der Europäischen Raumfahrt Agentur ESA rundet die Arbeit ab. Als Nachfolger der bekannten Hipparcos Mission wird dieser Satellit die hier gezogenen Schlussfolgerungen direkt überprüfen können. Er wird in der Lage sein, die Eigenbewegung von Sternen mit nie erreichter Präzision zu bestimmen. Außerdem wurde er konstruiert, um automatisch vollständige kinematische Analysen für eine große Anzahl an Sternen durchzuführen. Während seiner erwarteten Lebenszeit von fünf Jahren wird er bis zu einer Milliarde Sterne beobachtet haben und damit einen neuen Maßstab setzen.

Summary

Since their discovery, hyper-velocity stars have attracted great attention as they may be linked to the super-massive black hole in the Galactic centre.

Already in the late eighties it was predicted from numerical experiments that a binary could be disrupted by a massive black hole (MBH), leaving one star bound to the MBH and the other star ejected with velocities exceeding the escape velocity of the Galaxy. These stars have been called hyper-velocity stars (HVS) and can reach theoretical ejection velocities of $4,000 \text{ km s}^{-1}$. At that time there was no proof of a MBH in the Galactic centre (GC). Nevertheless the compact radio source Sagittarius A* was already known for decades. In 2002 astrometrical measurements confirmed the existence of a super-massive black hole (SMBH) with a mass of about $3 \times 10^6 M_{\odot}$ in the GC. However, HVS still had to be discovered. The only known considerably fast stars have been the high-velocity O and B type stars found at high Galactic latitudes. These stars have been termed runaway stars as the direction of their space velocity and their proximity to known gas-rich OB associations made it easy to believe that these stars originate from there. However the differentiation between these two object classes is not easy at all.

In 2005 the first three HVS have been discovered serendipitously, which triggered lots of interest, both from theoretical and observational side. After the first survey for hyper-velocity stars, all in all 16 of them are known today. Most of them have similar spectral type and are classified as late B-type main-sequence stars. Although there is no proof for these stars to originate in the GC, statistical argument support the idea. However already in 2005 the massive main-sequence HVS HE 0437–5439 was found to be too young to originate in the centre of the Galaxy. Its individual metal abundances strongly favour an origin in the Large Magellanic Cloud, which would also be consistent with its evolutionary lifetime.

However for late-type B-stars the determination of the stellar type can be very difficult and may lead to different solutions for the stellar mass, the distance, escape and transverse velocity. Especially in the region where the horizontal-branch and the main-sequence overlap in the characterising T_{eff} -log g-diagram, this is an important issue. Hence we decided to have a closer look again on the already known late-B type stars HVS 7 to 10 and applied our analysis also to new HVS candidates from the dedicated search for B-type HVS of W. Brown. For HVS 8 to 10 we re-analysed the spectra taken at the MMT with a new grid of synthetic model spectra for different hydrogen-to-helium abundances in order to reveal their nature. We found that all of them show fast rotation, hence a horizontal branch nature can be clearly excluded. Additionally our analysis revealed that HVS 8 and

HVS 10 do not lie in the discussed problematic region due to the respective low errors. For the other HVS candidates which we examined we could not exclude a horizontal-branch nature in all cases.

In the case of HVS 7 actually we obtained high-resolution spectra with UVES at the VLT and performed a detailed quantitative spectral analysis using state-of-the-art modelling techniques. We found that HVS 7 is an outstanding chemically peculiar late B-type star with moderate projected rotational velocity. This could have been expected as the fraction of chemical peculiar stars among late B-type main sequence stars is known to be high and adds another complication to the identification process of HVS. A severe caveat for the interpretation of HVS is the lack of proper motion measurements, which prevents a detailed kinematical analysis. Therefore we embarked on a project to study HVS candidates in the 6D phase space. As the known HVS are too faint for such an investigation, we had to select a brighter candidate sample.

The sample of more than 10,000 A-type stars from Xue et al. (2008) instantly attracted our interest, as they provided a list of heliocentric radial velocities, which is converted to the Galactic rest-frame (GRF) to search for HVS. Hence we focused on the fastest stars and tested for the first time our method to measure proper motions for HVS candidates. Therefore we used all available photographic plates to measure epochs and combined them with position measurements from various modern surveys to achieve the best possible time base. Together with the spectroscopic distance we can reconstruct and study the full phase space information. We used the method by Odenkirchen & Brosche (1992) in the standard Galactic potential of Allen & Santillan (1991) to perform a detailed kinematical analysis. Four stars of our sample showed a significant proper motion: J1553+0030 turned out to be a spectroscopic binary and was accordingly excluded from the analysis. J0136+2425 was found to be an A-type main-sequence star travelling at $\approx 590 \text{ km s}^{-1}$, possibly unbound to the Galaxy, which makes it an excellent HVS candidate. Most importantly we found the star to originate from the outer Galactic rim, nowhere near the Galactic centre, although this would be the favoured place of origin, if a super-massive black hole acted as a slingshot. Hence we conclude that there must exist a different ejection mechanism, similar to the case of HD 271791 (Heber et al. 2008a).

J1300+0422 was found to be a metal-poor blue straggler of population II on a wide retrograde halo orbit. For the first time a sophisticated NLTE analysis was performed and compared to the standard LTE approach. We classified its kinematics by using a sample of white dwarfs as reference. J1300+0422 is only marginally bound to the Galaxy in a standard Galactic potential.

Finally J1539+0239 was found to have very high negative radial velocity, i.e. is approaching us. It is a blue horizontal-branch star of Population II, travelling with the largest space velocity of any horizontal branch star known so far. The extreme kinematics of the star allows a significant lower limit to be put on the dark halo mass in order to keep it bound. Changing the average density and assuming the star to be bound we can constrain the mass of the Galactic halo to be $M_{\text{halo}} \geq 1.7_{-1.1}^{+2.3} \times 10^{12} M_{\odot}$. This value leads to a 80% higher total Galactic mass than that derived by Xue et al. (2008) but is consistent with other studies. In turn our finding has implication for the HVS as well

because, the Galactic escape velocity may be higher than presumed.

Until now only one old population HVS has been found: the subdwarf O star US 708. Such hot subdwarf stars come in two varieties (subdwarfs of O-, and B-type) and are rather unusual stars, due to their exceptional evolutionary state. As they already evolved away from the main-sequence they are burning helium in their core, which is surrounded by a very thin ($<0.02 M_{\odot}$) inert hydrogen envelope. In the case of subdwarf O stars almost no hydrogen is left in the envelope, which produces quite unique stellar spectra, dominated by helium absorption lines. Subdwarf B stars, however have masses of about $0.5 M_{\odot}$ and should evolve directly to the white dwarf cooling sequence, bypassing a second giant phase. Because the sdO star US 708 was discovered serendipitously, we can expect a larger population of these outstanding subdwarf hyper-velocity stars. Therefore we performed the Hyper-MUCHFUSS (Hyper-velocity stars or Massive Unseen Companions of Hot Faint Underluminous Stars from *SDSS*) project, which targets the detection of a fast (halo) population amongst hot subdwarf stars. We carried out the project at several observational sites, including e.g. the ESO Very Large Telescope in Chile. All the stars we analysed have to be either hot subdwarf binaries with massive compact companions, which are expected to show huge radial velocity variations or single hot subdwarf stars, which show constant high Galactic rest-frame velocities. We applied a sophisticated target selection method for hot subdwarfs with high Galactic rest-frame velocities to the enormous *SDSS* DR6 spectral database. These *SDSS* spectra served as first epoch observations for our project. We observed about one third of our targets and found 39 stars to have a high but constant radial velocity. For 15 stars we were able to measure a significant proper motion. From their stellar parameters ten stars turned out to be hot subdwarfs, 2 other are DA white dwarfs. Finally we performed a kinematical analysis, calculated possible trajectories and concluded on the origin of these 12 stars. Amongst them, we found the unbound hyper-velocity subdwarf J1211+1437 and traced the subdwarfs J1644+4523 and J0948+5516 back directly into the Galactic bulge during their last passage of the Galactic disk (GD). Overall 40% of our subdwarf stars show kinematics, consistent with such an origin, while another 30% seem to come from the outer rim of the Galaxy, at least told by their last GD passage.

Basically we conclude that there is the sought high-velocity subdwarf population, even including the first unbound subdwarf B star. At least two subdwarf stars are consistent with an origin in the bulge and may have been ejected via the so-called Hills mechanism. Six of our fast subdwarf population cannot originate from the Galactic centre within their last passage of the GD. Therefore we conclude that a high fraction of up to 60% of our fast population might be ejected via different scenarios, e.g. of the runaway type (see Chapter 7).

The sophisticated techniques we applied in the presented work can be easily used to extend the search for hyper-velocity stars. The final *SDSS* data release 7, as well as any other radial velocity based sample of stars is usable as starting point for an extended project. We closed by providing an outlook to the future Global Astrometric Interferometer for Astrophysics (GAIA) satellite mission by the European Space Agency. This successor to the famous ESA Hipparcos mission will instantly lead to a verification of the

provided conclusions by measuring highly accurate proper motions. Additionally it was built to provide complete kinematics for an unprecedented amount of stars. Within its lifetime of about five years it will observe up to a billion stars and set a new benchmark, if everything works as planned.

Chapter 1

Introduction

If you get to know an convincing archeoastronomer for the first time one can get the impression, that the natural science of astronomy has to be nearly as old as the mankind, because the dark night sky with its overwhelming amount of stars is one of the most fascinating miracles of nature. Therefore throughout all aeons men have reverentially trained their eyes on the skies. And so it is today (actually the year 2009) as we celebrate for the first time a worldwide International Year of Astronomy. Proclaimed by the 62nd General Assembly of the United Nations, it refers to the 400th anniversary of Kepler's "Astronomia nova" and the first telescopic discoveries of Galileo Galilei. One cannot overestimate the importance of this dedicated work, as it marked the breakthrough in peoples thinking of the world: away from a selfish earth(/men)-centred to a sun(/observer)-centred view. It was Copernicus in his book "De Revolutionibus Orbium Coelestium" who proposed the heliocentric world model (Copernicus 1543). Johannes Kepler made a precise description of the planetary motion and deduced the still fundamental laws of planetary motion (Kepler 1609). The era of the public breakthrough was heralded by publishing the "Astronomia nova" in 1609. Both Kepler and Galilei were convinced of the Copernican system and fighting against the common world view and the interpretation sovereignty of the Church. Galileo Galilei even had to swear off his ideas in front of the Holy Inquisition and was put under arrest. Otherwise he would have paid with his life for that. Finally this tragedy came to an end almost 400 years later as in 1992 Pope JP II officially apologised for that and Galilei was posthumously rehabilitated.

After building one of the first telescopes, Galilei used this new tool e.g. to discover that the Milky Way as an amount of numerous faint stars (Galilei 1610). For the next more than 300 years lots of speculations have been made about the shape of our own galaxy. Today we know a lot more about the detailed structure of other galaxies than our own, which is due to the fact that we are the outside beholder. Nevertheless our own galaxy is still much more difficult to explore.

Already in the 18th century William Herschel had the idea that we reside in a lens-shaped conglomeration of stars, which we see as the Milky Way (Herschel 1784). But Kapteyn (1922) was the first one to really observe the shape of the Milky Way and put it together into a quantitative model. To do this he used photographic star counts and statistical distance measurements for nearby stars through parallax and proper motions.

Finally he obtained a flattened disk with increasing stellar density towards the centre and came very close to the truth. Without accounting for dust extinction in the Galactic disk, he necessarily underestimated the real distances.

At the same time Shapley (1922) deduced the Galactic structure from his own work. He based his work on distance measurements especially of globular clusters using the variable RR-Lyrae stars. Finding a higher concentration of these clusters towards the constellation of Sagittarius, he suggested that the Galactic centre should reside there. Again no extinction correction was applied, hence he derived a flattened disk with a diameter of 100 kpc and a distance of 16 kpc to the centre of that disk.

The truth lies somewhere in between. Kapteyn (1922) underestimated the size, as he accounted only for nearby stars, which lie in the highest extinction region of the Galactic disk. And Shapley (1922) was accounting only for the distant globular clusters in the lowest extinction region. Hence he was overestimating the size. Finally Trumpler (1930) discovered interstellar extinction. He found that globular clusters are systematically too distant when the difference between apparent and absolute luminosity is not corrected for extinction.

This approach was the breakthrough to determine the shape of the Milky Way. Starting not only from the work of Herschel (1864), who prepared a huge catalogue of nebulae and clusters, the so-called “zone of avoidance” in the Galactic plane was a well known phenomenon. Today we know that the Galaxy consists of a thin and thick disk surrounded by a spherical halo. Our sun together with the complete thin disk is in an orbit with a circular velocity of $v_{\text{circ}} \approx 220 \text{ km s}^{-1}$ around the Galactic centre. In this centre there is a super-massive black hole called Sag A* with a mass of $3 \times 10^6 M_{\odot}$ at a distance of about 8 kpc, which is surrounded by a spherical bulge structure (e.g. Buser 2000).

Finding a SMBH in the Galactic centre was one of the most exciting discoveries of the last decade. Although the existence of a compact radio source called Sagittarius A* was already known for more than 50 years, nobody was able to conclude on its structure and its mass. Finally Schödel et al. (2002) succeeded to measure the elliptical orbit of stars moving around the GC. Applying Kepler’s laws they derive the mass of the black hole to be about $2.2 \times 10^6 M_{\odot}$. Later Hansen & Milosavljević (2003) even suggested the existence of at least another intermediate black hole (IMBH) in the GC. However the detailed structure of the Galactic centre is still not revealed today. The existence of such a SMBH has also some consequences for the stellar content of the Galaxy. One of them was e.g. described by Hills (1988) already well before the discovery of the SMBH. He suggested that in the vicinity of a MBH a binary could be disrupted, whereas one star is captured. The other star is ejected at almost orbital speed and was henceforth called hyper-velocity star (HVS).

But that is not the whole story. Beyond the stellar halo there must be something, which dominates the mass density and is the most massive part of the Galaxy by far. This can be deduced from the flat rotation curves of disk stars and gas in galaxies alone. The disk shows a constant rotation velocity over its whole extent (see Figure 1). A typical Keplerian potential for the mass concentrated in the Galactic core would lead to a $v \sim r^{-1}$ law, whereas solid body would produce a $v \sim r$ law. However in the inner part of the

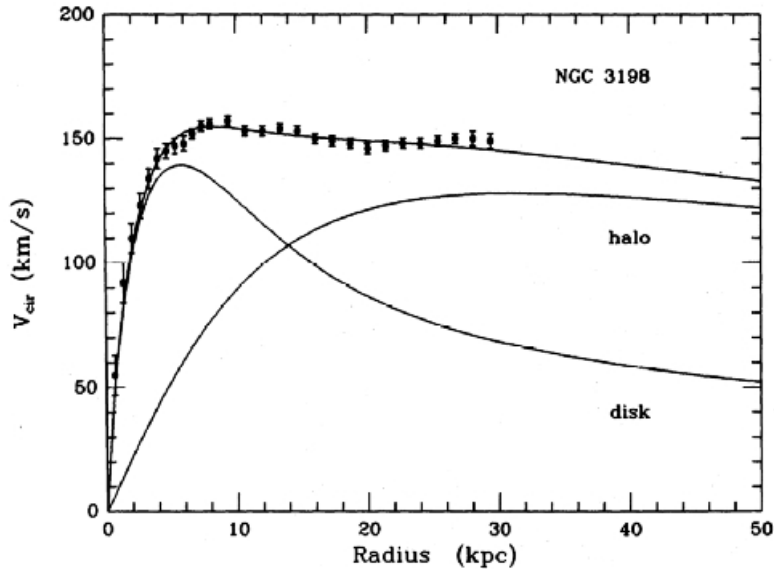


Figure 1.1: Circular velocity curve for the spiral galaxy NGC 3198 (van Albada et al. 1987).

disk the predicted disk potential is consistent with the observations. But as the stellar density is decreasing exponentially with radial distance from the centre we would expect the rotation to level off. Because the curve remains flat there must exist some dark (not luminous) matter, which is responsible for the flat rotation curve and the gravitational potential. Amazingly this holds not only for our own galaxy but for almost all spiral galaxies, as in Rubin et al. (1980), for example.

Furthermore Kahn & Woltjer (1959) found out that the local group is only stable if the Milky Way is much more massive than expected. The idea of a Cold Dark Matter (CDM) content of the halo, interacting only via gravitation was about to be born. Nowadays this dark halo mass is under active discussion due to several observational and theoretical constraints. By using 27 satellite galaxies and globular clusters and assuming that they bound, Wilkinson & Evans (1999) derived a total Galactic halo mass of $M_{\text{halo}} \sim 1.9^{+3.6}_{-1.7} \times 10^{12} M_{\odot}$. Basically one can say that larger halo masses of about $2 \times 10^{12} M_{\odot}$ were favoured earlier (Wilkinson & Evans 1999; Sakamoto et al. 2003), lower masses of about half this value were derived more recently (Battaglia et al. 2005; Smith et al. 2007; Xue et al. 2008). Navarro et al. (1996) used N-body simulations to derive a universal CDM density distribution, which is called the NFW model. Nowadays it is has become the benchmark in most studies to deduce the total halo mass (e.g. Xue et al. 2008).

From this point of view, especially hyper-velocity stars are perfectly suited to probe the structure of the Galaxy. Especially in case of the dark matter halo they might provide constraints on the total mass. This was already proven by Abadi et al. (2009), who set new important constraints by having a closer look at the known HVS. Therefore in

the following work I am convinced that I contribute my part to bringing light into the enormously puzzling "Ultimate Question of Life, the Universe, and Everything" (Adams 1979), which is commonly known as Astronomy.

This work is structured as follows: Chapter 2 gives a brief review on stellar evolution with a focus on blue stars and relates them to the fastest moving stars known, the recently discovered Hyper-velocity stars (HVS). In Chapter 3 a short introduction to the quantitative spectral analysis is given, while the applied advanced kinematical approach is presented in Chapter 4. Improved Analysis of some of the already known HVS can be found in Chapter 5. In Chapter 6 we present our search for A-type HVS based on the sample of Xue et al. (2008). The Hyper-MUCHFUSS project to find high-velocity subdwarfs in the halo can be found in Chapter 7. Finally we close with a brief outlook.

Chapter 2

The fast and the (UV-)luminous

Working in the field of stellar astronomy, you will never get along without using the Hertzsprung-Russell diagram (HRD, see Figure 2.1). This basic tool was invented 1913 by Henry Norris Russell and is based on the work of Ejnar Hertzsprung. Originally invented as a spectral type-magnitude diagram it turned out to represent more fundamental physical stellar properties. In that sense the spectral type of a star corresponds to its effective temperature, while its absolute magnitude can be transferred into luminosity, hence the emitted power.

The dominating structure is the main sequence, which is populated by hydrogen burning stars. As an ordinary star spends about 90% of its lifetime on the main sequence, most of the known stars can be found in that region. The heavier stars show increased burning rates, hence higher luminosity. Therefore the main sequence is also a mass sequence, with stellar masses varying from $0.1-100M_{\odot}$.

In order to make a more precise classification of a star, several extension systems have been provided. The most prominent system to do so, is the Harvard schema, which is based on pattern found in the optical wavelength of stellar spectra. An O-type star is defined by the presence of ionised helium lines (He II), whereas a B-type star shows lines produced by hydrogen and neutral helium (He I). If the star shows only hydrogen lines, together with calcium we speak of a A-type star. From type F to M the metal lines increase continuously in strength. In order to receive a better accuracy the types are subdivided into classes from 0 to 9, according to the strength of their characteristic pattern. The Harvard spectral classes can directly be converted to a physical measure, the temperature.

But there are more structures in a HRD, that can be separated according to their luminosity. Traditionally the structures are divided in to different classes, extending the common Harvard system. Most popular is the system developed by William Wilson Morgan and Philip. C. Keenan, the so-called MK-system. Typically seven luminosity classes are distinguished: I supergiants, II bright giants, III giants, IV sub-giants, V dwarfs, VI subdwarfs and VII white dwarfs. The main sequence stars correspond in general to the luminosity class V. But there are more classes of stars, like the hot subdwarfs, that can-

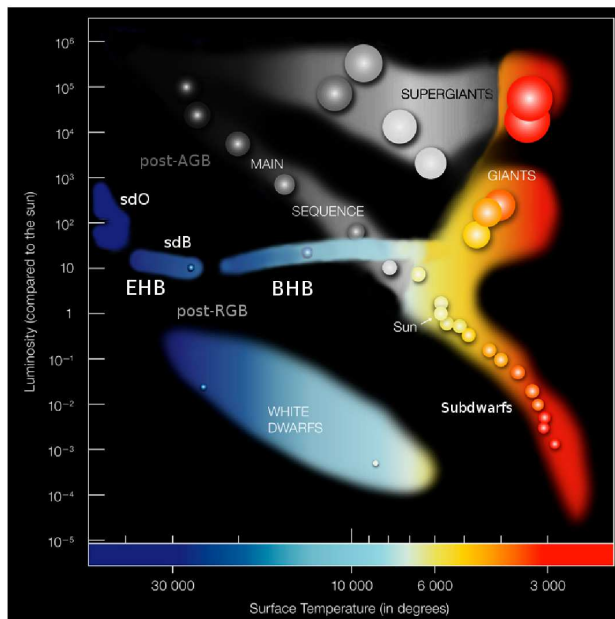


Figure 2.1: Hertzsprung-Russell diagram for different stellar types (ESO PR Photo 28c/07 with modifications by the author).

not easily be integrated into the MK classification system¹. A physical HRD showing the luminosity classification is shown in Fig 2.2.

More than 90% of all stars can be classified in the MK-system. In the following sections, I want to introduce several types of hot stars in more detail.

2.1 Blue star group

In the Hertzsprung-Russell diagram the blue B- and O-type stars, can be found at temperatures higher than 10,000 K. Their main characteristic feature in the optical spectrum is the presence of helium lines. B-type stars show both prominent Balmer and He I lines in their spectra, while O-type stars show ionised helium lines He II in addition to He I together with the Balmer lines, unless they are hydrogen deficient. These OB stars have an increased burning rate with an increasing temperature. Although they have high masses, and hence a large amount of fuel, they are short-lived as the faster burning cannot be compensated. Therefore they are often observed close to their place of formation. Additionally another factor has to be discussed. Empirical studies show that the number density dN in a stellar population drops steeply with increasing mass M , following

$$dN \sim M^{-\alpha} dM \quad (2.1)$$

. Based on the pioneering work of Salpeter (1955), the parameter α was regarded to be about 2.35 for massive stars. This means that massive stars form much less frequently

¹An extension of the MK procedure to classify hot subdwarfs has been proposed by Drilling (1994)

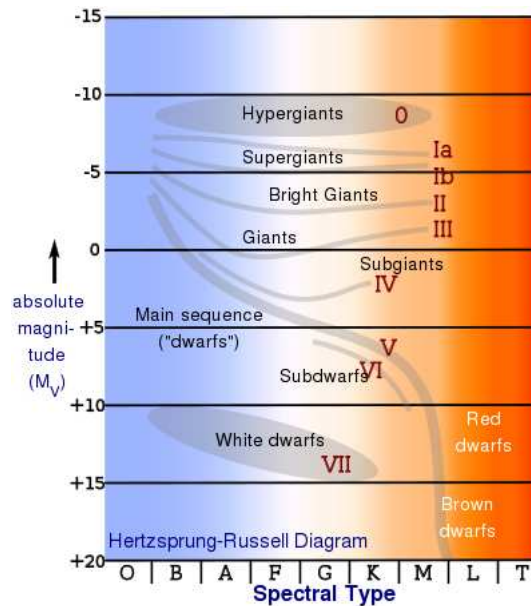


Figure 2.2: Hertzsprung-Russell diagram including MK- and Harvard classes. Excerpted from Wikipedia.

than low mass stars do. This has several important consequences. Compared to the rest, blue stars are very rare and so they have always been attractive for astronomy. On the main sequence the B-type stars are about 10^3 times more common than O-type ones. Additionally these stars are luminous and can therefore be seen over large distances. In the following we focus mainly on B-type stars, which can be found over a wide range of luminosities and hence also masses.

2.1.1 B-type stars on the main sequence

When B-type stars start their life on the main sequence (MS), they have masses between $2.0-16 M_{\odot}$ with radii between $1.8-6.6 R_{\odot}$. Compared to giants and supergiants they are rather small, hence also called dwarfs. Surrounded by a radiative shell, they burn hydrogen to helium in their convective core. The prominent features in their spectra are the neutral He I and the Balmer lines, which become weaker with increasing temperature. Additionally they often show lines produced by ionised carbon, oxygen and silicon. These stars have about solar metallicity and usually show a tendency to cluster. Due to their short lifetimes (below 100 Myr) B stars normally do not move very far away from their young active star formation region (e.g. Pleiades open star cluster) in the Galactic disk. Hence they belong to the so-called Population I of metal rich stars and can be found exclusively in the gas rich spiral arms of the Galactic disk, apart from very few halo exceptions (see Section 2.2 and Chapter 5).

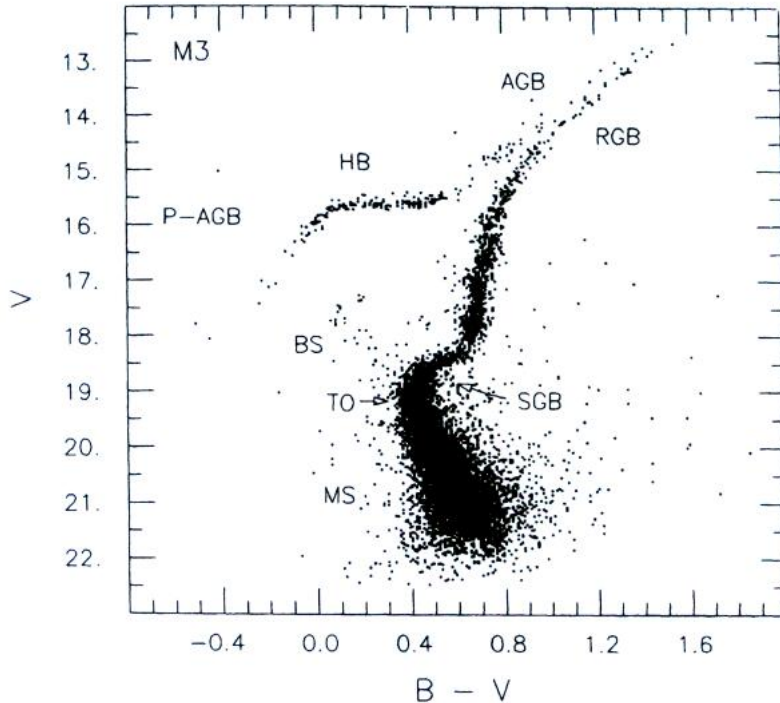


Figure 2.3: Colour-magnitude diagram in classical B-V vs V style for M3 (Renzini & Fusi Pecci 1988). Note the more left the bluer the stars.

2.1.2 Red giants and horizontal branch stars

In the Galactic halo, a sphere around the Galactic disk (GD) we find different B-type stars the so-called horizontal-branch (HB) stars. These stars are typically older than the sun, which is a Population I star, hence we call them Population II stars. They are mostly found in the old dense globular clusters and have a low stellar mass. In the standard HRD the HB crosses the main sequence at spectral type A0.

Horizontal-branch stars become obvious in the characterising colour-magnitude diagram (CMD), where they can be found in an horizontal region above the main sequence (see Figure 2.3). Globular Clusters are perfect examples for the study of stellar evolution as all the (> 50000) stars are located at almost the same place and formed out of the same material at the same time. As expected the dominant structure in the CMD (see Figure 2.3) is the main-sequence, an almost vertical bunch of stars in the lower centre. However the MS is short. At the upper end called turn-off (TO) the Red Giant Branch (RGB) diverges from the MS. Those stars evolve away from the MS along the RGB as the hydrogen fuel is almost exhausted and the core has enriched with helium ash. As the radiative pressure disappears the core contracts until it is stabilised by the degenerate electron gas and the stellar envelope expands strongly. This happens with increasing brightness although the envelope cools down and the star moves to the left and then up the RGB. On the tip of the red giant branch their core has been heated enough to

abruptly ignite helium core burning. For low mass stars ($< 2M_{\odot}$) this comes along with the helium flash, as the spontaneous ignition violently propagates through the stellar envelope. Depending on the envelope composition (metallicity) the flash might take away some material. After that the stars move to the horizontal branch and remain there for about 100 Myrs. They burn helium in their core, while in the outer parts they sustain hydrogen shell burning. Massive stars are found on the red side, while less massive stars fall to the left side of the HB. The line where the stars arrive on the HB is called the zero-age horizontal branch (ZAHB) and is hence a function of mass. When also their helium fuel is almost exhausted and their core consists out of carbon and oxygen ash they cross the terminal-age horizontal branch and evolve to higher brightness along the Asymptotic Giant Branch (AGB). Finally most of the stars evolve to white dwarfs and fulfil their destiny as an inert cooling degenerate object. At this point the active burning lifetime of the stars is over, but all these important stages can be exemplified in a CMD of a globular cluster.

In 1955 Arp (1955) discovered that the seven globular clusters he analysed looked indeed very similar in the CMD, with strong blue HBs. Additionally all of them turned out to be comparably metal poor. From that point it was clear that the stars in globular clusters must be chemically very homogeneous. Therefore they are perfectly suited as laboratories to follow the stellar evolution in the HRD. Applying this knowledge one can even estimate the age of a globular cluster. Assuming all stars have formed at the same time, the location of the turn-off point compared to the HB is therefore a suitable measure.

Nevertheless CMDs of globular clusters do not look the same. They particularly differ in the form of their HB. With the advent of the first charge coupled devices (CCD) in the 1980s the number of analysed globular clusters increased enormous. It turned out that the changes in the morphology are characterised primarily by metal abundance. In high metal abundance clusters the blue horizontal branch (BHB) often does not appear, whereas the red part is short and stumpy. Most of the metal poor globular cluster have distinct blue HBs sometimes extended with long dropping blue tails, which contain much fainter stars and are called the extreme horizontal branch (see Section 2.1.4).

But even in clusters with the same metallicity the morphology can be very different. In Figure 2.4 we show the CMDs of M3 and M13, which both have a metallicity of $[Fe/H] \approx -1.5$. Therefore we know that there is still a lack in understanding and metallicity cannot be the only reason. This is summarised under the term “second parameter problem”. Theoretical modelling of HBs showed that several parameters like age, rotation or helium surface abundance (Lee et al. 1990) can change the morphology of the cluster in the CMD and have to be discussed individually. Fortunately with the Hubble Space Telescope, imaging precision improved a lot and helped to analyse and understand these relations. Nowadays even tiny splittings in the MS and the TO of globular clusters have been detected (see Figure 2.5), which implies several stellar populations slightly different in age, but chemically distinct (Ventura et al. 2009). What remains is that horizontal branch stars are one key element in understanding stellar populations, as they are of the same kind (core helium burning objects), but can be very different. For a more detailed review on horizontal branch stars I want to refer to Catelan (2009), Philip (2000) and Layden

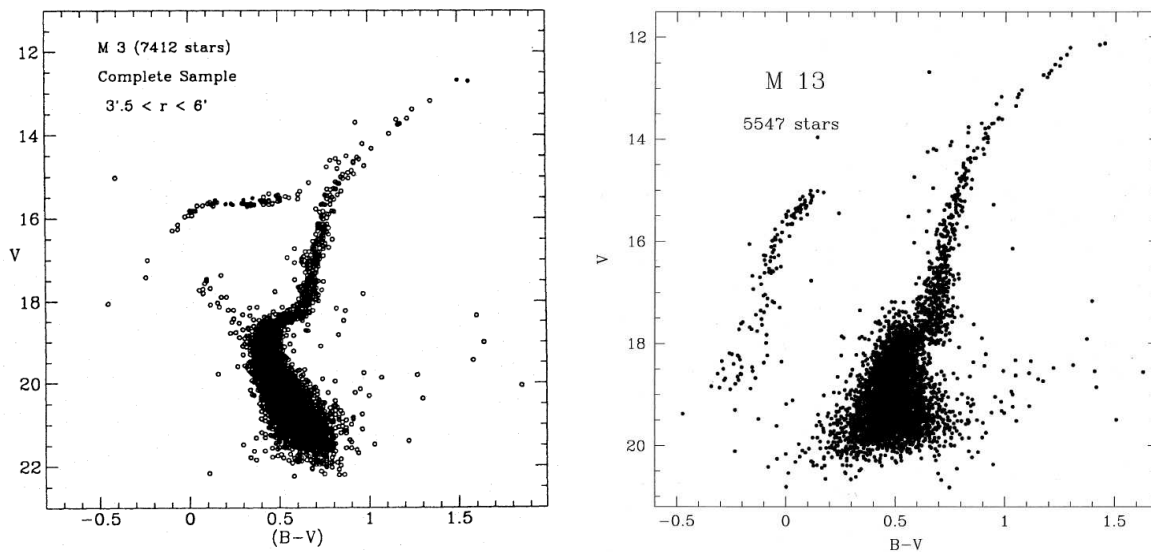


Figure 2.4: Comparison of the colour-magnitude diagrams for M3 (Buonanno et al. 1994) and M13 (Paltrinieri et al. 1998).

(1998), for example.

At first glance, some horizontal branch stars can look like normal dwarfs as their spectra look quite similar, although physically they are very different. Problematic especially for B stars is that the MS and HB populations intersect in the $T_{\text{eff}}\text{-log } g$ -diagram (see Chapter 7). In the intersection region around $T_{\text{eff}} \approx 12600 \text{ K}$ and $\log g \approx 4.0$ these stars can only be distinguished by additional information e.g. metallicity, rotation or alpha enhancement. It is therefore of critical importance to know about B-star occurrence, their different forms of appearance and to care about an accurate classification of these types of stars.

2.1.3 Blue stragglers

With the advent of advanced stellar photometry in the 1950's, the so-called blue-straggler enigma was discovered. Observing Globular Clusters revealed blue stars on the extension of the main-sequence beyond the turn-off point (see Figure 2.3). However, we do not expect stars in that area of the CMD as they should have already evolved to red giants or even further. As they seem to straggle around, independent of their destiny, Burbidge & Sandage (1958) introduced the term “Blue Stragglers“ (BS). At this time basically three scenarios were discussed: (1) the stars either have formed later than the rest of the Cluster, for which to date no reasonable argument could be provided. (2) They are already evolved, which means they are a kind of pseudo horizontal branch stars. This scenario could be excluded by several (multicolour) analysis in the following decades (e.g. Bond & Perry 1971). (3) Blue Stragglers are simply stars with an extended lifetime on the main sequence, which is still the current view. The reason for their prolonged lifetime is controversially discussed.

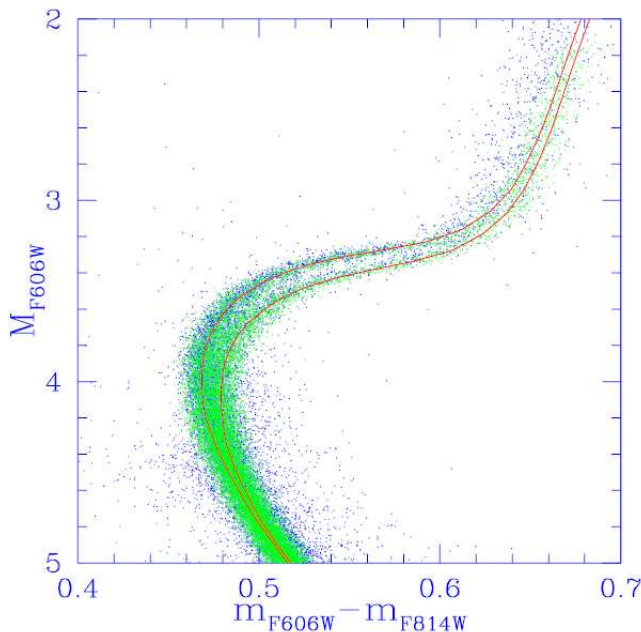


Figure 2.5: Colour-magnitude diagram for NGC 1851 (Ventura et al. 2009). Observations are blue, the model is green and the red lines are fits to the observations.

Several scenarios ranging from stellar collisions over several deep mixing theories to binary mass transfer have been proposed. Until today the most popular scenario is the merger of two stars. This merging could be the result of a stellar collision, but these events especially close ones are rare. Hence collisional mergers may easily account only for about 10 % of the BS (Leonard & Linnell 1992) in high stellar density regions like GCs.

Besides that, mergers can occur in close binary systems, but these scenarios are much more complex. Binaries might establish mass transfer via Roche-Lobe overflow or undergo a Common Envelope phase before the two cores spiral together. How these binary mergers exactly happen, depends on the participating masses and the orbit of the system. Assuming no significant mass loss of the system in this stage, the leftover is a star with fresh hydrogen to extend its lifetime. The problem is that after a merging event we expect fast rotation of the remnant. But observations show no evidence for the fast rotation of BSs; in the case of M 67 the rotation was found by Peterson et al. (1984). Therefore these stars have to lose angular momentum e.g. by magnetic braking, which works in case of sufficiently strong stellar winds. In general we believe that several scenarios could be responsible for the observed BSs, whereas the binary merger scenario seems to be the most observed one in nature. As a result we observe a long-lived main sequence star with a mass of, at most, the sum of the two progenitors.

Whether two types of BSs exist in clusters, which may result from the different suggested mechanisms has been discussed frequently in the literature. The discovery of two distinct sequences of BSs in the globular cluster M 30 (Ferraro et al. 2009) indicates that

indeed both formation mechanisms are at work.

In open clusters this does not seem to be the case, as Mathieu & Geller (2009) recently found a high frequency of binaries among the blue stragglers in the open cluster of NGC 188, most having eccentric orbits with periods of about 1000 days. Brown et al. (2009) argue that most if not all BS in open clusters arise from multiple star systems. This suggests that blue stragglers are formed in both ways in star clusters, with collisions/mergers becoming more common with increasing cluster density.

In the Galactic field it is more difficult to identify BSs because the stellar age can not be determined. Field blue stragglers are therefore usually identified as metal-poor main sequence objects that are hotter than globular cluster main-sequence turnoff stars. Nevertheless a lot of blue metal-poor stars $[Fe/H] < -1$ with main-sequence luminosities have been found to be hotter than the main-sequence turnoff of globular clusters and are therefore considered to be field analogs to the cluster BS population. Actually these stars seem to be so numerous that their specific frequency of appearance compared to regular horizontal branch stars was found to be higher than in globular clusters (Preston & Sneden 2000). As the stellar density is small in the field, binary star evolution and mass transfer is probably the most common path of formation among field BS stars. Carney et al. (2001, 2005) pointed out that some BS candidates among metal-poor halo main-sequence stars are not binaries. Hence binary star evolution and mass transfer may not be the only path. They argue that the apparently single stars could be the partial remnants of an accreted dwarf satellite galaxy whose star formation continued over a long period of time. Hence those metal-poor main-sequence stars are simply young stars.

For a more detailed discussion of the Blue Straggler phenomenon I refer to the reviews of Ferraro et al. (2009), Nemeč (1991), Stryker (1993) or Mathys (1987), for example.

2.1.4 Hot subdwarfs

Among the blue stars, the hot subdwarfs form a class of particular interest, as they are distinctly fainter than the associated main sequence stars. The first extensive search for faint B-type stars was performed in the 1940's by Humason & Zwicky (1947). During the spectroscopic follow-up the first subluminous B stars were found. In the following decades their number remained rather small. But with the Palomar-Green survey of the northern hemisphere their number increased rapidly and it turned out that the subdwarf B stars (sdBs) form a very homogeneous class in terms of their spectral properties. Indeed it was noticed that for magnitudes brighter than 18^m most faint blue objects seem to be subdwarfs, outnumbering even the well-known white dwarfs (WDs). Among these blue subdwarfs we can also find subluminous O-type stars (sdOs), which show a large variety of spectra. Basically they are characterised by strong He II Pickering lines, unblended from hydrogen Balmer lines (Ströer et al. 2005). The spectrum of these old population sdOs are mainly believed to be the descendants of the sdBs (Heber et al. 2006), although they are hotter as their inert hydrogen shell around the helium burning core is even thinner (or gone). In general subdwarf O stars are a blend of post-horizontal branch stars, post-giant branch stars and post-asymptotic branch stars.

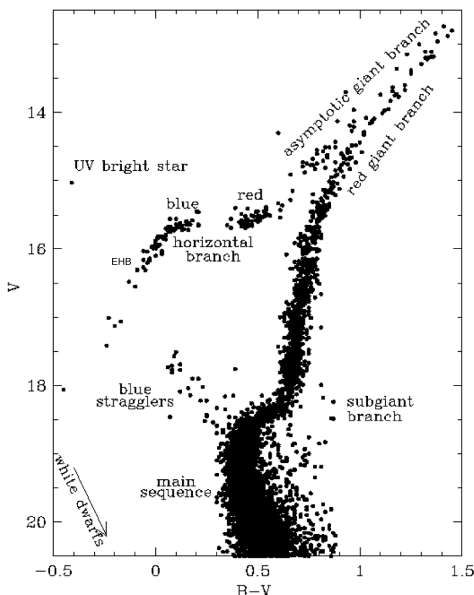


Figure 2.6: Colour-magnitude diagram with components for M3 from Buonanno et al. (1994) including the horizontal branch Excerpted from Moehler (2001).

The subluminescent B stars, are generally believed to be core helium burning stars with very thin ($<0.02 M_{\odot}$) hydrogen envelopes (Heber et al. 1984), which have masses around $\sim 0.5 M_{\odot}$. However, important questions still remain about their formation and the appropriate timescales. Following ideas outlined by Heber (1986), the sdBs can be identified with models for extreme horizontal branch (EHB) stars (see Figure 2.1). An EHB star bears great resemblance to a helium main-sequence star of half a solar mass and it should evolve similarly, i.e. directly to the white dwarf cooling sequence, bypassing a second giant phase.

To date EHB stars have been found in several different stellar populations. Within the Galactic field they are represented within the rather bright ($< 16^m$) PG survey sample. Hence these subdwarfs have been identified, analysed and studied in great detail (e.g. Saffer et al. (1994), Maxted et al. (2001) and Green et al. (2008)). Furthermore a large search search for subdwarfs within the extensive Sloan Digital Sky Survey (short: *SDSS*) was performed by Hirsch et al. (2008), whereas especially the helium rich objects have been analysed in detail as the *SDSS* spectral coverage is perfectly suited for this purpose. Apart from the Galactic field, subdwarfs can also be found in globular clusters. In the CMD these stars form an extension of the blue horizontal branch, especially distinct in metal poor clusters (see Section 2.1.2). Fig 2.6 shows the extended horizontal branch of M3. Due to their thin hydrogen layer sdBs cannot sustain shell burning and lack therefore about half the luminosity of a normal horizontal branch star. Like in M3, this extension is often separated by gaps where no stars are found. Suitable explanations are still under vigorous discussion. Some of them can be found in Moehler (2001), together with a detailed review on hot subdwarfs in globular clusters.

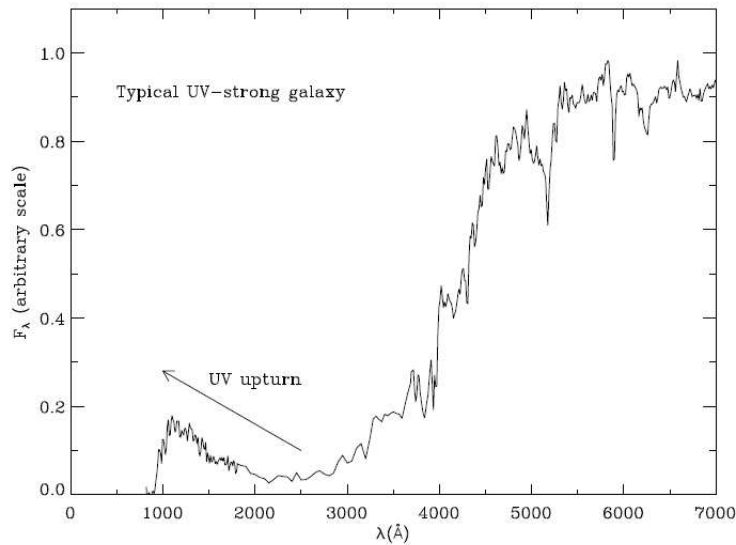


Figure 2.7: The composite spectrum of the giant elliptical galaxy NGC 4552 shows a classic example of the UV upturn (Ventura et al. 2009).

With the start of satellite UV astronomy a mysterious excess of UV light in seven early-type (elliptical and S0) galaxies was found (Code & Welch 1979). In spiral galaxies clearly the UV flux is dominated by the young most massive stars, which should not exist at all in old galaxies. Later, this result was confirmed during several space missions e.g. HUT (Brown et al. 1997). Fig 2.7 shows a typical UV upturn in an elliptical galaxy.

Although old hot subdwarfs seem to be the natural candidates for an UV excess, it was doubted for a long time if they are sufficiently numerous in galaxies. Besides in the Milky Way halo, hot subdwarfs have been resolved for the first time in the core of the dwarf elliptical galaxy M32 by Brown et al. (2000) using the Hubble Space Telescope (S T Imaging Spectrograph). Additionally the work of Busso et al. (2005) revealed subdwarfs in the central Galactic Bulge, which is the Galactic part most similar to elliptical galaxies. So considerable evidence has accumulated that these stars are sufficiently common to be the most likely source for the “UV upturn phenomenon” observed in elliptical galaxies and spiral galaxy bulges as proposed by Yi et al. (1997). For a more detailed review of the UV upturn phenomenon I refer to Yi (2008).

While the present state and future stages of sdB evolution seem to be well known, the question of the stars’ formation is widely unanswered. After all, three basic scenarios have been proposed: binary interaction e.g. Roche lobe overflow (Mengel et al. 1976), single star evolution with strong mass loss near the tip of the Red Giant Branch (D’Cruz et al. 1996), and the merger of two helium white dwarfs (Iben & Tutukov 1986). Nowadays, evidence is growing that close binary evolution plays an important role for the formation of sdB stars. A fraction of close binaries of two third was found by Maxted et al. (2001), while Morales-Rueda et al. (2003) and Napiwotzki et al. (2004a) found a slightly lower binary fraction of 48% and 39%, respectively.

The theoretical work of Han et al. (2003) brought remarkable progress. Three possible binary formation channels were studied: common envelope ejection, stable Roche lobe overflow, and the merger of two helium white dwarfs. Using binary population synthesis, 12 simulation sets could be created and one of them could satisfactorily reproduce the observed characteristics of the sdBs' characteristics (T_{eff} , $\log g$, binary fraction, orbital period distribution, etc) when compared to radial velocity studies of Maxted et al. (2001). One of the key results of the Han et al. studies was that the mass range of sdBs may be larger than previously thought. They found that sdB stars in binary systems may have masses as low as $0.36 M_{\odot}$ and still pass through a helium core burning phase. Until now, the mass of any sdB stars has mostly been assumed to be $\sim 0.5 M_{\odot}$ for the determination of luminosity or binary companion mass, however now it appears this may not be entirely appropriate. What is needed is a set of precise masses that can be compared with sdB formation models such as those of Han et al. (2003).

The growing field of Asteroseismology appears to be the perfect tool to face this challenge and probe stellar masses with a forward approach. The first pulsating subdwarf B star EC 14026–2647 was discovered by Kilkeny et al. (1997) and resides in a binary system. Photometric variations of small-amplitudes (≈ 0.012 mag) with a very short period of 144s were found. Kilkeny et al. (1997) even detected a second pulsation mode near 134s with a smaller amplitude of ≈ 0.004 mag, which might be variable. Consequently this discovery marked a new class of variable stars, which are now called sdBV_r stars (Kilkeny et al. 2010).

The sdB+M star eclipsing binary NY Vir was the Rosetta stone in this field, as it shows a strong reflection effect **and** short-period pulsations. Vučković et al. (2007) determined a stellar mass of $M = 0.466 \pm 0.006 M_{\odot}$ by using only the binary properties. This model is remarkably consistent with the asteroseismological result derived by fitting the 25 pulsation periods from the time-averaged spectroscopy (Charpinet et al. 2008). Unfortunately obtaining complete sets of modes derived by spectroscopic mode identification are extremely time-consuming and therefore rare. Nevertheless for some stars we have obtained a very detailed picture of their pulsational behaviour, e.g. PG 1325+101 (Telting & Østensen 2004), PG 1605+072 (Tillich et al. 2007) and Balloon 090100001 (Telting et al. 2008). For a detailed review on the observational efforts to analyse pulsating subdwarfs, I refer to the work of Kilkeny (2007). In future more such analyses together with a forward seismic modelling will hopefully lead to a bigger set of masses in order to improve the understanding of the formation of sdB.

2.2 Stars beyond the speed limit

Main sequence OB stars are luminous stars that can be seen to large distances. In the 1950s some of these stars have been found to move with astonishing high velocities and were named *runaway stars* by Oort & Spitzer (1955). Thinking of mechanisms to accelerate such an heavyweight was an interesting field shaped by the interplay of theoretical prediction and observational verification. While in the late 1980s the runaway stars apparently lost their attraction, as they are a natural outcome of the modern star cluster

simulations (see Section 2.2.1). But in 2005 a new class of high velocity objects attracted general interest. The proclamation of so-called hyper-velocity stars (short: HVS), linked these stars closely to a potential super-massive black hole (short: SMBH) origin (Hills 1988). This circumstance was perfectly suited to bring forward the search for massive black holes (see Section 2.2.2). Both kinds of stars are currently again of highest interest and share their main attribute: an atypical high velocity. Therefore they have attracted great interest as they allow implications on a wide field of astrophysics, which we intend to outline here.

2.2.1 Runaway stars

The first high-velocity O and B type stars have been found at high Galactic latitudes with galactic rest-frame (short: GRF) velocities in the range of $100 - 200 \text{ km s}^{-1}$ (Blaauw 1961). The direction of their space velocity and their proximity to known gas-rich OB associations made it easy to believe that these stars originate from there. Hence, these stars have been termed runaway stars. The authors pointed out that they are not a distinct subdivision of high-velocity OB stars, but merely those for which the direction of the space velocity is sufficiently accurately known and the distance the star has travelled is still small (Blaauw 1961). Within OB associations the expanding motion of the components can be naturally explained by star formation within fast hydrogen gas regions, which could be accelerated by a simple rocket effect (Oort & Spitzer 1955) observed in other gas clouds. However this effect cannot explain very fast stars, as high increase in velocity also provokes a high mass loss. According to their calculations the initial gas cloud must be at least as big as $3 \times 10^6 M_{\odot}$ for a increase of 200 km s^{-1} , which is unlikely to occur. Furthermore Oort & Spitzer (1955) stated, that if such clouds would exist, one would expect to find a large collection of O stars; this was obviously not the case.

Today we know two capable ejection mechanisms for runaway stars. Zwicky (1957) was the first to notice that a supernova in a binary could produce high velocity stars. Independently Blaauw (1961) suggested a massive binary in its final stage of life to explain his observed OB runaway stars. In the modern version of this binary scenario a massive star undergoes a core collapse explosion and its companion star is released at a high percentage of its orbital velocity (up to 200 km s^{-1}). Faster stars cannot be explained by that scenario as the orbital speed is limited by the huge dimension of such massive binaries.

The other ejection mechanism is based on close single star/binary (or binary/binary) encounters. N-body simulations of open clusters with an initial binary ratio of 50% produce stars with velocities up to twice as large as the binary orbital velocity due to binary-binary interaction (Leonard & Duncan 1988). Thus for OB-type stars these ejection velocities can reach up to 360 km s^{-1} . The binary ratio of the escaping stars decreases with increasing escape velocity.

These formation scenarios are also explained by the simulations of three-body scattering done by Gvaramadze et al. (2009). Following their studies $3-4 M_{\odot}$ stars can attain ejection velocities of $\gtrsim 300 - 400 \text{ km s}^{-1}$, while late B-type stars reach typically

$\gtrsim 200 - 400 \text{ km s}^{-1}$. Furthermore they found that, in some cases stars can even reach velocities exceeding the Galactic escape velocity. But this is only regularly the case for scattering on very massive stars of several hundred solar masses.

Observational efforts to discover more such runaway stars have been continuously increased since their discovery in the 1960s. House & Kilkenny (1978) analysed a sample of 138 OB-stars located at intermediate galactic latitudes. As no reliable proper motion was present for these stars, they compared their radial velocities with theoretical values from dynamical models. They found that the low-velocity stars have probably been ejected from the plane some time after formation, whereas the high-velocity stars have been ejected only a short time after formation. They concluded that the results are in reasonable agreement with origins from slingshot mechanisms and runaway scenarios.

In the following two decades a systematic and dedicated search for blue stars at high galactic latitudes was performed by Kilkenny (1989). All of these stars have been analysed using both photometry and spectroscopy combined with synthetic line profiles. This produced a first estimate for their distance and lead to good constraints on their current location. Unfortunately the lack of reliable proper motions prohibited combining it with the distance and the spectral radial velocity information to obtain the full 6D phase space information. In the first part Kilkenny & Lydon (1986) revealed a supergiant, which they possibly could assign to the SMC, and four population II stars. They considered these stars as related to the “UV-bright” stars detected in some globular clusters. Continuing their search they revealed also several new subdwarfs of O-, B-, and OB-type (Kilkenny & Pauls 1990; Kilkenny & Busse 1992).

But that was only the beginning: especially the Palomar-Green survey (Green et al. 1986) and the Edinburgh Cape survey (Kilkenny et al. 1991) have driven progress in the field, due to the discovery of an unprecedented amount of early-type stars at high Galactic latitudes (Saffer et al. 1997; Kilkenny & van Wyk 1990; Kilkenny et al. 1995). Naturally this also was of enormous importance for the field of hot subdwarfs as their number increased tremendously in consequence.

The suggested formation scenarios have met with considerable success to explain most of the observed runaway stars known (e.g. Conlon et al. 1990, 1992; Tobin & Kilkenny 1981; Kilkenny 1989; Kilkenny & van Wyk 1990). The Hipparcos-Satellite mission (Perryman et al. 1997)². had an enormous impact on the field because it provided accurate proper motions and allowed detailed kinematical studies.

Recently a very complex situation, produced by two runaway stars AE Aur and μ Col and the binary ι Ori, was successfully analysed by Hoogerwerf et al. (2001). Using accurate astrometry with proper motions and parallaxes from Hipparcos in a detailed kinematical study, they were able to resolve a common origin about 2.5 Myr ago. Additionally they found comparatively large velocities of the runaways a high eccentricity of the ι Ori binary. Hence they deduced that a double binary runaway scenario is indeed responsible for the observed trajectories.

The most recent example is HD 271791, the hyper-runaway B-type star HD 271791 which was found and analysed in detail by Heber et al. (2008a). With its high heliocentric

²The final calibration is given by van Leeuwen (2007).

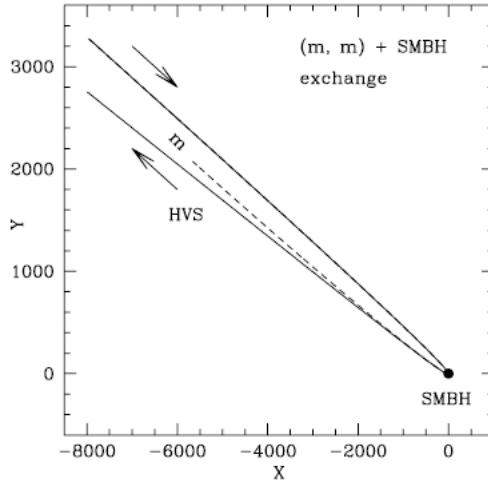


Figure 2.8: Example for the disruption of a massive binary by a SMBH. Excerpted from Gualandris et al. (2005).

radial velocity of $v_{rad} \approx 440 \text{ km s}^{-1}$ (Kilkenny & Muller 1989) this subgiant B star might appear easily in RV based surveys (see Table 2.1). The new proper motion measurement together with the detailed kinematical analysis of HD 271791 performed by Heber et al. (2008a), showed that the star originated from the Galactic outskirts. Furthermore the ejection velocity as well as a detailed study of abundance pattern by Przybilla et al. (2008a), provide evidence for an extreme case of the runaway scenario (Blaauw 1961) involving an hypernova.

But as such stars are mistaken as hyper-velocity stars we urge a clear classification based on a detailed analysis of the fastest stars.

2.2.2 Hills scenario and the super-massive black hole

The compact radio source Sagittarius A* in the Galactic centre (GC) has been known for decades. Hence the central mass of our Galaxy has long been suspected to be in that region. Due to the dynamics of gas in that central region, Oort (1977) has suggested the existence of a massive black hole (MBH) of more than $4 \times 10^6 M_{\odot}$. In the late eighties it was predicted from numerical experiments that a binary could be disrupted by a massive black hole, leaving one star bound to the MBH and the other star ejected with velocities exceeding the escape velocity of the Galaxy (Hills 1988). These hyper-velocity stars can theoretically reach an ejection velocity of 4000 km s^{-1} for a binary with a semi-major axis of 0.01 AU and therefore cannot be mistaken as runaway-stars. But only hard binaries with large orbital velocities are able to travel intact through the suspected high stellar density surrounding a MBH. In Fig 2.8 we show an example for such a binary disruption, which is also known as slingshot mechanism.

Up to 6000 such stars might exist inside the solar orbit of the Galaxy if one HVS

is produced per 10^3 yr. HVS might also have proper motions up to 100mas/yr in an 8kpc distance, which could be reached in only 2×10^6 yr. Therefore Hills suggested to use proper motion surveys to find these objects. Additionally he pointed out that the detection of one such HVS would be evidence for the existence of a massive black hole in the GC.

In the following years unfortunately nobody was able to detect such an object and so the MBH remained unproven. Finally Schödel et al. (2002) confirmed a SMBH with a mass of about $3 \times 10^6 M_\odot$ (Ghez et al. 2005) in the GC using astrometric measurements. Later Hansen & Milosavljević (2003) even suggested the existence of at least another intermediate black hole (IMBH) in the GC. Due to young massive main-sequence stars in the environment of the BH they favour a scenario where these stars have been dragged to the GC by an IMBH. The first IMBH candidate in the central region IRS 13E was meanwhile abandoned (Schödel et al. 2005) due to lack of an X-ray source, hence lack of evidence for accretion.

From that point it was clear that HVS should exist and the efforts in this field have been increased. Based on three different ejection scenarios, Yu & Tremaine (2003) predicted for the first time formation rates for HVS ($> 10^3\text{km s}^{-1}$). They completely ruled out close encounters of two single stars with a negligible formation rate of $10^{-11}/\text{yr}$, whereas the tidal disruption of a binary leads to a formation rate of $10^{-5}(\eta/0.1)/\text{yr}$, which increases with the binary fraction η . With $\eta = 0.1$ one HVS should be ejected every 100000yr , resulting in a total number within the solar orbit ($< 8\text{kpc}$) of ≈ 100 , assuming solar mass binary stars and a typical semi-major axis of 0.1AU . For the first time a binary black hole scenario, applied on single stars, was examined. In that case the ejection rate even increases to $10^{-4}/\text{yr}$ with a total number of 1000 HVS within the solar orbit (Yu & Tremaine 2003). The time was ready for the first HVS to be found...

2.2.3 The first hyper-velocity stars

In 2005 the first three HVS have been found serendipitously. Brown et al. (2005) analysed a sample of BHB stars from the Sloan Digital Sky Survey (short: *SDSS*) in order to trace the velocity structure in the halo, when they found the first HVS. After a follow-up observation it was clear that they found a faint B-type star J090745.0+024507 (= HVS 1) with a heliocentric RV of 853km/s , travelling at a galactic rest frame velocity of 709km s^{-1} . The temperature of the star was found to be $T_{\text{eff}} \sim 10500\text{K}$ (hence B9), which lies exactly in the region, where the main sequence crosses the horizontal branch. From the roughly solar metallicity of the star they suggest that it resides on the main sequence, which they admit not to be a compelling argument. In any case such an assumption is not justified as shown in Section 2.1. Later, a BHB nature could be excluded, as Fuentes et al. (2006) detected slow pulsation in HVS 1. This indicates strongly a main sequence nature for the star and hence a distance of $d_{MSB} = 71\text{kpc}$. Although no proper motion is available, HVS 1 is unbound due to its high GRF velocity (Brown et al. 2005). Nevertheless they found its travel time to be $\leq 80\text{Myr}$, which is consistent within the main sequence lifetime for a B9-star of about 350Myr .

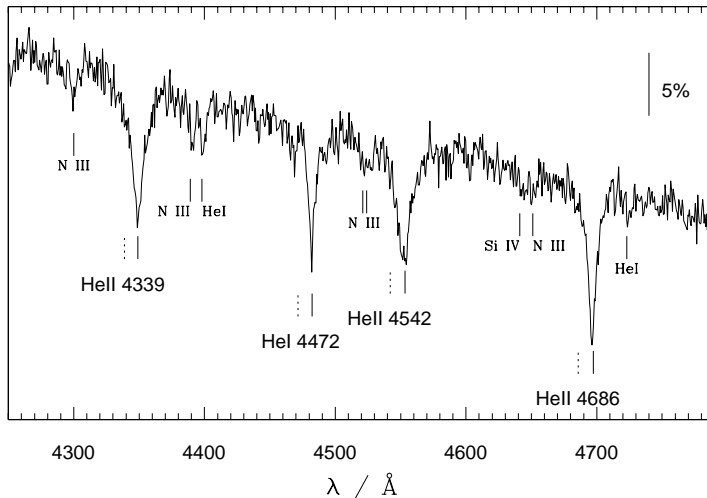


Figure 2.9: Spectrum of the subdwarf O star US 708 (= HVS 2), which was found to be a HVS. Note the highly red-shifted He II Pickering lines. Excerpted from Hirsch et al. (2005).

Independently members of our group (Hirsch et al. 2005) discovered the subdwarf O star US 708 to be a HVS, soon thereafter. The faint ($V = 19.0$) blue object J093320.86+441705.4 (also HVS 2) at high Galactic latitude ($l_{II} = 175.99^\circ, b_{II} = +47.05^\circ$) was also rediscovered by *SDSS* and analysed within a search campaign for subdwarf O stars (sdO). Remarkably a redshift of almost 10 \AA was measured, which is demonstrated in Fig 2.9. This converts into a heliocentric RV of $708 \pm 15 \text{ km s}^{-1}$ and results in a GRF velocity of 751 km s^{-1} which defines the star as unbound in Standard Galactic potentials. HVS 2 belongs to the so-called subclass of He-sdOs, as can be seen from the strong He II lines unblended from hydrogen Balmer lines (Ströer et al. 2005). Applying a χ^2 -fit of synthetic model spectra the atmospheric parameters are determined to $T_{\text{eff}} = 45560 \pm 675 \text{ K}$, $\log g = 5.23 \pm 0.12$ and $\log n_{\text{He}}/n_{\text{H}} = 0.99 \pm 0.18$, typical for sdO-stars. Hence a spectroscopic distance of $d = 19_{-2.7}^{+3.1} \text{ kpc}$ was calculated (Hirsch et al. 2005). From a trial test they found a trajectory with a proper motion of $\mu_\alpha \cos(\delta) = -2.2 \text{ mas yr}^{-1}$ and $\mu_\delta = -2.6 \text{ mas yr}^{-1}$ originating in the GC with a time of flight of $\text{TOF} = 32 \text{ Myr}$, shorter than the evolutionary lifetime of a sdO ($t_{\text{evol}} \approx 100 \text{ Myr}$). Since the merger of a close binary of two helium white dwarfs is a suggested available scenario for sdO formation, this might have happened during the encounter with the SMBH in the GC.

These two independent discoveries within a very short time easily got the ball rolling and triggered tremendous attention. The next section gives an overview of the new projects and ideas, which arose following this discovery.

2.2.4 Blue stars near the Galactic centre

After the discovery of the SMBH in the GC and of HVS, following the Hills (1988) scenario the question was raised: where are the binary remnants, which have been captured by

Table 2.1: Table of the known HVS following Brown et al. (2009)

ID	Type	M_V (mag)	V (mag)	R_{GC} (kpc)	l (deg)	b (deg)	v_{\odot} km s^{-1}	v_{GRF} km s^{-1}	Catalog name
HVS1	B	0.3	19.83	111	227.33	+31.33	840	696	SDSS J090744.99+024506.91
HVS2	sdO	+2.6	19.05	26	175.99	+47.05	708	717	US 708
HVS3	B	2.7	16.20	62	263.04	40.91	723	548	HE 0437-54393
HVS4	B	0.9	18.50	82	194.76	+42.56	611	566	SDSS J091301.01+305119.84
HVS5	B	0.3	17.70	45	146.23	+38.70	553	649	SDSS J091759.48+672238.34
HVS6	B	0.3	19.11	78	243.12	+59.56	626	528	SDSS J110557.45+093439.55
HVS7	B	1.1	17.80	60	263.83	+57.95	529	416	SDSS J113312.12+010824.95
HVS8	B	0.3	18.09	53	211.70	+46.33	489	407	SDSS J094214.04+200322.16
HVS9	B	0.3	18.76	68	244.63	+44.38	628	485	SDSS J102137.08005234.86
HVS10	B	0.3	19.36	87	249.93	+75.72	478	432	SDSS J120337.85+180250.46
HVS11	A	+0.6	19.70	70	238.76	+40.63	482	336	SDSS J095906.48+000853.4
HVS12	A	+0.6	19.76	70	247.11	+52.46	552	429	SDSS J105009.60+031550.7
HVS13	B	0.3	20.16	125	251.65	+50.64	575	443	SDSS J105248.31000133.9
HVS14	B	0.3	19.89	112	241.78	+53.20	532	416	SDSS J104401.75+061139.0
HVS15	B	0.3	19.33	85	266.51	+55.92	463	343	SDSS J113341.09012114.2
HVS16	B	0.3	19.49	90	285.86	+67.38	443	367	SDSS J122523.40+052233.8

the SMBH? In general the stars in the central parsec of the GC are blue ($T_{\text{eff}} \approx 30000\text{K}$), hence seem to be young. However the nature of these so-called S-stars remained under controversial discussion, as their orbits come so close to the SMBH that tidal forces prevent star formation in situ, leading to a birth problem (Ghez et al. 2003). Hence Hansen & Milosavljević (2003) suggested another intermediate massive black hole (short: IMBH) in the GC, which dragged this stars to their current location. Eisenhauer et al. (2005) found 9 out of 10 stars in the central 0.4" region to be main-sequence B stars. A detailed analysis of their trajectories showed a random orbital orientation, hence they concluded that these S-stars neither inhabit the inner central region as a group nor are formed in any disk and migrated inwards. This obviously disagrees with common star forming theories in the Galactic disk. Davies & King (2005) argue that the S-stars may actually be the remnants of low to intermediate mass red giants that have been tidally stripped by the SMBH but Goodman & Paczynski (2005) disagree with this interpretation. But none of these scenarios explains what mechanism might bring a substantial number of massive-star binaries to a distinct area where the SMBH can grab the S-stars. So the situation can be described perfectly as: "feeding delicacies to monsters" (Gould & Quillen 2003).

2.2.5 The Multiple Mirror Telescope survey for hyper-velocity stars

If the Hills (1988) scenario is valid, HVS can naturally provide constraints on the SMBH in the GC. In that way to focus on HVS instead of the centre itself, is the other side of the coin. A dedicated systematic survey for late B-type stars has been successfully performed by Brown et al. (2006a). Together with an extended survey, Brown et al. (2009) reported the discovery of an additional 13 HVS (Brown et al. 2009), which are listed in Table 2.1.

These stars have been found by applying colour cuts to the *SDSS* spectral database

in order to select A- and B-type stars. Then the radial velocities are measured and transferred into GRF velocities, assuming zero proper motion. As all stars in the sample are a priori assumed to be main sequence star, spectroscopic distances can easily be calculated. Brown et al. (2007a) introduced the new class of bound HVS with GRF velocities of more than 275 km s^{-1} , which have most likely been ejected by the SMBH in the GC but obviously do not exceed the local Galactic escape velocity. In fact for most of them we do not have an evidence for their stellar type not to mention their precise location.

The most important attribute of HVS is, that they provide insight into the environment of the SMBH and its nature as well as on the shape and density distribution of the Galactic dark matter halo. Gnedin et al. (2005) showed that accurate proper motion measurements of a couple of HVS in the order of $\sigma \approx \mu\text{as yr}^{-1}$ would provide significant constraints on the triaxial dark halo. They especially pointed out that the distance of the stars has to be known accurately enough ($< 10 \%$). The simulations of Bromley et al. (2006) showed that different Galactic mass models produce different velocity distribution. Besides the unbound stars, the simulations also produce a number of bound stars, which may be identified with the already found “bound population” by Brown et al. (2007a). Remarkably it is not yet clear if all observed really originate from the Galactic centre.

Due to the parameters of the performed HVS surveys, 13 out of 16 HVS are of late B-type. However a discrimination between a main sequence and a horizontal branch nature remains difficult, as both branches overlap in the HRD. Only with the help of quantitative spectroscopy one can analyse these stars in great detail and draw conclusions as to their nature. Recently one of these stars was discovered to be a chemically peculiar (CP) main sequence star and is introduced here in Section 5.1 (Przybilla et al. 2008c). Another star seems to originate in the LMC (Przybilla et al. 2008b) and is presented in the next Section 2.2.6.

Only one of the currently known HVS, belongs to an old stellar population: US 708. Therefore we performed a dedicated survey for such old population HVS, which is carried out in more detail in Chapter 7.

Lately another subclass among the high-velocity stars was introduced by Brown et al. (2007a). Evaluating the the total velocity distribution of their survey, they noticed an excess of B-type stars with large radial velocities in the Galactic rest-frame (GRF) of $275 \text{ km s}^{-1} < v_{rad}^{GRF} < 450 \text{ km s}^{-1}$. In Figure 2.10 we show the velocity histogram of their sample. They called this population the “bound“ HVS and suggested formation via ejection from the GC on bound orbits. Based only on their observed velocity distribution, they proposed a value of $v_{rad}^{GRF} > 275 \text{ km s}^{-1}$ to distinguish between runaway stars and HVS (Brown et al. 2007a). Furthermore they also noticed that the distribution of HVS on the sky should be anisotropic for a survey complete to a fixed limiting apparent magnitude (see Figure 2.10), if an ejection origin in the Galactic centre ejection is correct. But this definitely does not exclude contamination of the sample with runaway stars.

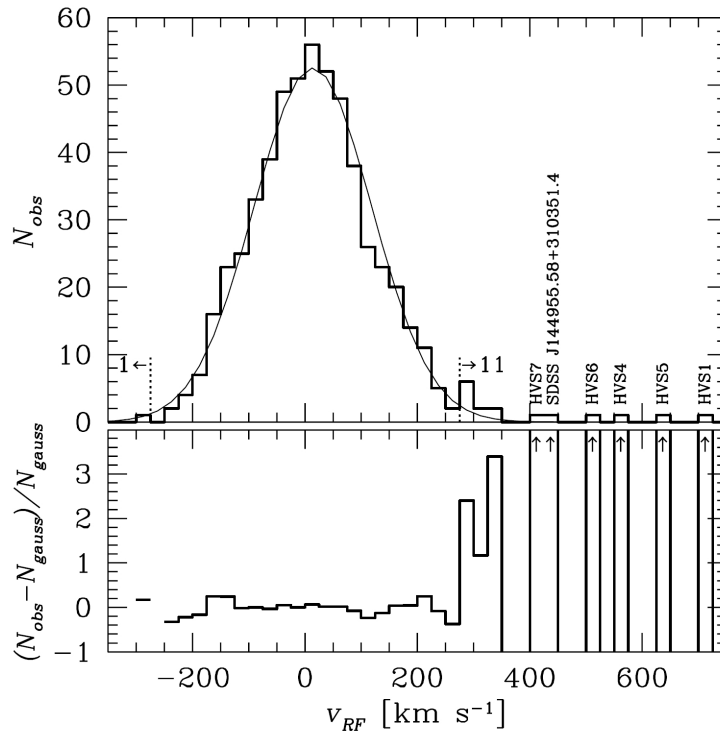


Figure 2.10: Galactic rest-frame velocity histogram of the sample of Brown et al. (2007a). The best-fit Gaussian is shown as thin line. The bottom panel plots the residuals of the observations from the best-fit Gaussian, normalised by the value of the Gaussian. Note the anisotropic distribution. Excerpted from Brown et al. (2007a)

2.2.6 A hyper-velocity star from the Large Magellanic Cloud

Edelmann et al. (2005) discovered the third HVS HE 0437–5439 (also HVS 3) almost simultaneous to the first two. Again it is a faint blue star ($V = 16.2^m$) at high galactic latitude ($l_{II} = 263.04^\circ$, $b_{II} = -40.88^\circ$) from the Hamburg/ESO survey, searching for hot subdwarf stars. Outstanding is the high heliocentric RV of $723 \pm 3 \text{ km s}^{-1}$, which converts to a GRF velocity of 563 km s^{-1} . Hence HVS 3 is unbound according to Standard Galactic potentials. Its spectrum belongs to a typical B-type star with the stellar parameters $T_{\text{eff}} = 20354 \pm 116 \text{ K}$, $\log g = 3.77 \pm 0.02$ and $\log n_{\text{He}}/n_{\text{H}} = -0.94 \pm 0.02$ derived by an LTE analysis (Edelmann et al. 2005). A comparison with the evolutionary tracks for main sequence B stars (Schaller et al. 1992) shows that HVS 3 is a young massive MSB star with a mass of $M = 8.0 \pm 0.5 M_{\odot}$ and an evolutionary lifetime of $t_{\text{evol}} \approx 25 \text{ Myr}$ ($t_{\text{evol}} \approx 35 \text{ Myr}$ for a slightly lower metallicity $Z=0.008$). The corresponding $T_{\text{eff}}\text{-log } g$ -diagram with evolutionary tracks is shown in Figure 2.11.

Due to the high rotational broadening $v \sin i = 54 \pm 4 \text{ km s}^{-1}$ and the solar photospheric helium abundance as well as roughly solar metallicity derived from high resolution UVES spectra, a BHB nature can certainly be excluded. The kinematical analysis of HVS 3

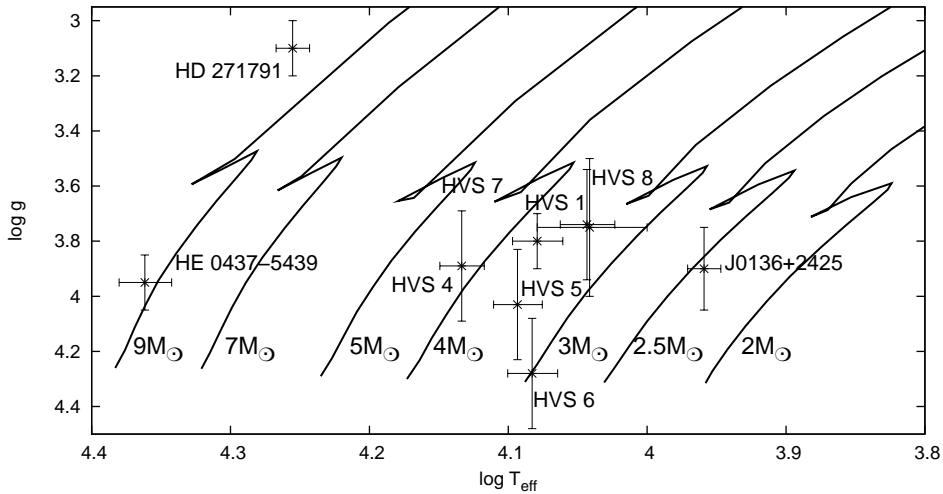


Figure 2.11: The $(T_{\text{eff}}, \log g)$ diagram with evolutionary tracks of Schaller et al. (1992) for solar metallicity in order to determine stellar masses. The positions of typical HVS (HVS 1, 4, 6, and 7, from Heber et al. 2008b) as well as for HD 271791, HE0437–5439 and J0136+2425 are also shown. Note that the mass of J0136+2425 is quite similar to that of the typical HVS.

revealed interesting properties. For the faint but massive star the spectroscopic distance is very high $d = 61 \pm 12$ kpc. Applying again a trial test one can find a trajectory in the Galactic potential of Allen & Santillan (1991) originating in the GC with a time-of-flight of $\text{TOF} = 99 \pm 19$ Myr. For that purpose only a tiny proper motion of $\mu_{\alpha} \cos(\delta) = 0.55 \text{ mas yr}^{-1}$ and $\mu_{\delta} = 0.09 \text{ mas yr}^{-1}$ is required. As the TOF greatly exceeds the t_{evol} , only a blue straggler scenario could explain a Galactic origin. In that case a close binary could be ejected through the disruption of the hierarchical multiple system by the SMBH in the GC. Later the binary merges and continues its journey as a blue straggler, which is very difficult to distinguish from a common MSB. But as this complicated scenario requires a lot of fine-tuning, Edelmann et al. (2005) suggested a Large Magellanic Cloud (LMC) origin for HVS 3. In that case the $\text{TOF} = 35$ Myr equals the t_{evol} for the lower (LMC-like) metallicity. Hence the star could have been ejected from somewhere around the centre of the LMC shortly after its birth. Finally Edelmann et al. (2005) pointed out, that this scenario can be checked either by a detailed abundances study of HVS 3 to search for an LMC pattern or by measuring the proper motion, which is predicted to be about 2 mas yr^{-1} .

Based on high resolution spectroscopy obtained from UVES/VLT, Przybilla et al. (2008b) performed a detailed quantitative NLTE analysis and compared the results to stars of different location. In Figure 2.12 we show a comparison of the abundance pattern for HE 04375439. They found them to be inconsistent with stars near the GC and ruled out such a birthplace. An origin from the outskirts of the Galactic Disk, seems unlikely, as the flight time from there is more than three times higher than the main sequence

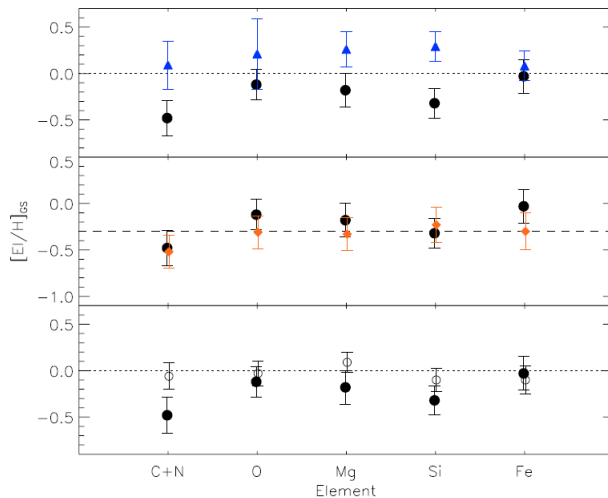


Figure 2.12: Comparison of metal abundances in HE 04375439 (black dots) with a sample of stars close to the GC (blue triangles) in the upper panel, the LMC reference star NGC 2004-D15 (red diamonds) in the middle panel, and the solar neighbourhood reference star HR 3468 (circles) in the lower panel. Error bars account for statistic and systematic uncertainties. Excerpted from Przybilla et al. (2008b).

lifetime of the star. The best consistency is reached with abundance pattern from stars belonging to the LMC. Therefore one might suggest the LMC to host an MBH, which in this case must have at least a mass of $M_{BH} \geq 10^3 M_{\odot}$ (Gualandris & Portegies Zwart 2007). They argued that such an object can most likely be found even in the young dense star clusters. Most of them, however, are either too old or too lightweight. Therefore Gualandris & Portegies Zwart (2007) regard NGC 2004 and NGC 2100 to be the most promising birth candidates for HVS 3.

Howsoever, what remains is the fact that for HVS 3 an GC origin can be excluded. This is challenging the SMBH paradigm (Przybilla et al. 2008b) and we have to turn our view to alternative stellar ejection scenarios in the next section.

2.2.7 Further scenarios

Until now none of the unbound stars could be definitely traced back to the Galactic centre. Mainly this is due to the lack of proper motions and the uncertainties in the distance. But remarkably, every time a complete kinematical analysis of an unbound star was possible, all-but-certain a GC origin was excluded (Heber et al. 2008a; Edelmann et al. 2005; Irrgang et al. 2010). Related studies are presented in the following chapters. Hence the classical Hills (1988) mechanism cannot be the only way to produce unbound stars. Over the years a lot of different formation channels have been proposed.

Yu & Tremaine (2003) extended the formation theory of Hills and studied two new different scattering processes. Based on the current data on the structure of the Galaxy, they calculated appropriate scattering cross sections. Close stellar encounters of two single

stars as they may appear in dense stellar regions, have very small ejection rates in the order of 10^{-11}yr^{-1} for a solar mass star. The ejection rate is strongly influenced by the finite size of a star, which means that stars with a lower mass are have higher rates but are much less luminous, hence more difficult to detect. The second new scenario involved for the first time a binary black hole for scattering of single stars. This produced a ten times higher ejection rate of $10^{-4}/\text{yr}$ compared to the former Hills (1988) scenario. Following the estimation of Brown et al. (2006a), we expect the Galactic halo to hold ≈ 2000 HVS in a sphere of 120 kpc radius. However the mass of the Galactic dark matter halo is still under vigorous discussion (see Chapter 1 and Section 6.4). Furthermore we still miss the very fast HVS with GRF velocities $v_{GRF} \geq 1000 \text{ km s}^{-1}$, which are also predicted by the Hills (1988) scenario. Concerning a higher dark halo mass of $3.42 \times 10^{12} M_{\odot}$ (Li & White 2008) provides a considerable higher escape velocity of $\sim 600 \text{ km s}^{-1}$ at 50 kpc. Hence the lack of very fast HVS is even more significant.

Gualandris et al. (2005) carried out theoretical simulations for the first HVS discovered. Using the tripartite galactic mass model suggested by Miyamoto & Nagai (1975), adapted and applied by Paczynski (1990) they calculated random trajectories to the GC for the two possible spectroscopic distances. In the case of a main sequence nature, HVS 1 has a predicted proper motion of $\mu_{\alpha} \cos(\delta) = 0.7214 \pm 0.0002 \text{ mas yr}^{-1}$ and $\mu_{\delta} = 1.1917 \pm 0.0003 \text{ mas yr}^{-1}$. Generally the proper motion is expected to lie in the range of $1 - 3 \text{ mas yr}^{-1}$ and is too small to be directly measureable with today's instrumentation. Additionally they confirmed the analysis of Yu & Tremaine (2003) by showing that most likely HVS are formed by star scattering by the SMBH. Due to the high ejection velocity of $v_{ej} = 1250 \text{ km s}^{-1}$ they excluded a supernova runaway origin and calculated the semimajor axis of the binary progenitor ($0.05 \text{ au} \leq a \leq 0.3 \text{ au}$).

The second HVS was found to be an old population subdwarf O star. Interestingly most of their progenitors, the subdwarf B stars, are believed to have most likely formed out of binaries, via several ways of mass transfer (see Section 2.1). Hence subdwarf HVS might also have formed out of binaries after they have been ejected by a slingshot mechanism. Lu et al. (2007) carried out a numerical analysis for that scenario. They showed that binary stars may preserve their integrity during scattering at a massive binary black hole and can reach velocities up to $1,000 \text{ km s}^{-1}$. Accordingly, high-velocity binaries are unlikely to be produced by a single MBH. Hence Lu et al. (2007) propose a search for HVS binaries and claim that the discovery of one HVS binary, would be the definitive evidence for the existence of a binary MBH in the GC.

Not only the Milky Way seems to shelter a SMBH. Recently, a disk of blue stars orbiting the very centre of M31 has been discovered and allowed the mass of the SMBH in the centre of M31 to be constrained to $(1.1 - 2.3) \times 10^8 M_{\odot}$ (Bender et al. 2005). They conclude that the disk could be formed by a single star burst 200 Myrs ago. As for the Galactic centre, this poses a difficult challenge for star formation theory. Demarque & Virani (2007), however, point out that a population of blue horizontal branch stars and stellar mergers cannot be ruled out.

Sherwin et al. (2008) focused their work on HVS ejected from M31 (Andromeda) galaxy. They examined three scenarios: disrupting binaries by a galactocentric MBH,

ejection by in-spiralling of a IMBH and scattering of stars by stellar BHs orbiting the MBH. By numerically calculating trajectories they derived spacial distributions and found many of these stars approaching with large velocities ($< -500 \text{ km s}^{-1}$). While especially the fastest stars are unbound to the Local Group, stars with lower velocities might be gravitationally drawn and captured by the Milky Way (MW). Sherwin et al. (2008) pointed out that high-mass stars should only be found in the vicinity of M31, while ejected low-mass stars ($\approx 1 M_{\odot}$) could be found in the MW as well, as their lifetime exceeds the travel time. They expect about 1000 M31 HVS to exist within the virialized halo of the MW.

As the central Galactic region ($< 0.1 \text{ pc}$) is expected to contain segregated stellar black holes O’Leary & Loeb (2008) discussed their eminent role for ejection mechanisms. This scattering of stars by BHs alone can eject stars up to a velocity of $\sim 2000 \text{ km s}^{-1}$ at a rate comparable to the estimated rate only by the Hills scenario. They claim that under certain conditions this mechanism can even dominate the production of HVS in the Galaxy and suggest that therefore the expected velocity and mass distributions should show at least bi-modality.

Abadi et al. (2009) noticed that in Galactic projection the known HVS seem to cluster in the constellation of Leo, sharing a travel time between $100 - 200 \text{ Myr}$. Therefore they suggest that, the observed HVS might have been expelled from a dwarf galaxy near the central SMBH on its last pericentric passage. If such a companion passes on its orbit too close to the SMBH a tidal tail should be stripped off the dwarf and is therefore composed of stars with similar types and velocities. After these stars have travelled quite a while, they simply look as if they would cluster, consistent with the observations. Abadi et al. (2009) propose to extend the surveys and test their scenario and the observed enhancement in the Leo constellation. Accordingly they also postulate the existence of returning stars from the tail with a high negative velocity and suggest to check existing surveys for close stars for unusual velocity patterns.

Huang et al. (2009) discovered lately the typical main sequence B star HD 69686 to have a large proper motion of $\mu_{\alpha} \cos(\delta) = 86.17 \pm 0.67 \text{ mas yr}^{-1}$ and $\mu_{\delta} = 7.21 \pm 0.42 \text{ mas yr}^{-1}$. They traced back its path and found the birth region to be located at the outer part of the Galaxy well below the Galactic Disk. Amazingly they found several similar stars, in terms of proper motion and photometry, located on the projected path of HD 69686 in the sky. This co-moving group allows some further implications; it suggests tidally triggered star formation in a high velocity cloud as origin for the stars. This mechanism was proposed by de la Fuente Marcos & de la Fuente Marcos (2008) and explains star formation at high galactic latitudes. In their scenario star formation is triggered by the fly by of massive star clusters, e.g. globular clusters in the Galactic halo. Alternatively Huang et al. (2009) suggest that the co-moving group could be the remnant of a merged galaxy.

Various scenarios for certain fast stars have been introduced so far. But remarkably almost all these suggestions have been required to explain the observed stars. Hence the variety of formation scenarios is certainly not complete and will have to be adapted in the future.

Chapter 3

Quantitative spectral analysis

Basically our data set, consists mainly out of low-resolution spectra. Therefore in most of the cases the analysis of the observed stellar spectrum has been performed using fixed model grids of synthetic spectra. Before we used an automatic fitting routine, we manually selected a set of initial parameters for every stellar spectrum. Depending on this parameters the corresponding grid and the expected absorption lines have been chosen.

In order to analyse observed stellar spectra we used the FITSB2 routine following Napiwotzki et al. (2004b). FITSB2 performs χ^2 -fitting of synthetic spectra to determine the velocity, T_{eff} and $\log g$ together with the appropriate statistical errors (e.g. by a bootstrapping or a Monte-Carlo procedure), within grids of different metallicities $[m/H]$ or helium fractions $\log n_{\text{He}}/n_{\text{H}}$. In the literature the RV is very often measured by using only one or two lines (e.g. Xue et al. 2008), which we regard as highly insufficient. Hence we used our synthetic model spectra for the appropriate stellar types even for the RV fitting, which leads to a more accurate measurement as we have to adapt the total line profile. Due to the combination with a statistical approach for our error calculation we derive reliable errors. A typical fit for a *SDSS* spectra is shown in Figure 3.1. To achieve the best result, we focused on all visible lines in the spectra. As we use only low-medium resolution spectra, there are only a few strong lines to analyse. In the case of hot subdwarfs our spectra do only contain hydrogen and helium lines. For the hotter subdwarf OB or O stars ($T_{\text{eff}} \gtrsim 33,000$ K), we had to account for NLTE-effects as well (Napiwotzki et al. 2004b). Hence we used a grid, calculated with a new version of PRO2 (so-called NGRT) that employs a temperature correction scheme and uses more sophisticated model atoms (Werner & Dreizler 1999). For the cooler subdwarf B stars ($T_{\text{eff}} \lesssim 33,000$ K) we used a grid of metal-line blanketed LTE spectra (Heber et al. 2000). The white dwarfs have been analysed using a model grid from Koester (2002). In the temperature range $10,000$ K $\lesssim T_{\text{eff}} \lesssim 20,000$ K the the horizontal branch crosses the main sequence in the T_{eff} - $\log g$ -diagram, hence a new grid was calculated. For this purpose the ATLAS9 and SURFACE codes have been used. With the help of ATLAS9 we produced plane-parallel model atmospheres based on converging Opacity Distribution Functions (ODFs) (Castelli & Kurucz 2003). Then we created synthetic spectra with various $\log n_{\text{He}}/n_{\text{H}}$ using the SURFACE package, using model atoms for hydrogen and helium. Finally we received a grid with a stepwidth of $\Delta T_{\text{eff}} = 2000$ and $\Delta \log g = 0.25$ ranging from $3.0 \lesssim \log g \lesssim 4.5$,

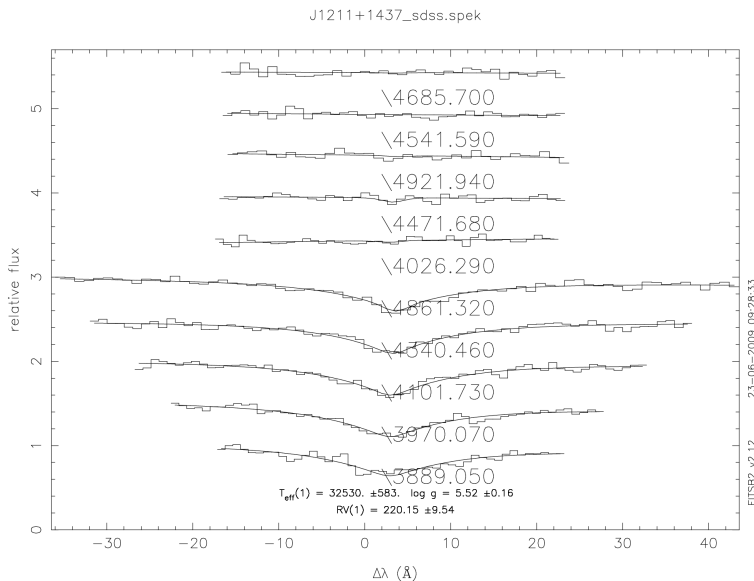


Figure 3.1: Fit of the subdwarf B star J1211+1437 from an *SDSS* spectrum produced by FITSB2.

which we used especially for stars with temperatures above the maximum of the Balmer lines.

In Figure 3.2 we show a comparison of observed data with our newly calculated model grid.

For cooler stars ($T_{\text{eff}} \lesssim 10,000$ K) below this maximum the characteristic signatures change dramatically as metal lines get significantly stronger. Therefore we focused also on metals (e.g. O, Ca and Fe) by varying the metallicity $[m/H]$ instead of analysing only hydrogen and helium by varying $\log n_{\text{He}}/n_{\text{H}}$. We used the synthetic spectral database provided by Munari et al. (2005) in order to create the required model grids.

In particular cases where we obtained high-resolution or high S/N spectra (see Section 5.1, 6.2, 6.3 and 6.4) another, more sophisticated approach was necessary. Hence we followed the methodology discussed by Przybilla et al. (2006). Initially line-blanketed LTE model atmospheres were computed with ATLAS9 (Kurucz 1993) or ATLAS12 (Kurucz 1996). Then NLTE (and LTE) line-formation calculations were performed using updated versions of DETAIL and SURFACE (Giddings 1981; Butler & Giddings 1985). Many astrophysically important chemical species were treated in NLTE, using state-of-the-art model atoms (H: Przybilla & Butler 2004a; C I: Przybilla et al. 2001b; N I: Przybilla & Butler 2001; O I: Przybilla et al. 2000; Mg I/II: Przybilla et al. 2001a; Ti II and Fe II: Becker 1998).

We determined the effective temperature T_{eff} and the surface gravity $\log g$ from the Stark-broadened Balmer lines and any observable ionisation equilibrium (e.g. in case of A-type stars we used Si II/III). The quality of the match of the spectral indicators within the given S/N limitations constrained the uncertainties in the stellar parameters (T_{eff} ,

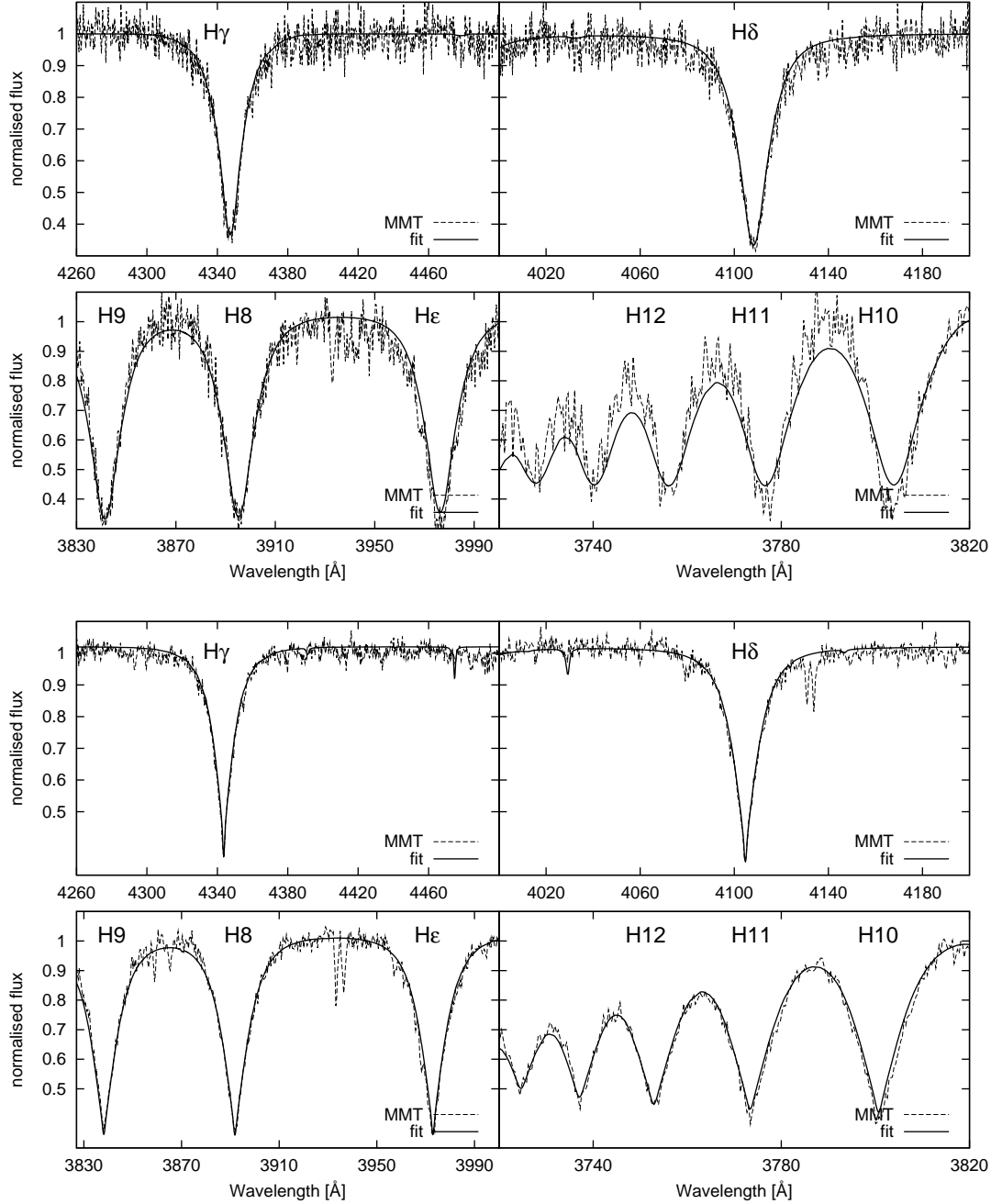


Figure 3.2: Comparison between the synthetic model with the observed spectrum from the MMT for the main-sequence stars HVS8 (top) and BCAND371 (bottom). The synthetic spectrum of HVS 8 had to be broadened with $v_{\text{rot}} \sin i = 280 \text{ km s}^{-1}$ to achieve a good match, while BCAND371 does not show rotation at all. Note the overall good agreement.

$\log g$). Figure 3.3 shows a comparison between an observed spectrum and a synthetic spectrum. Detailed comparisons of NLTE and LTE profiles are therefore shown in the corresponding insets.

The combination of a higher T_{eff} and the diminished line blocking because of the low metal content results in a hardened radiation field. Hence NLTE effects on many diagnostics lines become stronger. This NLTE strengthening is found for the Doppler core of $\text{H}\alpha$ – in line with the behaviour in cooler (e.g. Przybilla & Butler 2004b) as well as in hotter stars (e.g. Nieva & Przybilla 2007) –, while the inner line wings are weakened (see Figure 3.3). The higher Balmer and Paschen lines show much lower deviations from LTE.

The microturbulence velocity ξ was derived in the standard way by demanding that the line abundances within Fe II be independent of equivalent width. In case weak metal lines are visible in the spectrum the rotational broadening can be measured accurately. For our sdB stars we only obtained low-resolution spectra, which show solely the Balmer and helium absorption lines.

The detection of rotational broadening $v_{\text{rot}} \sin i$ of absorption lines is a very important part of our analysis. Due to the rotation of a star one part of the stellar surface approaches us, while the other does the opposite. This produces Doppler shifts, which have to be intergrated over the whole surface of the star. This leads to a broadening of the absorption lines as well as to a flattening of the line cores and is demonstrated in Figure 3.2. Especially the weak metal lines are very sensitive to this effect. But unfortunately we can only observe such weak lines in the high resolution spectra we obtained. Due to stronger pressure broadening Balmer and helium lines are much less sensitive to rotational broadening than metal lines. Therefore only strong rotational broadening ($v_{\text{rot}} \sin i \gtrsim 100 \text{ km s}^{-1}$) can be detected in the low resolution spectra.

The elemental abundances have been determined from visual fits to profiles of isolated lines or lines with resolved blends (see Figure 3.3). In case of comparatively high $v_{\text{rot}} \sin i$ the identification of the line blends has to be considered carefully.

Chapter 4

Advanced Kinematics

In the following chapter the kinematical approach as well as the used standards will be presented.

The equatorial coordinate system, involving right ascension and declination, is required in astronomy to describe stellar positions in the sky independent of the earth's rotation. However from an extrasolar point of view, the Galactic coordinate system is the natural way to describe projected stellar positions. As the sun, together with the rest of the Galactic disk (GD), orbits the Galactic centre (GC) the Galactic plane forms the first axis, called the longitude l . The second axis, called the latitude b , is perpendicular to the Galactic plane pointing at the so-called north Galactic pole (NGP) at 12h 49m and $+27.4^\circ$ (see equation 4), which was defined by the IAU (1959). The origin of the Galactic coordinate system has the coordinates 17h 45m 37.224s 28 56' 10.23" (J2000) (266.405100° , -28.936175°) and is not far away from the radio source Sagittarius A*, which is the best tracer for the GC (Schödel et al. 2002). The longitude ranges from 0 - 360° into the direction of the Sagittarius tangent, while the latitude is measured from -90° to $+90^\circ$ and is positive towards the NGP. Figure 4.1 shows the relation between the equatorial and the galactic coordinate system.

One can derive the Galactic coordinates (l, b) easily from the Equatorial coordinates (α, δ) in the 1950.0 system (Lang 1999), following

$$b = \sin^{-1}(\cos \delta \cos 27.4^\circ \cos(\alpha - 192.25^\circ) + \sin \delta \sin 27.4^\circ) \quad (4.1)$$

$$l = \tan^{-1}(\sin \delta - \sin b \sin 27.4^\circ / [\cos \delta \sin(\alpha - 192.25^\circ) \cos 27.4^\circ]) + 33^\circ.$$

For kinematical studies we have to change from these co-rotating systems to a stationary system, the so-called Galactic rest-frame (GRF). The velocity vector \vec{v} is 3 dimensional, but only one component is easy to obtain. Based on the *SDSS* spectral database, radial velocities are directly at hand and can be transferred to lower limit of the GRF velocities by using the Galactic coordinates (l, b) and accounting for the sun orbiting the GC with $v_{circ} \approx 220 \text{ km s}^{-1}$.

$$v_{rad}^{rf} = v_{rad}^{helio} + (10 \cos l \cos b + 5.2 \sin l \cos b + 7.2 \sin b) + 220 \sin l \cos b \quad (4.2)$$

determined in $[F] = [\frac{\text{erg}}{\text{cm}^2\text{s}}]$. We can assume that the emitted total energy of a star has to be conserved and distance d can be derived by

$$\oint F = 4\pi r^2 F = 4\pi d^2 f = \oint f \Leftrightarrow d = \sqrt{\frac{r^2 F}{f}} \quad (4.5)$$

The total flux F intergrated over the stellar surface with radius r , equals the flux f integrated over a sphere at our distance d . We have to be aware that what we measure is the astrophysical flux $F_V = F_V/\pi$, hence the average intensity over the stellar disk. Unfortunately it is very hard to obtain the total flux of a star, hence we have to specify the flux at a certain wavelength λ . The apparent visual magnitude m_V can be transferred into the observed flux f_V in the visual band following

$$f_V = 3.607 \times 10^{-9} \frac{\text{erg}}{\text{cm}^2\text{s}\text{\AA}} \times 10^{-0.4m_V}. \quad (4.6)$$

As we focus especially on data from Sloan Digital Sky Survey (short: *SDSS*) we have to use the provided ugriz-colours to calculate the visual magnitude. Jordi et al. (2006) presented the empirical transformation

$$m_V = m_g(-0.5690.007) \times (m_g - m_r) + (0.0210.004), \quad (4.7)$$

which was found for metal poor population II stars, while the discrepancies to metal rich stars are negligible within the overall errors in the colours (Adelman-McCarthy et al. 2008). We accounted for the interstellar reddening in two ways. Either the interstellar colour excess was determined by comparing the observed colours to synthetic ones from the model spectral energy distribution. Or we used correction values from the maps of Schlegel et al. (1998), who used the dust infrared emission to estimate the interstellar reddening in cases where it was necessary. From Newton's law of gravitation we can write the stellar radius as

$$g = \frac{GM}{r^2} \Leftrightarrow r = \sqrt{\frac{GM}{g}}. \quad (4.8)$$

Combining all this equations with equation 4.5 we receive

$$d(m_V, M, T_{\text{eff}}, \log g) = 1.11 \text{ kpc} \sqrt{\frac{M}{M_{\odot}} \frac{\text{cms}^{-2}}{g} \frac{F_V(T_{\text{eff}}, \log g)}{10^8 \text{ergcm}^{-2}\text{s}\text{\AA}^{-1}}} 10^{0.4m_V}. \quad (4.9)$$

The rest of the unknown variables are the stellar mass and the atmospheric parameters $(T_{\text{eff}}, \log g)$, including the metallicity $[m/H]$ and the helium fraction $\log n_{\text{He}}/n_{\text{H}}$.

4.2 Evolutionary tracks and errors

Finally the last missing parameter is the stellar mass. We derive the stellar masses by applying the stellar parameters to different evolutionary tracks. For the main sequence

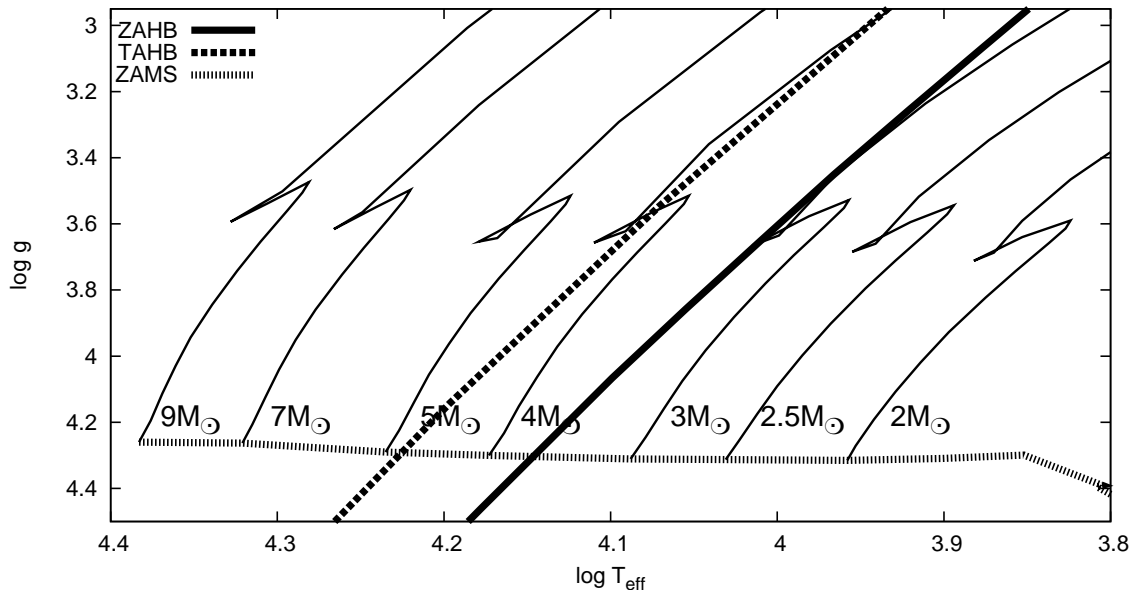


Figure 4.2: T_{eff} - $\log g$ -diagram for all analysed HVS with the evolutionary tracks of Schaller et al. (1992). The horizontal branch for subsolar metallicity is shown for reference, following Dorman (1992).

stars we used the tracks from Schaller et al. (1992). The stellar mass can be interpolated directly from the position of the star in the T_{eff} - $\log g$ -diagram shown in Figure 4.2 using the tracks with the respective metallicity. The same tracks are valid for the blue stragglers, as they are believed to be MS stars with an extended main sequence lifetime (see Section 2.1). For the blue horizontal-branch stars we used the tracks from Dorman (1992) applying the same method. Much easier to handle are the subdwarf B stars. As they are mostly believed to have a canonical mass, we used a fixed value of $0.48 M_{\odot}$, which is supported by the fact that most of the observed sdB masses seem to be consistent with this value (e.g. Vučković et al. 2007). Due to misclassification we also have some white dwarfs (WD) in our sample. Such degenerate objects are believed to have a characteristic mass-radius relation of $R \propto M^{-1/3}$ (e.g. Kippenhahn & Weigert 1990). If we would have such an explicit universal relation, one could easily determine their mass by applying Newton law of gravitation (see equation 4.8). Unfortunately this relation is insufficient, due to the fact that there is no general agreement about their evolutionary cooling tracks. Hence, for simplicity we did not infer the mass of a white dwarf from atmospheric parameters and used a fixed mass of $0.5 M_{\odot}$.

The uncertainties of all the previously discussed quantities propagate through equation 4.9 and produce a significant distance error. In order to evaluate this error we used a Monte-Carlo technique with a depth of 10,000. We randomly varied the input parameters of equation 4.9 within the full range of the respective errors. The standard deviation gives a good measure for the expected errors. We additionally calculated the conservative error propagation using partial derivatives and found it to be slightly higher than from our

Monte-Carlo approach. Due to the fact that our input uncertainties from χ^2 -fitting are statistical, we used the errors from our Monte-Carlo approach throughout the analysis. Note that the stellar mass is not an independent variable as it is derived from T_{eff} and $\log g$ together with the atmospheric composition exclusively. Hence the mass is not randomly distributed, but interpolated from evolutionary tracks for main-sequence or horizontal branch stars, while for the white dwarfs and the subdwarfs it is kept fixed.

4.3 Proper motion measurement

Proper motions are urgently required to provide a detailed kinematical analysis. Firstly we collected all available independent position measurements on Schmidt plates (APM - McMahon et al. (2000); SSS - Hambly et al. (2001)) and combined them with the *SDSS* and other available positions (CMC14 Carlsberg-Meridian-Catalog (2006); 2MASS - Cutri et al. (2003); UKIDSS - Lawrence et al. (2007)). The proper motion can then be easily derived from a simple linear regression fit. Unfortunately in most of the cases these values are not enough to obtain a reliable solution. Therefore we also measured stellar position on our own. By checking the Schmidt plates from the Digitised Sky Surveys¹ we found up to 14 different epochs, in case of overlapping plates. Then we extracted FITS images of 15 by 15 arcmin size from all available plates and used the ESO MIDAS tool CENTER/GAUSS to measure positions. For this purpose, we initially had to find and identify compact background galaxies from the *SDSS*. It is highly important to obtain enough galaxies well distributed over the image, although galaxies tend to cluster. In Figure 4.3 we show POSS-O and POSS-E photographic plates with the reference galaxies for calibration purposes. Initially we searched for background galaxies, which are visible on the two oldest plates, via the *SDSS* EXPLORE tool. We used the "Navigate" function for investigating the field around the respective star. In the first instance almost every object with a sharp contour is most likely a star and can be excluded. Hence the small objects with fuzzy contours attracted our interest. Galaxies with g-magnitudes below 19.5 mag turned out to be useless for calibration in most cases. In general such faint targets are unlikely to be visible in all filter ranges of the photographic plates.

The photometric classification of *SDSS* turned out to be a rather reliable indicator. Hence an object in *SDSS* can be classified as extended ("GALAXY") or point-like ("STAR") based on the difference between the point spread function (PSF) magnitude psfMAG and the cmodel magnitude cmodelMAG. The psfMAG is an optimal measure of the flux in a certain band and is derived by fitting a PSF model to the object. The cmodelMAG is obtained from the best fitting linear combination of the best-fitting de Vaucouleurs and exponential model for an object's line profile². If the condition

$$\text{psfMAG} - \text{cmodelMAG} > 0.145 \quad (4.10)$$

is fulfilled, the type is set to GALAXY for that band. Otherwise, the type is set to STAR. The global type objc_type is set according to the same criterion, applied to the summed

¹http://archive.stsci.edu/cgi-bin/dss_plate_finder

²<http://www.sdss.org/DR7/glossary/index.html>

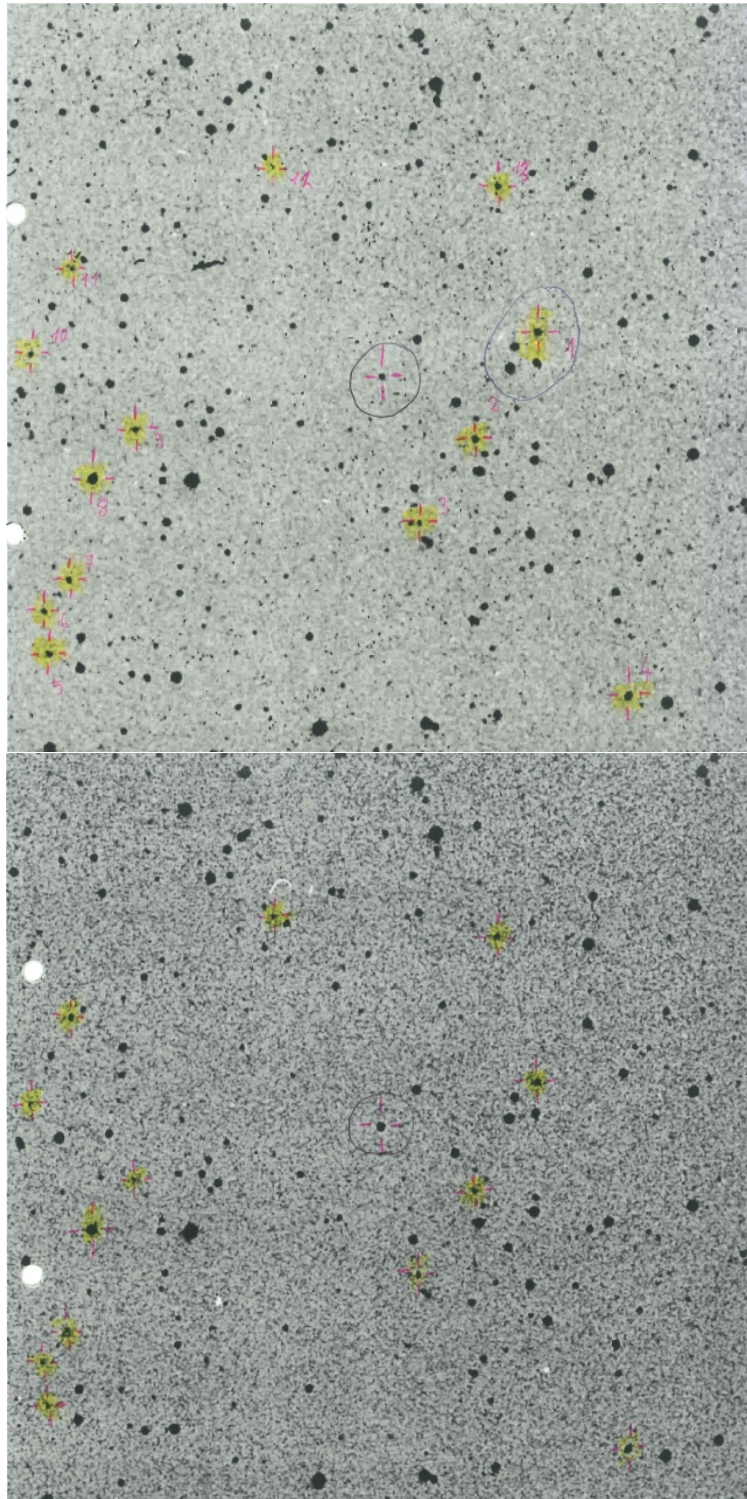


Figure 4.3: Photographic plates POSS-E (top) and POSS-O (bottom) for the subdwarf B star J1644+4523 taken at the epoch 1955.244. The used set of calibration galaxies have been marked.

fluxes from all bands in which the object is detected³. In the optimal case a galaxy can be confirmed beyond doubt, if also a spectra is available in the database. Unfortunately this is only the case for a few galaxies. Figure 4.3 shows the photographic plates POSS-E (red) and POSS-O (blue) and the used reference frame of compact background galaxies. In Figure 4.4 we also show the new plates taken in the R-band from POSS-II and from *SDSS* in order to document the quality differences of the various data. Especially in the new plates with higher quality the galaxies significantly gain more structure, which makes the fitting of their positions more accurate.

In the next step the coordinates of the reference galaxies have been extracted from *SDSS* and included into a MIDAS table for further calculations. We fitted a 2D Gaussian function by using the MIDAS CENTER/GAUSS routine, accounting only for the smallest possible region on the plate. Additional care is required in this step, as the resolution of the plates differs even within one epoch. Particularly good results are not only achieved for very compact objects but also for galaxies with a distinct (bright) central region.

We used at least 10 galaxies per measurement and determined the position of the star relative to the reference galaxies. Finally we transformed the target positions on all the Schmidt plates to the *SDSS* system. The small fields allowed us to apply a simple model (shift+rotation). We obtained one position per epoch and used linear regression to derive the proper motions. Fig 4.5 shows such a proper motion fit. Additionally we confirmed our proper motions with a robust regression technique, adding artificial outliers to our data. Especially for the old POSS-I epochs systematic discrepancies occurred sometimes between the positions obtained in different colour filters. Basically the galaxies simply look different in different colour filters. However these discrepancies do not occur in all the measurements and are therefore rather randomly distributed. However might be a direct relation between the choice of the reference galaxies and this effect, which is particularly strong for the old epochs. Another reason may therefore be, that with less quality of the plates the galaxies do not show a detailed structure, which makes the fitting of their positions less accurate. As the overall number of epochs is small, we did not eliminate measurements. The best way to handle these systematics is simply to use the same set of reference galaxies for every epoch. We regard a PM detection as confirmed, if the position measurements do not show a large spread relative to the linear fit and the derived proper motion is significant. Hence the proper motion errors σ of both components have to be below $\approx 3 \text{ mas yr}^{-1}$ and at least one of the PM components has to be significantly different from zero (above 3σ).

In Fig 4.5 we show a special case in order to demonstrate the advantages of our method. J2156+0036 (= PB 5010) was a preferred target in the *SDSS* and therefore has 15 epochs within 5 years. Adelman-McCarthy et al. (2008) derived its proper motion to be $\mu_\alpha \cos(\delta) = -1 \pm 3 \text{ mas yr}^{-1}$ and $\mu_\delta = -7 \pm 3 \text{ mas yr}^{-1}$. Neglecting the *SDSS* epochs, we measured a PM of $\mu_\alpha \cos(\delta) = -0.7 \pm 2.6 \text{ mas yr}^{-1}$ and $\mu_\delta = -8.5 \pm 1.9 \text{ mas yr}^{-1}$, which is perfectly consistent with the older value. Applying all available 26 epochs we obtained a final PM of $\mu_\alpha \cos(\delta) = -1.3 \pm 1.6 \text{ mas yr}^{-1}$ and $\mu_\delta = -7.4 \pm 1.2 \text{ mas yr}^{-1}$ for J2156+0036. Using a time base of almost 60 years the error is reduced by more than a

³<http://www.sdss.org/dr2/algorithms/classify.html>

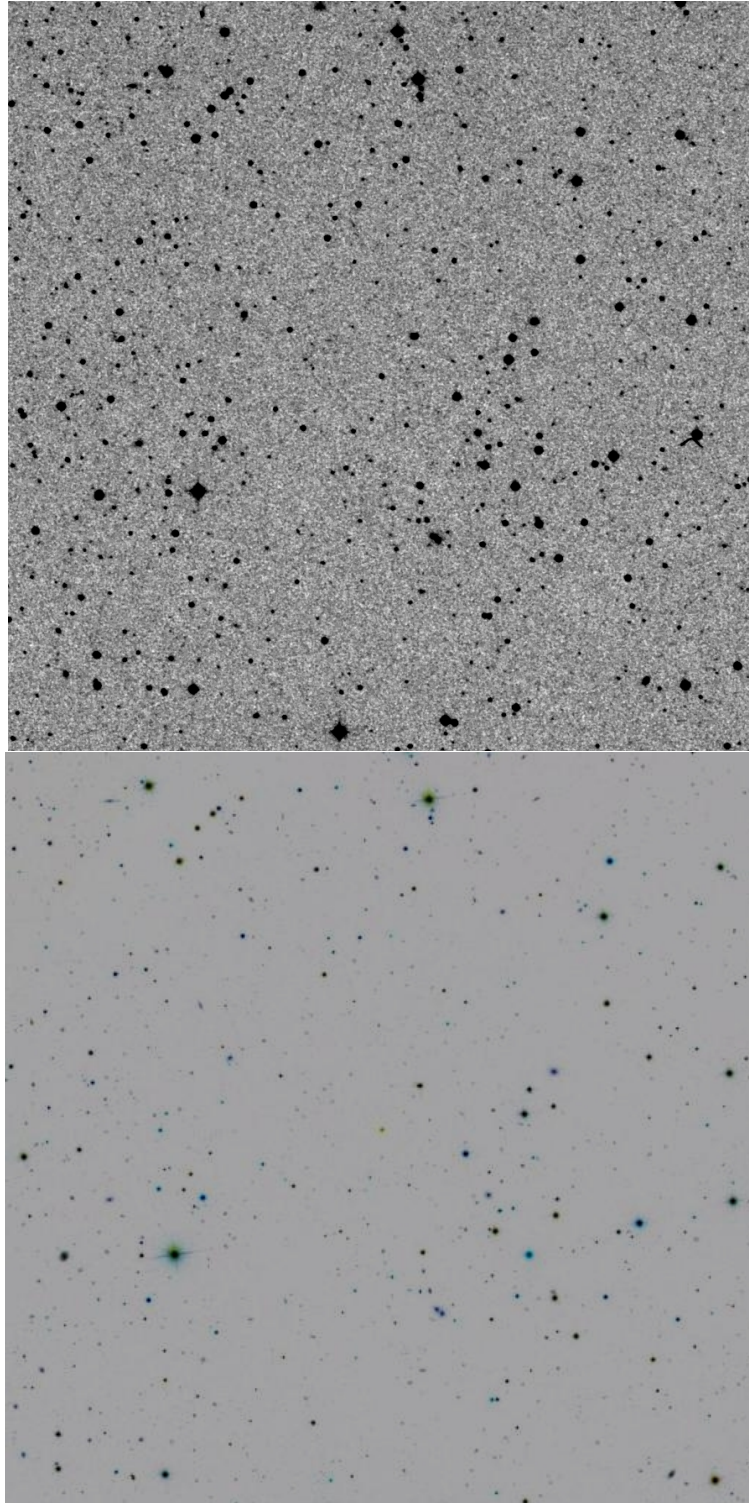


Figure 4.4: Photographic plates from POSS II-R (top, epoch 1991.299) and *SDSS* (bottom, epoch 2001.220) for the subdwarf B star J1644+4523. Note the improved resolution compared to the POSS-I plates.

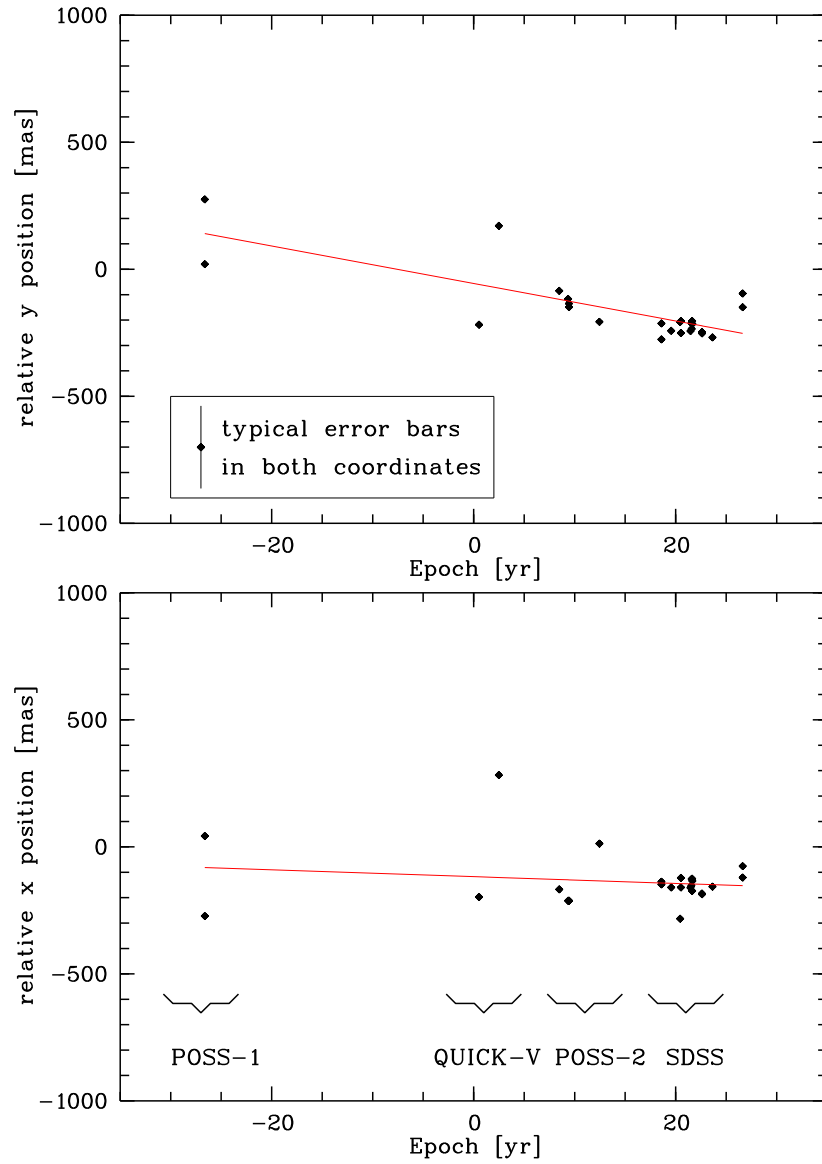


Figure 4.5: Proper motion fit for J2156+0036 (= PB5010) from our position measurements. Note that the points around epoch +20 yr are 15 *SDSS* measurements, which go perfectly with the rest, whereas 1981.196 is the zero epoch.

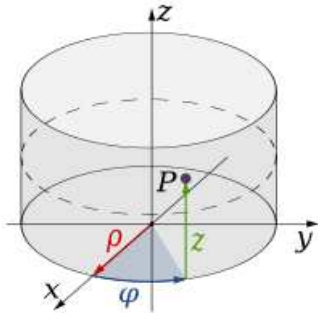


Figure 4.6: Schema of the used Cylindrical coordinates system (excerpted from www.wikipedia.de).

factor of 2, allowing a reliable kinematical study.

As we have a total number of 26 epochs for J2156+0036 we also tested the robust regression, proposed by Rousseuw & Leroy (1987). We applied the MIDAS routine REGRES/ROBUS for the fit, which uses the least median of squares method. Basically all data points are weighted, according to their discrepancy from the fit. We derived for J2156+0036 a proper motion of $\mu_\alpha \cos(\delta) = -2.9 \pm 0.5 \text{ mas yr}^{-1}$ and $\mu_\delta = -8.3 \pm 1.2 \text{ mas yr}^{-1}$ respectively. This is perfectly consistent with our values, derived by simple regression. The robust regression method works best with big data sets, which include a significant number of outliers. However for the rest of our targets it is unfortunately not applicable, as our data set consists of only a rather low number of epochs.

4.4 Integrating in the Galactic Potential

Using the ORBIT6 routine from Odenkirchen & Brosche (1992), we integrated in a Galactic potential Φ_{Gal} . We used the cylindrical space coordinates (ρ, z, φ) , with ρ radial and φ tangential, both parallel to the Galactic plane and z parallel to the direction of the NGP (see Fig .4.6). As Galactic potential Φ_{Gal} we used the one suggested by Allen & Santillan (1991), which consists out of a central bulge component, a disk and a halo component. The total mass of the bulge is $1.41 \times 10^{10} M_\odot$, whereas the respective potential is

$$\Phi_{bulge}(\rho, z) = -\frac{M_1}{(\rho^2 + z^2 + b_1^2)^{1/2}}. \quad (4.11)$$

Note that it cannot be used to reproduce the detailed and complicated dynamics in the innermost Galactic bulge (short: GB). Nevertheless it describes especially eccentric orbits where the stars spend only a short time in the central region, much better than a central mass point potential. The disk potential is described by

$$\Phi_{disk}(\rho, z) = -\frac{M_2}{\{\rho^2 + [a_2 + (z^2 + b_1^2)^{1/2}]^2\}^{1/2}}, \quad (4.12)$$

which corresponds to a disk with a local mass density of $0.15 M_\odot \text{ pc}^{-3}$ and a total disk mass of $8.56 \times 10^{10} M_\odot$. The Galactic dark halo is the most uncertain part of the potential

Table 4.1: Table of constants from Allen & Santillan (1991). Note that the Galactic mass constant is $M_{gal}^{const} = \frac{100 \text{ km}^2 \text{ s}^{-2} 1 \text{ kpc}}{G} = 2.32 \times 10^7 M_{\odot}$.

part	mass constants (M_{gal})	scale lengths (kpc)
bulge	$M_1 = 606.0$	$b_1 = 0.3873$
disk	$M_2 = 3690.0$	$a_2 = 5.3178 \quad b_2 = 0.2500$
halo	$M_3 = 4615.0$	$a_3 = 12.0$

even in terms of the total mass. A total halo mass of $8 \times 10^{11} M_{\odot}$ with an arbitrary cut at 100 pc, together with the simplification $R^2 = \rho^2 + z^2$ results in the halo potential

$$\Phi_{halo}(R) = - \left[\frac{M_3(R/a_3)^{2.02}}{(1 + (R/a_3)^{1.02})R} \right] - \left(\frac{M_3}{1.02a_3} \right) \left[\ln(1 + (R/a_3)^{1.02}) - \frac{1.02}{1 + (R/a_3)^{1.02}} \right]_R^{100}. \quad (4.13)$$

Note that here the density profile shows asymptotic behaviour $\rho \sim r^{-3}$, which was much later proposed by Navarro et al. (1997) based on theoretical N-body simulations and is now regarded as state-of-the-art potential. The complete Galactic potential Φ_{Gal} is the superposition of this three components

$$\Phi_{Gal} = \Phi_{bulge} + \Phi_{disk} + \Phi_{halo}, \quad (4.14)$$

and the adopted observational constants can be found in Table 4.1. Thus our applied potential is static, nonspherical but symmetric with respect to the Galactic plane and the NGP axis. We can write the equations of motions based on the two conserved quantities: the energy E and the angular momentum $\vec{M} = \vec{r} \times m \dot{\vec{r}}$.

Following Landau & Lifschitz (1972) the equations of motions for the movement in a given potential can be easily derived from the Lagrange formalism. Thus for a particle with mass m at the location $\vec{r} = (\rho, z, \varphi)$ in a potential $U(\vec{r})$ the Lagrange function is

$$\begin{aligned} L &= \frac{m}{2} \dot{\vec{v}}^2 - U(\vec{r}) = \frac{m}{2} (\dot{\vec{r}})^2 - U(\vec{r}) \\ &= \frac{m}{2} (\dot{\rho}^2 + \dot{z}^2 + \rho^2 \dot{\varphi}^2) - U(\vec{r}) \end{aligned} \quad (4.15)$$

and together with the Lagrange equation

$$\frac{d}{dt} \frac{\partial L}{\partial \dot{\vec{v}}} = \frac{\partial L}{\partial \vec{r}} \quad (4.16)$$

we obtain that the equations of motions can be reduced to the motion in the meridional plane with ρ, z and an effective potential $U_{eff} = U + \frac{M^2}{2m\rho^2}$. Hence the equation can be described fairly simply by

$$m \dot{\vec{v}} = - \frac{\partial U}{\partial \vec{r}} \quad (4.17)$$

and as

$$p_\varphi = \frac{\partial L}{\partial \dot{\varphi}} = m\rho^2\dot{\varphi} = M = M_z \quad (4.18)$$

with the constant energy

$$\begin{aligned} E &= \frac{m}{2}(\dot{\rho}^2 + \dot{z}^2 + \rho^2\dot{\varphi}^2) + U(\vec{r}) \\ &= \frac{m}{2}(\dot{\rho}^2 + \dot{z}^2) + \frac{M^2}{2m\rho^2} + U(\vec{r}) \\ &= \frac{m}{2}(\dot{\rho}^2 + \dot{z}^2) + U_{eff}(\vec{r}) \end{aligned} \quad (4.19)$$

In order to solve the equation of motion numerically ORBIT6 uses a modified Bulirsch-Stoer algorithm. The integrator is accurate enough except for the very centre of the Galaxy (Hanke 2006). Therefore we obtain numerical solutions to our ordinary differential equations with high accuracy and comparatively little computational effort. From the potential energy at $t = 0$ we calculated the local escape velocity simply by solving

$$E_{t=0}^{pot} - E_{t=0}^{kin} = 0 \Leftrightarrow v_{esc} = \sqrt{\frac{2E_{t=0}^{pot}}{m}}. \quad (4.20)$$

Applying ORBIT6 allows to calculate a complete trajectory if the location \vec{r} and the velocity \vec{v} are known.

4.5 Error propagation

In order to account for uncertainties in the measured values (see Sections 4.1,4.3) we used again a Monte-Carlo technique for error propagation throughout the analysis. Therefore we varied \vec{r} and \vec{v} randomly within the determined errors and calculated the first two moments (the statistical mean and its standard deviation) in a high depth of 10,000. Note that the error in the location \vec{r} is exclusively considered as distance error, whereas for the velocity \vec{v} the transverse components are highly dominant. This happens due to the fact that the measured proper motion μ is an angular velocity and can be transferred into a tangential velocity by

$$v_{tan} = \mu d, \quad (4.21)$$

where d is the distance. Hence a proper motion of $\mu = 1$ as/yr⁻¹ in distance $d = 1$ pc corresponds to a tangential velocity of $v_{tan} = 4.74$ km s⁻¹. The errors in distance multiply with those from the proper motion and produce a large spread in the space velocities, when interpreting the statistics. Figure 4.7 shows such a Monte-Carlo analysis for a certain set of starting parameters. Finally we also checked the trajectories for a possible origin most favoured in the Galactic disk. Therefore we extracted from our set of trajectories the intersection with the disk and calculated the statistical moments for them. In the case we could not identify an origin in the disk, we derived a distribution for a certain time $t = t_{event}$. The size and the direction of such distribution often leads to a detailed picture

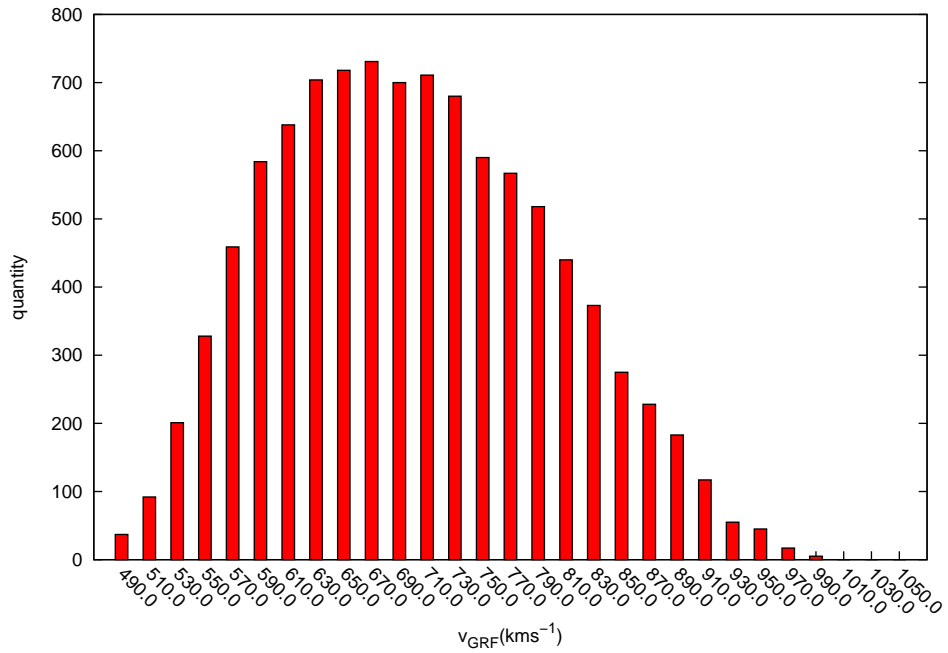


Figure 4.7: A Galactic restframe velocity distribution derived from a Monte-Carlo analysis with a depth of 10,000. The input parameters are those of J1539+0239 (see Section 6.4). Note that the velocity distribution is asymmetric, due to the logarithmic distance distribution.

for possible origins and the time of flight. In any case by applying this Monte-Carlo analysis we are able to exclude unlikely scenarios from the respective picture.

Chapter 5

Analysis of known Hyper-velocity stars

In the following chapter the results of detailed spectral analysis for some of the already known HVS is presented. All of them have been discovered by the Multiple Mirror Telescope (MMT) survey for HVS (Brown et al. 2006b, 2009). Following the predictions of Yu & Tremaine (2003) that a total number of about 1,000 HVS exist in the Galaxy. Hence HVS are expected to be a rather scarce phenomenon. It is then obvious that the inspected volume has to be large. Brown et al. (2006a) stated that even in a complete survey up to 1 kpc, the probability of finding a HVS is $\sim 0.1\%$. There are at least three good reasons for searching for B-type HVS out in the halo. Certainly the dust extinction in the Galactic disk prohibits a deep survey, which is the primary reason to check the halo. Secondly the stellar density declines following approximately r^{-3} , whereas the HVS density drops with r^{-2} if the production rate is constant. Hence stars far out in the halo are much more likely HVS than in Galactic disk (GD) neighbourhood. Thirdly most of the halo stars are metal-poor old stars of late stellar types, hence early type stars stick out, as they are not expected to belong to the stellar halo population. Another advantage is that these stars are so luminous that a search for faint ones of that kind naturally targets distant stars. While O-type stars are too short-lived to reach the outer halo, B- and later type stars are able to reach the halo within their lifetime (see Section 2.1). Nevertheless in the case of A-type stars a much bigger problem appears. In that spectral class it is only possible to reliably distinguish heavier main-sequence stars from less massive evolved horizontal branch stars by a detailed spectral analysis (Xue et al. 2008; Tillich et al. 2009b). Hence, a photometric preselection for massive distant main-sequence stars, should provide good results. Late B-type stars are therefore the most promising targets for a HVS search, as they are sufficiently long-lived, but less likely to be misclassified with blue straggler and HB A-type stars.

The Sloan Digital Sky Survey (short: *SDSS*, Adelman-McCarthy et al. 2008), which combines multicolour photometric with spectroscopic observations, is nowadays the perfect tool for this task. Errors and accuracy in the database are well-evaluated and allow us to apply colour cuts to create a target sample. Figure 5.1 shows the colour-colour of

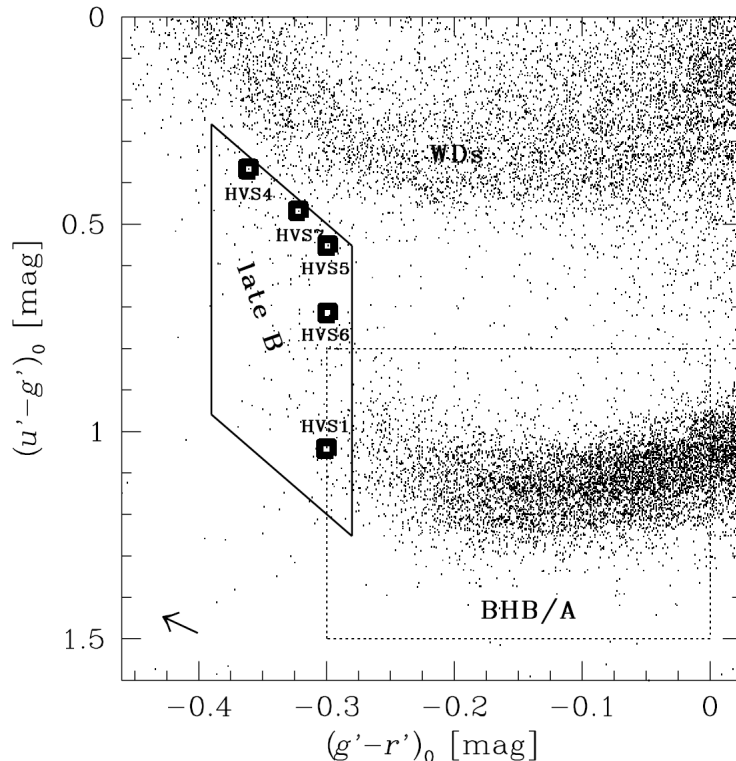


Figure 5.1: Section of *SDSS* data release 4 with target selection. The dotted box is the region where BHB/A-type stars are expected by Yanny et al. (2000). The late B-type stars are located in the full drawn box, which indeed contains all HVS known at that time, proving the efficiency of the search strategy. The arrow indicates the amplitude and the direction of the median reddening applied to the targets. Diagram excerpted from Brown et al. (2006b).

SDSS targets and the selected data sample of Brown et al. (2006b).

Unfortunately as soon as late-B stars are targeted in a survey the contamination with A-type (and BHB) stars increases to the red end. But even in the late-B type region the sample can never be pure. Hence in the next sections we show our detailed spectral analysis for some HVS (candidates) to unravel their nature. The following section is based on partially published work (Przybilla et al. 2008c).

5.1 HVS 7

*SDSS*J113312.12+010824.9 (= HVS 7) is one of the brightest late-B type HVS known and was discovered by Brown et al. (2006b), during their survey for late-B type HVS from *SDSS* data release 4. Although HVS 7 is assumed to be a main-sequence star even from its spectral morphology, it is also consistent with a blue horizontal-branch nature following Heber et al. (2008b). Therefore we obtained high-resolution spectra with UVES at the

Table 5.1: Stellar parameters & elemental abundances of HVS 7

T_{eff} (K)	$12\,000\pm 500$	M/M_{\odot}	3.7 ± 0.2
$\log g$ (cgs)	3.8 ± 0.1	R/R_{\odot}	4.0 ± 0.1
ξ (km/s)	3 ± 1	L/L_{\odot}	300 ± 50
$v \sin i$ (km/s)	55 ± 2	τ_{evol} (Myr)	150 ± 10

Ion	$\varepsilon^{\text{NLTE}}$	ε^{LTE}	#	Ion	ε^{LTE}	#
He I ¹	8.90 ± 0.11	9.17 ± 0.11	2	Ca II	6.60	1
C II ²	≤ 6.50	≤ 6.47	...	Sc II	4.00	1
N II ³	≤ 7.50	≤ 7.60	...	Cr II	6.40 ± 0.12	10
O I ⁴	≤ 7.70	≤ 8.20	...	Mn II	≤ 6.50	...
Mg II ⁵	6.00	5.80	1	Co II	6.82 ± 0.21	5
Si II ⁶	8.69 ± 0.13	8.61 ± 0.15	12	Sr II	5.00	1
Si III ⁶	8.65	8.80	1	Y II	5.02 ± 0.18	5
S II ⁷	7.35 ± 0.12	7.44 ± 0.14	2	Eu II	5.05 ± 0.16	3
Ti II ⁸	6.20 ± 0.11	5.64 ± 0.11	7	Gd II	5.93 ± 0.13	4
Fe II ⁸	8.44 ± 0.13	7.78 ± 0.16	26	Dy II	6.00 ± 0.23	5
P II	...	7.13 ± 0.21	2	Dy III	4.83 ± 0.18	3
Cl II	...	7.92 ± 0.21	5	Hg II	4.90	1

$\varepsilon(X) = \log(X/H) + 12$. Error estimates consist of statistical 1σ -uncertainties derived from line-to-line scatter (# lines) plus 0.1 dex for continuum placement uncertainty (added in quadrature); realistic uncertainties, including systematic effects e.g. if a magnetic field were present, are expected to be larger. The detailed line lists and the references for the NLTE model atoms are given in Przybilla et al. (2008c).

VLT and performed a quantitative spectral analysis at a high level, using state-of-the-art modelling techniques to constrain the nature of HVS 7 (Przybilla et al. 2008c).

Between April 15 and May 10, 2007, a number of 17 spectra with a total integration time of ~ 6.8 h have been obtained (Proposal 079.D-0756(A)), covering the range of 3750 to 4950 Å and 5700 to 9000 Å at a resolving power of $R \approx 35000$. The data has been reduced following Koester et al. (2001). Additionally we obtained a spectrum of the DC white dwarf WD 1055–072 for a reliable normalisation of the continuum. Within the detection limits no radial velocity variations have been detected within the respective errors. By co-adding the spectra we achieved a peak S/N of ≈ 80 in the blue channel.

At the first glance a high number of absorption lines can be seen in the spectrum (see Figure 5.2). The line identification was rendered difficult because many absorption lines showed up, which are not present in normal B-type stars. A detailed inspection of atomic data bases allowed us to identify many lines produced by rare elements such as e.g. chlorine and cobalt, which implies a strong enrichment of these elements in the atmosphere of HVS 7. The presence of chlorine, strong phosphorus and cobalt lines in the spectrum renders HVS 7 peculiar even for a Cp star. Amazingly even heavier species up to rare-elements and mercury have been found. Moreover, carbon nitrogen and oxygen are absent within the present detection limit. Overall many absorption lines remain

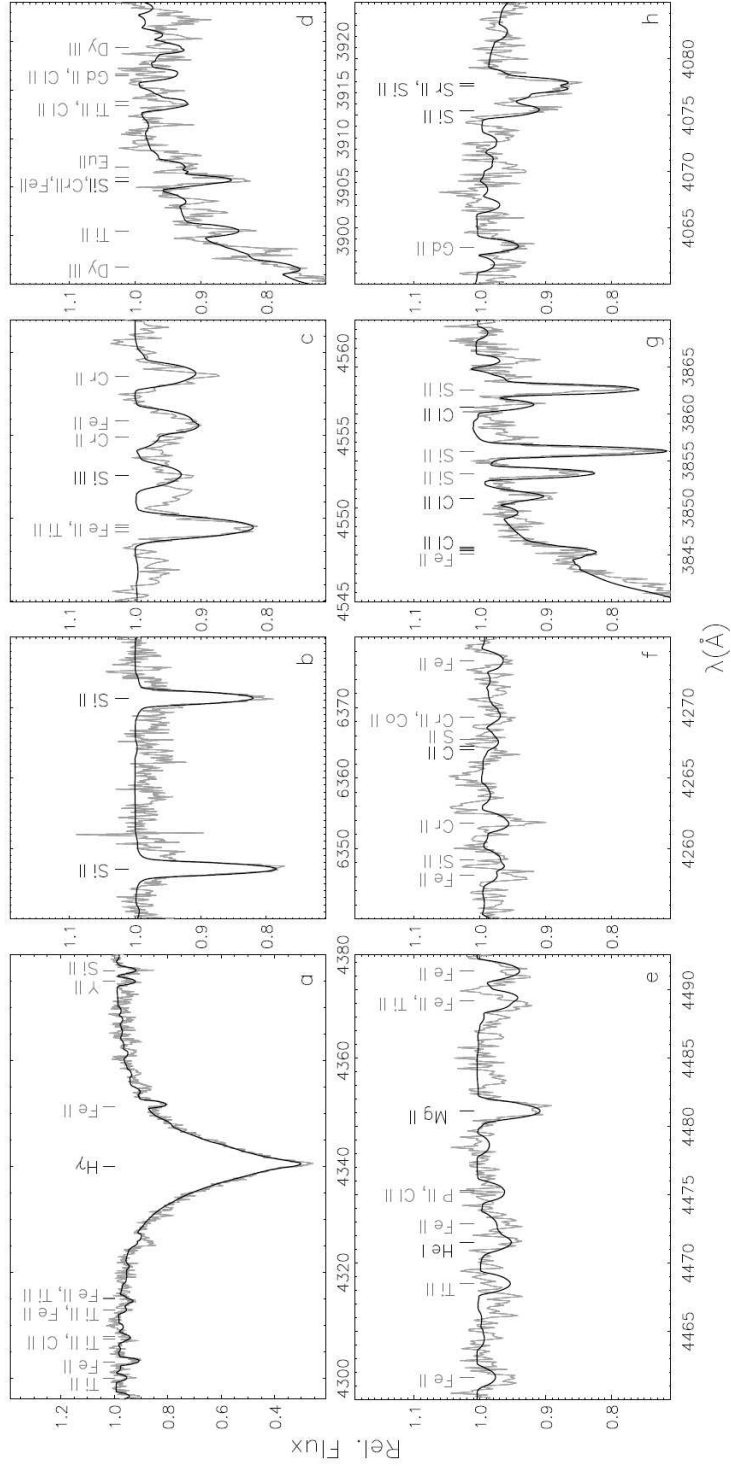


Figure 5.2: Comparison of spectrum synthesis for HVS 7 (full line, best fit for abundances as in Table 1) with observations (grey) as examples for some strategic regions.

unidentified, especially in the red spectral region.

All this indicates that HVS 7 is a chemically-peculiar (CP) late B-type (Bp) star with moderate projected rotational velocity (Przybilla et al. 2008c). While the helium lines are extremely weak, obviously strong silicon lines dominate the metal line profile. By using the NIST Atomic Spectral Database¹ a high number of metal absorption lines have been identified in the spectrum, which was shifted to rest wavelength for that purpose. Most of the α -process elements, as well as most of the iron group elements have been found.

For the quantitative spectral analysis we used the standard assumptions in the Cp field, in particular a chemically homogeneous atmosphere. First crude abundances have been determined by comparing the data with synthetic spectra containing metals with fixed abundances, which have been calculated in LTE. These estimates have been the starting point for a more detailed NLTE analysis as already described in Chapter 3. The chemical peculiarity of HVS 7 naturally required an iterative approach in order to obtain a consistent atmospheric model. The derived parameters and abundances are summarised in Table 5.1.

Note that the present results of our analysis are in excellent agreement with the results of Heber et al. (2008b), who derived $T_{\text{eff}} = 12\,600 \pm 500$ K, $\log g = 3.71 \pm 0.2$ from a LTE analysis. The abundance upper limits for C, N and O have been derived from the strongest predicted lines. Unfortunately the only available Hg line is blended and the respective abundance is therefore regarded as uncertain.

The synthetic spectrum compared to the observation in some sample regions is shown in Figure 5.2. Note that overall good agreement is achieved also for the blended lines, which have been omitted from the analysis. It is reassuring that they provide a good match. The Figure clearly illustrates the T_{eff} and $\log g$ determination from Balmer lines (H_γ in panel a)) and the Si ionisation equilibrium: Si II is shown in panel b), Si III and Si I in panels c) and d) respectively. Note the strong Si II lines in panel b) indicative of a Si overabundance. Panel e) illustrates the weakness (deficiency) of He I and Mg II, f) the absence (deficiency) of C II, g) the presence (strong enrichment) of Cl II. In panel h) we show a blend of Sr II and Si II. Iron group elements are highlighted in panel c) and rare-earth elements in d). Other prominent spectral lines are identified in Figure 5.2.

Nevertheless, some observed lines are not reproduced in the synthetic spectrum. This is a common problem in the field of Cp stars and occurs due to the lack of atomic data for some elements. Basically we find increased abundance with increasing atomic weight. The helium abundance is extremely low ($<1/100$ solar), C, N and O are absent within the detection limits ($<1/100$, $\lesssim 1/3$, $<1/10$ solar, respectively) and magnesium is markedly underabundant ($\sim 1/30$ solar). Silicon is the most abundant metal ($>10 \times$ solar) and chlorine, cobalt and phosphorus are pronouncedly overabundant (~ 440 , 80 and $40 \times$ solar). All heavier elements are largely overabundant: $\sim 10 \times$ solar values for iron group elements and $\sim 10\,000 \times$ solar values for rare-earth elements and mercury.

The differences between the LTE and NLTE analysis are mostly similar to those found in main-sequence stars of normal composition by Hempel & Holweger (2003). Prominent exceptions are found for Ti II and Fe II, where the differences of $\sim 0.6 - 0.7$ exceed even the

¹<http://physics.nist.gov/PhysRefData/ASD>

effect found in supergiants (Przybilla et al. 2006). The main NLTE mechanisms in these cases are an overionisation of the ground state and the energetically low levels. Because of the large overabundances the lines form at much smaller depths in the atmosphere than under normal conditions (though avoiding saturation), so that the level populations deviate strongly from detailed equilibrium values.

The position of HVS 7 in the $T_{\text{eff}}\text{-log } g$ -diagram is shown in Figure 5.4. Based on that alone, one cannot decide whether it is an intermediate-mass star of $3\text{-}4M_{\odot}$, close to the main-sequence or a low mass star of $\sim 0.5\text{--}0.7M_{\odot}$ on the horizontal branch (Heber et al. 2008b). Another important constraint is also the rotational velocity, which is in general low ($< 8\text{ km s}^{-1}$) for blue horizontal branch stars. HVS 7 shows a $v \sin i$ of 55 km s^{-1} , which does not necessarily exclude a HB nature, as the star might have been spun up by tidal locking to the orbital motion before the binary was disrupted (Hansen 2007) to release the HVS. The chemical composition of the star is also an important constraint for the distinction (see Section 2.1). Although similar chemical peculiarities can be found in both populations, the high density of metal lines in HVS 7 clearly favours a main-sequence nature. Note that chemical peculiarities only affect the outer layers of the star and they have developed with time, so we can apply standard evolutionary models for HVS 7. The comparison with the evolutionary tracks of Schaller et al. (1992) leads directly to the stellar mass M , radius R , its luminosity L and the evolutionary lifetime τ_{evol} , given in Table 5.1. The spectroscopic distance is then $59 \pm 6 \text{ kpc}$, in excellent agreement with the distance estimate of Brown et al. (2006b). Unfortunately HVS 7 does not show a significant proper motion applying our measurement described in Section 4.3. Therefore a detailed calculation of a 3D trajectory cannot be performed. Nevertheless based on numerical experiments we found that the lifetime of HVS 7 ($\sim 150 \text{ Myr}$) is consistent with a possible time-of-flight from the GC of about 120 Myr . Hence HVS 7 is a Cp main-sequence star, possibly ejected by the SMBH in the GC.

5.2 HVS 8,9,10

Based on the past discoveries Brown et al. (2007) extended their survey for late-B type HVS on *SDSS* data release 5. Simultaneously they increased their target sample by loosening the colour criteria and raising the limiting magnitude. Hence as first result the number of targets for their observational project doubled.

Finally Brown et al. (2007b) discovered the HVS 8, 9 and 10 during this extended survey for late-B type HVS. Warren Brown kindly provided his low resolution spectra for HVS 8,9 and 10. The spectra were obtained at the 6.5m MMT telescope with the MMT Blue Channel spectrograph. They provide a wavelength coverage of $3650\text{-}4500\text{\AA}$ at a spectral resolution of 1.2\AA . The exposure times were adapted to the luminosities of the targets aiming at an S/N of about 15. As for HVS 7, the colour analysis of the stars showed that they might possibly be main-sequence stars. Hence, in the advent of our own forthcoming HVS project, a detailed spectroscopic analysis might shed light on the MS or BHB nature of the stars. Due to the poor S/N we expected no metal lines in the spectra to be detectable. We calculated a grid of synthetic model spectra for different

Table 5.2: Results of the quantitative spectroscopic analysis for HVS 8, 9 and 10.

	HVS8	HVS9	HVS10
V (mag) ^a	18.09 ± 0.02	18.76 ± 0.03	19.36 ± 0.04
T_{eff} (K)	10400 ± 250	11770 ± 550	10450 ± 400
log g(cgs)	3.8 ± 0.1	3.9 ± 0.2	4.0 ± 0.2
log $n_{\text{He}}/n_{\text{H}}$ (cgs)	< -2.0	< -2.0	< -2.0
M/ M_{\odot}	3.00 ± 0.10	3.50 ± 0.10	2.75 ± 0.10
v_{rad}^a (km s ⁻¹)	500.0 ± 3.0	619.3 ± 4.5	472.0 ± 5.2
v_{rad}^b (km s ⁻¹)	503.8 ± 3.0	626.2 ± 4.7	470.1 ± 5.4
$v_{\text{rot}} \sin i$ (km s ⁻¹)	280	250	170
$v_{\text{rad}}^{\text{rf}}$ (km s ⁻¹)	420	480	425

hydrogen-to-helium abundances and used FITSB2 for the fitting, as already described in Chapter. 3.

At the first glance, only the Balmer lines are visible in the spectra. The determined parameters of the stars are given in Table 5.2. We did not detect any helium absorption lines in the spectra, hence we apply a upper limit of $\log n_{\text{He}}/n_{\text{H}}=-2.0$ for the helium content in HVS 8, 9 and 10. This is similar to HVS 7, where helium is also depleted in the stellar atmosphere. Furthermore we found indication for rotational broadening in the H_{γ} and H_{δ} line. Unfortunately the spectra do not cover the H_{β} or H_{α} lines, where this effect would emerge even stronger. However, the projected rotation velocity is so large (170 – 280 km s⁻¹), that the detection appears reliable.

The comparison between our synthetic model and the observed data for HVS 9 is shown in Figure 5.3. Obviously the centre of the broad Balmer lines H_{γ} and H_{δ} is flat, which is called rotational broadening. In order to achieve the best match between data and observation we had to apply a $v \sin i$ of 250 km s⁻¹. In this context even the weak helium lines fit in the picture. Due to the high rotation, the metal lines get even weaker, hence more difficult to detect. As for the other two stars the situation is comparable, the spectral plots can be found in Figure 3.2 and the appendix (Figure A.1). We connected the derived stellar parameters to the evolutionary tracks (see Figure 5.4) and obtained a complete and consistent result.

HVS 7 and 9 lie in the overlapping region of main-sequence and horizontal branch, hence their nature cannot be revealed from the T_{eff} -log g-diagram alone. For the bright HVS 7 we performed an detailed quantitative analysis based on high resolution spectra and found a chemically peculiar main-sequence star (see Section 5.1). HVS 8, 9 and 10 show no helium in their spectra, which is not exceptional accounting for the low-resolution, the high rotation and the well known peculiarity of stars at that temperature. Hence additional arguments are required to unravel their nature. As for HVS 9 a high rotation is present in the data, we clearly favour a main-sequence nature with 3.5 M_{\odot} . In the case of HVS 8 and 10 their location in the T_{eff} -log g-diagram (accounting also for errors) alone,

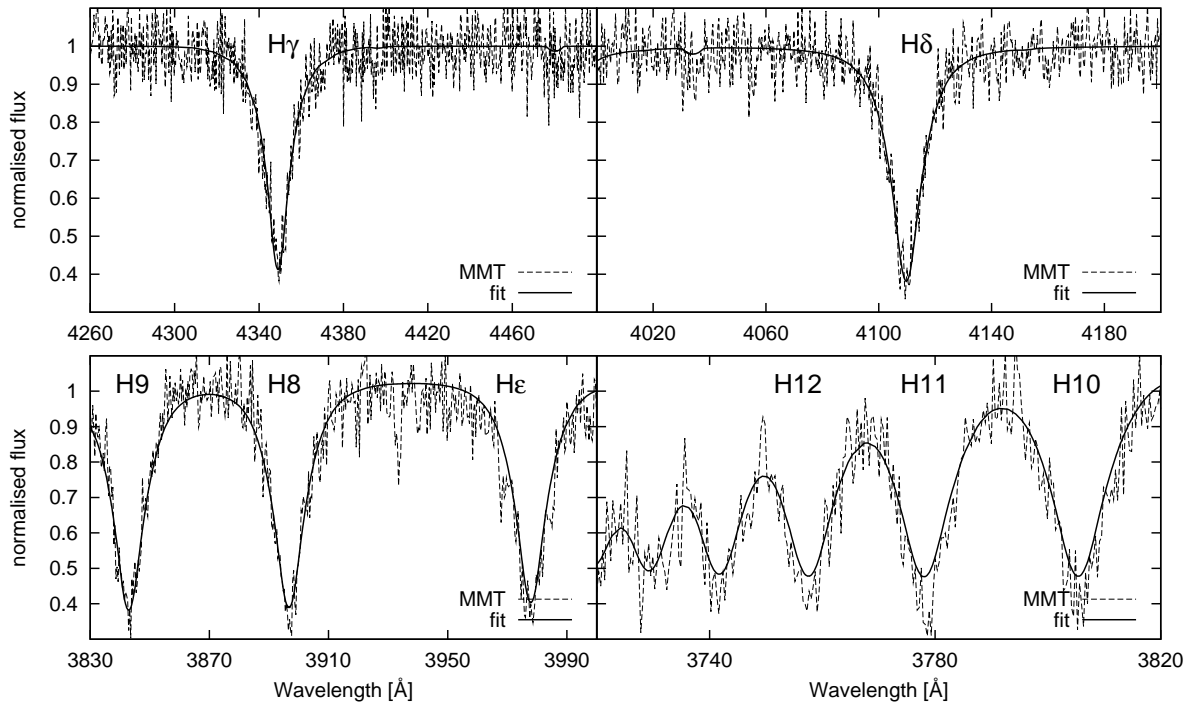


Figure 5.3: Comparison between the synthetic model with the observed spectrum from the MMT for HVS 9. The synthetic spectrum had to be broadened with $v_{\text{rot}} \sin i = 250 \text{ km s}^{-1}$ to achieve a good match. Note the overall good agreement. The poorer match of the higher Balmer lines is due to the problem of matching the continuum and rectification artefacts.

speaks for a main-sequence nature. Together with the fast rotation a horizontal branch nature can be clearly excluded.

This means at the same time, that the distance estimates of Brown et al. (2007b) are rather accurate and the stars are likely to be unbound.

5.3 Further candidates

Encouraged by this clear result, additional MMT spectra for potential HVS were kindly provided by W. Brown, which have been obtained in his survey. As these candidates are from the bright survey $15.5 < V < 16.5$ the spectra are of much higher S/N and can be analysed in higher precision (Brown et al. 2007a). Unfortunately the spectra do not cover a suitable ionisation equilibrium for a highly accurate temperature measurement. As in the previous analysis we rely only on our grid of synthetic spectra including exclusively hydrogen and helium. From the fitting of synthetic spectra we found only the candidate star BCAND364 to show a high projected rotational velocity of $v_{\text{rot}} \sin i = 260 \text{ km s}^{-1}$. A comparison between the data and the best fit is shown in Figure 5.5.

Although the lines are strongly rotationally broadened, we clearly detect He I absorp-

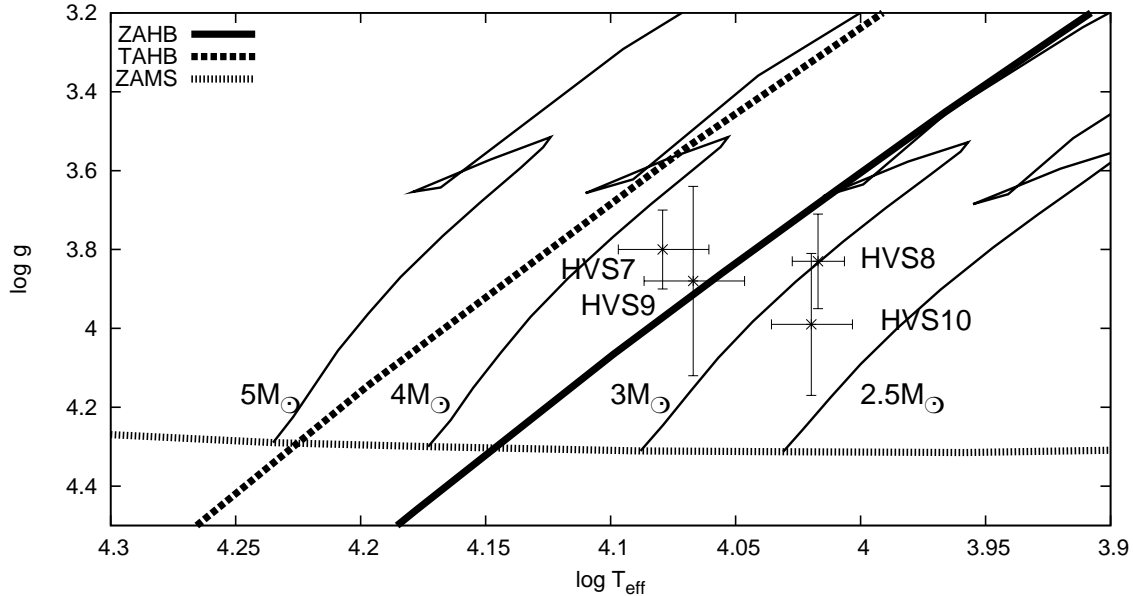


Figure 5.4: T_{eff} - $\log g$ -diagram for HVS 7, 8, 9, 10 with evolutionary tracks from Schaller et al. (1992). For clarity we marked the ZAMS, the ZAHB and the TAHB.

tion lines, hence determine a significant helium content. Only the Ca II-3933 line is not broadened as it is of interstellar origin. Additionally we see small atmospheric Si II-4131 and C II-4267 absorption features, which are just above the noise and indicate a high abundance for these elements. As the star rotates so fast no other metal absorption lines are visible. All this points are arguments for a main-sequence origin for BCAND364, hence it is very similar to HVS 8 to 10. As the spectra of the other candidates are not strongly rotationally broadened they form a different group, more similar to HVS 7. The results of the quantitative spectral analysis are given in Table 5.3, while the corresponding spectral comparison plots can be found in Figure 3.2 and in the appendix (Figures A.1 and A.2).

Due to the fact that no rotation is present, the clear He I absorption features in BCAND485 and BCAND563 give good constraints on the atmospheric helium content. In both stars we additionally see strong silicon (e.g. Si II-4131), magnesium (e.g. Mg II-4481) and carbon (e.g. C II-4367) absorption features, which are a clear indication for a main sequence nature. For two of the candidates, BCAND371 and BHVS462 we could not detect any He I absorption lines. Nevertheless for BCAND371 we can clearly identify red-shifted and therefore atmospheric calcium Ca II-3933 apart from the typical interstellar component (Ca II-3933) at rest-wavelength. Also silicon absorption lines were clearly identified in the stellar spectra (e.g. Si II-3856, Si II-3863, Si II-4131) and also prominent magnesium lines show up (e.g. Mg II-4481). Many more weaker metal lines seem to be hidden in the spectra, which are at the identification limit due to insufficient S/N (e.g. Sr II-4078). We find exactly the same situation for BHVS462 and additionally even a mercury absorption in the wing of the H_{ϵ} Balmer line (Hg II-3984). We conclude that

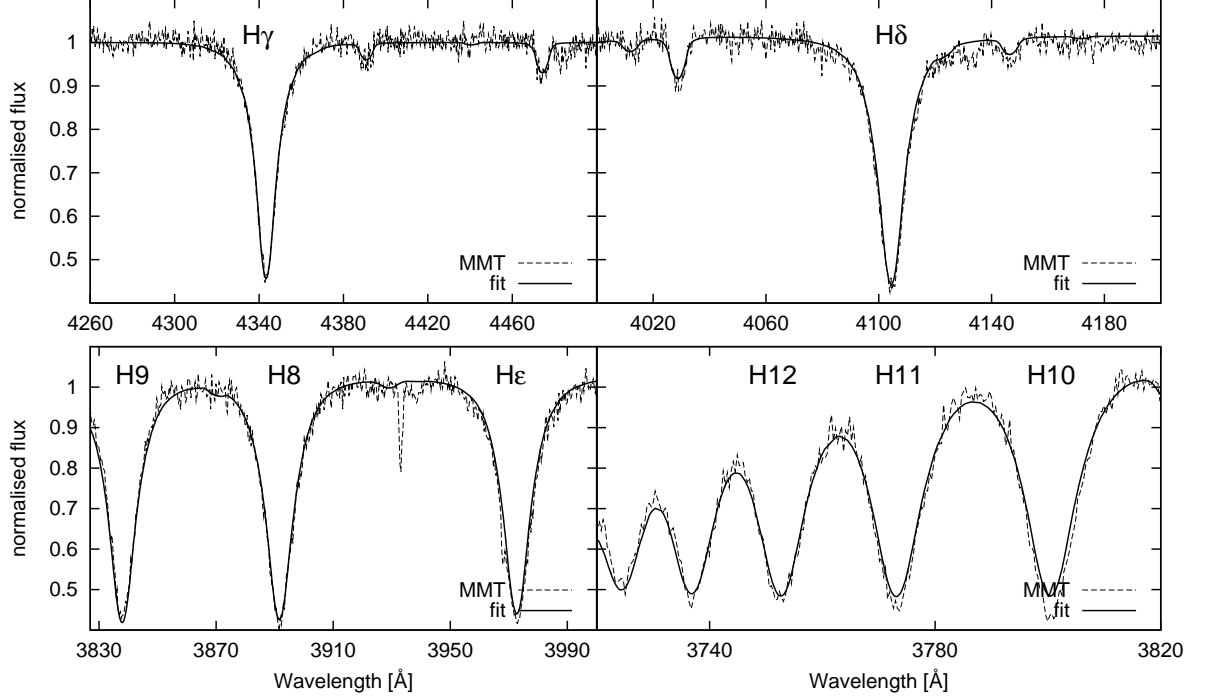


Figure 5.5: Comparison between the synthetic model with the observed spectrum from the MMT for BCAND364. The synthetic spectrum had to be broadened with $v \sin i = 260 \text{ km s}^{-1}$ to achieve a good match. Note the overall good agreement, even for the highest Balmer lines.

Table 5.3: Result of the quantitative spectroscopic analysis for further candidates.

	BCAND364	BCAND371	BCAND485	BCAND563	BHVS462
V (mag)	16.48 ± 0.02	15.72 ± 0.02	16.32 ± 0.02	15.93 ± 0.02	15.77 ± 0.02
T_{eff} (K)	12500 ± 250	13750 ± 200	15650 ± 300	15000 ± 250	13000 ± 300
$\log g$ (cgs)	3.6 ± 0.1	4.4 ± 0.1	3.8 ± 0.1	3.8 ± 0.1	3.9 ± 0.1
$\log n_{\text{He}}/n_{\text{H}}$ (cgs)	-0.8	< -2.0	-1.3	-0.8	< -2.0
M/M_{\odot}	$4-4.5 \pm 0.2$	-	5.2 ± 0.15	5.0 ± 0.15	-
v_{rad} (km s^{-1})	201.5 ± 5.0	220.0 ± 3.0	418.2 ± 5.0	314.0 ± 4.0	-398.0 ± 5.0
$v_{\text{rot}} \sin i$ (km s^{-1})	260	-	-	-	-
$v_{\text{rad}}^{\text{rf}}$ (km s^{-1})	225	259	379	324	-364

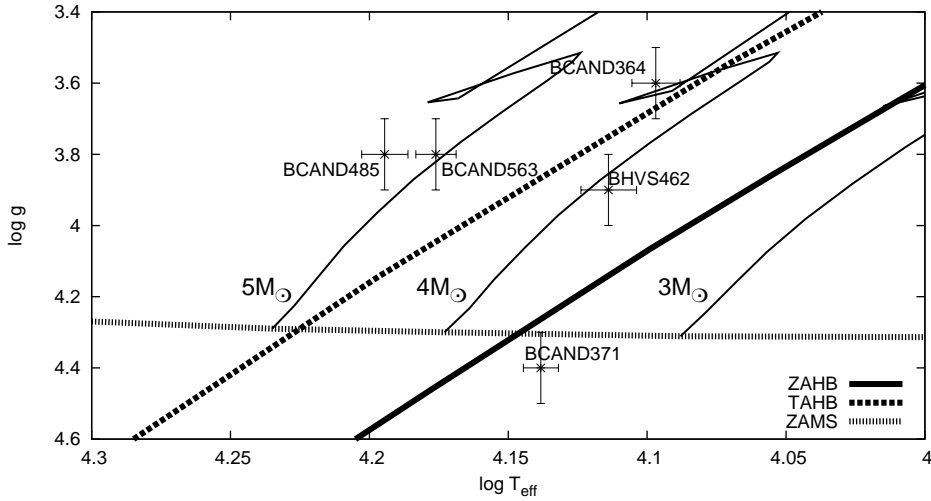


Figure 5.6: T_{eff} - $\log g$ -diagram for the further candidates with evolutionary tracks from Schaller et al. (1992). For comparison we marked the ZAMS, the ZAHB and the TAHB.

some of these elements are highly overabundant, while such typical elements like helium, carbon and oxygen seem to be untraceable. This leads to that conclusion that both stars belong to the chemical peculiar stars and are pretty similar to HVS 7. However, a detailed quantitative spectral analysis would require high resolution spectroscopy as for HVS 7 (see Section 5.1).

In Figure 5.6 we show the position of the candidates in the characterising T_{eff} - $\log g$ -diagram (accounting also for errors). The detection of the metal features in BCAND485 and BCAND563 together with their location, clearly outside the typical horizontal branch region, is an argument to favour a main-sequence nature for those two stars.

In the T_{eff} - $\log g$ -diagram BCAND364 and BHVS462 are located in the overlapping region of BHB and MS, where we cannot conclude on their nature based on that fact alone. The same holds for BCAND371, which is located very close to that region. Due to the fact that we found evidence for the chemical peculiarity of BCAND371 and BHVS462, both of them might be main-sequence stars, similar to HVS 7. But only the additional measurement of a high projected rotational velocity would be final evidence. However the case of BCAND364 is clear. Although it is situated in the problematic region, the detection of helium and metals together with its fast rotation are strong arguments to clearly favour a main-sequence nature beyond doubt. Unfortunately BCAND364 is located in the T_{eff} - $\log g$ -diagram where the evolutionary tracks of Schaller et al. (1992) show a loop. Therefore an accurate mass estimate is prevented, as several tracks overlap and we are left with a crude stellar mass range of $4-4.5 \pm 0.2M_{\odot}$.

While the previous chapter showed what can be done with our powerful quantitative spectral analysis if applied to already known HVS, the next chapters are dedicated exclusively to the search for new and unknown HVS among various types of A stars (see Chapter 6) and most importantly among hot subdwarf stars (see Chapter 7).

Chapter 6

Wanted - A sample of A-type Hyper-velocity star candidates

Systematic searches for HVS took advantage of the huge *SDSS* database (Adelman-McCarthy et al. 2008) for target selection and revealed a population of HVS; the latest compilation lists 16 of these stars (Brown et al. 2009). These surveys are based on RV measurements alone. However, a well known problem within late-B type surveys is to derive the distance of a HVS star, as there are different types of stars populating the same region in the $T_{\text{eff}}\text{-log } g$ -diagram (Heber et al. 2008b). Therefore blue horizontal-branch stars can not be easily distinguished from main-sequence stars but unfortunately they have very different distances. Nevertheless almost all HVS are assumed to be main-sequence and not blue horizontal branch stars. Detailed spectroscopic analyses have confirmed these assumptions only for HVS 1, HVS 3, HVS 7, and HVS 8 (Przybilla et al. 2008b,c; Heber et al. 2008b; López-Morales & Bonanos 2008, see also Chapter 5).

In the absence of proper motion measurements, the trajectories have not been derived for any individual HVS so far. Heber et al. (2008a) succeeded in investigating the trajectory of the high-velocity B star HD 271791 from accurate proper motions, radial velocity, and spectroscopic distance. The star was found to be probably unbound to the Galaxy and to originate in the outer rim of the Galaxy rather than in its centre, demonstrating that a mechanism other than that of Hills (1988) must have operated. Hence, it is rewarding to measure proper motions of high-velocity stars.

In order to address this topic and to find more such stars we used a sample published by Xue et al. (2008), which was also based on *SDSS*.

6.1 Just an A-type sample

The advantage of the approach via *SDSS* is primarily the huge amount of data, especially the over 1 million spectra, which are directly accessible. Furthermore *SDSS* is evaluated in terms of accuracy and errors to a very high level. Hence many recent studies, involving a high number of stars have made use of this powerful tool.

One of them is the work of Xue et al. (2008), which analysed the kinematics of 2,400

Table 6.1: Proper motion measurements for the positive detections. We found significant proper motions only for the four brightest stars.

name	V mag	$\mu_\alpha \cos(\delta)$ (mas yr $^{-1}$)	μ_δ (mas yr $^{-1}$)	$n_{\text{ep}}/n_{\text{gal}}$
J1300+0422	15.12	-11.9 ± 1.7	-19.7 ± 1.4	12/15
J1539+0239	15.72	-10.6 ± 1.6	-10.0 ± 2.3	17/7
J0136+2425	16.17	-2.2 ± 1.3	-8.2 ± 2.2	9/16
J1553+0030	17.36	-10.2 ± 2.1	$+3.1 \pm 1.4$	17/10

blue horizontal-branch candidates from a sample of 10,000 A-type stars, which were a mix of HB A-type stars, blue stragglers and MS stars. Finally they concluded on the Galactic halo mass from the reconstructed circular velocity curve of their BHB stars. Initially they applied colour cuts to especially focus on A-type stars. In order to separate main-sequence, blue straggler and horizontal-branch stars, they used two compulsory criteria based on the normalised line profile of the H_γ and H_δ Balmer lines. The first one is the $D_{0.2}$ versus f_m method (Pier 1983), which involves the width $D_{0.2}$ of the Balmer line at 20% below the continuum and the relative flux f_m in the line core. The second is the *scale width versus shape* method (Clewley et al. 2002), based on fitting a parametrised profile to the H_γ line. Both of the methods are highly insensitive, if applied to lower S/N data. Hence the same star, with several spectra may have several different classifications. For the HB stars, they derived the absolute magnitude from the colours following Sirko et al. (2004). Consequently the respective distance was calculated and the circular velocity curve was obtained from the $\sim 2,400$ HB stars. Finally the virial mass for the Milky Way’s dark matter halo of $M_{\text{halo}} = 1.0_{-0.2}^{+0.3} \times 10^{12} M_\odot$ was estimated by fitting the velocity profiles from Navarro et al. (1996) to the data.

Fortunately Xue et al. (2008) presented the radial velocities for more than 10,000 blue stars from the *SDSS*, with effective temperature between roughly 7,000 and 10,000 K according to their colours. We converted the radial velocities to Galactic ones and focused on the 17 fastest stars in terms of large RV in the Galactic rest-frame (GRF) using equation 4.2 (limits $|v_{\text{rad}}^{\text{GRF}}| > 350 \text{ km s}^{-1}$). We found 11 stars to show a positive radial velocity, which are discussed in the next Sections 6.2 and 6.3. But we also included 6 stars with highly negative velocity i.e. approaching us and discuss them in Section 6.4. Significant proper motion was measured for 4 stars only, which is presented in Table 6.1. Hence for them we have the full phase space information and a detailed kinematic analysis was possible.

Unfortunately a closer look at the spectrum of SDSSJ155352.41+003012.0 (J1553+0030 for short) showed it to be a spectroscopic binary. In the spectrum we found the Ca II IR triplet and to lesser extent the Mg I b triplet to be unusually strong. This is most likely produced by a cool companion contributing to the spectra. Hence we had to exclude J1553+0030 from the rest of our analysis. In order to confirm this result, we re-observed J1553+0030 with the TWIN spectrograph at the 3.5m telescope on Calar Alto in May

2009 and detected additionally a high spectral variability. However its proper motion fit is shown in the appendix A.

One star was found to be a metal-poor blue straggler (J1300+0422) of population II, as shown in Section 6.3. The remaining main-sequence star J0136+2425 turns out to be the first typical HVS, originating in the outer Galactic disk and will be presented in the next section. The following sections are based on partially published work (Tillich et al. 2009b, 2010d; Przybilla et al. 2010).

MJD	v_{rad}^{helio} km s ⁻¹	instrument
J0136+2425		
53327.16339	324 ± 6	SDSS combi
55035.59195	313 ± 13	TWIN/CAHA
55035.64608	306 ± 13	TWIN/CAHA
55036.62592	317 ± 13	TWIN/CAHA
55036.64492	301 ± 11	TWIN/CAHA
55039.62192	298 ± 13	TWIN/CAHA
55039.66335	324 ± 13	TWIN/CAHA
J1300+0422		
52669.50747	505 ± 8	SDSS combi
54978.97774	515 ± 6	TWIN/CAHA
J1539+0239		
52026.43391	-373 ± 6	SDSS combi
54979.88191	-367 ± 3	TWIN/CAHA
J1553+0030		
51692.28655	316 ± 9	SDSS combi
54980.97777	355 ± 17	TWIN/CAHA

Table 6.2: Details on the obtained data for the sample of Xue et al. (2008). The *SDSS* spectra are a combination of at least three consecutive single spectra of 15 minutes exposure time each and cover a range of 3800 – 9200 Å at a spectral resolution ranging from 1850 to 2200. The TWIN spectra covers a range of 3600 – 5600 Å in the blue channels with a dispersion of 72.62 Å/mm and 6000 – 7600 Å in the red channel with a dispersion of 73.46 Å/mm.

6.2 J0136+2425 - the first late B-type HVS from the Galactic rim

Based on our selection and priority criterion, J0136+2425 was the most promising target. Luckily it is comparatively bright, as significant proper motions were found for the four brightest stars only. Regarding only the measurement procedure, this is a bit unexpected from the point, as there is no direct relation between the measurability and the magnitude, as long as the star is present on the plates. Nevertheless the rest of the targets are almost two magnitudes fainter. Although darker targets are in average at a higher distance and therefore expected to have a smaller PM, it is generally possible to obtain detections also for fainter stars, which can be seen in Chapter 7. Conducting the measurement as presented in Section 4.3, we obtained for J0136+2425, $\mu_\alpha \cos(\delta) = -2.2 \pm 1.3 \text{ mas yr}^{-1}$ and $\mu_\delta = -8.2 \pm 2.2 \text{ mas yr}^{-1}$ (see Figure 6.1). We confirmed our proper motion again with robust regression, adding artificial outliers to our data.

6.2.1 Spectroscopy

In order to exclude RV variability, we re-observed J0136+2425 at ESO with EFOSC2 mounted on the NTT in October 2008 and with the TWIN spectrograph at the 3.5m telescope on Calar Alto in July 2009; during the latter run, six spectra for J0136+2425 distributed over three days were obtained. Details on the obtained data are given in Table 6.1.

Radial velocities were derived by χ^2 -fitting suitable synthetic spectra over the full spectral range. Since we used many spectral lines, our results differ from that of Xue et al. (2008) who used the H δ line only.

The radial velocities from individual spectra agree to within their respective error limits, indicating that the star is not RV variable within a few kilometers per second on timescales of days.

A quantitative analysis was carried out following the hybrid NLTE approach discussed by Przybilla et al. (2006). The effective temperature T_{eff} and the surface gravity $\log g$ were determined by fits to the Stark-broadened Balmer and Paschen lines and the ionisation equilibrium of Mg I/II. The stellar metallicity was derived by model fits to the observed metal-line spectra. Results are listed in Table 6.3 and a comparison of the resulting final synthetic spectrum with observations in the selected regions around the Balmer lines, the higher Paschen series, Mg II-4481Å, the Mg I b and the near-IR O I triplets, is shown in Figure 6.2. Overall, excellent agreement is obtained for all strategic spectral lines throughout the entire wavelength range. The uncertainties in the stellar parameters were constrained by the quality of the match of the spectral indicators within the given S/N limitations.

Its T_{eff} and gravity places J0136+2425 on the main sequence (see Figure 6.3). In addition the star is rapidly rotating at 250 km s^{-1} and its metallicity is solar, which strengthens the conclusion that it is an intermediate-mass A-type main-sequence star of $2.45 M_\odot$ as derived by comparing the position of the star to predictions of the evolutionary

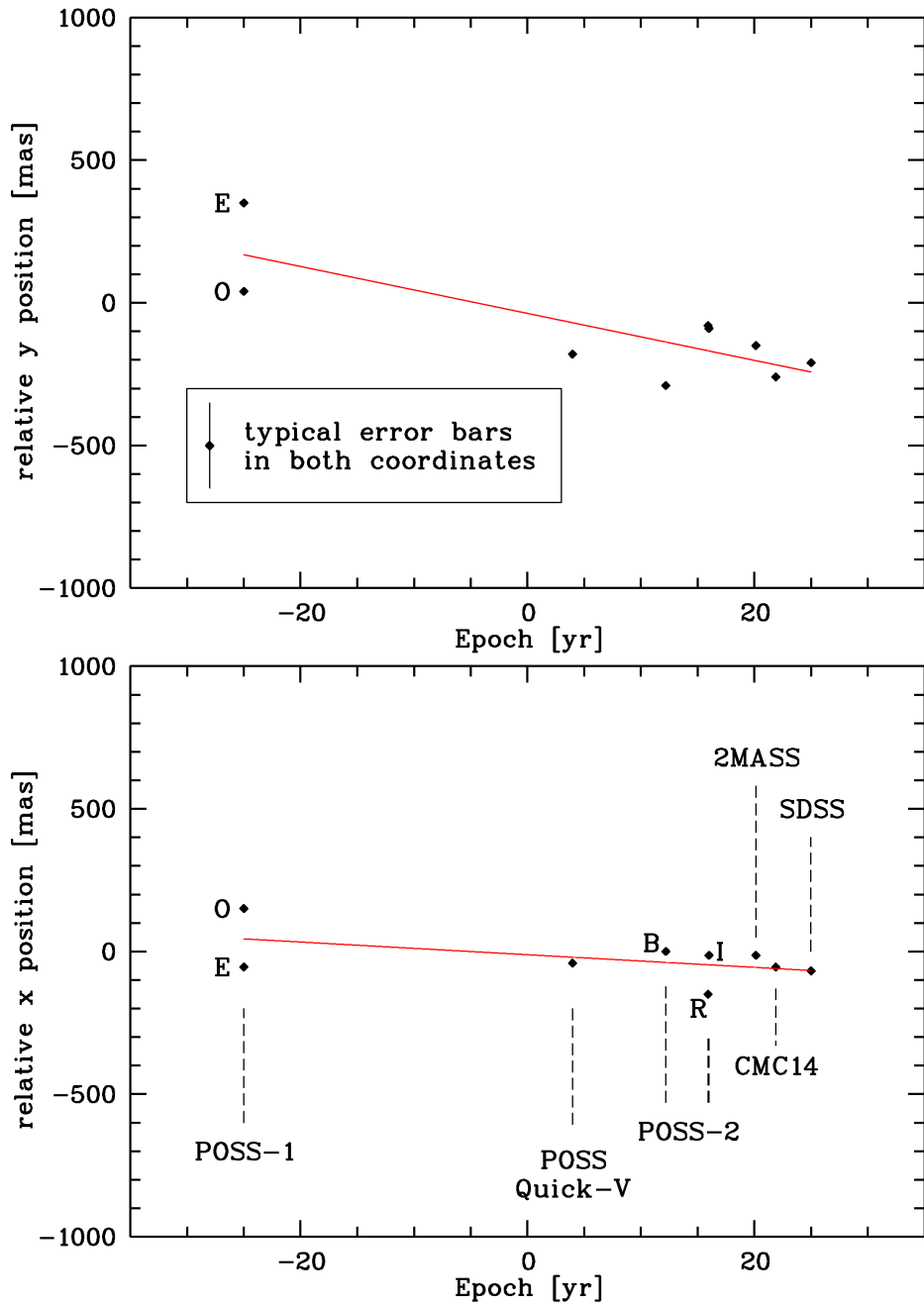


Figure 6.1: Linear fit of the position measurements for J0136+2425, whereas 1979.74 is taken as zero epoch.

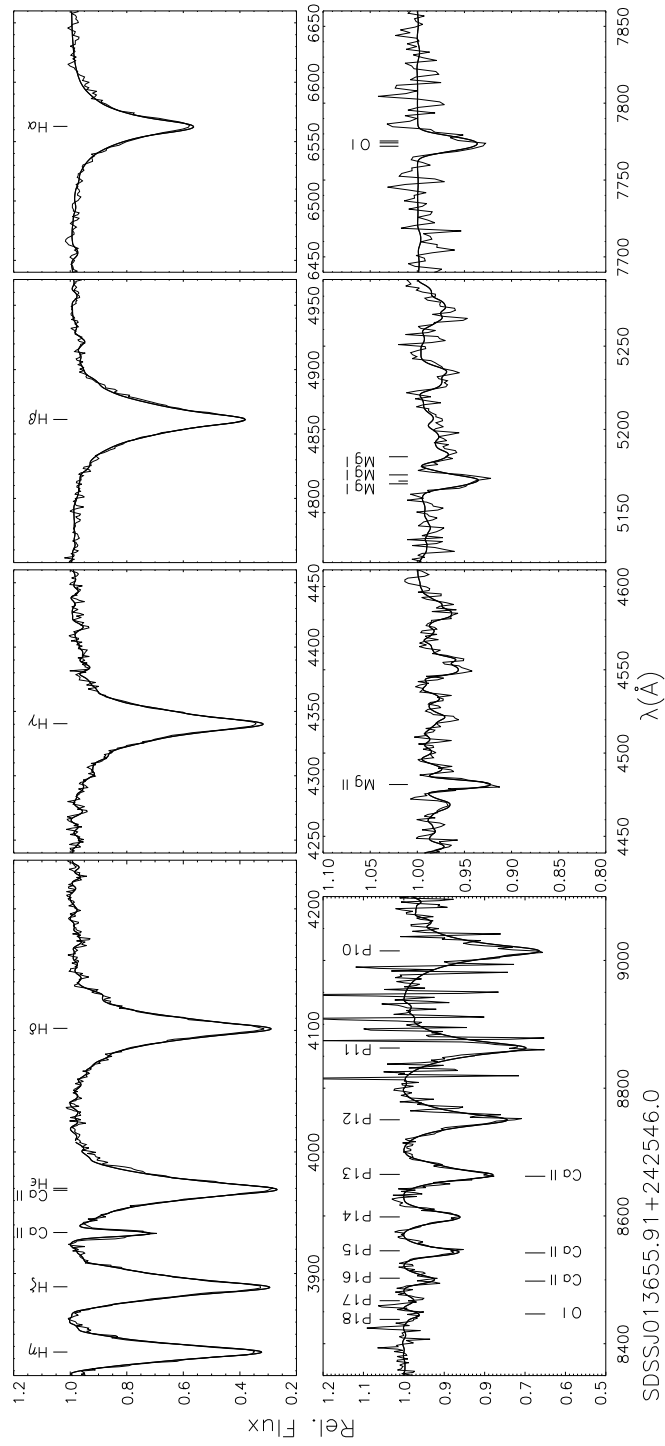


Figure 6.2: Comparison of NLTE spectrum synthesis (thick line) with observation (thin wiggly line) for J0136+2425(*left*) and J1539+0239(*right*). Displayed are selected regions around the Balmer lines, the higher Paschen series, Mg II $\lambda 4481$ Å, the Mg I b and the near-IR O I triplets.

Table 6.3: Results of the quantitative spectroscopic and kinematic analysis of J0136+2425. The resulting GRF velocity v_{GRF} and the local escape velocity v_{esc} are given.

V (mag) ^a	16.17 ± 0.02	$E(B - V)$ (mag) ^b	0.16 ± 0.02
$\mu_{\alpha} \cos(\delta)$ (mas yr ⁻¹)	-2.2 ± 1.3	μ_{δ} (mas yr ⁻¹)	-8.2 ± 2.2
T_{eff} (K)	9100 ± 250	$\log g$ (cgs)	3.90 ± 0.15
$[m/H]$	0.0	M/M_{\odot}	2.45 ± 0.20
v_{rad} (km s ⁻¹)	324.3 ± 5.9	$v_{\text{rot}} \sin i$ (km s ⁻¹)	250
d (kpc)	10.90 ± 2.00	v_{grf} (km s ⁻¹)	587^{+144}_{-89}
v_{ej} (km s ⁻¹)	551	v_{esc} (km s ⁻¹)	466
TOF (Myrs)	12 ± 1.3	t_{evol} (Myrs)	245

^a The visual magnitude derived following Jordi et al. (2006)

^b The interstellar colour excess $E(B - V)$ was determined by comparing the observed colours to synthetic ones from the model spectral energy distribution.

models of Schaller et al. (1992).

In Figure 6.3, we compare the position of J0136+2425 in the T_{eff} - $\log g$ -diagram to those of five late B-type HVS for which these parameters are available (Przybilla et al. 2008b,c; Heber et al. 2008b; López-Morales & Bonanos 2008) as well as those of the massive B star HE 0437–5439 originating in the LMC (see Section 2.2.6), and the B giant HD 271791. The vast majority of HVS are of late B type because they were discovered by targeted searches. Hence, we shall term them typical HVS. J0136+2425 is slightly cooler and less massive than the other known HVS. However, its mass and evolutionary lifetime is similar to that of the typical HVS (3–4 M_{\odot} , ≈ 100 Myrs), while HE 0437–5439 and HD 271791 are far more massive (9–11 M_{\odot}) and short-lived (≈ 20 Myrs).

6.2.2 Kinematics

Using the mass, effective temperature, gravity, and extinction-corrected apparent magnitude, we derive the distance as described in Section 4.1 (see Equation 4.9) using the fluxes from the final model spectrum. The distance error is dominated by the gravity error.

Applying the Galactic potential of Allen & Santillan (1991), we calculated orbits and reconstructed the path of the star back to the Galactic plane with the program of Odenkirchen & Brosche (1992) as described in detail in Section 4.4.

Since the radial velocity (RV) is well known, the error in the space motion is made up of that of the distance, which is controlled mainly by the gravity error, and those of the proper motion components. Varying these three quantities within their respective errors by applying a Monte Carlo procedure with a depth of 1000 (see Section 4.5 for details), we determined the intersection area of the trajectories with the Galactic plane and the time-of-flight. From these Monte Carlo simulations, we derived the median GRF velocities at

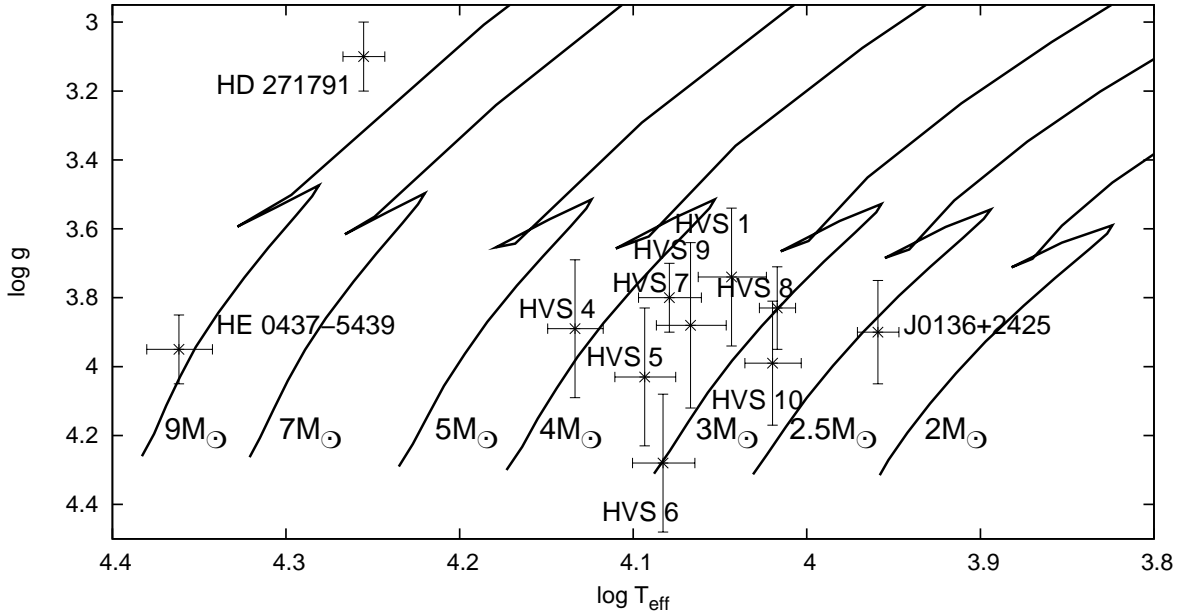


Figure 6.3: J0136+2425 in the $(T_{\text{eff}}, \log g)$ diagram with evolutionary tracks of Schaller et al. (1992) for solar metallicity. The positions of typical HVS (HVS 1, 4 and 6 to 10, from Heber et al. 2008b, and Chapter 5) as well as for HD 271791 and HE0437–5439 are also shown. Note that the mass of J0136+2425 is quite similar to that of the typical HVS.

the present location and their distribution (see Figure 6.4) and compared these with the local escape velocity calculated from the Galactic potential of Allen & Santillan (1991).

For J0136+2425, the GRF velocity of 587_{-89}^{+144} km s $^{-1}$ slightly exceeds the local escape velocity. Whether the star is bound to the Galaxy depends on the Galactic potential adopted, in particular for the dark matter halo, as pointed out by Abadi et al. (2009). Allen & Santillan (1991) adopted a halo mass out to 100 kpc of $M_{\text{Halo}} = 8 \times 10^{11} M_{\odot}$. Xue et al. (2008) derived a somewhat lower mass whereas Abadi et al. (2009) favoured a higher one of $M_{\text{Halo}} = 3.42 \times 10^{12} M_{\odot}$. If the former were correct, J0136+2425 would be unbound, while it would be bound in the latter case. As can be seen in Figure 6.5, its place of origin is found to be in the outer part of the Galactic plane at Galactic radii between 12.5 kpc and 18 kpc, nowhere near the GC. The time of flight (12 ± 1.3 Myr) is much shorter than the star’s lifetime (450 Myr).

6.2.3 Conclusion

J0136+2425 was found to be a rapidly rotating A star of solar composition and therefore classified as a main-sequence star of $2.45 M_{\odot}$. The kinematic analysis excludes an origin at the GC and hence the Hills mechanism for ejection of the star. Its place of origin was found to be in the outer part of the Galactic plane at Galactic radii between 12.5 kpc

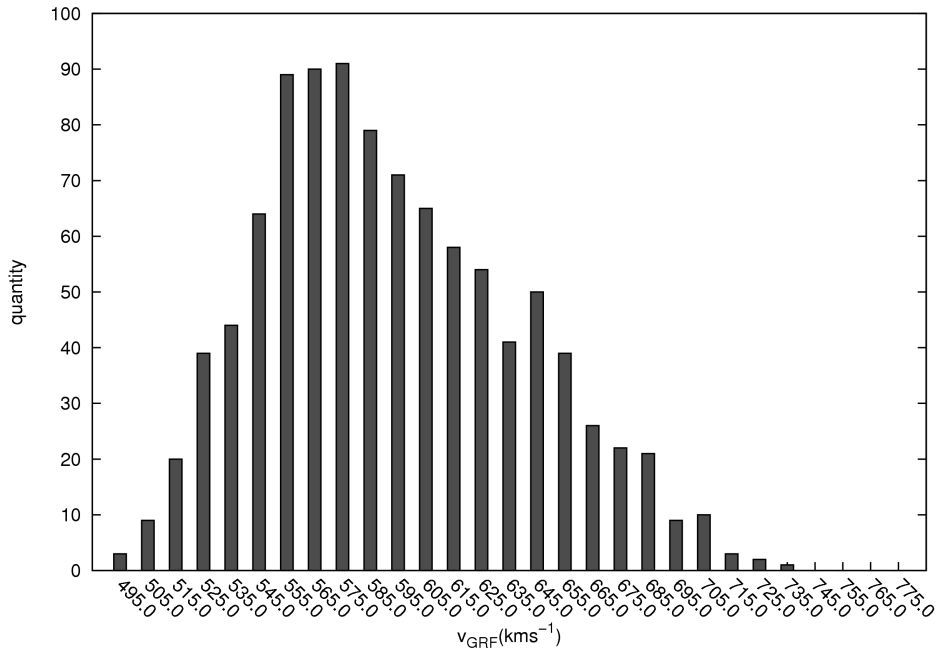


Figure 6.4: Galactic rest-frame velocity distribution for J0136+2425.

and 18 kpc. This is very similar to the cases of the massive B stars HD 271791 (Heber et al. 2008a) and HIP653 (Irrgang et al. 2010), which were the first ultra-high-velocity star whose proper motions exclude a GC origin. The ejection mechanism for both stars was proposed to be an extreme binary supernova, which also explained its enrichment in α elements. However, we find no evidence of α -enhancement in J0136+2425 from the existing spectra. The star is more metal-rich than expected on average for an object born at such a large Galactocentric distance. Due to the presence of Galactic abundance gradients (Rudolph et al. 2006), we expect the outer parts of the Galaxy to be less metal-rich than the Sun. The metallicity of J0136+2425 is compatible with the high end of the abundance distribution in the outer disk.

The required ejection velocity from the disk is so high (550 km s^{-1}) that an extreme supernova binary scenario as proposed for HD 271791 (Przybilla et al. 2008a) is very unlikely. We want to point out, that J0136+2425 is already the third star with particular high space velocity for which a GC origin can be ruled out. A fourth example is HE 0437–3954 believed to be ejected from the LMC, which has already been described in Section 2.2.6.

Most known HVS are late B-type stars of about $3 M_{\odot}$. With a mass of $2.45 M_{\odot}$, J0136+2425 resembles such a typical HVS much more than HD 271791 ($M = 11 M_{\odot}$) does. Hence, this is the first time that a typical HVS is found not to originate in the GC and excludes the SMBH slingshot mechanism. Accordingly typical HVS may have been ejected by different mechanisms other than that proposed by Hills.

Once more, this calls for an alternative ejection scenario to the Hills mechanism such

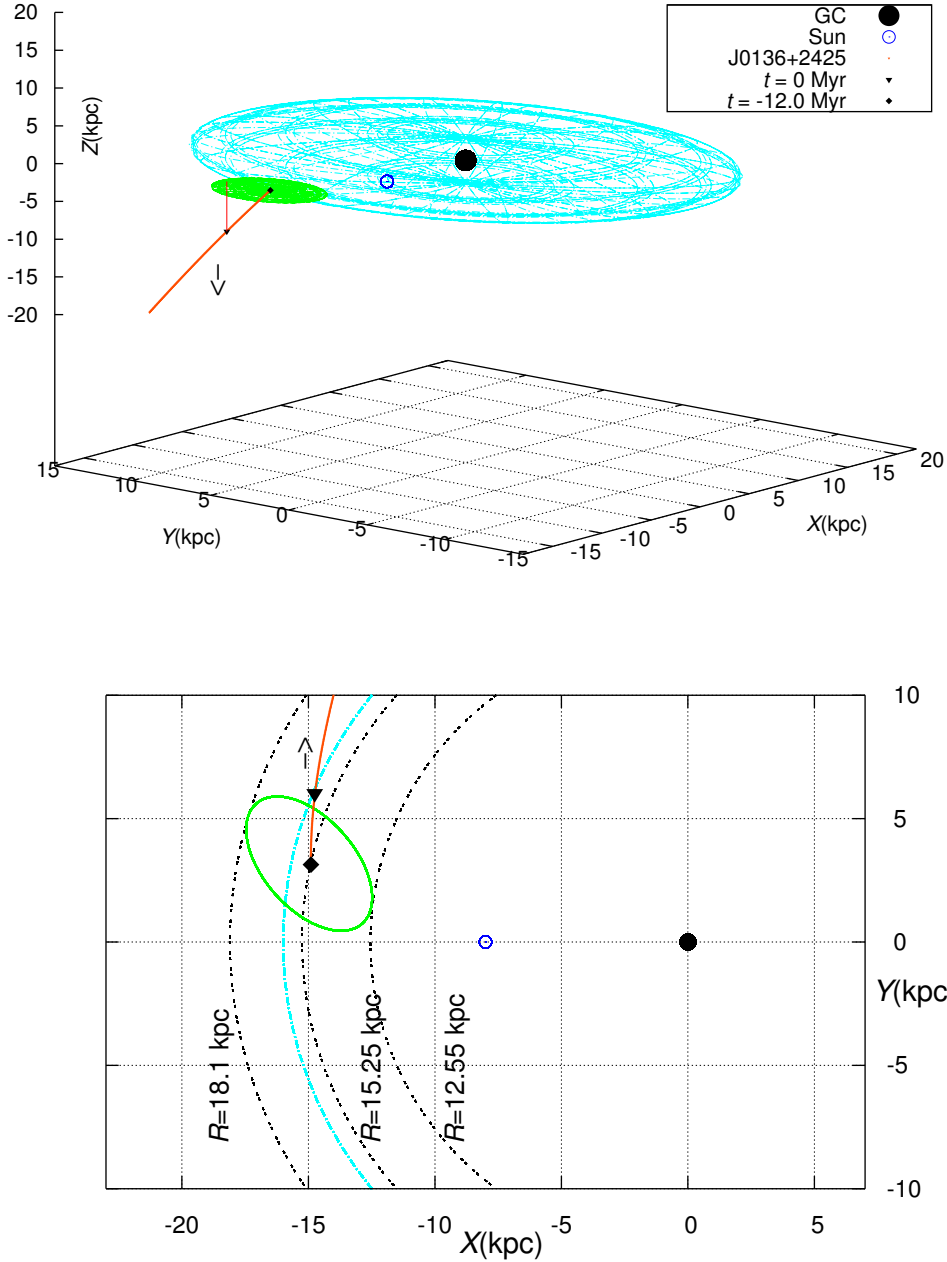


Figure 6.5: **Upper panel:** Trajectory for J0136+2425 with place of birth marked in green (3σ -error), relatively to the Galactic disk (light blue). The current position and the point of intersection with the Galactic plane are marked. Note that the Galactic centre is far from the plane intersection area. Hence it can not originate from the GC. **Lower panel:** Galactic disk (light blue) projection of the trajectory for J0136+2425 and intersection of the bunch of trajectories (green). The characteristic radii are indicated. as well as the current position and the point of intersection with the Galactic plane calculated with the best fitting parameters. Note that the GC is far from the plane intersection area.

as dynamical ejection from clusters or binary supernovae (see Gvaramadze et al. 2009). Hence, we are left with the dynamical ejection scenario or tidal disruption of a satellite galaxy, as proposed by Abadi et al. (2009). They noticed a clustering of more than half of the known HVS in a region of 26° -diameter in the constellation of Leo ($l_{II} \approx 230^\circ$, $b_{II} \approx 60^\circ$). They suggested that if these stars stem from a disruption event of a dwarf galaxy, more high velocity stars should be found in that area. However, J0136+2425 ($l_{II} = 136^\circ$, $b_{II} = -37^\circ$) is located far from Leo and is therefore probably unrelated.

The results presented in this section have already been published by Tillich et al. (2009b).

6.3 J1300+0422 - A halo blue straggler on a highly eccentric retrograde orbit

The second star with a high positive Galactic restframe velocity from the Xue et al. (2008) sample for which we could measure the proper motion was SDSSJ130005.62+042201.6 (J1300+0422 for short). This star was classified as a blue straggler by Xue et al. (2008).

Blue straggler (BS) stars were first discovered as an unusual subclass of stars in globular clusters (Sandage 1953). They lie on or near the main sequence but are more luminous than the turn-off stars, indicating that they are of higher mass than the latter. Apparently, BS are present in all the Galactic globular clusters (Piotto 2003).

Because the stars in a cluster are believed all to have formed at the same time, whereas the stellar turn-off age decreases with mass, BS should have evolved off the main sequence to become giants and white dwarfs long ago. It is generally believed that blue stragglers are coeval to the rest of stars in the cluster and originate from normal main-sequence stars that gained mass through a recent accretion episode. Most formation scenarios evoke mass transfer in and/or the merger of binary stars or collisions of stars.

Whether two types of BS exits in clusters, which may result from the different suggested mechanisms, has been discussed frequently in the literature. The discovery of two distinct sequences of BS in the globular cluster M 30 (Ferraro et al. 2009) indicates that indeed both formation mechanisms are at work.

In open clusters this does not seem to be the case, as Mathieu & Geller (2009) recently found a high frequency of binaries among the blue stragglers in the open cluster NGC 188, most having eccentric orbits with periods of about 1000 days. Brown et al. (2009) argue that most if not all BS in open clusters arise from multiple star systems. This suggests that blue stragglers are formed in both ways in star clusters, with collisions/mergers becoming more common with increasing cluster density.

In the Galactic field it is more difficult to identify BS because the stellar age can not be determined. Field blue stragglers are therefore usually identified as metal-poor main sequence objects that are hotter than globular cluster main-sequence turn-off stars. Nevertheless a lot of blue metal-poor stars $[Fe/H] < -1$ with main-sequence luminosities have been found to be hotter than the main-sequence turn-off of globular clusters and are therefore considered to be field analogs to the cluster BS population. Actually these stars seem to be so numerous that their specific frequency of appearance compared to regular horizontal-branch stars was found to be higher than in globular clusters (Preston & Sneden 2000). As the stellar density is small in the field, binary star evolution and mass transfer is probably the most common path of formation among field BS stars. Carney et al. (2001, 2005) pointed out that some BS candidates among metal-poor halo main-sequence stars are not binaries. Hence binary star evolution and mass transfer may not be the only path. They argue that the apparently single stars could be the partial remnants of an accreted dwarf satellite galaxy whose star formation continued over a long period of time. Hence those metal-poor main-sequence stars are simply young stars.

A detailed spectral analysis of a blue metal-poor star sample in the field by Preston & Sneden (2000) showed a very high binary fraction of at least 67%, dominated by long

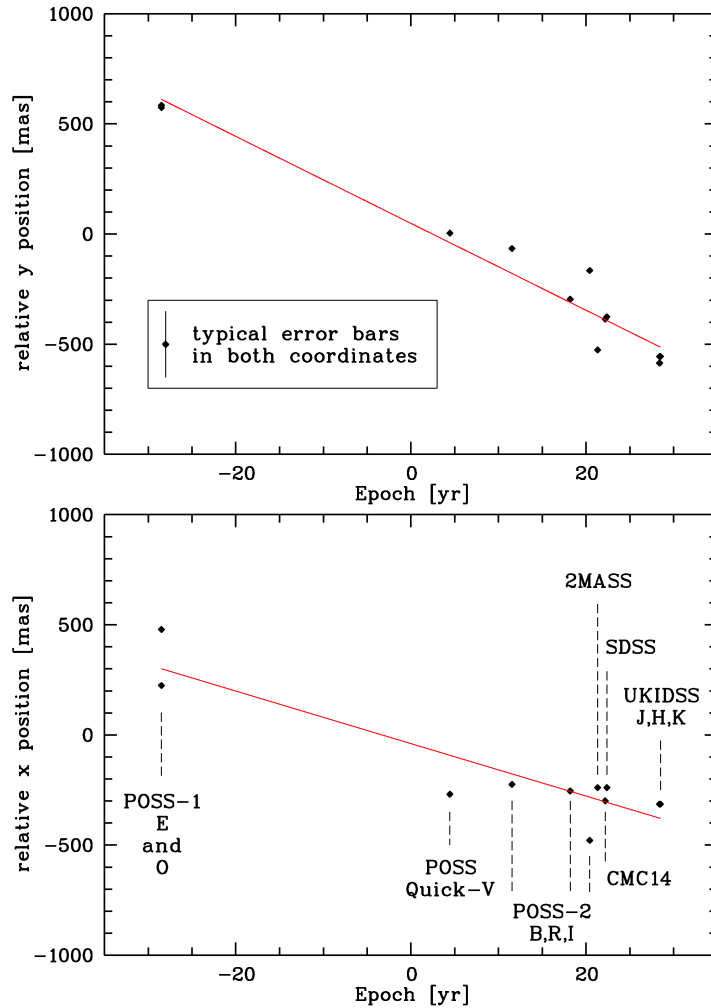


Figure 6.6: Linear fit of the position measurements for J1300+0422, where 1978.84 is the zero epoch.

period (wide) binaries. This population appears to be very similar to that of the open cluster NGC 188 (Mathieu & Geller 2009). Assuming a formation by Roche lobe overflow during the red giant branch stage of the primary, Preston & Sneden (2000) identified at least half of the blue metal-poor stars in their survey as blue stragglers. This is supported by more recent and much larger surveys for faint blue stars in the halo. For example, Xue et al. (2008) found that blue stragglers account for half of their sample of more than 10 000 A-type stars.

In the following sections we present a detailed quantitative spectral analysis of J1300+0422 and study its kinematics.

6.3.1 Spectroscopy

J1300+0422 is the brightest of our 17 targets (see Section 6.1) for which we conducted a proper motion measurement as described in Section 4.3. We found a highly significant proper motion of $\mu_\alpha \cos \delta = -11.9 \pm 1.7 \text{ mas yr}^{-1}$ and $\mu_\delta = -19.7 \pm 1.4 \text{ mas yr}^{-1}$, which is shown in Figure 6.6.

In order to search for radial velocity variations, we re-observed J1300+0422 with the TWIN spectrograph at the 3.5m telescope on Calar Alto on May 2009. The radial velocity (heliocentric $v_{\text{rad}} = 515.3 \pm 8 \text{ km s}^{-1}$) was derived by χ^2 -fitting of adequate synthetic spectra over the full spectral range.¹ It was found to be consistent with that measured from the *SDSS* spectrum (heliocentric $v_{\text{rad}} = 504.6 \pm 5 \text{ km s}^{-1}$). Details on the obtained data are given in Table 6.1.

We also inspected three individual *SDSS* spectra which were taken one after the other. No variations were found. This indicates that large radial velocity variations on small timescales are unlikely, but we can not rule out small RV variations over long periods as observed in many BS (Carney et al. 2005).

A quantitative analysis of the co-added *SDSS* spectrum of J1300+0422 was carried out following the hybrid NLTE approach discussed by Przybilla et al. (2006). The effective temperature T_{eff} and the surface gravity $\log g$ were determined by fits to the Stark-broadened Balmer and Paschen lines and the ionisation equilibrium of Mg I/II (see Chapter 3). A microturbulent velocity of 2 km s^{-1} was adopted and a mixing-length to pressure scale-height ratio ℓ/H of 1.25 for the convective atmosphere. The stellar metallicity was derived by model fits to the observed metal line spectra. Results are listed in Table 6.4 and a comparison of the resulting final synthetic spectrum with observation is shown in Figure 3.3. Overall, excellent agreement is obtained for the strategic spectral lines throughout the entire wavelength range. The uncertainties in the stellar parameters were constrained by the quality of the match of the spectral indicators within the given S/N limitations.

It may be instructive at this point to take a closer look on the spectrum synthesis in NLTE and LTE, as this has so far not been done for Population II blue straggler stars². A few comparisons of NLTE and LTE profiles are therefore shown in the insets in Figure 3.3. The combination of a higher T_{eff} than typically found for Population II stars and the diminished line blocking because of the low metal content results in a hardened radiation field which leads to pronounced NLTE effects on many diagnostic lines. NLTE strengthening is found for the Doppler core of $\text{H}\alpha$ – in line with the behaviour in cooler (e.g. Przybilla & Butler 2004b) as well as in hotter stars (e.g. Nieva & Przybilla 2007) –, while the inner line wings are weakened. The higher Balmer and Paschen lines show much lower deviations from LTE. Our calculations predict the majority of the weak metal-lines to be described well by the assumption of LTE. On the other hand, many of the stronger

¹As we made use of many spectral lines our results differ from that of Xue et al. (2008) who used cross-correlation for RV and the $\text{H}\gamma + \text{H}\delta$ lines for stellar type determination only.

²De Marco et al. (2005) presented global fits of partially line-blanketed NLTE model atmospheres to several blue straggler stars in globular clusters. However, the differences between NLTE and LTE model spectra were not elaborated there.

Table 6.4: Results of the quantitative spectroscopic and kinematic analysis of J1300+0422 using the maps of (Schlegel et al. (1998)). The resulting GRF velocity v_{grf} and the local escape velocity v_{esc} , also in a more massive halo $v_{\text{esc}}^{\text{a}}$, are given.

V (mag) ^a	15.12 ± 0.02	$E(B - V)$ (mag) ^b	0.05 ± 0.02
T_{eff} (K)	7350 ± 200	$\log g$ (cgs)	4.00 ± 0.15
$[m/H]$	-1.2α	M/M_{\odot}	1.15 ± 0.10
v_{rad} (km s ⁻¹)	504.6 ± 5	$v_{\text{rot}} \sin i$ (km s ⁻¹)	-
d (kpc)	3.25 ± 0.62	v_{grf} (km s ⁻¹)	467^{+41}_{-21}
v_{esc} (km s ⁻¹)	529	$v_{\text{esc}}^{\text{a}}$	708

^a The visual magnitude has been derived from *SDSS* photometry following Jordi et al. (2006)

^b The interstellar colour excess $E(B - V)$ has been determined by comparing the observed colours to synthetic ones from the model spectral energy distribution.

metal lines, as e.g. those shown in the insets in Figure 3.3, show pronounced NLTE strengthening.

In order to reproduce the NLTE equivalent widths of these particular lines, abundance corrections need to be applied of about +0.2 dex (Mg I/II, Fe II), +0.5 dex (O I) and +0.8 dex (C I) in LTE. Note, however, that these lines are close to saturation. LTE computations with increased abundances can therefore not reproduce the NLTE line depths at all, instead stronger line wings develop. Abundance studies based on equivalent widths may therefore be misleading, as such differences remain unnoticed. An investigation at high spectral resolution would therefore be worthwhile in order to facilitate the NLTE effects to be studied in detail.

Its T_{eff} and gravity places J1300+0422 on the main sequence (see Figure 6.7) at a mass of $1.15 M_{\odot}$ as derived by comparing the position of the star to predictions of the evolutionary models of Schaller et al. (1992). No rotational broadening was detected. The metallicity is lower than solar by a factor of almost 20 and the abundances of the α -elements (those from O to Ti) are enhanced by ~ 0.3 – 0.4 dex, which is typical for the halo population. This suggests the star to be a halo blue straggler. All results are summarised in Table 6.4.

6.3.2 Kinematics

As for the other two stars, we performed the same analysis as described in Section 6.2.2 and derived the median GRF velocity from the Monte-Carlo distribution in Figure 6.8. The local escape velocity is calculated from the Galactic potential of Allen & Santillan (1991). Hence the GRF velocity of 467^{+41}_{-21} km s⁻¹ is still below the local escape velocity of $v_{\text{esc}} \approx 529$ km s⁻¹ and J1300+0422 is bound to the Galaxy.

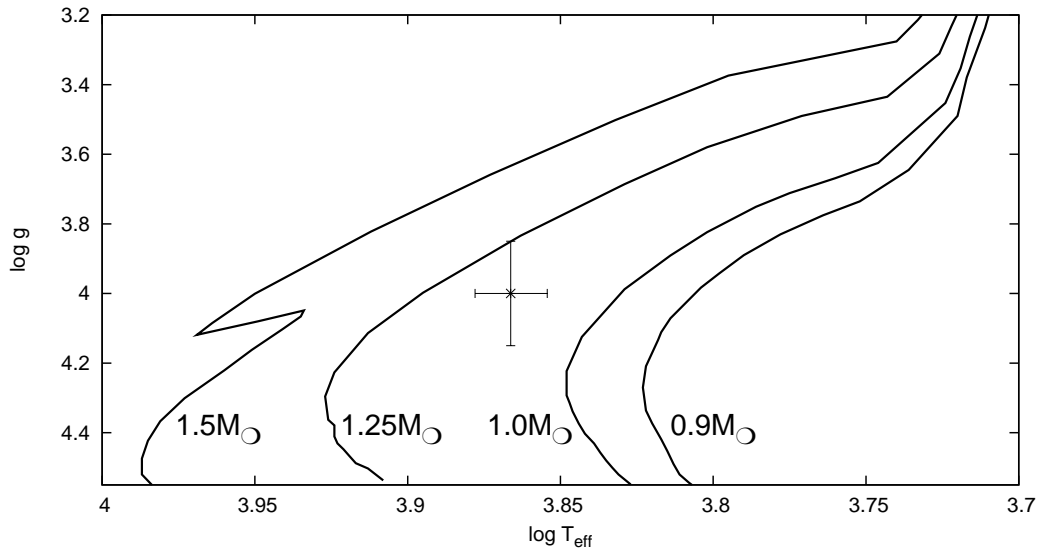


Figure 6.7: Comparison of the position of J1300+0422 in the $(T_{\text{eff}}, \log g)$ diagram to evolutionary tracks of Schaller et al. (1992) for sub-solar metallicity ($Z = 0.001$) in order to determine its mass.

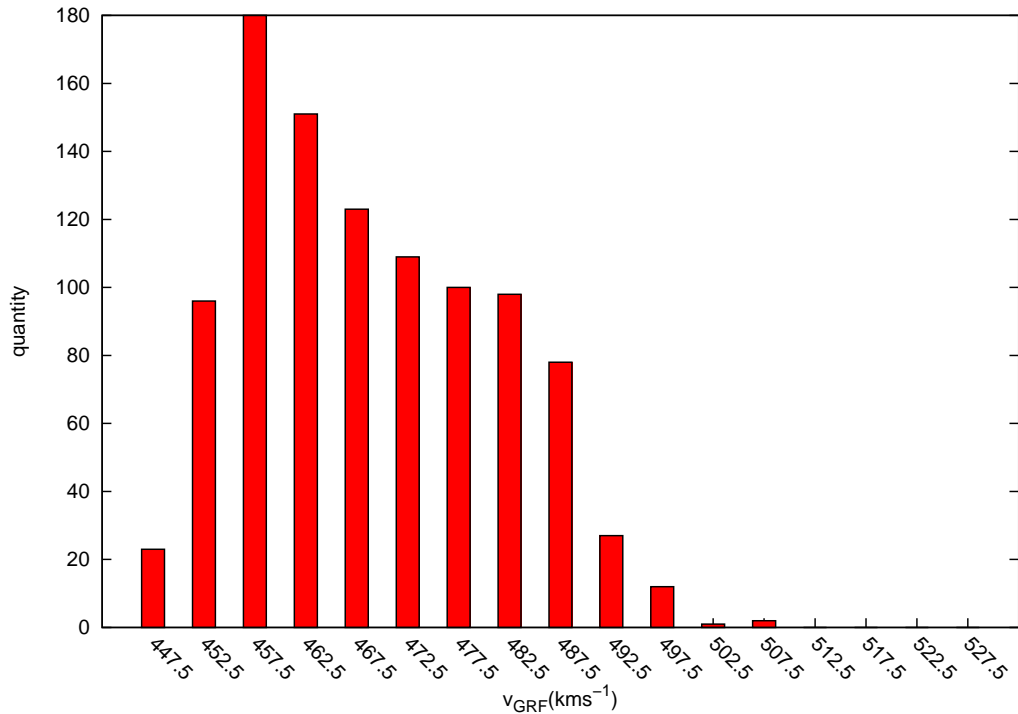


Figure 6.8: Galactic restframe velocity distribution for J1300+0422 derived from a Monte Carlo procedure with a depth of 1000.

To further quantify the kinematics of the star, we made a comparison to the work of Pauli et al. (2006). Based on the 3D-orbit, the $V - U$ diagram and the eccentricity e together with the Z -component of the angular momentum J_Z they introduced a kinematic population classification scheme and combined it with age information. They analysed 398 DA white dwarfs from the SPY project, which is the largest homogeneous sample of that kind and performed a detailed kinematic analysis accounting for errors by means of a Monte Carlo error propagation code, similar to our method. Finally they performed a consistency check with a sample of typical main-sequence stars and derived the 3σ -contours for the $V - U$ diagram on which the classification is based. For the $-e - J_Z$ diagram a “Region B” is defined such that it excludes as many thin-disk stars as possible. The last criterion is the 3D-orbit, which is classified by comparison with template Galactic orbits (Pauli et al. 2003). A substantial thick disk fraction of 7% was found, while only 2% of the DA show characteristic halo properties.

Following this approach we revealed that J1300+0422 clearly belongs to the halo population. This is obvious in Figure 6.9, which shows the characteristic $V - U$ and $e - J_Z$ diagrams in relation to the reference white dwarf sample of Pauli et al. (2006). Note that the orbit of J1300+0422 is retrograde and highly eccentric. Furthermore the star probes far out into the halo up to distances of more than 100 kpc (see Figure 6.10). Whether the star is bound to the Galaxy depends on the Galactic potential adopted, in particular on the dark matter halo, as pointed out by Abadi et al. (2009). In our standard potential (Allen & Santillan 1991) we adopted a halo mass out to 100 kpc of $M_{\text{Halo}} = 8 \times 10^{11} M_{\odot}$. The analysis of J1539+0239 (Przybilla et al. 2010, see also Section 6.4) suggested a higher halo mass. Hence we repeated our analysis accordingly and found a higher escape velocity of $v_{\text{esc}} \approx 708 \text{ km s}^{-1}$, which means that the star would be bound in any case. The effect on the angular momentum was negligible, while the orbit became significantly less eccentric (see Figure 6.9). Hence the star might have crossed the disk even more often within its lifetime.

6.3.3 Conclusion

We reported the quantitative spectral analysis of a high-velocity star from the sample of faint blue stars in the halo of Xue et al. (2008). Radial velocity, proper motion and spectroscopic distance were derived and a detailed kinematical analysis was performed using the Galactic potential of Allen & Santillan (1991) as well as an modified one, that accounts for a more massive Galactic dark matter halo.

The metal-poor A-type star J1300+0422 was identified as a blue straggler of $1.15 M_{\odot}$ due to its main-sequence gravity. A detailed NLTE analysis was performed, which we compared to the standard LTE approach. Significant differences were found especially for C I and O I. With its low metallicity of $[Fe/H] = -1.2$ and the characteristic enhancement of α -elements it would fit perfectly in the sample of Preston & Snenen (2000), apart from the huge space velocity of the star. The kinematical characteristics (U, V, J_Z) confirm the halo membership of J1300+0422 beyond any doubt. Additionally, its trajectory probes far out into the halo and might have crossed the Galactic disk severalfold within its lifetime.

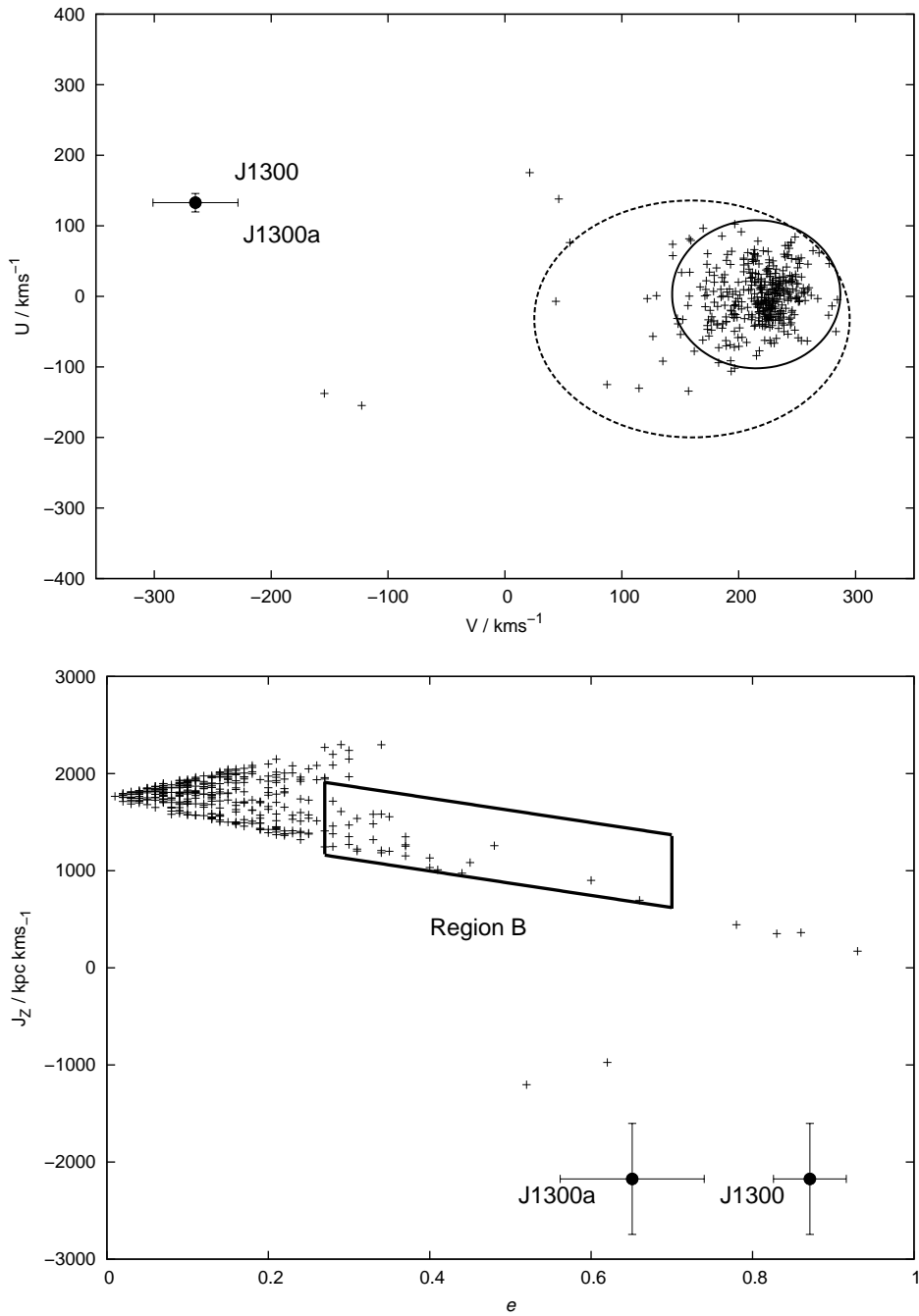


Figure 6.9: $V - U$ (*top*) and $e - J_z$ diagram (*bottom*) for J1300+0422. The white dwarf sample (+) of Pauli et al. (2006) serves as reference. The ellipses in $U - V$ diagram show the thin and thick disk contours (solid and dashed lines respectively), halo stars lie outside of these ellipses. In the lower panel, the left-hand triangle-shaped cloud of stars are the thin disk white dwarf population while the solid box marks the thick disk region (Region B). Note that in both diagrams J1300+0422 lies far away from the disk populations. In case of a higher Galactic halo mass (Przybilla et al. 2010) the position is marked with J1300a.

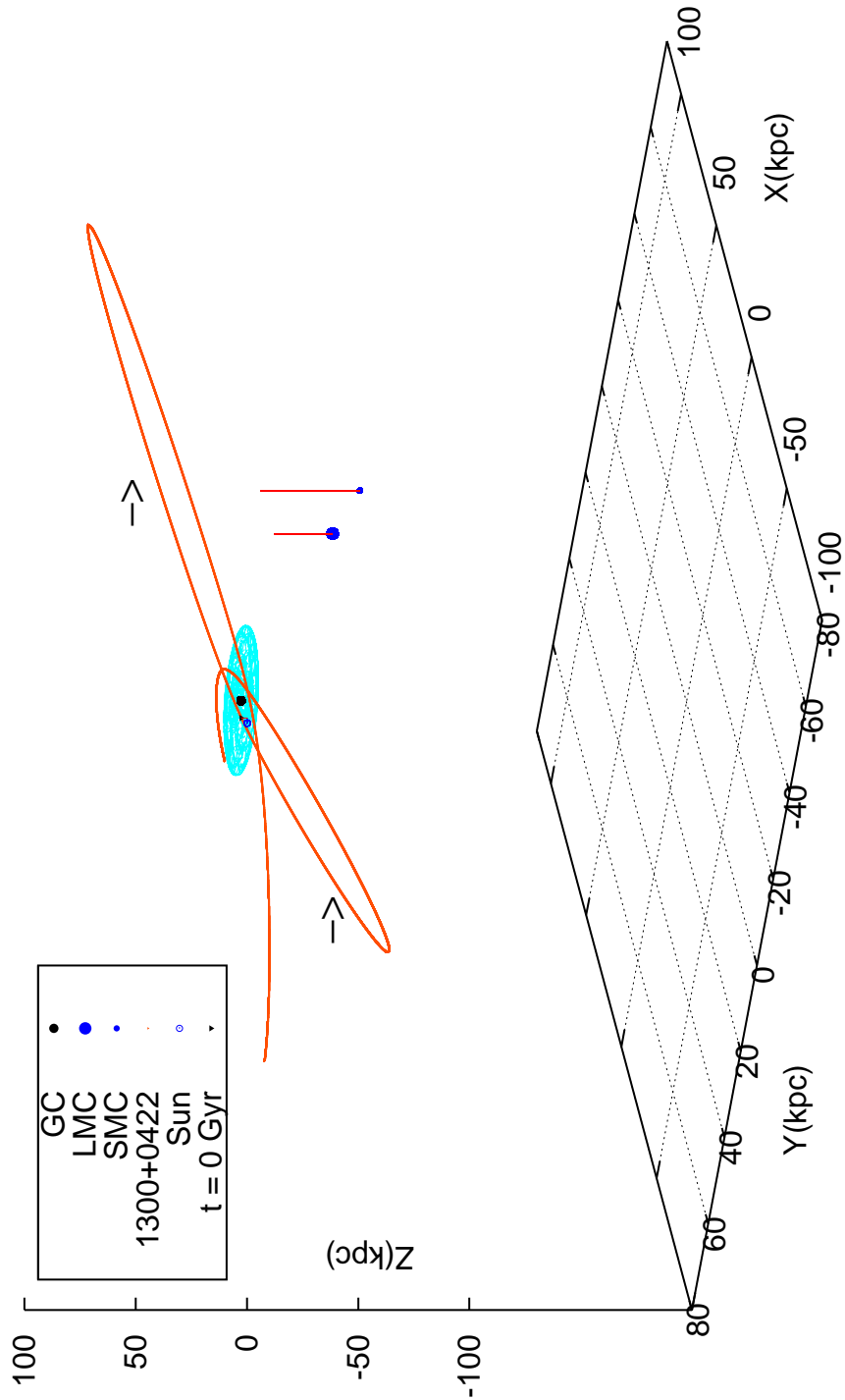


Figure 6.10: Trajectory for the metal-poor blue straggler J1300+0422, relative to the Galactic disk (light blue), calculated for ± 2 Gyrs in time. The arrows show the travel direction and current position is marked.

Many blue stragglers were found to be long period binaries (with periods of several 100 to 1,000 days; Carney et al. 2005; Mathieu & Geller 2009) with low radial velocity semi-amplitudes ($K \sim 5 - 10 \text{ km s}^{-1}$, Carney et al. 2001, 2005). Whether or not J1300+0422 is such a binary needs to be verified by an extensive radial velocity study.

The results of this section have been submitted for publication to A&A (Tillich et al. 2010d).

6.4 J1539+0239 - weighing the Galactic dark matter halo: a lower mass limit from the fastest halo star known

In Section 6.1 we introduced the sample of Xue et al. (2008), which already served as input for a search for high GRF velocity objects. Here we discuss the stars with negative RVs, i.e. approaching us, which are completely different high-velocity objects as they cannot be unbound HVS ejected from the SMBH in our Galactic centre. Nevertheless these extreme halo objects can be of tremendous importance to constrain the Galactic halo mass.

Knowledge of the properties of dark matter halos is an important issue for our understanding of galaxy formation and evolution, and for unveiling the nature of dark matter. The halo of the Milky Way therefore is of highest interest, as it allows unique observational constraints to be obtained for testing theoretical models (e.g. Navarro et al. 1996). Several observational campaigns – e.g. the Sloan Digital Sky Survey (York et al. 2000), the Radial Velocity Experiment (*RAVE*, Steinmetz et al. 2006), the Sloan Extension for Galactic Understanding and Exploration (*SEGUE*, Yanny et al. 2009) – provide the tracers for studying halo properties such as the total mass of the halo and its extent.

Several studies in the past decade determined the halo mass from ever increasing samples of halo stars, globular clusters and/or satellite galaxies. While larger halo masses of about $2 \times 10^{12} M_{\odot}$ were favoured earlier (Wilkinson & Evans 1999; Sakamoto et al. 2003), lower masses of about half this value were derived more recently (Battaglia et al. 2005; Smith et al. 2007; Xue et al. 2008). The precise value determines, among others, whether satellite galaxies like the Magellanic Clouds (e.g. Kallivayalil et al. 2006; Costa et al. 2009) or hyper-velocity star candidates (Abadi et al. 2009) are on bound orbits, or not.

Amazingly one star alone can already put constraints on the Galactic dark halo, if the kinematics are remarkably enough. *SDSS*J153935.67+023909.8 (J1539+0239 for short) from the sample of Xue et al. is one of that kind (see Section 6.4.3).

J1539+0239 is the brightest of the 6 targets with negative RV and the second brightest of the total GRF sample. We measured its proper motion (see Section 4.3) and found it to be highly significant with values of $\mu_{\alpha} \cos \delta = -10.6 \pm 1.6 \text{ mas yr}^{-1}$ and $\mu_{\delta} = -10.0 \pm 2.3 \text{ mas yr}^{-1}$. Figure 6.11 shows the plot for our measurement.

6.4.1 Spectroscopy

In order to exclude radial velocity (RV) variability, we re-observed J1539+0239 with the TWIN spectrograph at the 3.5m telescope on Calar Alto in May 2009. Radial velocities were derived by χ^2 -fitting of adequate synthetic spectra over the full spectral range, yielding a heliocentric radial velocity of $v_{\text{rad}} = -366.6 \pm 4.0 \text{ km s}^{-1}$ for the TWIN spectrum, which is consistent with the $v_{\text{rad}} = -372.6 \pm 5.8 \text{ km s}^{-1}$ measured from the *SDSS* data within the mutual uncertainties. We use the latter value for the kinematic study. Details on the obtained data are given in Table 6.1.

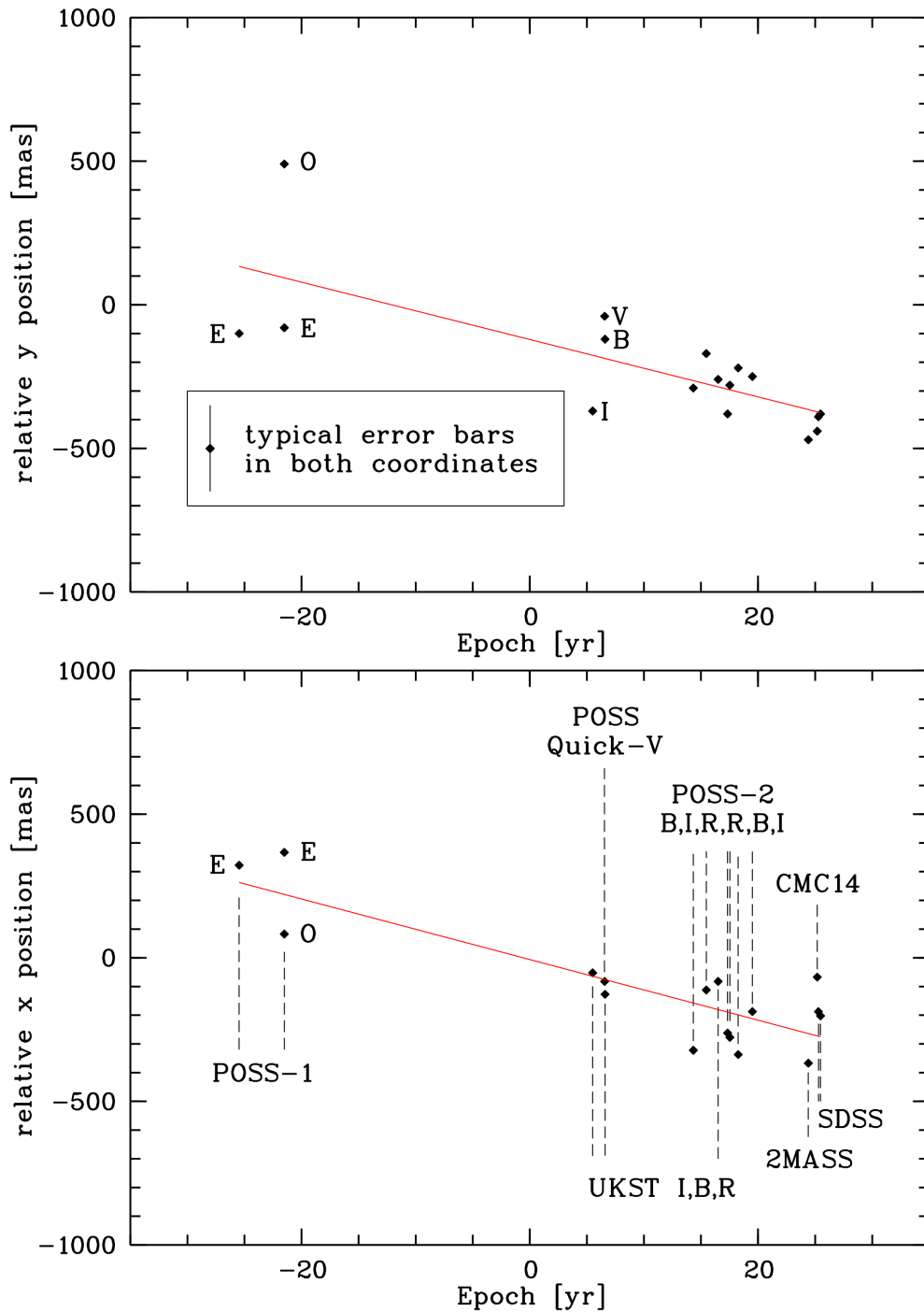


Figure 6.11: Linear fit of the position measurements for J1539+0239, where 1975.39 is taken as zero epoch.

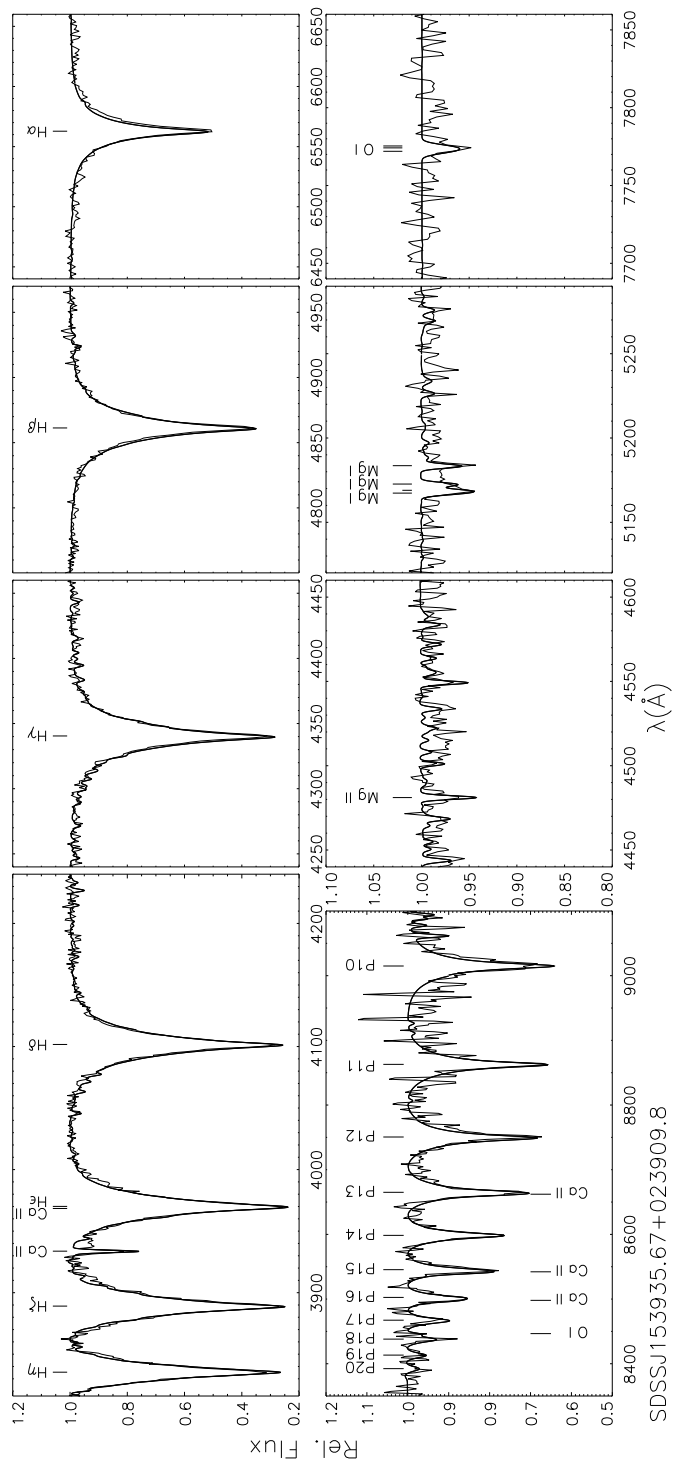


Figure 6.12: Comparison of NLTE spectrum synthesis (thick line) with observation (thin wiggly line) for J1539+0239. Displayed are selected regions around the Balmer lines, the higher Paschen series, Mg II $\lambda 4481\text{\AA}$, the Mg I b and the near-IR O I triplets.

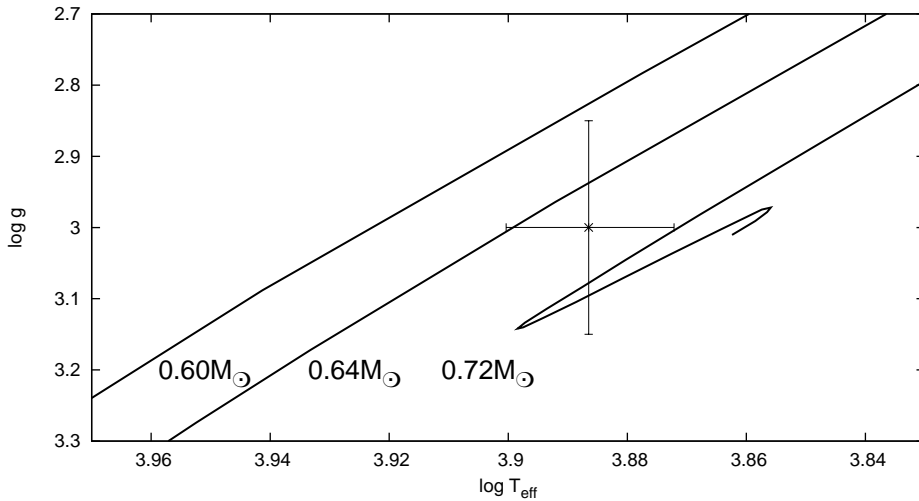


Figure 6.13: J1539+0239 in the $(T_{\text{eff}}, \log g)$ diagram with evolutionary tracks of Dorman (1992) for subsolar metallicity.

Again a quantitative analysis of J1539+0239 was carried out, in analogy to the one for J0136+2425 (Section 6.2.1). Following the hybrid NLTE approach described in Chapter 3 using the Stark-broadened Balmer and Paschen lines and the ionisation equilibrium of Mg I/II in this particular case to determine stellar parameters. Results are listed in Table 6.5 and a comparison of the resulting final synthetic spectrum with observation is shown in Figure 6.12. Overall, excellent agreement is obtained for the strategic spectral lines throughout the entire wavelength range. Our stellar parameters ($T_{\text{eff}} = 7700 \pm 250$ K, $\log g = 3.00 \pm 0.15$) are consistent with those derived in the LTE analysis by Xue et al. (2008): $T_{\text{eff}} = 7807$ K, $\log g = 3.16$. However our values are regarded as more accurate as we use all spectral lines. We constrained the errors in the stellar parameters by the quality of the match of the spectral indicators within the given S/N limitations.

Its parameters place J1539+0239 on the horizontal branch (see Figure 6.13) at a mass of $0.68 \pm 0.05 M_{\odot}$ as derived by comparing the position of the star in the $T_{\text{eff}} - \log g$ -diagram to predictions of the evolutionary models of Dorman et al. (1993). No rotational broadening was detected at the resolution of the *SDSS* spectrum. The metallicity is lower than solar by a factor of 100 and the abundances of the α -elements are enhanced by 0.4 dex with respect to iron, which is typical for the halo population. We conclude that the star is a horizontal branch star of Population II. All results are summarised in Table 6.5.

6.4.2 Kinematics

We performed the same analysis as described in Section 6.2.2 and derived the median GRF velocity from the Monte-Carlo distribution in Figure 6.14.

For J1539+0239 the GRF velocity of 694_{-221}^{+300} km s $^{-1}$ is above the local escape velocity of $v_{\text{esc}} \approx 519$ km s $^{-1}$ in the potential of Allen & Santillan (1991). Furthermore J1539+0239

Table 6.5: Results of the quantitative spectroscopic and kinematic analysis of J1539+0239. The resulting GRF velocity v_{GRF} and the local escape velocity v_{esc} are given.

V (mag) ^a	15.72 ± 0.02	$E(B - V)$ (mag) ^b	0.04 ± 0.03
$\mu_{\alpha} \cos \delta$ (mas yr ⁻¹)	-10.6 ± 1.6	μ_{δ} (mas yr ⁻¹)	-10.0 ± 2.3
T_{eff} (K)	7700 ± 250	$\log g$ (cgs)	3.00 ± 0.15
$[m/H]$	-2.0α	$[\alpha/\text{Fe}]$	$+0.4$
M/M_{\odot}	0.68 ± 0.05	d (kpc)	12.0 ± 2.3
v_{rad} (km s ⁻¹)	-372.6 ± 5.8	v_{GRF} (km s ⁻¹)	694^{+300}_{-221}
v_{esc} (km s ⁻¹)	519		

^a The visual magnitude has been derived from *SDSS* magnitudes following Jordi et al. (2006)

^b The interstellar colour excess $E(B-V)$ has been determined by comparing the observed colours to synthetic ones from the model spectral energy distribution.

is the fastest halo star known, superseding even the previous record holder CS 22183-0014 (at $v_{\text{GRF}} = 635 \pm 127$ km s⁻¹ Sakamoto et al. 2003).

J1539+0239 is located in the northern Galactic hemisphere ($l = 9.0$, $b = 42.95$), in the direction close to the Sagittarius stream (Belokurov et al. 2006; Fellhauer et al. 2006) and in particular close to the globular clusters *NGC 5904* and *Palomar 5*, with its tidal tail (Odenkirchen et al. 2003). However, it is unlikely that J1539+0239 is related to either of those because of its distinct space motion and its position in the foreground.

In order to keep the trajectory of J1539+0239 bound to the Galaxy, the dark matter halo mass needs to be adjusted. We carried out numerical experiments increasing the halo density by a constant factor. Finally we found a bound trajectory for a minimum mass of $M_{\text{halo}}^{\text{new}} = 1.7 \times 10^{12} M_{\odot}$. The apocentre distance of the star’s trajectory is located far out in the halo, at ~ 250 kpc in this case. If we take into account the full velocity distribution (see Figure 6.14) of the star we even can derive solutions for the extrema, which correspond to the absolute errors. In that case the total halo mass of the Galaxy is determined to $M_{\text{halo}}^{\text{new}} \geq 1.7^{+2.3}_{-1.1} \times 10^{12} M_{\odot}$. This value corresponds to an upper limit of 5.9% for the fraction of visible to dark matter in the Galaxy.

Whether the star is bound to the Galaxy highly depends on the Galactic potential adopted, in particular on the mass of the dark matter halo, as pointed out by Abadi et al. (2009). Remarkably our value is similar to several recent studies. Wilkinson & Evans (1999) used 27 satellite galaxies and globular clusters, by assuming that they are bound and derived a total Galactic halo mass of $M_{\text{halo}} \sim 1.9^{+3.6}_{-1.7} \times 10^{12} M_{\odot}$. This value matches our derivation but has a larger uncertainty. Sakamoto et al. (2003) used 11 satellite galaxies, 137 globular clusters and 413 field horizontal branch stars to derive a total Galactic mass. They used only the half of objects for which proper motions were measured as they noticed that the potential is largely determined by a few high velocity objects. The exclusion of Leo I from their sample would lower the total Galactic mass

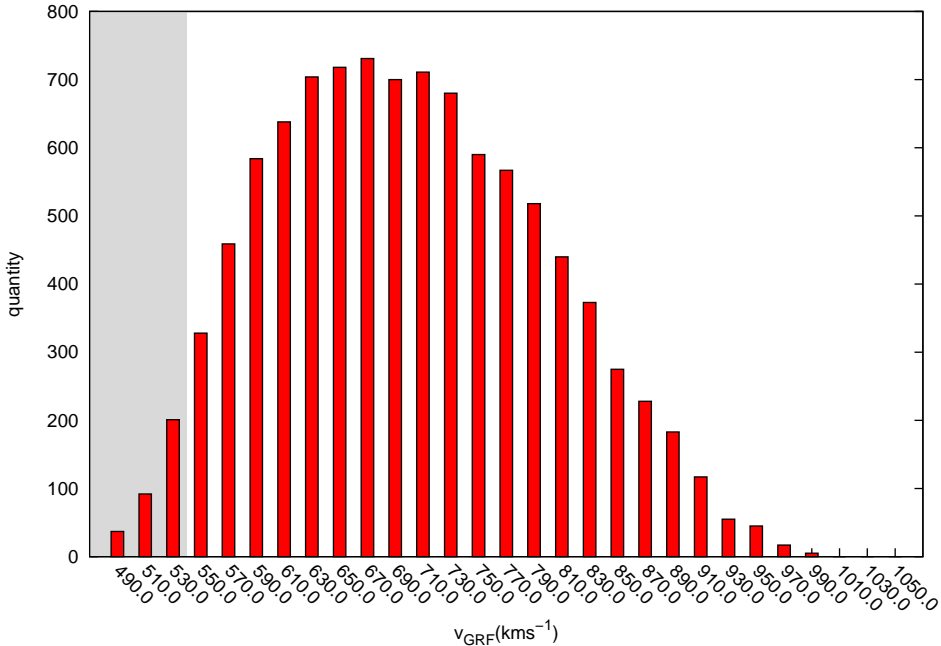


Figure 6.14: Galactic restframe velocity distribution for J1539+0239 derived from a Monte Carlo procedure with a depth of 10,000. The grey shaded area indicates the fraction of trajectories that would be bound for $M_{\text{halo}} = 1.0 \times 10^{12} M_{\odot}$, the most likely halo mass of Xue et al. (2008).

from $M_{\text{total}} \sim 2.5_{-1.0}^{+0.5} \times 10^{12} M_{\odot}$ to a value of $M_{\text{total}} \sim 1.8_{-0.7}^{+0.4} \times 10^{12} M_{\odot}$, again both values are in excellent agreement with our finding.

On the other hand, our lower limit is just about consistent with the $M_{\text{halo}} = 1.0_{-0.2}^{+0.3} \times 10^{12} M_{\odot}$ derived by Xue et al. (2008) from the RV study of ~ 2400 blue horizontal-branch stars, including J1539+0239. Less than 4% of the trajectories resulting from our MC simulations would be bound for the most likely mass of Xue et al. (grey shaded area in Figure 6.14). The halo mass of Xue et al. therefore tends to be underestimated.

6.4.3 Conclusion

We performed the quantitative spectral analysis of a high-velocity star from the sample of faint blue halo stars of Xue et al. (2008). J1539+0239 was confirmed to be a Population II horizontal branch star with a low metallicity of $[\text{Fe}/\text{H}] = -2.0$ and the characteristic enhancement of α -elements. Radial velocity, proper motion and spectroscopic distance were derived and a detailed kinematical analysis was performed.

Carrying out kinematical numerical experiments using the Galactic potential of Allen & Santillan (1991) in order to obtain an orbit of J1539+0239 gravitationally bound to the Milky Way, we found that the mass of the dark halo has to be at least $M_{\text{halo}} \sim 1.7_{-1.1}^{+2.3} \times 10^{12} M_{\odot}$. This mass limit is in good agreement with several previous studies (Wilkinson

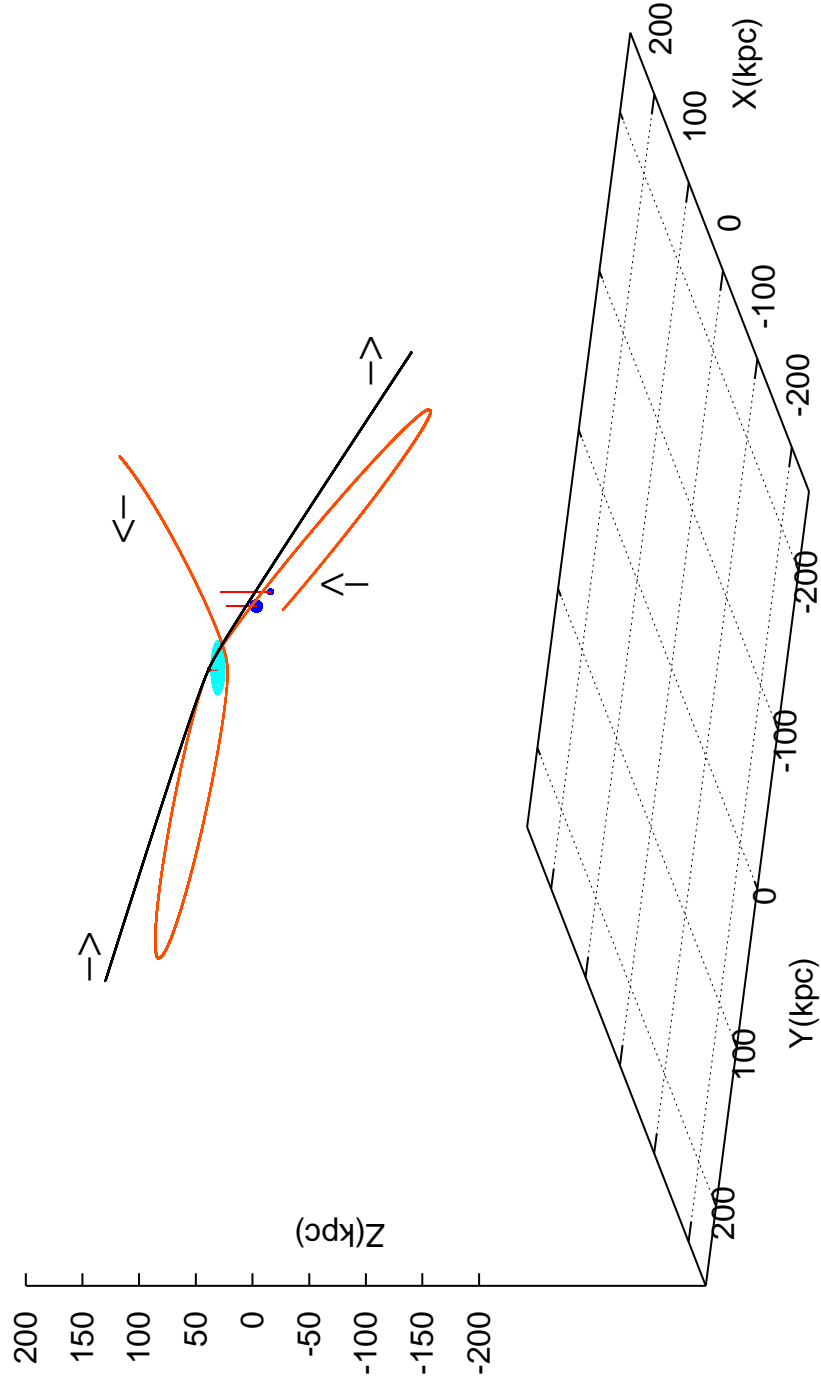


Figure 6.15: Trajectories for the metal-poor horizontal branch star J1539+0239, relatively to the Galactic disk (light blue). Applying a standard potential (Allen & Santillan 1991) the trajectory is unbound (black, $t \approx \pm 0.5$ Gyr), while increasing the halo density we found a bound trajectory (red, $-3 \text{ Gyr} \lesssim t \lesssim +2 \text{ Gyr}$). For reference the Magellanic Clouds and the current position are marked.

& Evans 1999; Sakamoto et al. 2003; Abadi et al. 2009) but just about consistent with the results from the analysis of the sample that J1539+0239 was drawn from Xue et al. (2008), which in consequence tends to underestimate the Galactic dark halo mass.

We conclude, that because the kinematics of this halo star is extraordinary enough, and the errors within the analysis are sufficiently small, even *this one* star alone can provide a significant lower limit to the dark matter halo mass, and to the total mass of the Milky Way, here $M_{\text{total}} \geq 1.8_{-1.1}^{+2.3} \times 10^{12} M_{\odot}$. The determining factor is that full kinematic information is available, as it will become routine in the era of the GAIA space mission, at much higher precision.

The results of this section are submitted for publication in ApJ (Przybilla et al. 2010).

Chapter 7

The Hyper-MUCHFUSS project

In the Galactic halo most of the stars can be found in the remarkable densely packed globular clusters, which consist of metal-poor stars only. When Arp (1955) analysed seven globular clusters, he found them to look indeed very similar in the colour-magnitude diagram. They all show strong blue horizontal branches, which characterises a population of evolved stars already in the helium burning phase. Additionally all of them turned out to be comparably metal-poor. From that point it was clear that the stars in globular clusters must be chemically very homogeneous and the horizontal branches define their morphology. Furthermore their kinematics are very similar, which is the reason why they are excellent tracers to probe the gravitational potential of their host galaxies (Dinescu et al. 1999; Hwang et al. 2008). Nevertheless there are still important unsolved problems in the understanding of globular cluster like the “second parameter problem”. Even in clusters with the same metallicity the morphology can be very different. Theoretical modelling of HB showed that several parameters like age, rotation or helium surface abundance (Lee et al. 1990) can change the morphology of the cluster and have to be discussed individually.

But there are also other stars found in the halo, which are not obviously linked to Globular clusters. Maybe the most interesting ones of these stars are subdwarf B stars. A detailed introduction of subdwarfs is given in Section 2.1.4. Briefly hot subdwarf stars (sdB/sdOs) are considered to be helium core burning stars with very thin ($<0.02 M_{\odot}$) inert hydrogen envelopes and masses around $0.5 M_{\odot}$. Due to their exceptional evolutionary state, their spectra are quite unique. Following ideas outlined by Heber (1986), the sdBs can be identified with models for extreme horizontal-branch stars (Greenstein & Sargent 1974). An EHB star bears great resemblance to a helium main-sequence star of half a solar mass and it should evolve similarly, i.e. directly to the white dwarf cooling sequence, bypassing a second giant phase. Up to now, the only kinematical study of such sdBs in the halo was performed by Altmann et al. (2004). From a sample of 114 sdBs they found only 15 to have orbits which differ considerably from disk orbits, while the vast majority is consistent with a thick disk population. This is in high contrast to the cooler HB A-type stars, which are predominantly or even exclusively halo objects. Hence it can be doubted, whether both types are of the same origin. Various runaway scenarios such as binary interaction inside star clusters (Leonard & Duncan 1988) or ejection by binary supernova

explosion (Blaauw 1961) might provide useful explanations.

However, finding subdwarfs in the halo and unravelling their kinematics may shed light on their evolution and is of high interest, as it provides extraordinary insight into the halo dynamics. Therefore the Hyper-MUCHFUSS (Hyper-velocity stars or Massive Unseen Companions of Hot Faint Underluminous Stars from *SDSS*) project targets the detection of a fast (halo) population amongst hot subdwarf stars. The following sections are based on partially published work (Tillich et al. 2009a, 2010a,b,c).

7.1 Aims

In the Hyper-MUCHFUSS project we devised a search strategy that allows us to follow two aims simultaneously. It combines the MUCHFUSS projects with the search for a Hyper-velocity subdwarf population.

MUCHFUSS originally was initiated to search for close binaries of high radial velocity amplitude (several hundred km s^{-1}) by taking spectra at random epochs for stars selected from the *SDSS* with high heliocentric RVs. MUCHFUSS was motivated by the recent discovery of massive unseen companions to hot subdwarfs (Geier et al. 2010). These systems have a massive unseen companion (white dwarfs, neutron stars, black holes) and low orbital inclination orbits assuming tidal locking of the sdBs. Their high inclination counterparts might reach radial velocity semi-amplitudes of up to 500 km s^{-1} at orbital periods of less than 0.5 days. The assumption of tidal locking has been verified from ellipsoidal light variations and asteroseismology in some cases. Hence the method is applicable for orbital periods of up to at least 0.6 d, which is the case for more than half of the sample. In a first study about 4-8% of these massive companions were found to exceed the Chandrasekhar mass limit. A massive main-sequence companion can be excluded as it would outshine the sdB. The companions are therefore most likely neutron stars or black holes. Considering the fraction of 4-8% together with the very low number of known neutron star or black hole binaries, which are detected as X-ray sources, a confirmation would mean a tremendous rise of the total number of these heavy compact objects in the Galaxy. But in order to discuss these targets we need to measure the complete orbit. Obviously this work is very time consuming and is not yet done.

Only 55.7% of the Hyper-MUCHFUSS targets turned out to be RV variable. The RV constant stars of high-velocity are interesting in their own right, as they may be HVS candidates. So far only one hot subdwarf US 708 (alias HVS 2, see Section 2.2.3) has been found serendipitously to be a HVS. However these old population stars are perfect probes for the Galactic potential as they are long-lived.

Finally, our method is also the most promising approach for finding a **HVS binary**, as we are focussing on subdwarfs, which have a particularly high binary fraction. The existence of such an object coming from the GC would imply that two massive black holes must be present there (Lu et al. 2007).

7.2 Survey

The enormous *SDSS* database is pretty well evaluated in terms of errors and accuracy and is the perfect starting point for our survey. In order to select subdwarf candidates, we used several indicators, e.g. colour, visual classification and velocity. Figure 7.1 shows a flowchart of the target selection method. We selected sdO/B candidates by colour and pre-classified their spectra by visual inspection. Measuring the RV by fitting synthetic models, we selected only stars faster than $\pm 100 \text{ km s}^{-1}$ and converted the hel. RV to the Galactic rest-frame (short: GRF) using equation 4.2. Most of the sdB stars belong to the thin disk and therefore have small radial velocities. Almost half of the known sdBs are in close binaries and show RV variations up to 350 km s^{-1} . For most of the sdB binaries however the RV semi-amplitudes are below 100 km s^{-1} . Hence the radial velocity of a sdB binary will rarely exceed 100 km s^{-1} in absolute value. We especially focused on stars with RVs in the rest-frame of more than 275 km s^{-1} . This observational cut was introduced by Brown et al. (2007a) to define the so-called bound HVS and separate them from ordinary halo-stars. Henceforth the RV in the rest-frame served as priority criterion for the target sample, in which we filtered out disk stars including low amplitude RV variables. The remaining sample should consist of halo stars, high amplitude RV variables and HVS candidates. More information on the process of target selection are presented by (Geier et al. 2010, in prep.).

A total amount of 265 targets with measured radial velocity remained on the targets list, serving as a first epoch. The survey part, to obtain the second epochs, started in 2007 using VLT/FORS, WHT/ISIS, CAHA-3.5m/TWIN and NTT/EFOSC2. Up to now we observed 88 stars, which is about one third of our targets. We measured the RVs by χ^2 -fitting of adequate synthetic spectra and regard a star as RV constant if its velocity is consistent with the first epoch within the respective error limits and call it a preferential HVS candidate if $|v_{\text{GRF}}| > 275 \text{ km s}^{-1}$.

7.3 Kinematics

A kinematical analysis can only be done if we know the star's location and space velocity. Hence we measured proper motions for all our HVS candidates applying the method presented in Section 4.3.

Again we obtained systematic discrepancies between the positions, especially for the old POSS-I epoch, due to the different colour filters and quality of the plates. The best way to handle this systematics is simply to use the same set of reference galaxies for every epoch, although this reduces the number of reference galaxies. We regard a proper motion as detected, if the position measurements do not show a large spread relative to the linear fit and the derived proper motion is significant. 24 stars turned out to have a proper motion consistent with zero, while for 15 of our 39 candidate HVS ($\approx 38\%$) we measured a significant proper motion. Additionally we confirmed our proper motions with the robust regression technique, adding artificial outliers to our data. The robustness of our technique has already been demonstrated on the example of the sdB J2156+0036 (=

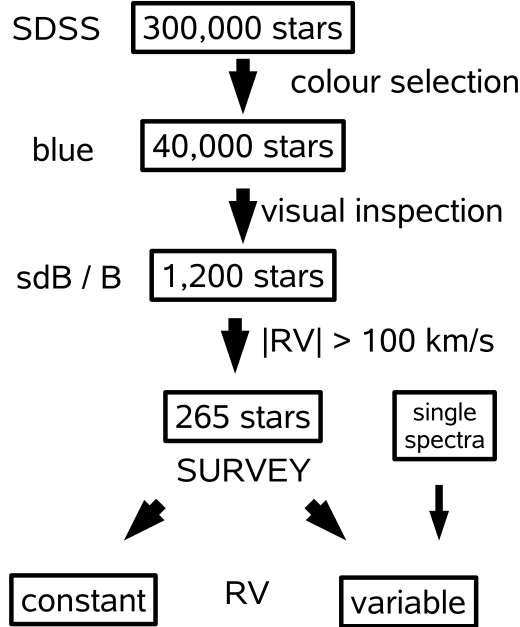


Figure 7.1: Target selection method based on *SDSS*. Stars are selected for which the absolute value of the RV exceeds 100 km s^{-1} . Hence disk stars are efficiently removed.

PB 5010) in Section 4.3. All the plots for our measurements can be found in the appendix.

We analysed the stellar spectra following the methods described in Chapter 3. In most of the cases the stellar spectra from the *SDSS* provide sufficient S/N and resolution. We applied χ^2 -fitting of synthetic line profiles to the Balmer and helium lines in order to determine the atmospheric parameters and abundances. Naturally our sample contains misclassifications, as we also found e.g. main sequence/horizontal branch stars and white dwarfs. Therefore we had to use several model grids, appropriate for the stellar type under study, which was already carried out in Chapter 3. As already described in Section 4.1 we infer the stellar masses and derive the distance.

We performed the same analysis as described in Section 6.2.2 and derived the median GRF velocity from the Monte-Carlo distribution in Figure 7.5. The local escape velocity is calculated from the Galactic potential of Allen & Santillan (1991). Furthermore from kinematic characteristics (e.g. U , V , J_z) we obtained additional information about the halo membership of the stars. Following the trajectories backwards we can even put constraints on the origin of the stars, applying the same Monte-Carlo method.

Table 7.1: Proper motion measurements for the significant detections from the Hyper-MUCHFUSS project. The number of used reference galaxies and epoch are also given.

name	V mag	$(\mu_\alpha \cos(\delta))$ mas/yr	μ_δ mas/yr	n_{ep}/n_{gal}	
J0758+1158	18.82 \pm 0.03	+3.0 \pm 1.7	-12.0 \pm 1.1	9/10	
J0844+1139	16.11 \pm 0.02	-11.5 \pm 2.6	-11.9 \pm 2.1	6/ 7	sdB
J0845+1352	17.42 \pm 0.02	-10.7 \pm 2.3	-3.7 \pm 2.6	5/14	sdB
J0849+1455	18.85 \pm 0.03	-49.5 \pm 1.8	+6.4 \pm 1.6	8/ 9	DA
J0948+5516	18.59 \pm 0.03	-1.9 \pm 2.9	-7.4 \pm 1.7	7/12	sdB
J1020+0137	16.91 \pm 0.02	-2.4 \pm 1.3	-7.3 \pm 1.2	12/15	sdB
J1125+0333	19.85 \pm 0.04	+10.0 \pm 1.2	-10.6 \pm 1.3	5/13	
J1211+1437	17.87 \pm 0.03	-12.1 \pm 1.8	-27.2 \pm 1.4	13/14	sdB
J1358+4729	18.03 \pm 0.03	+76.1 \pm 2.4	+14.4 \pm 2.4	14/15	DA
J1556+4708	18.61 \pm 0.03	-6.3 \pm 1.9	+1.3 \pm 1.8	10/14	sdB
J1629+1307	18.30 \pm 0.03	+0.8 \pm 1.7	-5.7 \pm 1.4	9/17	
J1632+2051	17.62 \pm 0.03	-12.5 \pm 3.0	-1.6 \pm 3.6	7/16	sdB
J1644+4523	17.36 \pm 0.02	+4.7 \pm 2.8	-26.1 \pm 3.3	8/13	sdB
J2156+0036	17.91 \pm 0.03	-1.3 \pm 1.6	-7.4 \pm 1.2	26/13	sdB
J2244+0106	18.14 \pm 0.02	+2.1 \pm 0.8	-3.7 \pm 1.3	30/14	sdB

7.4 Results

The first step of the project consisted of obtaining second epoch observations for all possible targets (survey) and is completed at a level of 33%. The second step, which aims at measuring the RV curves for the detected binaries (follow-up) requires a lot more of observations and is still in progress. The first results for this binary part will be presented soon in a dedicated paper (Geier et al. 2010, in prep.).

Until now we observed and analysed 88 out of our 265 targets, i.e. \approx 33%. Accordingly 39 of these stars have constant RV within our detection limits and 49 stars show indication for binarity, leading to a lower limit for the binary fraction of 55.7%. For 29 of our 39 constant stars we derived preliminary stellar parameters of subdwarf B stars, whereas for the rest we could not find a clear solution or the S/N is simply too low. These 29 sets of preliminary parameters can be found in Table A.1 of the appendix. Accounting only for the hot subdwarfs we derived a slightly higher binary fraction of at least 57.3%, which goes well with previous estimates (40-70%, e.g. Maxted et al. 2001). Then we measured the proper motion (PM) for the remaining 29 stars. A number of 15 targets showed a significant PM and has been analysed in detail using quantitative spectroscopy. We identified in our sample 10 subdwarfs stars together with 2 DA white dwarfs. The remaining three stars show lower T_{eff} and $\log g$ can be either main sequence or blue horizontal-branch stars. Higher resolution spectroscopy may put constraints on their nature, but is unfortunately not available. As the resulting mass spread avoids a faithful

Table 7.2: Stellar parameters for the remaining stars with PM.

name	T_{eff} K	log g	log $n_{\text{He}}/n_{\text{H}}$
J0844+1139	28604. \pm 738.	5.331 \pm 0.124	-2.63 \pm 0.60
J0845+1352	24570. \pm 1066.	5.586 \pm 0.169	<-3.00
J0849+1455	27746. \pm 833.	7.324 \pm 0.153	-2.00 \pm 0.00
J0948+5516	33891. \pm 557.	5.836 \pm 0.202	-1.45 \pm 0.20
J1020+0137	28960. \pm 762.	5.387 \pm 0.135	<-3.00
J1211+1437	32530. \pm 583.	5.524 \pm 0.159	-2.94 \pm 0.54
J1358+4729	10636. \pm 111.	8.100 \pm 0.074	<-3.00
J1556+4708	34410. \pm 1275.	5.343 \pm 0.254	<-3.00
J1632+2051	26869. \pm 609.	5.310 \pm 0.086	-2.07 \pm 0.24
J1644+4523	31682. \pm 413.	5.782 \pm 0.114	-2.93 \pm 0.33
J2156+0036	29083. \pm 808.	5.600 \pm 0.149	-2.49 \pm 0.27
J2244+0106	33578. \pm 684.	4.750 \pm 0.200	-1.47 \pm 0.71

distance estimation and does not allow a kinematical studies (see Tillich et al., 2009), we excluded these objects from our analysis. The derived stellar parameters for the remaining 12 stars are shown in Table 7.2, while the respective RV list can be found in Table A.2 of the appendix. In Figures 7.4 and 7.6 we show the comparison of the observed data with the synthetic line profile for four stars. The rest can be found in Figures A.11, A.12, A.13 and A.14 of the appendix. Note that, after our analysis, the two targets with the highest measured PMs naturally turned out to be DA white dwarfs. The proper motion measurement is therefore a suitable tool to find such nearby white dwarfs. For two of our stars we derive parameters not consistent with a typical extreme horizontal-branch (EHB) nature. In Figure 7.4 we show a T_{eff} -log g-diagram for the 10 subdwarfs in comparison to the reference sample of the SPY subdwarfs analysed by Lisker et al. (2005). Obviously 8 of our subdwarf B stars reside on the extended horizontal-branch within the respective errors. However, the stars J1556+4708 and J2244+0106 have already evolved away from the horizontal branch and are currently in a post-EHB state. Figure 7.4 shows that our subdwarf B sample goes perfectly together with the SPY sample. Based on these parameters we determined the distances as described in Section 4.1, which are given in Table 7.3. We applied a Monte-Carlo method and derived a distribution of the GRF velocities based on the determined uncertainties. Together with the median space velocity we also obtained the escape velocity in the Galactic potential of Allen & Santillan (1991). Hence the data set for the 12 stars was completed and Figure 7.7 shows the space distribution of the targets, for which we carried out a detailed kinematical analysis. To further quantify the kinematics of the star, we again made a comparison to the work of Pauli et al. (2006), as already described in Section 6.3.2.

Following this approach we see that the sdB J0845+1352 and the white dwarf J1358+4729 show thick disk kinematics (see Figure 7.3). The other white dwarf J0849+1455 clearly

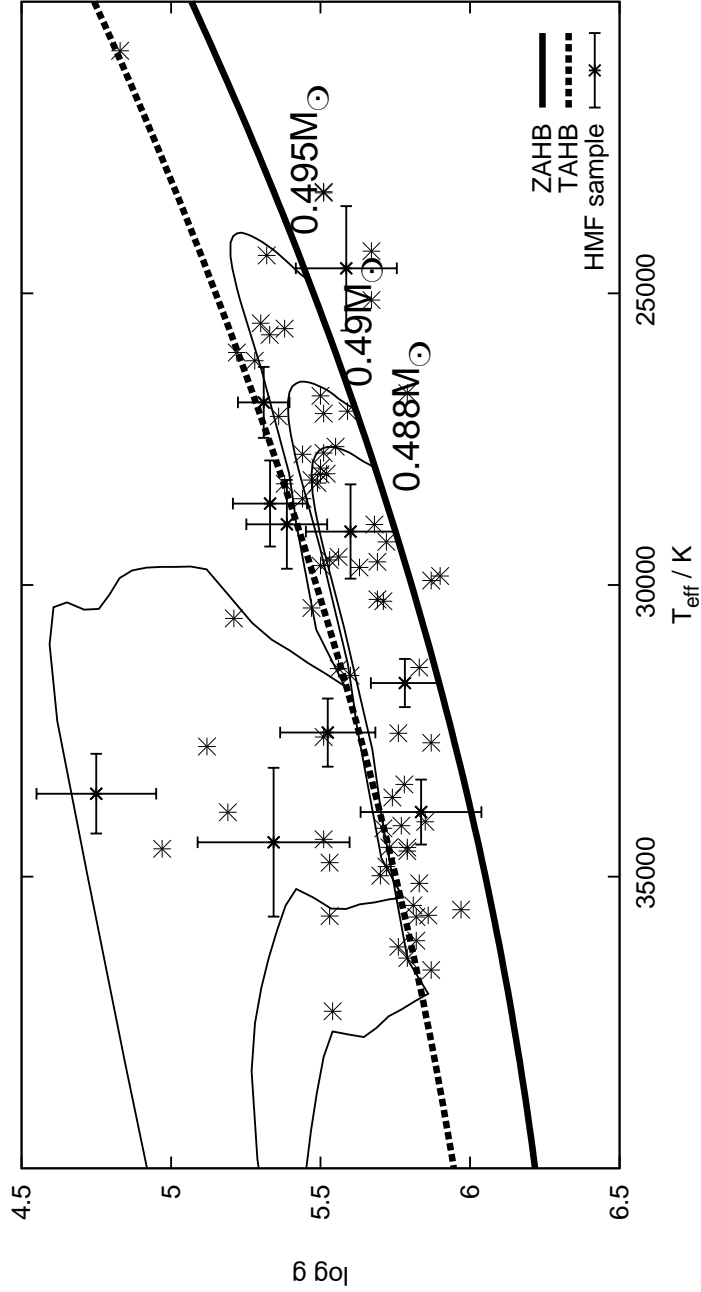


Figure 7.2: Comparison of the position of the 10 subdwarfs (with error bars) from HMF projects in the $T_{\text{eff}}\text{-log } g$ -diagram to evolutionary tracks of Dorman et al. (1993). The SPY subdwarf B sample is given as reference (Lisker et al. 2005). The ZAHB and the TAHB are extended from a polynomial fit. Note that 2 subdwarfs have already left the EHB.

Table 7.3: Calculated distance, escape and median Galactic rest-frame velocities together with the respective errors.

name	dist kpc	v_{rad} km s^{-1}	v_{GRF} km s^{-1}	v_{esc} km s^{-1}	
J0844+1139	3.14 ± 0.26	202.7 ± 5.0	202^{+55}_{-46}	513	halo
J0845+1352	3.50 ± 0.38	115.1 ± 9.6	230^{+70}_{-61}	511	thick disk
J0849+1455	1.11 ± 0.11	119.0 ± 37.2	354^{+33}_{-34}	531	halo DA
J0948+5516	6.51 ± 0.88	-142.1 ± 8.6	106^{+78}_{-35}	490	halo
J1020+0137	4.31 ± 0.39	238.0 ± 8.3	107^{+20}_{-13}	513	halo
J1211+1437	6.45 ± 0.68	220.1 ± 9.5	713^{+155}_{-139}	507	retrograde orbit
J1358+4729	0.14 ± 0.01	-260.6 ± 14.2	295^{+10}_{-11}	541	thick disk DA
J1556+4708	11.76 ± 2.03	-385.4 ± 7.4	353^{+174}_{-106}	487	retrograde orbit
J1632+2051	6.09 ± 0.36	-236.1 ± 3.2	275^{+120}_{-110}	544	retrograde orbit
J1644+4523	3.68 ± 0.27	-314.1 ± 4.5	468^{+104}_{-90}	534	halo
J2156+0036	5.37 ± 0.54	-177.2 ± 6.5	85^{+58}_{-44}	534	halo
J2244+0106	18.29 ± 2.45	-166.0 ± 5.8	200^{+186}_{-156}	458	retrograde orbit

belongs to a the halo population. Amazingly these three stars are also the only ones to show highly prograde orbits. The remaining 9 stars can be divided into two groups: the first group consists of 5 stars clustering around zero in the angular momentum J_z and reside at a rather high eccentricity. This might be an indication for a halo membership, as they reside also at a V -velocity (= tangential component) of about zero. In contrast to that, the four stars of the second group show retrograde orbits at various eccentricities. This retrograd kinematics combined with the fact that they have throughout negative V -velocities, could be an indication of a runaway origin of these stars.

However, all of these 9 sdB stars possess halo characteristics, as they reside clearly outside the 3σ thick disk contour in the diagrams. Furthermore all the 3D-trajectories of our sample are all clearly in favour of a halo membership. The situation for J2244+0106 is a bit special, as it shows a more circular orbit, but is directed perpendicular to the Galactic plane. However, for 10 stars at least two of three indications are present, which renders them as halo stars, following Pauli et al. (2006).

We now shall focus and comment on individual objects. **J1211+1437** stands out as it has a high GRF velocity ($v_{GRF} = 713^{+155}_{-139} \text{ km s}^{-1}$), clearly exceeding the local Galactic escape velocity of $v_{esc} = 507 \text{ km s}^{-1}$. A comparison between observed and synthetic spectrum is shown in Figure 7.6. Fig 7.5 shows the velocity distribution of the subdwarf J1211+1437. Unfortunately tracing back the star to the GD comes along with high uncertainties, which did not allow us to determine the origin for the star. Figure 7.8 shows a 3D plot in order to determine its origin. However, it is clear that the star cannot

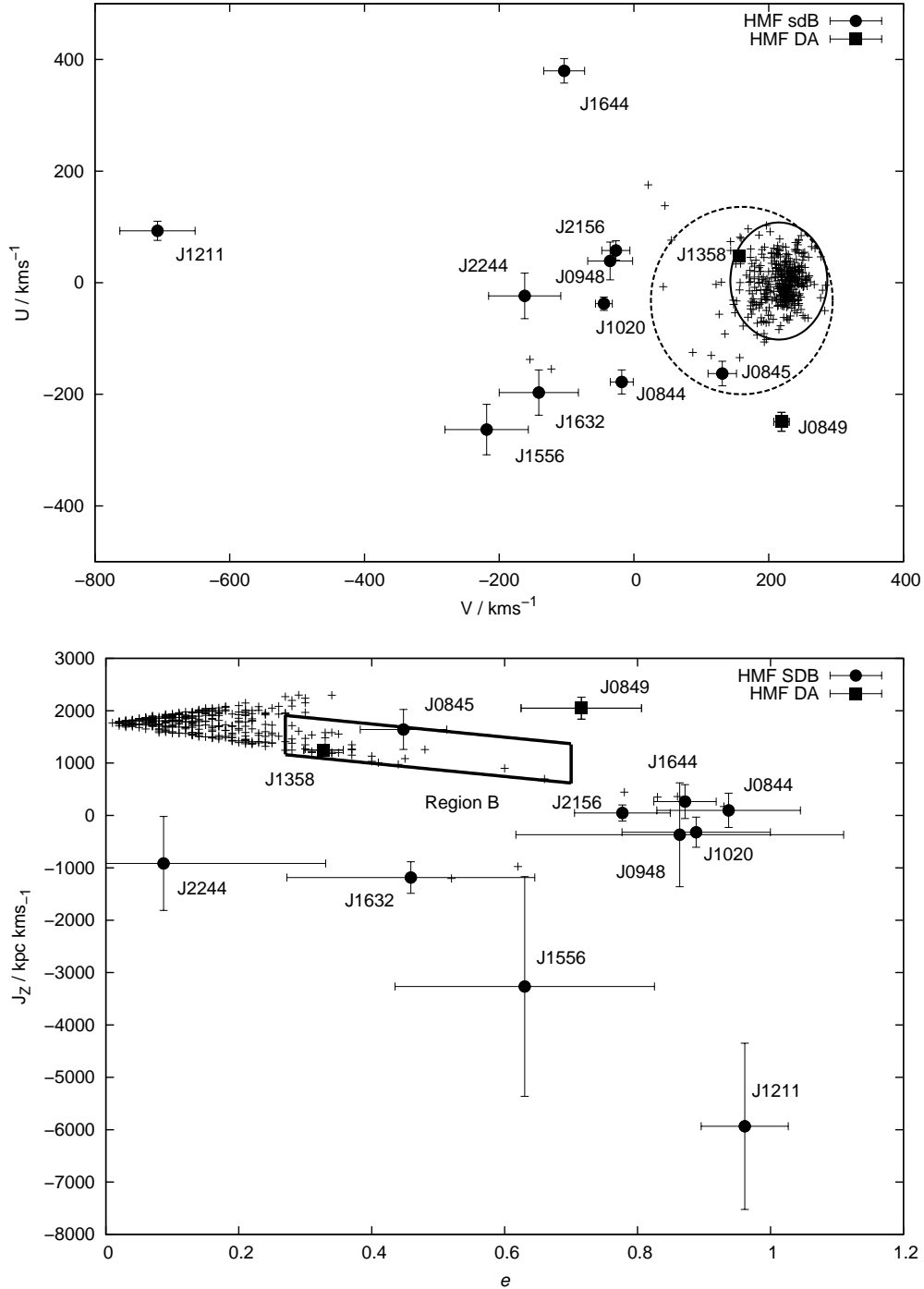


Figure 7.3: $V-U$ (*upper*) and $e-J_z$ diagram (*lower*) for our 12 targets. The white dwarf sample (+) of Pauli et al. (2006) serves as reference. The ellipses render the 3σ -thin and thick disk contours (solid and dashed lines respectively), while the solid box (lower panel) marks the thick disk region (Region B). Note that except for two stars, all our targets are far far away from the disk population in both diagrams.

come from the GC and it is unbound in the Standard Galactic potential. The rest of the sample is bound to the Galaxy, although the subdwarfs **J1556+4708** and **J1644+4523** might exceed the escape velocity within their respective errors. Nevertheless there is growing evidence for the underestimation of the Galactic dark matter halo (e.g. Wilkinson & Evans 1999; Sakamoto et al. 2003; Abadi et al. 2009; Przybilla et al. 2010). In that case the escape velocity could be as high as $v_{esc} \approx 900 \text{ km s}^{-1}$ in the vicinity of the sun and almost no unbound stars remain. Hence even **J1211+1437** would be bound and may have already completed several orbits within its lifetime. Hence a GC origin could not be excluded. The most astonishing trajectory was found for the subdwarf **J1644+4523**. A comparison between observed and synthetic spectrum is shown in Figure 7.4. We measured a GRF velocity of $v_{GRF} = 468_{-90}^{+104} \text{ km s}^{-1}$, which is below the escape velocity of $v_{esc} = 534 \text{ km s}^{-1}$, hence the star is probably bound. As the star is approaching us, we calculated the trajectory backwards into the past and revealed that the star has crossed directly through the Galactic bulge (short: GB), which can be seen from Figure 7.7. The high ejection velocity of $v_{ej} = 597 \text{ km s}^{-1}$ suggests a formation scenario involving a MBH in the GB. The time-of-flight (short: TOF) is much longer ($TOF = 1.27 \text{ Gyr}$) than the helium core burning phase lasts ($\approx 200 \text{ Myr}$). In case **J1644+4523** was ejected when crossing the GD the last time, this means that **J1644+4523** evolved to a subdwarf a long time after it was ejected by a MBH in the GB. In this case it could have been ejected as binary HVS, following the sdB formation scenarios (Han et al. 2003). Nevertheless the star might have undergone single star evolution as well with strong mass loss near the tip of the Red Giant Branch to become a sdB. Additionally we repeated the kinematical calculations for a higher dark halo mass, adopting a total dark halo mass of $M_{halo}^{new} = 3.4 \times 10^{12} M_{\odot}$ as suggested by Abadi et al. (2009) with a mass distribution out to 100 kpc, following Allen & Santillan (1991). The place of origin remains almost unchanged but the time-of-flight is strongly reduced to $TOF = 145 \text{ Myr}$, which is consistent with the lifetime of hot subdwarfs. Hence the star could have been ejected as subdwarf and did not have to evolve after the ejection. We also adopted a halo mass of $M_{halo}^{new} = 1.7 \times 10^{12} M_{\odot}$ as suggested from our analysis of J1539+0239 (see Section 6.4, Przybilla et al. 2010). In that case the time-of-flight is still reduced to $TOF = 359 \text{ Myr}$, which is also consistent with the lifetime of hot subdwarfs. However **J1644+4523** is the first high-velocity star, which comes from the GB and was most likely ejected by a MBH in the GB (see Figure 7.7). For the subdwarf B star **J0948+5516** we found a similar behaviour, although in that case the errors are large (see Figures 7.9 and 7.10). With a GRF velocity of $v_{GRF} = 106_{-35}^{+78} \text{ km s}^{-1}$ it resides on a highly bound orbit. Nevertheless we reconstructed its trajectory back directly into the GB, where it might have been ejected $TOF = 109 \text{ Myr}$ ago, experiencing an ejection velocity of $v_{ej} = 492 \text{ km s}^{-1}$.

All our 12 stars have been traced back to the GD in order to assess their possible origin during their last passage of the disk. For the 2 white dwarfs we can exclude a GC origin during their last passage of the disk, which is shown in Fig 7.10. We found 4 subdwarf stars (40%), which are consistent with an origin in the GB. Figure 7.9 shows their intersection with the GD. For the first time, 2 stars can be traced back directly into the GB, where they may have been ejected by the Hills mechanism.

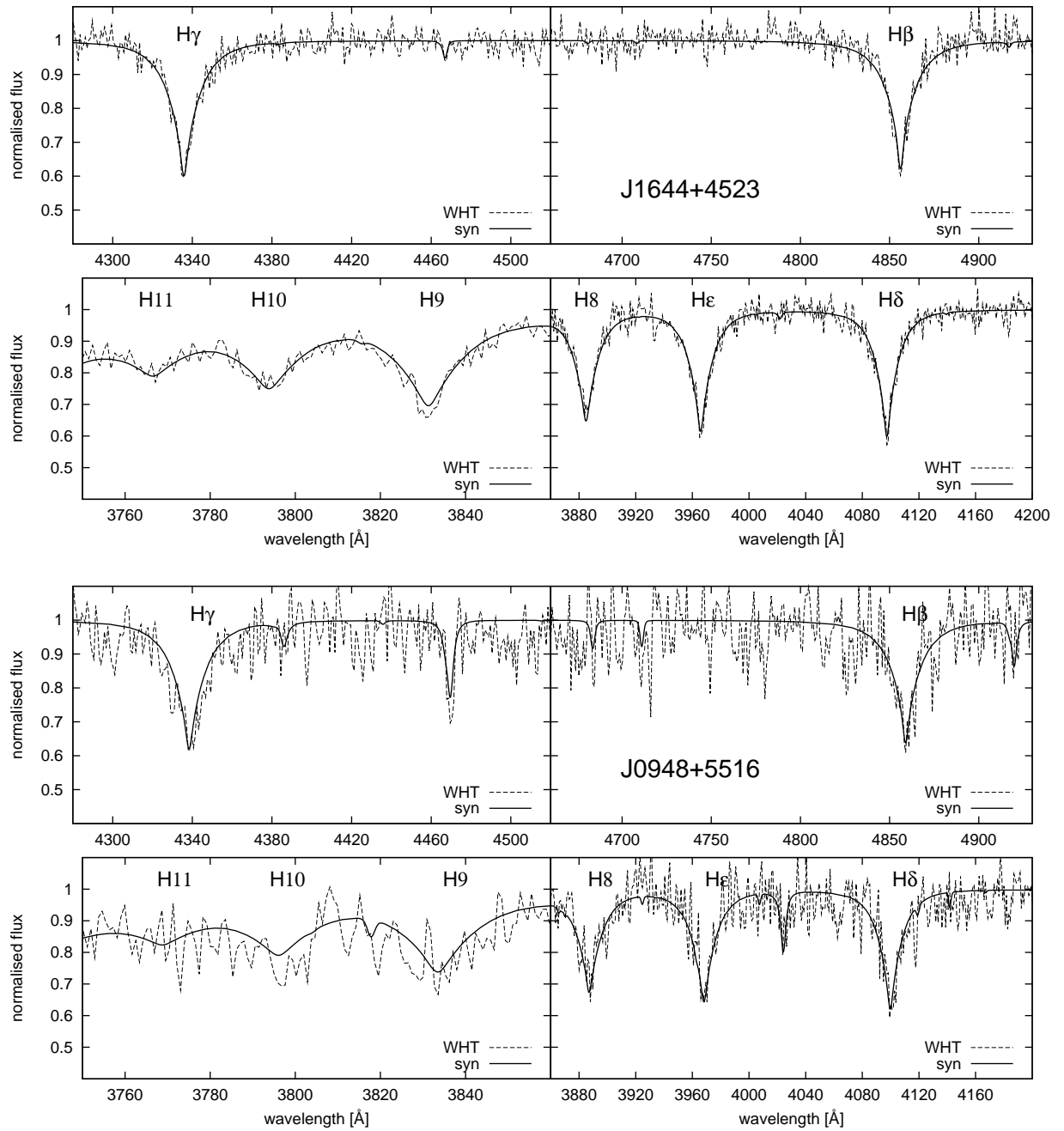


Figure 7.4: Comparison between the synthetic model with the observed spectrum from the WHT for the sdBs J1644+4523 (top) and J0948+5516 (bottom). Note the overall good agreement.

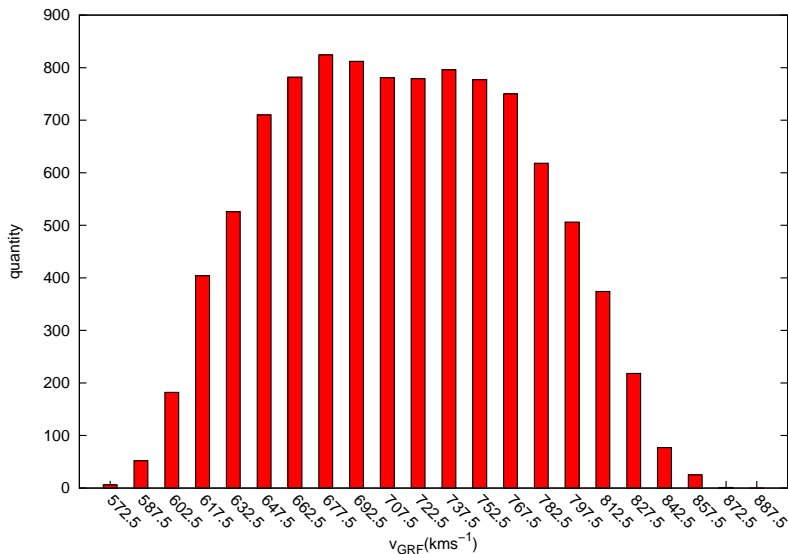


Figure 7.5: Galactic restframe velocity distribution for J1211+1437 derived from a Monte Carlo procedure with a depth of 10,000.

Another 3 subdwarf stars may originate in the outer Galactic rim. Although the errors are large in some cases, these stars have clearly not passed the inner part of the GD during their last passage. Such a behaviour is pretty similar to the case of the main-sequence star J0136+2425 (Tillich et al. 2009b).

The remaining 3 stars are not consistent with a GC origin during their last disk passage. However we have to mention, that this is an alternative. Perhaps the most obvious one is, that all of these stars are population II stars, i.e. very old. Hence they might have crossed the GD already several times within their lifetime.

7.5 Conclusion

Our Hyper-MUCHFUSS project was carried out successfully. We found 9 new halo subdwarfs and one of the thick disk population (**J0845+1352**) together with two new white dwarfs: the thick disk WD **J1358+4729** and the new halo WD **J0849+1455**. Based on the detailed analysis of these objects we can finally draw three important conclusions.

We discovered the unbound subdwarf B star **J1211+1437** with a GRF velocity of $v_{\text{GRF}} = 713_{-139}^{+155} \text{ km s}^{-1}$, which is above the local Galactic escape velocity in the Standard Galactic potential. Additionally we found 3 subdwarfs that could be reckoned as HVS following Brown et al. (2007a). Hence US 708 is not the only subdwarf with high-velocity properties. As the evolution of hot subdwarfs is closely connected to binary stars, this is not completely unexpected as we know several scenarios in which binaries or their remnants might be accelerated to very high velocities (e.g. Lu et al. 2007; Tutukov & Fedorova 2009). Recently Przybilla et al. (2010) found the fastest halo star known, namely

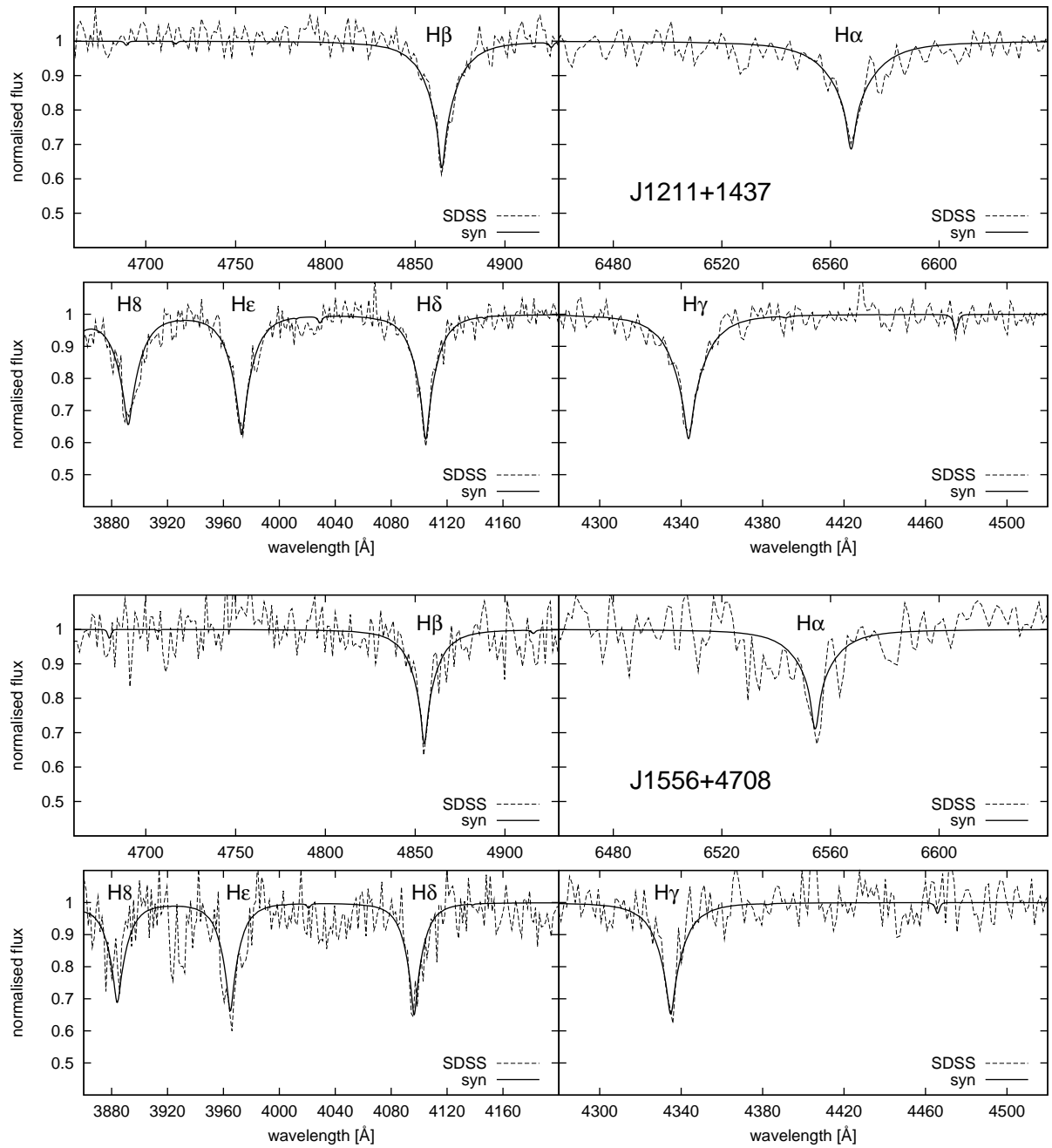


Figure 7.6: Comparison between the synthetic model with the observed spectrum from the WHT for the sdB J1644+4523 (top) and the post-EHB star J1556+4708 (bottom). Note the overall good agreement.

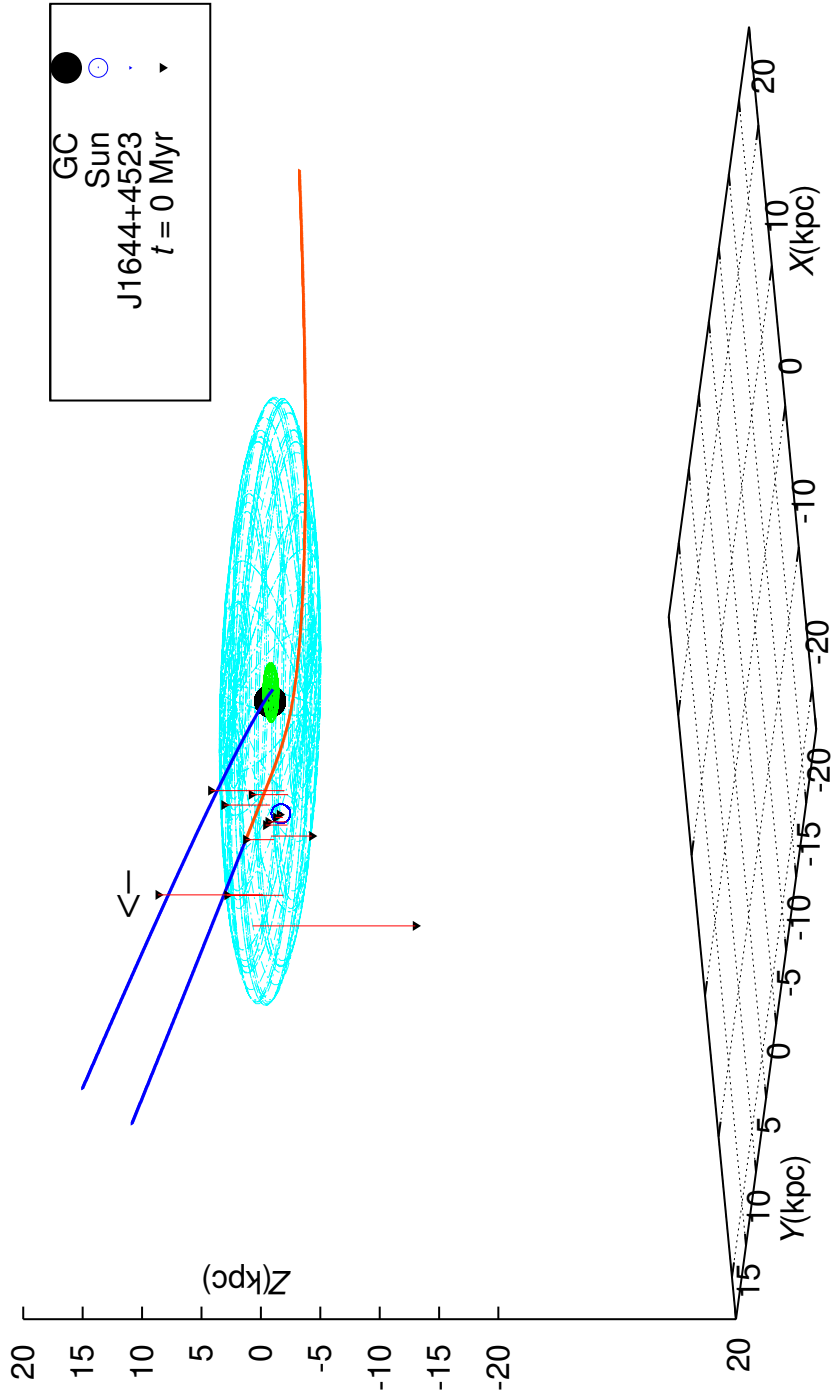


Figure 7.7: 3D plot of the current positions of our 12 stars (black triangle) relative to the Galactic Disk (light blue), showing also the trajectory for J1644+4523 (past:blue, future:red) in the potential of (Allen & Santillan 1991).

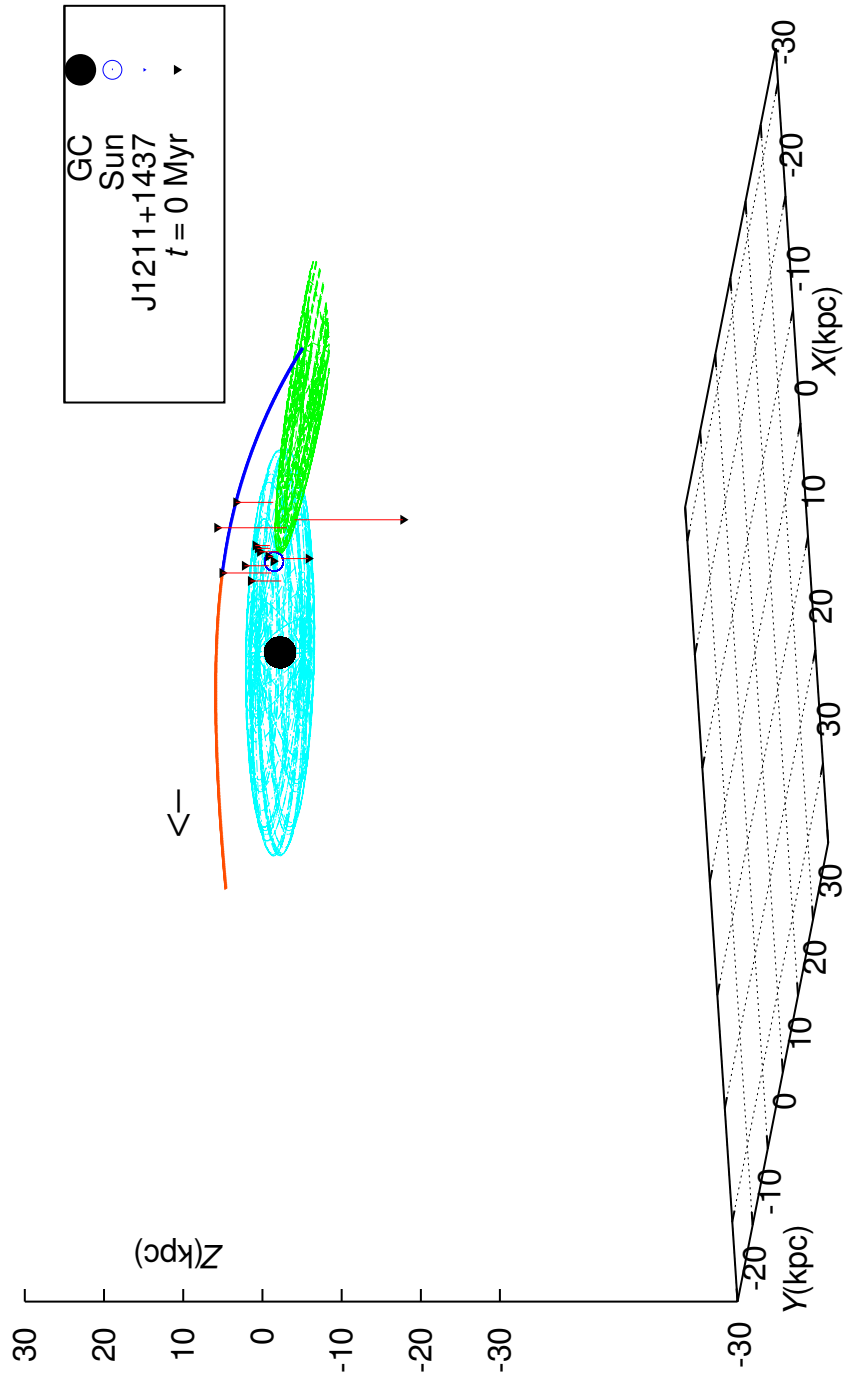


Figure 7.8: 3D plot of the current positions of our 12 stars (black triangle) relative to the Galactic Disk (light blue), showing also the trajectory for J1211+1437 (past:blue, future:red) in the potential of (Allen & Santillan 1991).

the blue horizontal branch star J1539+0239, which is also an evolved star of population II. We conclude that there exists indeed a population of evolved HVS, apart from the known main-sequence HVS. However subdwarf B stars of population II are a very rare phenomenon. Altmann et al. (2004) carried out a kinematical analysis of a sample of 114 subdwarfs from various surveys (e.g. Palomar Green, Hamburg/ESO). They found 16 subdwarfs ($\approx 14\%$), which kinematically belong to the Galactic halo and are therefore population II stars. Our survey is exclusively dedicated to find such objects, hence we can add 9 more halo subdwarfs to that list, whereas only one shows thick disk behaviour.

The subdwarf B stars **J1644+4523** and **J0948+5516** could be traced back directly to the GB. Furthermore they show extreme kinematical properties and ejection velocities of $v_{\text{ej}} = 597 \text{ km s}^{-1}$ and $v_{\text{ej}} = 492 \text{ km s}^{-1}$ respectively. Hence they are consistent with a slingshot mechanism proposed by Hills (1988). Two more subdwarf B stars are consistent with a origin in the GB and show ejection velocities of $v_{\text{ej}} \approx 350 \text{ km s}^{-1}$. We conclude that these objects may have ejected by the Hills mechanism. However, this is only one possibility for such long-lived population II stars. More likely they may have crossed the Galactic disk already several times.

6 out of 10 subdwarf stars (60%) have not crossed the Galactic bulge during their last passage of the Galactic disk. Furthermore for **J1211+1437** an origin in the GC can be excluded due to its unbound trajectory coming from the outer Galactic rim (see Figure 7.8). As all the stars in our sample are long-lived, the rest might have crossed the GD several times. The uncertainties grow with every passage simply due to the factor of time and a clear determination of the origin cannot be performed. However from the existence of **J1211+1437** we conclude, that there are other efficient acceleration mechanisms than the Hills scenario, which produce unbound subdwarfs.

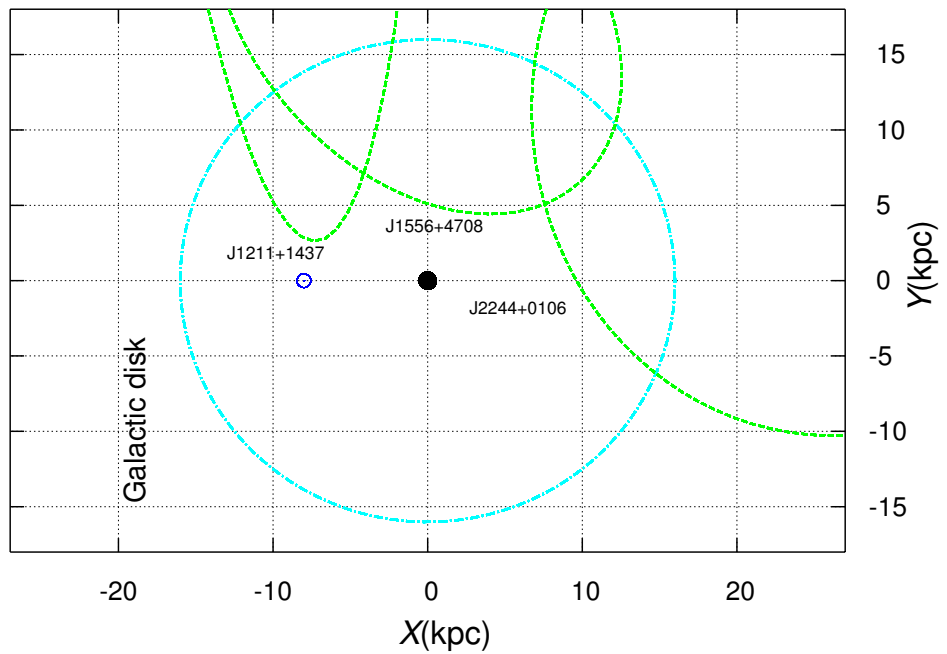
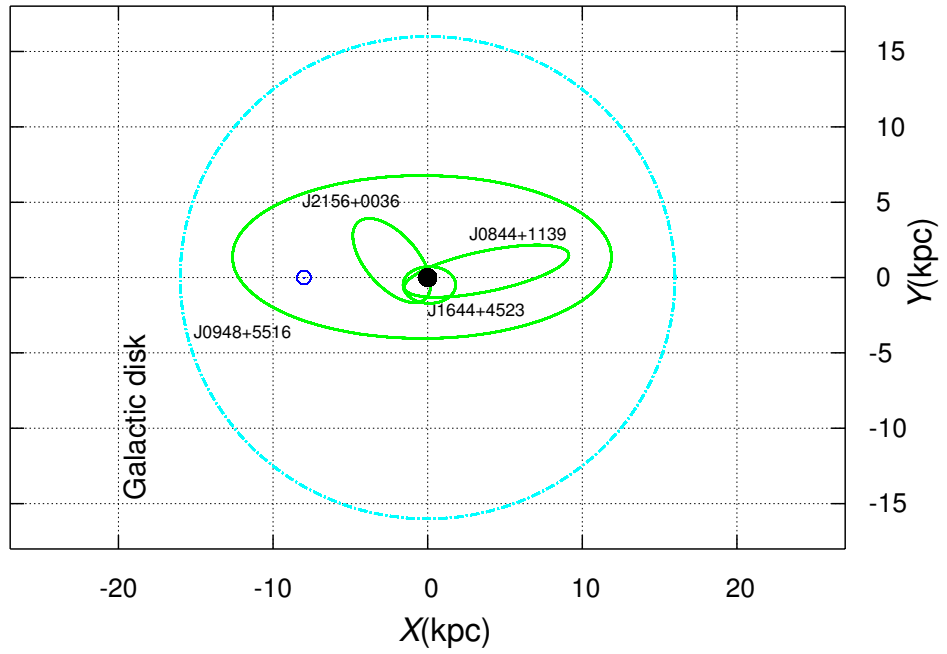


Figure 7.9: Intersection region of the targets' past trajectories with the GD in order to conclude on their origin. Note that 4 subdwarfs are consistent with a GB origin (*top*), 3 subdwarfs might originate in the outer Galactic rim (*bottom*). For orientation the position of the sun is marked as well (open circle).

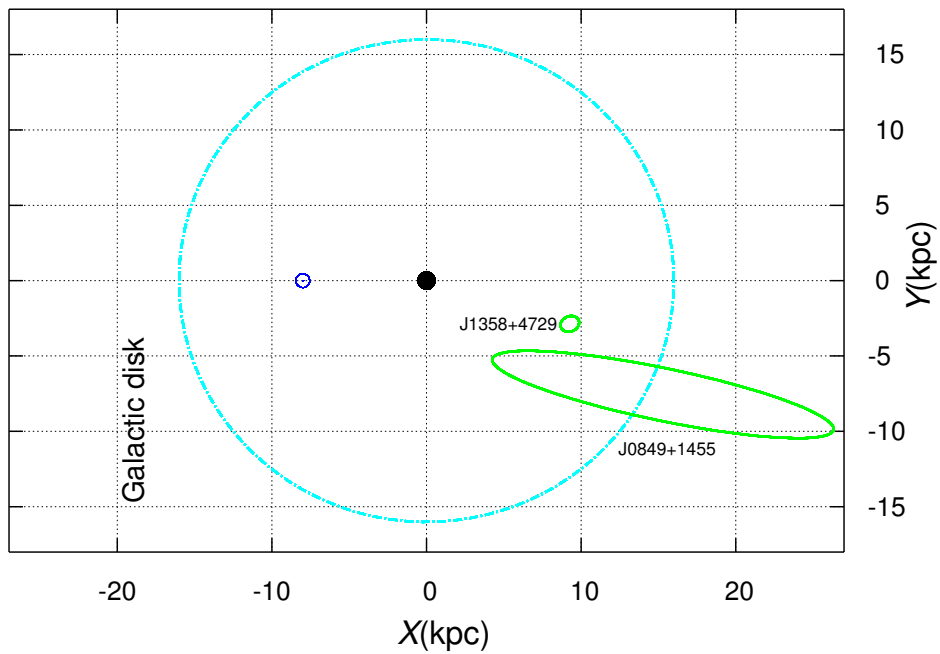
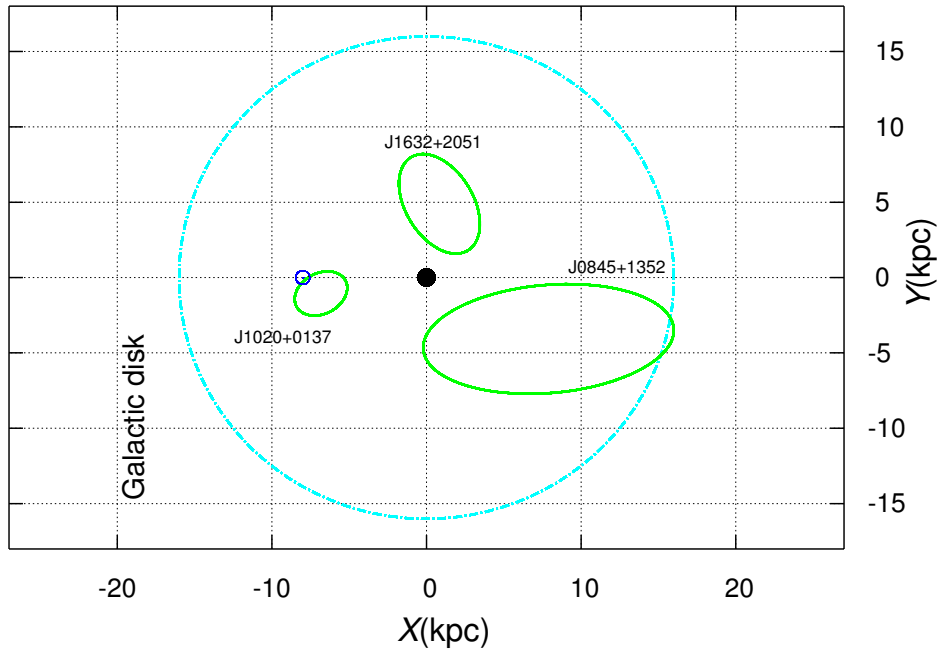


Figure 7.10: Intersection region of the targets' past trajectories with the GD in order to conclude on their origin. Note that 3 subdwarfs come from the inner GD (*top*) and the two white dwarfs do not originate in the GC (*bottom*). For orientation the position of the sun is marked as well (open circle).

Chapter 8

Outlook

In the previous chapters several new results concerning the field of hyper-velocity stars have been presented. We analysed spectra of the already known HVS 8, 9 and 10, which we kindly received from W. Brown using quantitative spectroscopy in order to conclude on their true nature. After we detected fast rotation for all three of them, determined their atmospheric helium abundance and checked their position with respect to stellar evolutionary model, we confirmed that they belong to the main-sequence population. The same holds for the majority of HVS candidates sampled from the extended survey (Brown et al. 2009), although the situation is not clear in all cases.

High resolution spectra have been obtained for **HVS 7** with UVES/VLT. After applying a detailed quantitative analysis using state-of-the-art modelling techniques we discovered, that HVS 7 is a extraordinary chemically peculiar late-B type star with moderate projected rotational velocity. The detailed analysis of high-resolution spectra is of fundamental importance to understand the evolutionary history of HVS.

We conducted a survey for A-type HVS based on the sample of Xue et al. (2008), which is a mix of blue horizontal-branch-, main-sequence stars and blue stragglers. Combining the results from quantitative spectroscopy and proper motion measurements we were able to obtain the full phase space information for three stars. We discovered **J0136+2425**, which is the first late B-type HVS from the Galactic rim. The halo blue straggler **J1300+0422** was found to be on a highly eccentric retrograde orbit. And finally we have weighed the Galactic dark matter halo and derived a lower mass limit from the kinematics of **J1539+0239**, which is the fastest halo star known. The search for more such stars with extreme kinematics is a perfect tool to directly constrain the mass of the Galactic dark matter halo.

We performed the Hyper-MUCHFUSS project in order to find more high-velocity hot subdwarfs. We created a sample using a sophisticated target selection and obtained stellar spectra at various telescopes. Finally we were able to perform a full kinematical analysis for 12 stars. 9 new halo subdwarf B stars and one new halo white dwarf were found. 4 subdwarf B stars turned out to be highly consistent with an origin in the Galactic bulge during their last passage of the Galactic disk. We discovered the unbound subdwarf B star **J1211+1437**, which originates in the outer Galactic rim. Finally the subdwarf B star **J1644+4523** was found to be on a trajectory, which is directly crossing the Galactic

bulge and is bound as it is already on its way back. Hence it may have been ejected via the Hills mechanism. However, the fact that the majority of the sdB stars show kinematics, which are not directly and mandatory related to the GC, suggests that other formation mechanisms than the classical one () must be sought. Especially the possibility that some stars seem to be kinematically related to the Galactic rim has to be examined by further dedicated extended surveys.

When Hills (1988) presented his theoretical work on the disruption of binaries in the vicinity of SMBHs he simply called the remnants hyper-velocity stars, because they might reach very high velocities. After the observational evidence for such stars by Brown et al. (2005), this HVS nomenclature was immediately raised to a definition. But there is also the possibility to define the prefix hyper-velocity as unbound to the Galaxy. However in that case the “bound” HVS, which have been introduced by Brown et al. (2007a), would be no HVS at all. As the time passed by, the confusion about this terminology continuously grew. Today we know e.g. HVS 3 and J0136+2425, which are HVS and even unbound, but cannot originate in the GC.

The problem with the first definition is, that from an observers point of view it is pretty difficult to find out, where a star is from. Responsible for that is the lack of applicable proper motions, which are necessary to reconstruct the full trajectories. Due to this problem, so far none of the known HVS has been proven to come from the Galactic centre. But also the second definition has some severe disadvantages. The local escape velocity is rather well constrained in the direct vicinity of the sun. But when we find stars out in the halo, it highly depends on the assumed mass of the dark matter halo. Unfortunately this value is under vigorous discussion, as it is not known very accurately. Hence none of the recently used definition for hyper-velocity works properly; at least not in combination with what we know today.

Furthermore there is also the class of runaway stars, which makes the situation even more complicated. It is evident that there must be some overlap between these two classes, but only at the low end of the HVS distribution (Heber et al. 2008a). Recently Heber et al. (2008a) and Irrgang et al. (2010) found the first two runaway stars, which might be unbound. Hence we also need a demarcation between hyper-velocity and runaway stars. The only way out of this dilemma is to find more such objects and perform a complete kinematical analyses to define possible trajectories with high accuracy.

In order to find more high-velocity objects, one can easily think of an extension of our dedicated search. Every stellar survey sample with measured radial velocities is usable to serve as starting point to search for hyper-velocity stars. Naturally early-type stars on the main-sequence are in general very luminous and high mass stars. Hence if they are found at faint magnitudes, they are most likely far away. In such a case it is even more precious to measure a significant proper motion, as it will increase the transverse velocity components tremendously.

Therefore the most obvious extension project would be to look at the final data release 7 for the *SDSS*, which was published in 2009 and provides the completion of the project (Abazajian et al. 2009). Data release 7 strikingly extends DR6 as it provides spectra from 577 new plates and raises the total number of spectra to more 1.6 billion objects. Fur-

thermore the data from astrometry based on *SDSS* imaging positions are also published in the CAS Schema Browser¹. This also allows now a preselection of high proper motion targets in order to find earlier type stars and analyse their kinematics. As our work only covers data release 6, there are surely unidentified high-velocity or even hyper-velocity stars to be found in this sample.

Another approach for an extension could be a dedicated search for high proper motion objects. Similar to the SuperCOSMOS Sky Survey² one could collect all the available position information from all available archives. A simple linear fit of these data will easily produce a reliable measure for the priority of the target. As this will produce an enormously large target list, it is important to simultaneously obtain photometric information. Hence, in order to ensure that the high proper motion leads to high tangential velocities, we have to ensure that the distance of the target is large enough. Therefore our targets, for which we then would conduct a real proper motion measurement, are therefore sufficiently blue and faint.

But at the latest with the launch of the Global Astrometric Interferometer for Astrophysics (abbrev: GAIA) satellite, the most demanding part in the analysis of HVS will reach another level: proper motion measurements will reach an accuracy $\leq 0.1 \text{ mas yr}^{-1}$ for all stars down to $V=20$ mag. Hence it is also called the successor to the famous ESA Hipparcos mission, although it provides more than interferometry. By using a narrow band spectrometer from $8470 - 8740 \text{ \AA}$ It will also measure the RV and additionally identify stellar types by using multicolour photometry, which is a highly demanding task (see Section 4.1). The satellite is supposed to be launched in 2012 with a Soyuz rocket from French Guiana. It will fly to the Lagrange point L2 located approximately 1.5 million kilometers from earth, which is a stable point keeping pace with the earths yearly revolution around the sun. This stable thermal environment has to be ensured. As the satellite creates its power mainly by solar panels, solar eclipses of the sun by the earth should be avoided. Hence it will orbit the L2 on a Lissajous orbit. The mission is conducted for about five years and will observe about one billion stars in our Galaxy and throughout the Local Group, which corresponds to about 1% of the Galactic stellar population.

For all these objects GAIA should be able to determine positions, distances and 3D space motions simply on its own. Nevertheless in the current work we have showed that this can be a very demanding task and has to be performed with great care. In case of GAIA it is much more a factor a the size of the target sample, as it will provide the first full kinematical study of stars in very high detail. But apart from that, it will surely also lead to new great discoveries and set a new benchmark in astrometry, in case everything works out right. So let's keep our fingers crossed.

¹A powerful graphical browser, which makes it very easy to access the manifold *SDSS* data.

²<http://www-wfau.roe.ac.uk/ss>

Appendix A

name	T_{eff} K	log g	$n_{\text{He}}/n_{\text{H}}$	v_{rad} km s ⁻¹
J0019304+1355306	28770 ± 1100	5.29 ± 0.20	0.063 ± 0.002	-236 ± 6
J0120161-0047057	30190 ± 890	6.40 ± 0.29	9.433 ± 0.647	-69 ± 18
J0758477+1158063	19740 ± 1550	4.70 ± 0.18	0.003 ± 0.095	169 ± 5
J0844470+1139100	29550 ± 530	5.23 ± 0.13	0.002 ± 0.001	198 ± 5
J0845568+1352113	24310 ± 1110	5.51 ± 0.18	0.000 ± 0.001	111 ± 10
J0948505+5516317	34930 ± 700	5.99 ± 0.21	0.040 ± 0.007	-135 ± 32
J0950220+0815576	34080 ± 640	5.08 ± 0.12	0.003 ± 0.002	318 ± 4
J1005358+2239521	28630 ± 1120	5.53 ± 0.23	0.002 ± 0.001	-140 ± 8
J1020572+0137512	28470 ± 820	5.31 ± 0.14	0.001 ± 0.001	250 ± 5
J1025061+1200223	27020 ± 790	5.21 ± 0.12	0.008 ± 0.003	420 ± 4
J1125198+0333424	21560 ± 620	4.37 ± 0.14	0.050 ± 0.001	199 ± 3
J1157164+6124107	29920 ± 530	5.44 ± 0.15	0.000 ± 0.001	-174 ± 12
J1211503+1437162	33740 ± 1620	5.98 ± 0.43	0.001 ± 0.003	193 ± 43
J1229587+0101497	39150 ± 1440	5.84 ± 0.29	2.512 ± 0.269	151 ± 6
J1232042+5225482	39670 ± 1070	7.38 ± 0.22	0.003 ± 0.001	-150 ± 46
J1335557+1251376	32470 ± 450	5.63 ± 0.13	0.003 ± 0.001	-13 ± 7
J1351085-0115554	38900 ± 450	5.76 ± 0.09	0.398 ± 0.008	256 ± 5
J1437528+3127346	38080 ± 850	5.02 ± 0.13	0.000 ± 0.001	-259 ± 8
J1528485+1911365	24750 ± 960	4.71 ± 0.14	0.002 ± 0.001	-203 ± 4
J1554541+1826149	40880 ± 2230	4.91 ± 0.14	0.001 ± 0.002	-193 ± 10
J1556358+4708518	37780 ± 880	4.93 ± 0.13	0.000 ± 0.002	-385 ± 8
J1606232+3630054	33430 ± 130	6.87 ± 0.05	0.004 ± 0.002	66 ± 5
J1632131+2051240	25970 ± 1000	5.19 ± 0.17	0.004 ± 0.005	-230 ± 3
J1644194+4523267	33430 ± 360	5.55 ± 0.13	0.013 ± 0.001	-306 ± 3
J1709574+2227450	53090 ± 1470	5.72 ± 0.17	5.012 ± 0.006	-370 ± 11
J2050304-0619579	49680 ± 4500	5.82 ± 0.22	9.953 ± 2.641	-531 ± 14
J2156487+0036207	30400 ± 520	5.62 ± 0.15	0.005 ± 0.001	-164 ± 13
J2239134+1338106	31770 ± 430	5.33 ± 0.11	0.001 ± 0.001	-34 ± 3
J2345452-0009332	41270 ± 490	6.03 ± 0.18	0.398 ± 0.022	-393 ± 13

Table A.1: Preliminary stellar parameters for the 29 subdwarf stars with constant RV.

Table A.2: RV table for the 12 stars discussed here

name	OBS	MJD	v_{rad} km s ⁻¹
SDSSJ075847.74+115806.3(short J0758+1158)	SDSS	2453674.936059	+161 ±23
J0758+1158	NTT	2454756.83980383	+126 ±40
SDSSJ084447.00+113910.0(short J0844+1139)	SDSS	2453801.1251331	+203 ±5
J0844+1139	NTT	2454755.86312183	+219 ±30
SDSSJ084556.85+135211.3(short J0845+1352)	SDSS	2453799.765353	+115 ±10
J0845+1352	NTT	2454756.86725607	+ 92 ±15
SDSSJ084938.85+145503.2(short J0849+1455)	SDSS	2453818.6548958	+119 ±37
J0849+1455	NTT	2454757.87125523	+ 83 ±34
SDSSJ094850.47+551631.7(short J0948+5516)	SDSS	2451991.6335069	-138 ±12
J0948+5516	WHT	2454588.38583304	-137 ±27
J0948+5516	WHT	2454588.39188542	-142 ±9
J0948+5516	WHT	2454587.46586414	-159 ±18
SDSSJ102057.16+013751.3(short J1020+0137)	SDSS	2451997.186412	+243 ±8
J1020+0137	FORS	2454638.47892508	+237 ±9
J1020+0137	FORS	2454638.48049004	+238 ±8
SDSSJ112519.75+033342.4(short J1125+0333)	SDSS	2452376.6870428	+194 ±15
J1125+0333	FORS	2454575.74971284	+121 ±999
J1125+0333	FORS	2454613.52800169	+202 ±3
SDSSJ121150.27+143716.2(short J1211+1437)	SDSS	2453466.7114641	+220 ±9
J1211+1437	FORS	2454575.76724424	+205 ±37
J1211+1437	FORS	2454575.76996466	+224 ±62
SDSSJ135824.61+472931.6(short J1358+4729)	SDSS	2452723.9695428	-261 ±14
J1358+4729	WHT	2454586.54874204	-257 ±14
SDSSJ155635.80+470851.8(short J1556+4708)	SDSS	2452354.493235	-393 ±20
J1556+4708	WHT	2454586.60330613	-385 ±7
SDSSJ162916.05+130742.8(short J1629+1307)	SDSS	53915-2203-222	-278 ±7
J1629+1307	FORS	2454656.60586742	-286 ±7
J1629+1307	FORS	2454662.67907158	-284 ±7
SDSSJ163213.05+205124.0(short J1632+2051)	SDSS	2453224.6422685	-239 ±7
J1632+2051	FORS	2454656.61760853	-236 ±3
J1632+2051	FORS	2454656.62612829	-236 ±3
SDSSJ164419.44+452326.7(short J1644+4523)	SDSS	2452051.9386574	-314 ±5
J1644+4523	WHT	2454586.71567501	-313 ±12
SDSSJ215648.71+003620.7(short J2156+0036)	SDSS	2452933.5838194	-177 ±7
J2156+0036	NTT	2454755.66955594	-136 ±48
J2156+0036	NTT	2454755.70668008	-151 ±36
J2156+0036	NTT	2454757.70342858	-190 ±37
SDSSJ224451.81+010630.9(short J2244+0106)	SDSS	2452146.8122801	-166 ±6
J2244+0106	NTT	2454756.61349441	-149 ±19

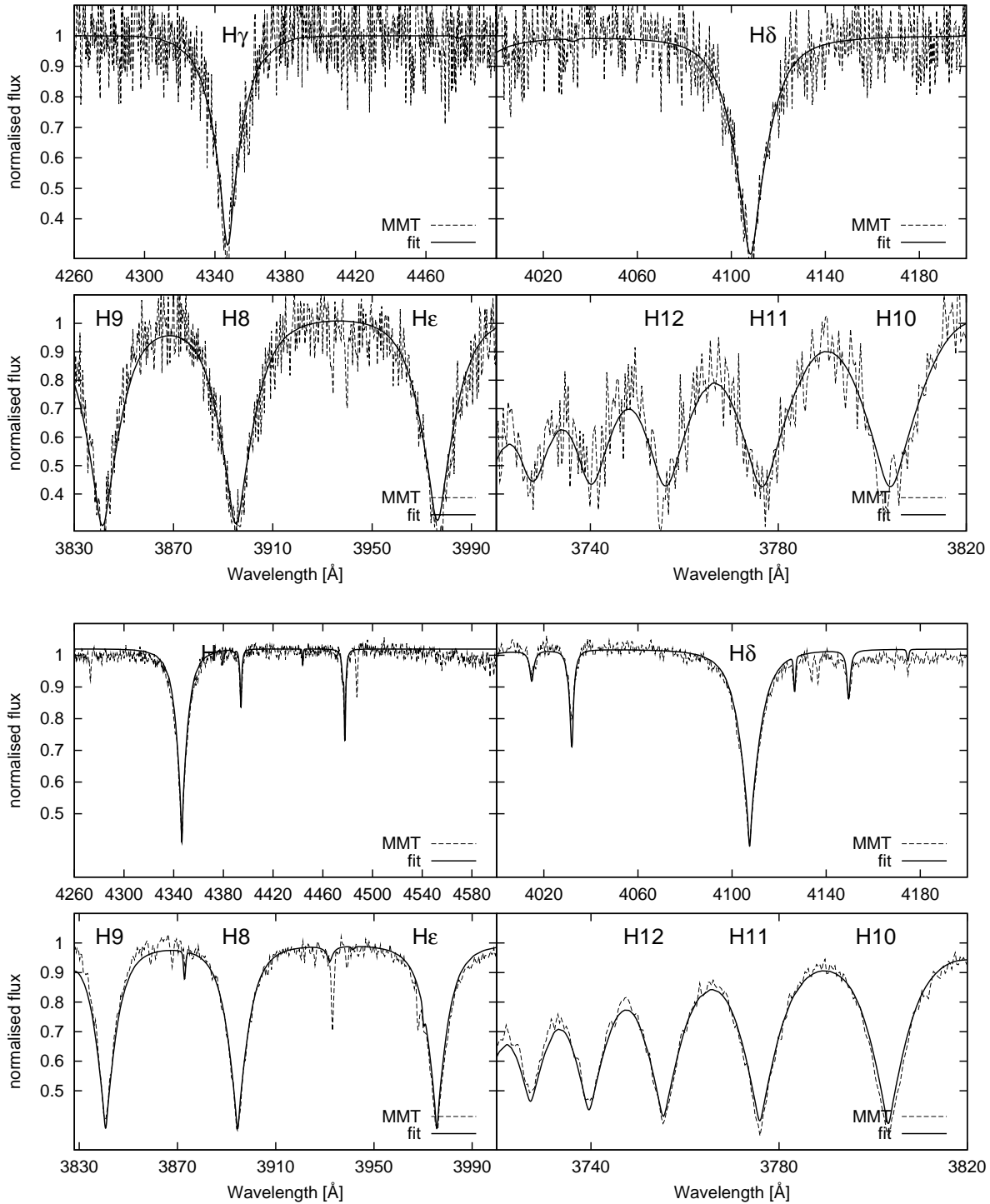


Figure A.1: Comparison between the synthetic model with the observed spectrum from the MMT for HVS 10 (top) and BCAND485 (bottom). The synthetic spectrum of HVS 10 had to be broadened with $v_{\text{rot}} \sin i = 170 \text{ km s}^{-1}$ to achieve a good match, while BCAND485 does not show rotation at all. Note the overall good agreement.

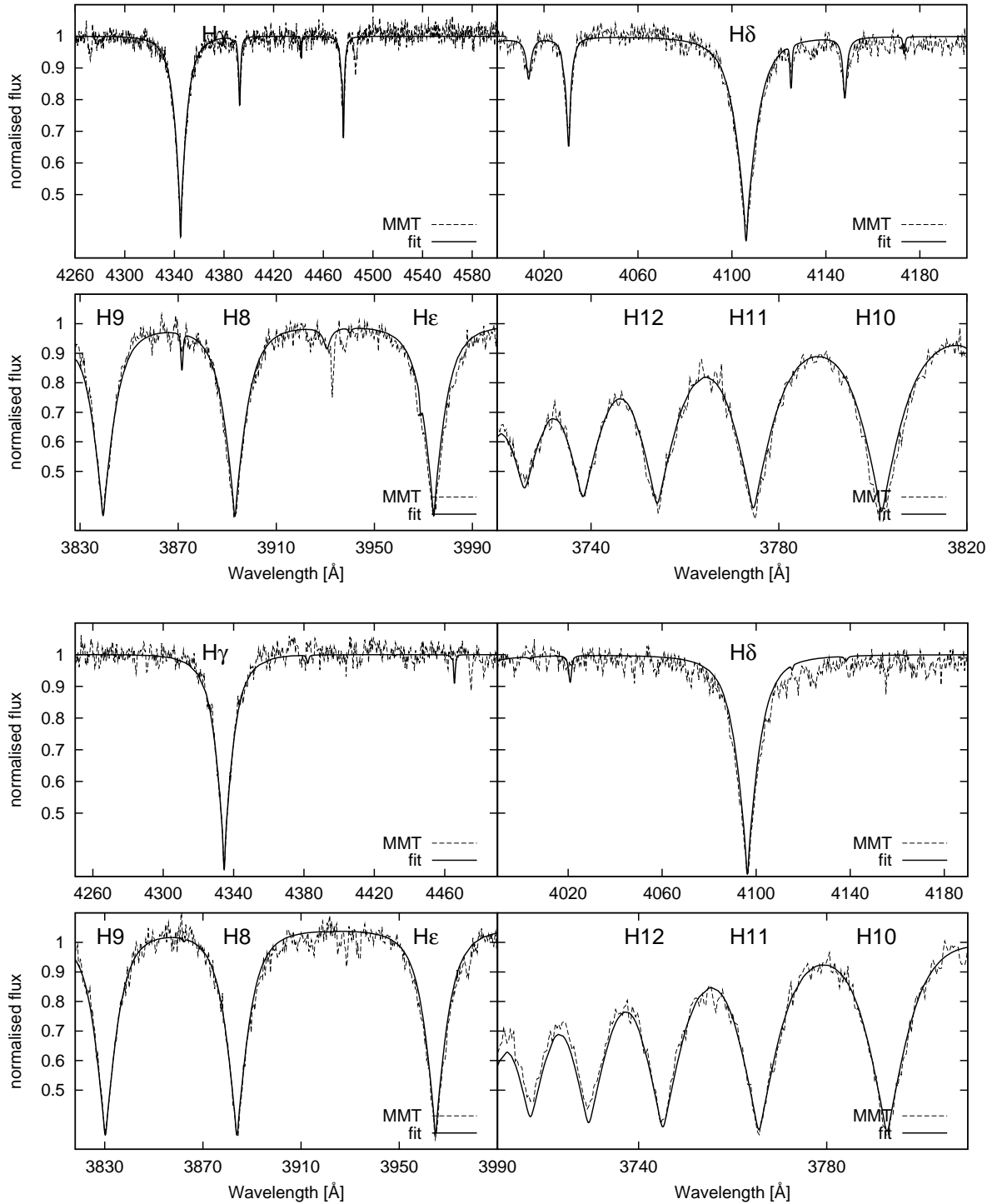


Figure A.2: Comparison between the synthetic model with the observed spectrum from the MMT for BCAND563 (top) and BHVS462 (bottom). Both stars show no rotation at all. Note the overall good agreement.

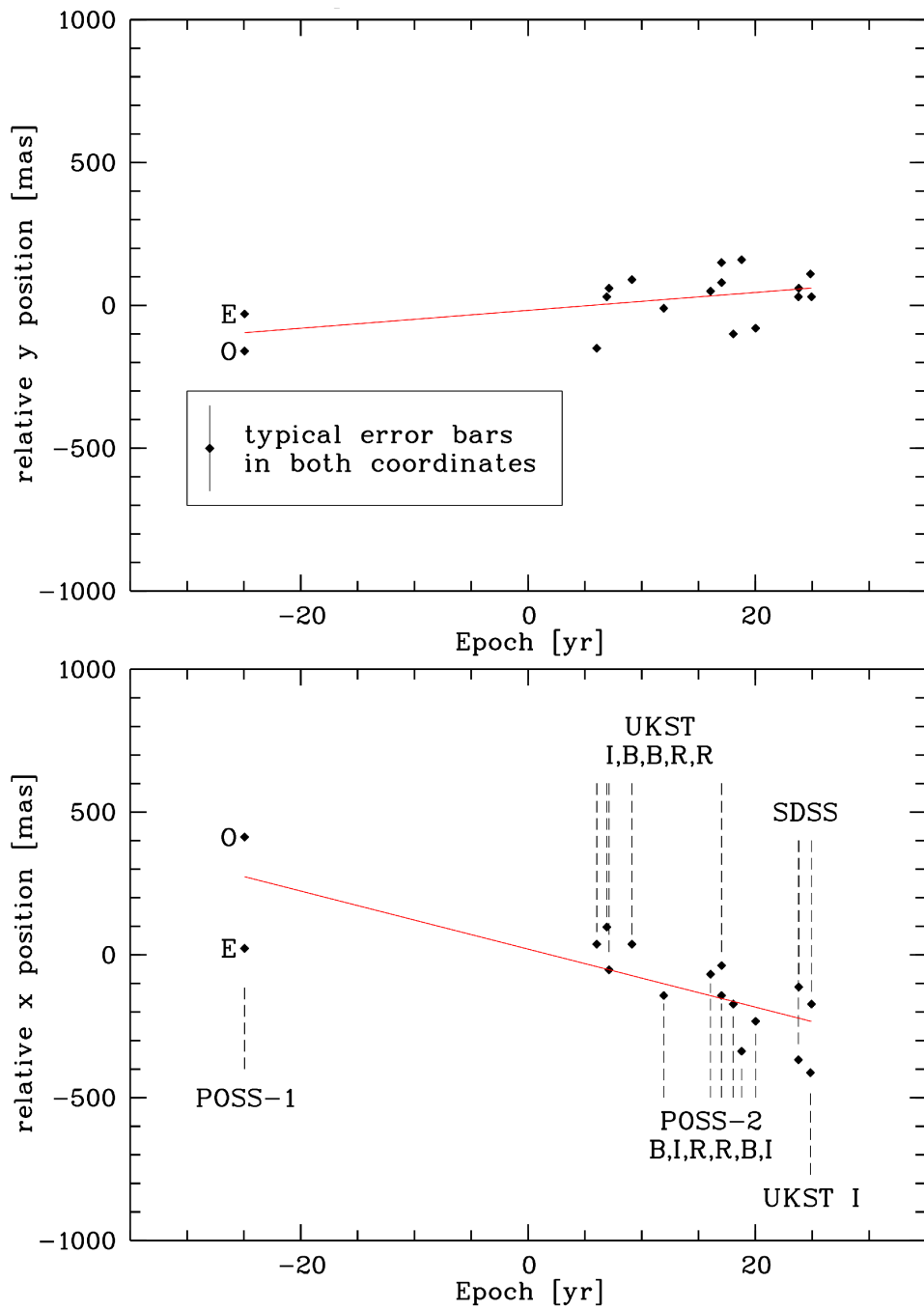


Figure A.3: Linear fit of the position measurement for spectroscopic binary J1553+0030, whereas 1975.40 is the zero epoch.

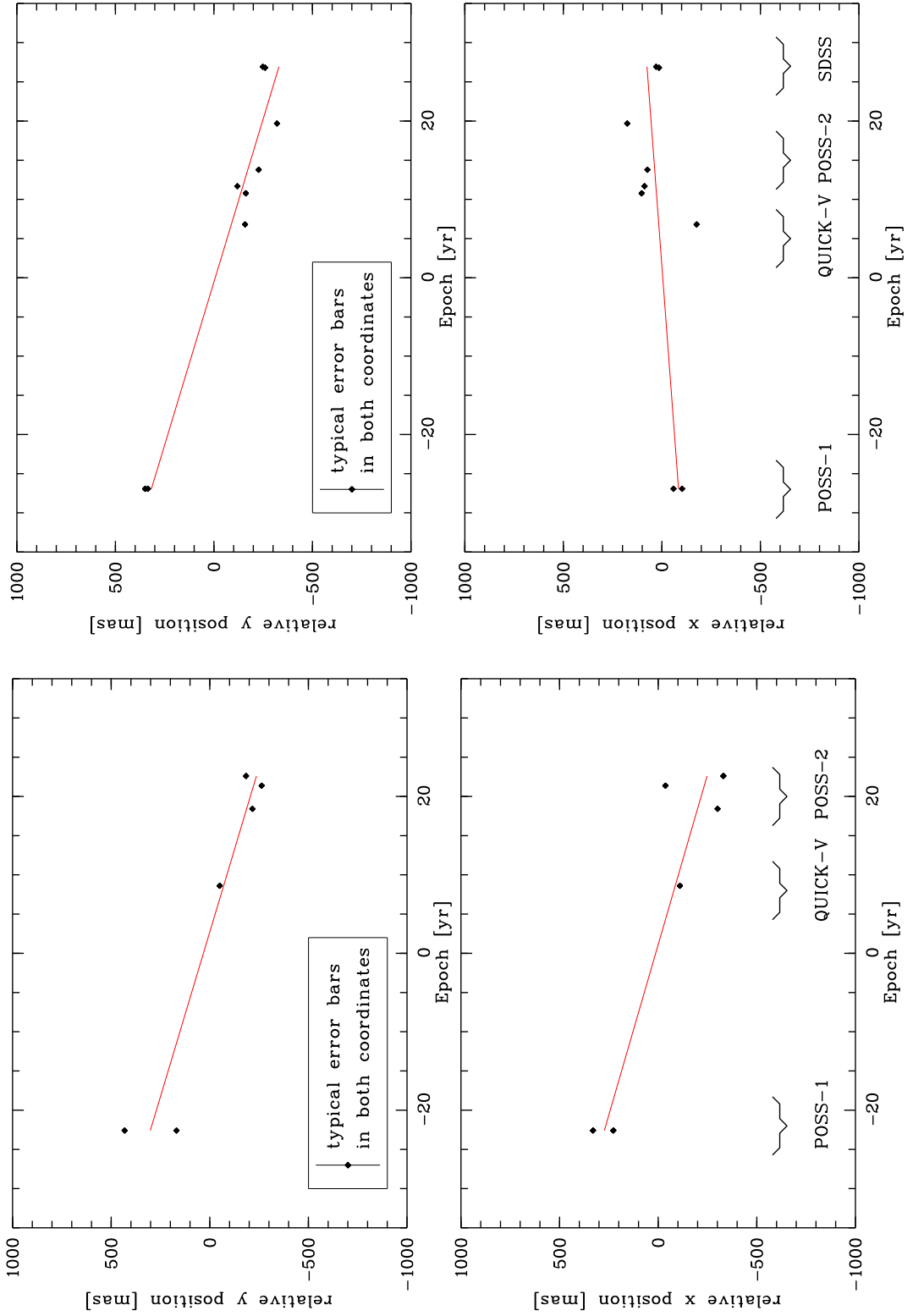


Figure A.4: Linear fit of the position measurement for J0758+1158(top) and J0844+1139(bottom), whereas 1978.165 and 1974.507 respectively are the zero epochs.

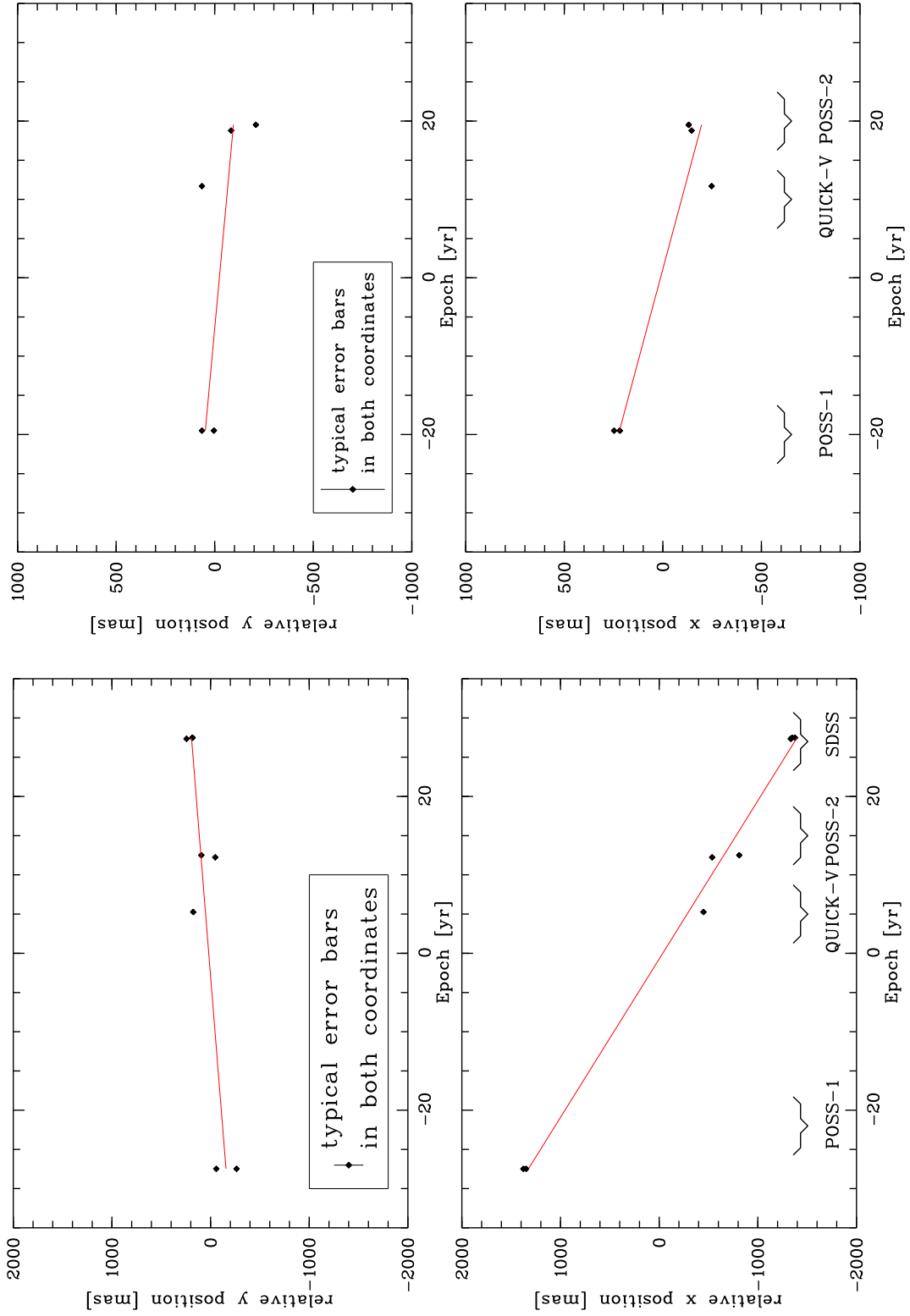


Figure A.5: Linear fit of the position measurement for J0845+1352(top) and J0849+1455(bottom), whereas 1971.422 and 1977.702 respectively are the zero epochs.

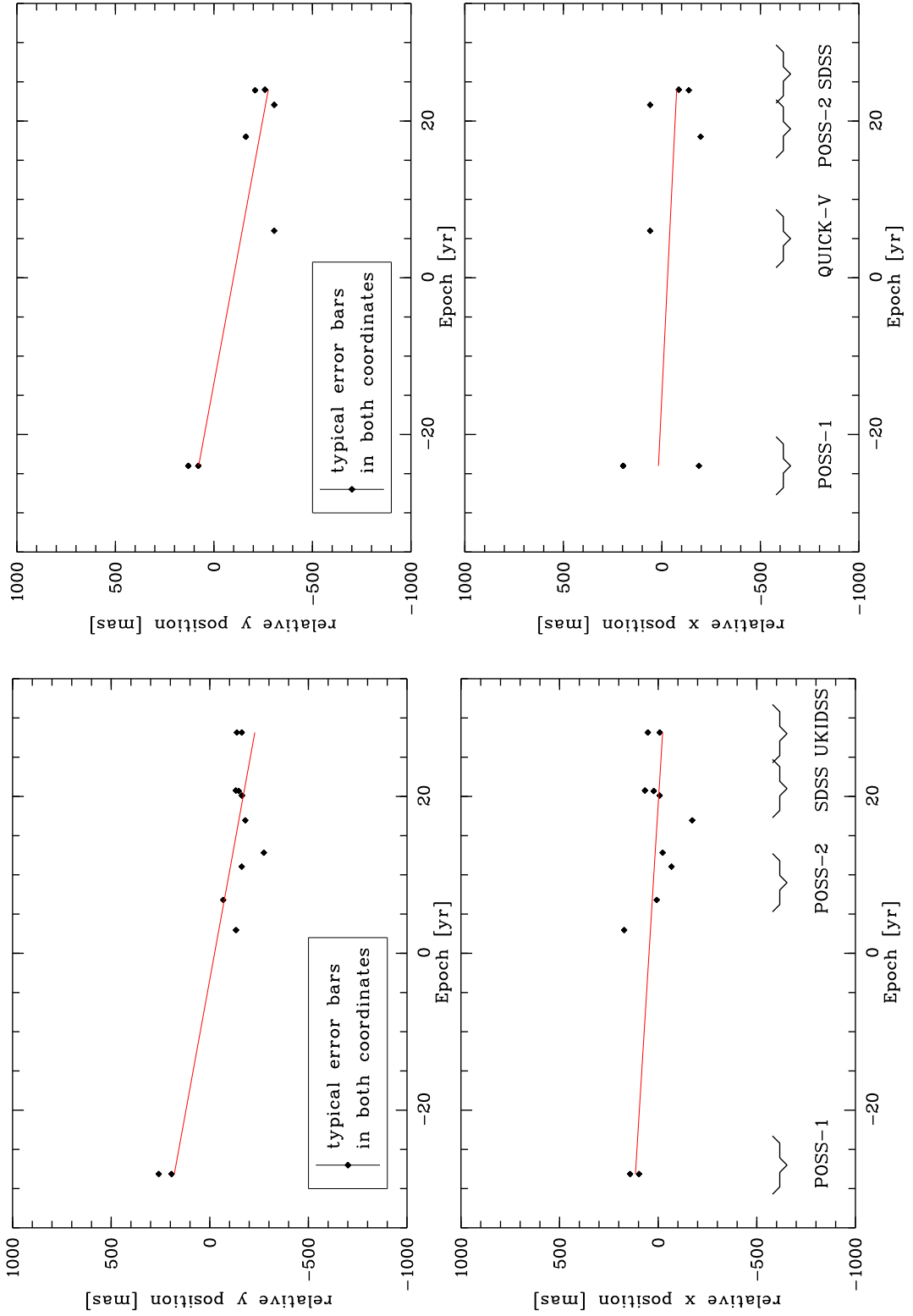


Figure A.6: Linear fit of the position measurement for J0948+5516(top) and J1020+0137(bottom), whereas 1977.142 and 1980.228 respectively are the zero epochs.

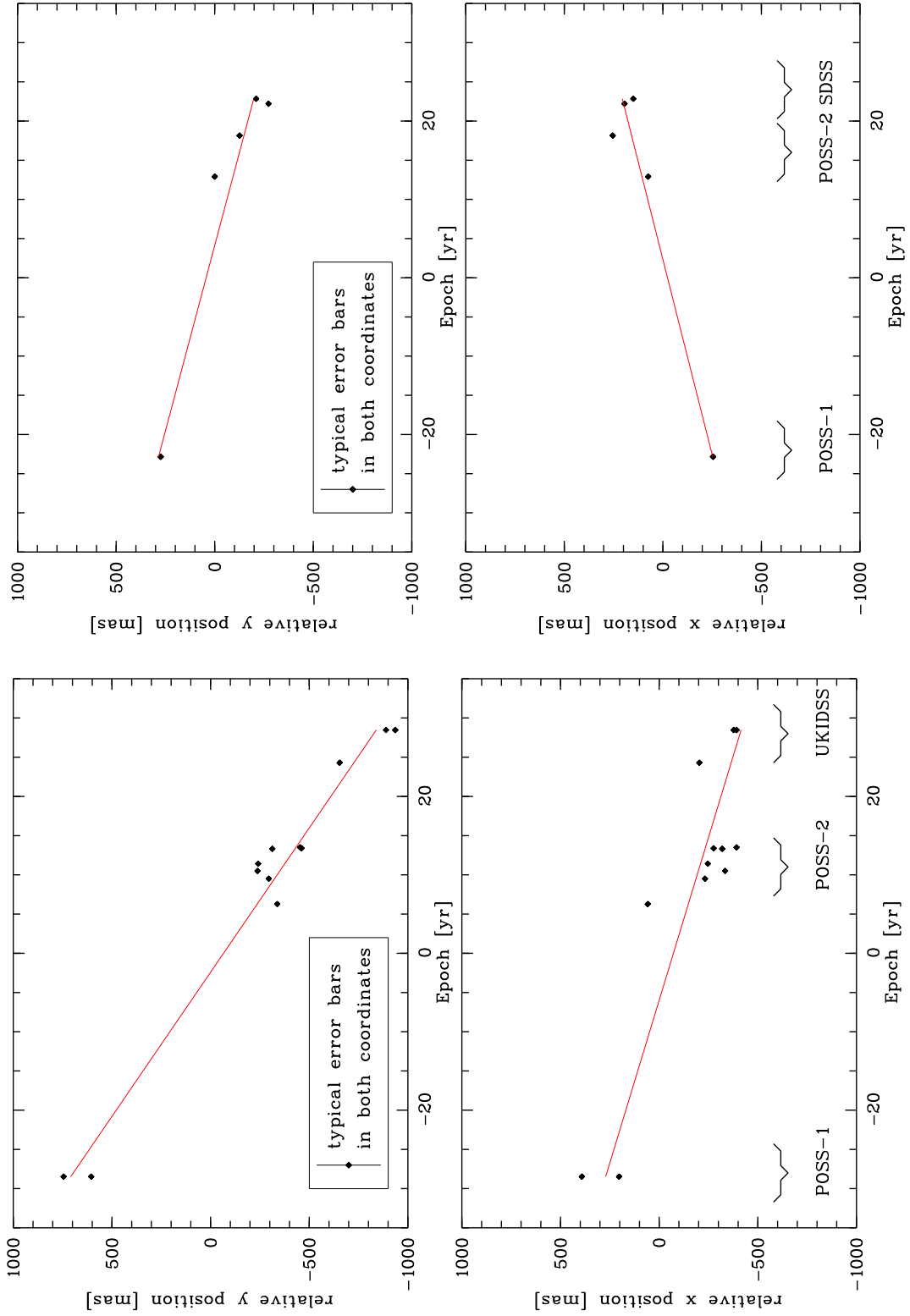


Figure A.7: Linear fit of the position measurement for J1125+0333(top) and 1211+1437(bottom), whereas 1978.131 and 1978.770 respectively are the zero epochs.

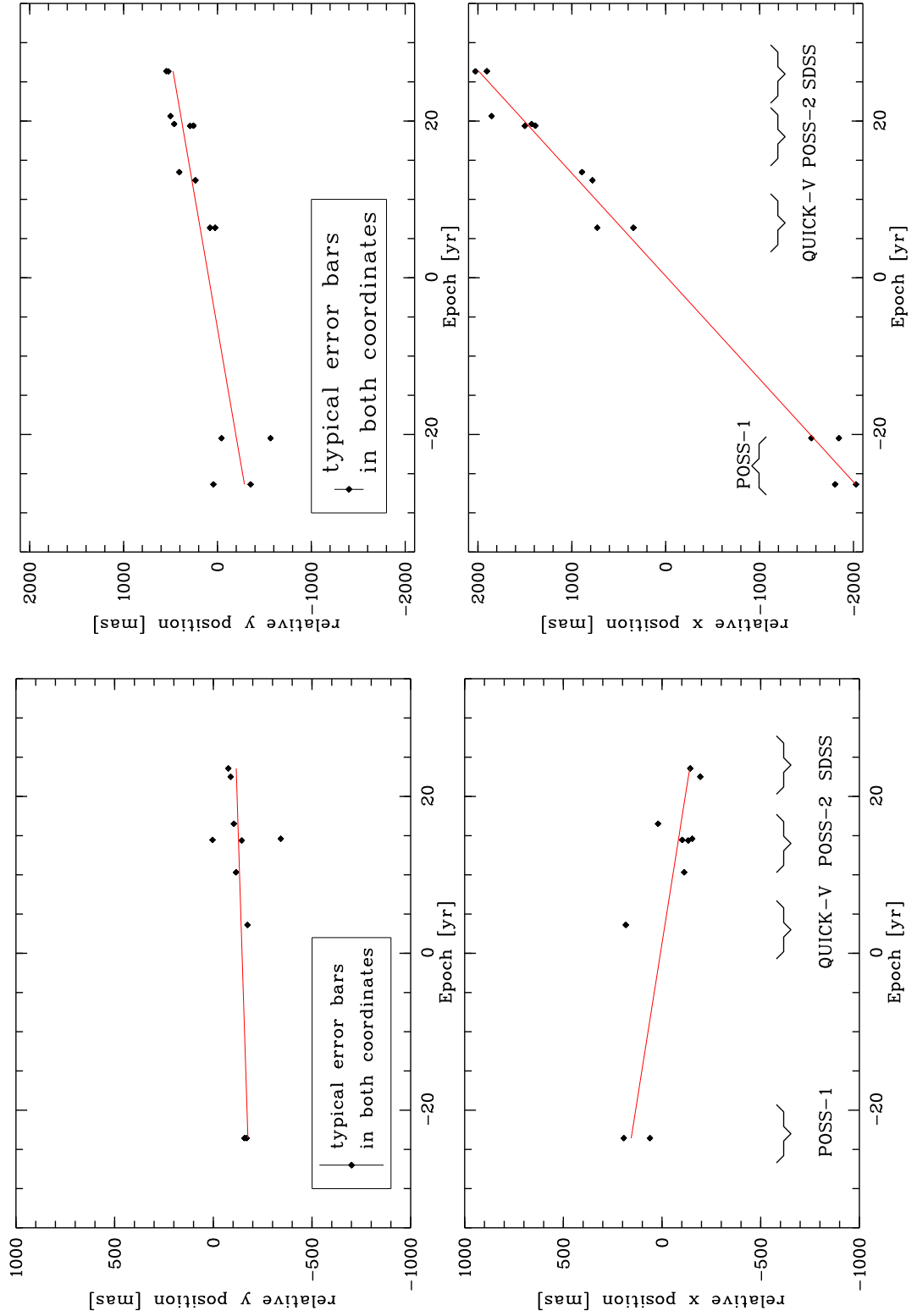


Figure A.8: Linear fit of the position measurement for J1358+4729(top) and J1556+4708(bottom), whereas 1976.743 and 1978.866 respectively are the zero epochs.

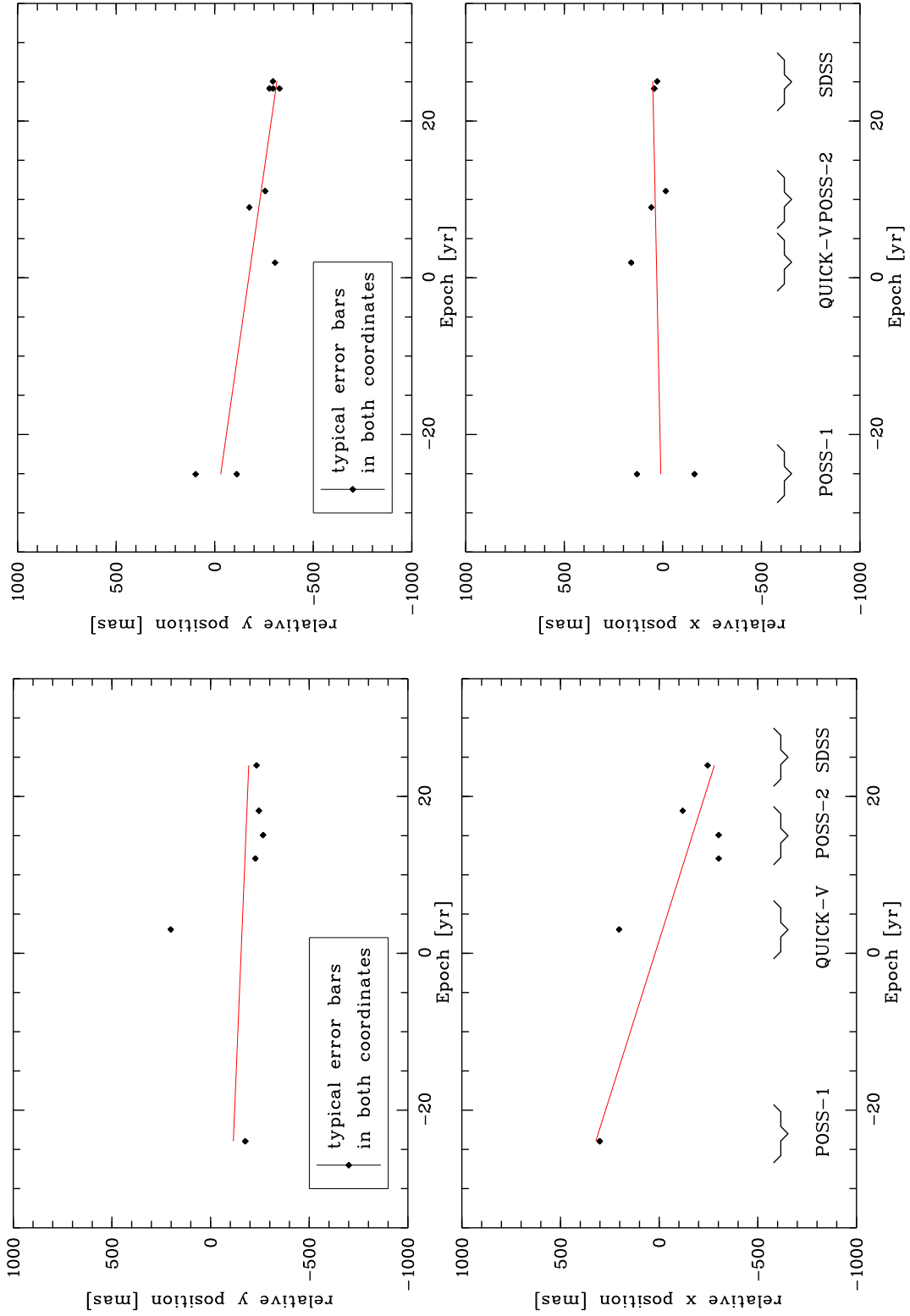


Figure A.9: Linear fit of the position measurement for J1629+1307(top) and J1632+2051(bottom), whereas 1980.295 and 1979.349 respectively are the zero epochs.

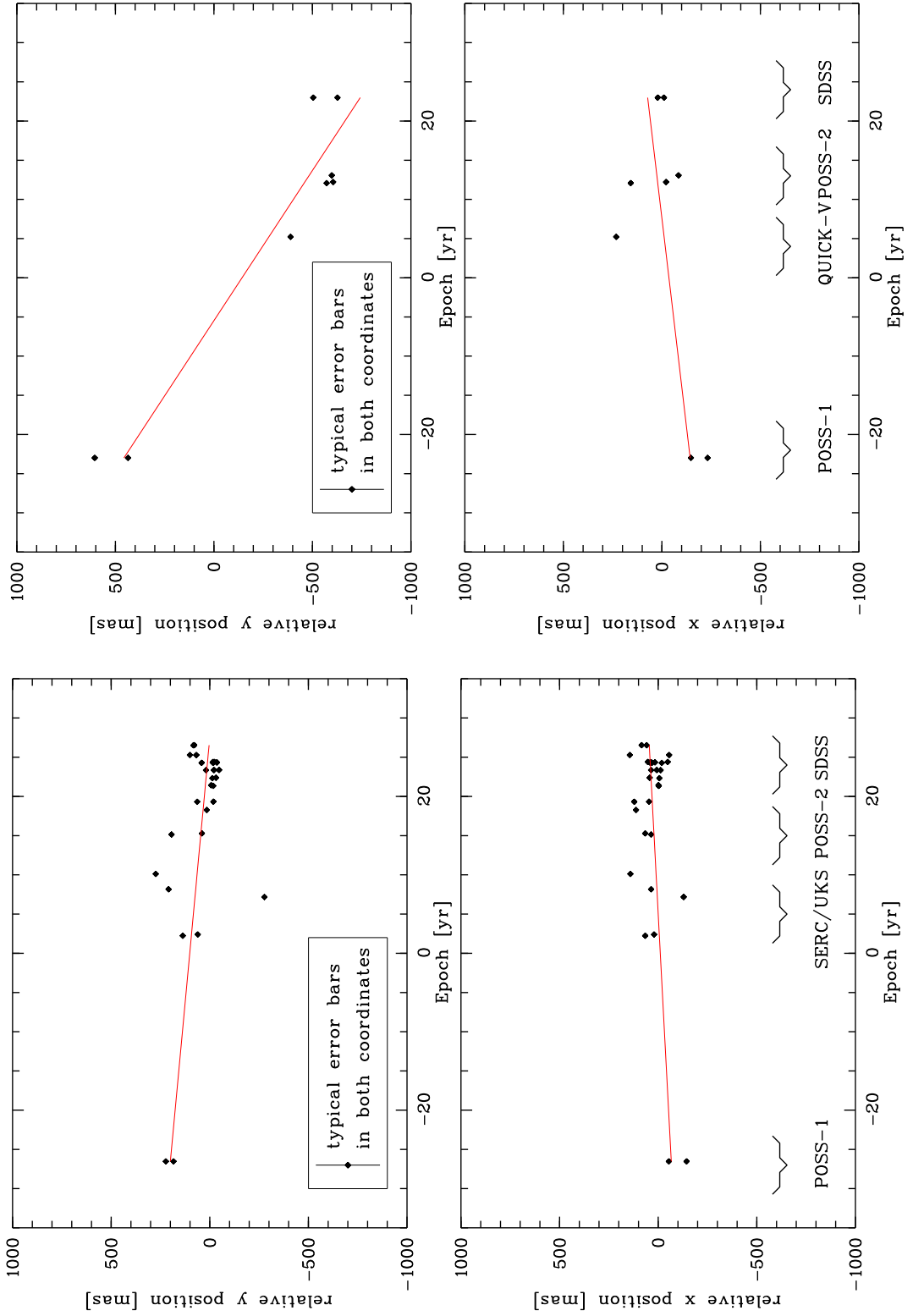


Figure A.10: Linear fit of the position measurement for J1644+4523(top) and J2244+0106(bottom), whereas 1978.232 and 1980.445 respectively are the zero epochs.

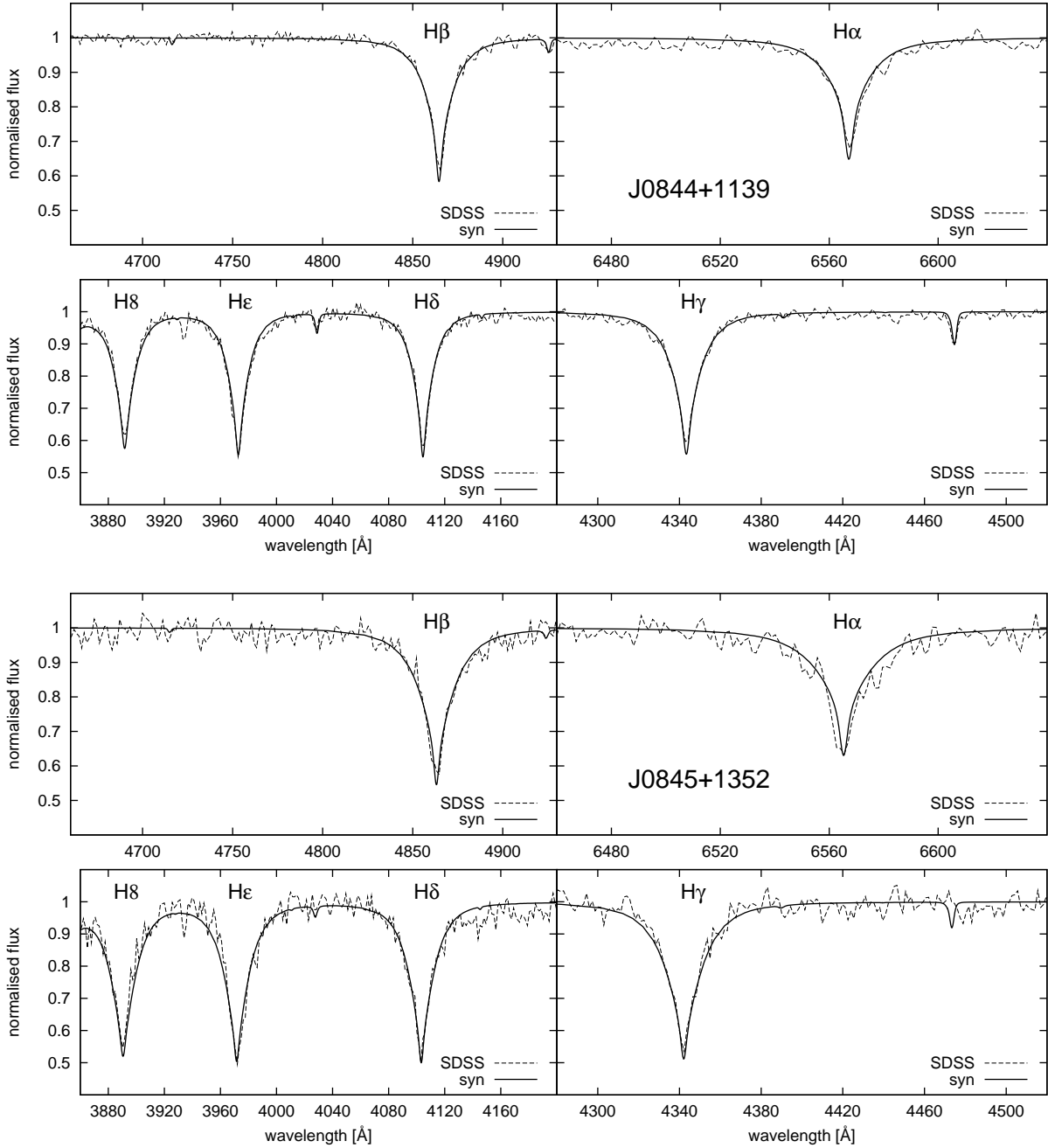


Figure A.11: Comparison between the synthetic model with the observed spectrum from the WHT for the sdBs J0844+1139 (top) and J0845+1352 (bottom). Note the overall good agreement.

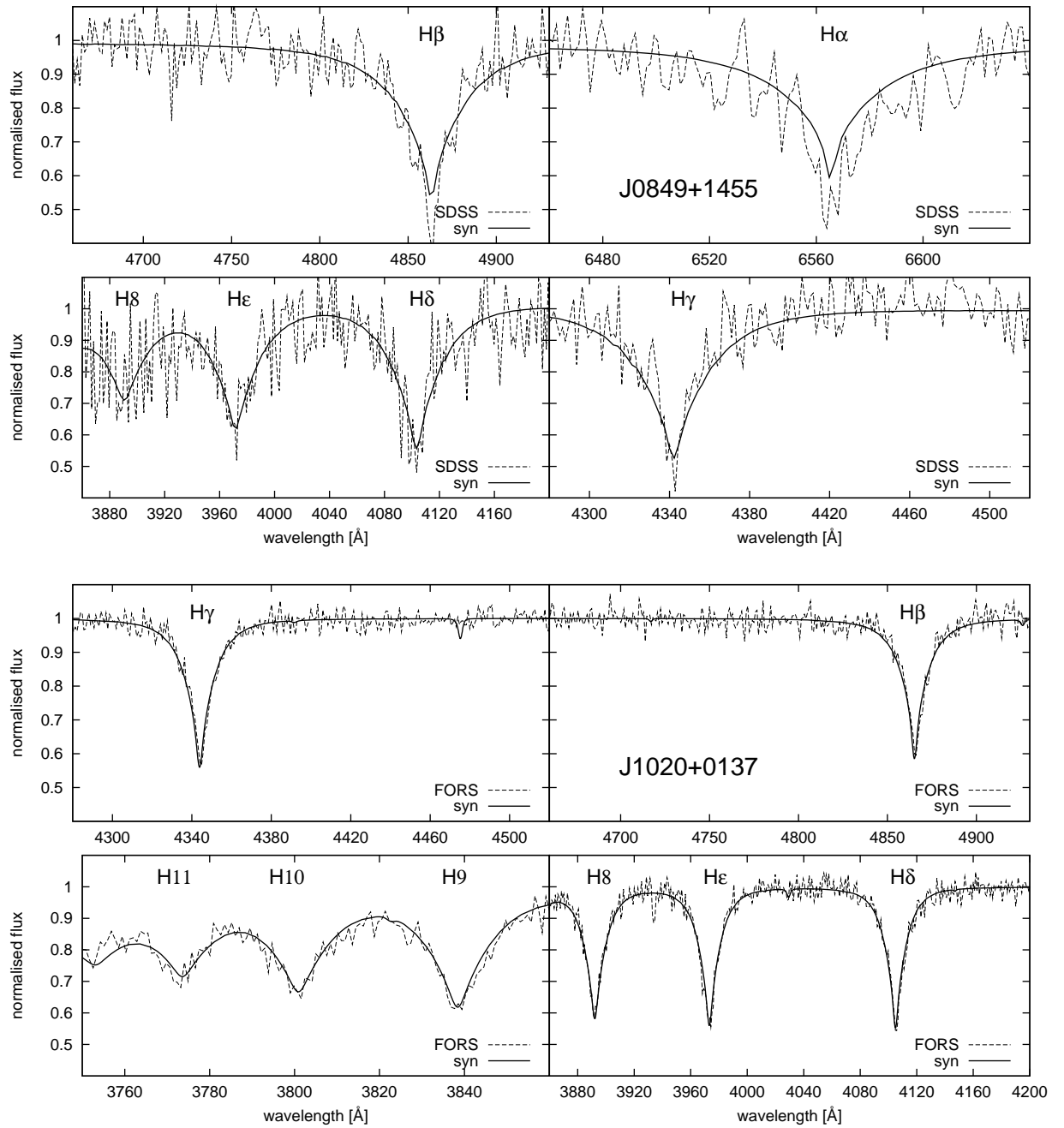


Figure A.12: Comparison between the synthetic model with the observed spectrum from the WHT for the DA J0849+1455 (top) and the sdB J1020+0137 (bottom). Note the overall good agreement.

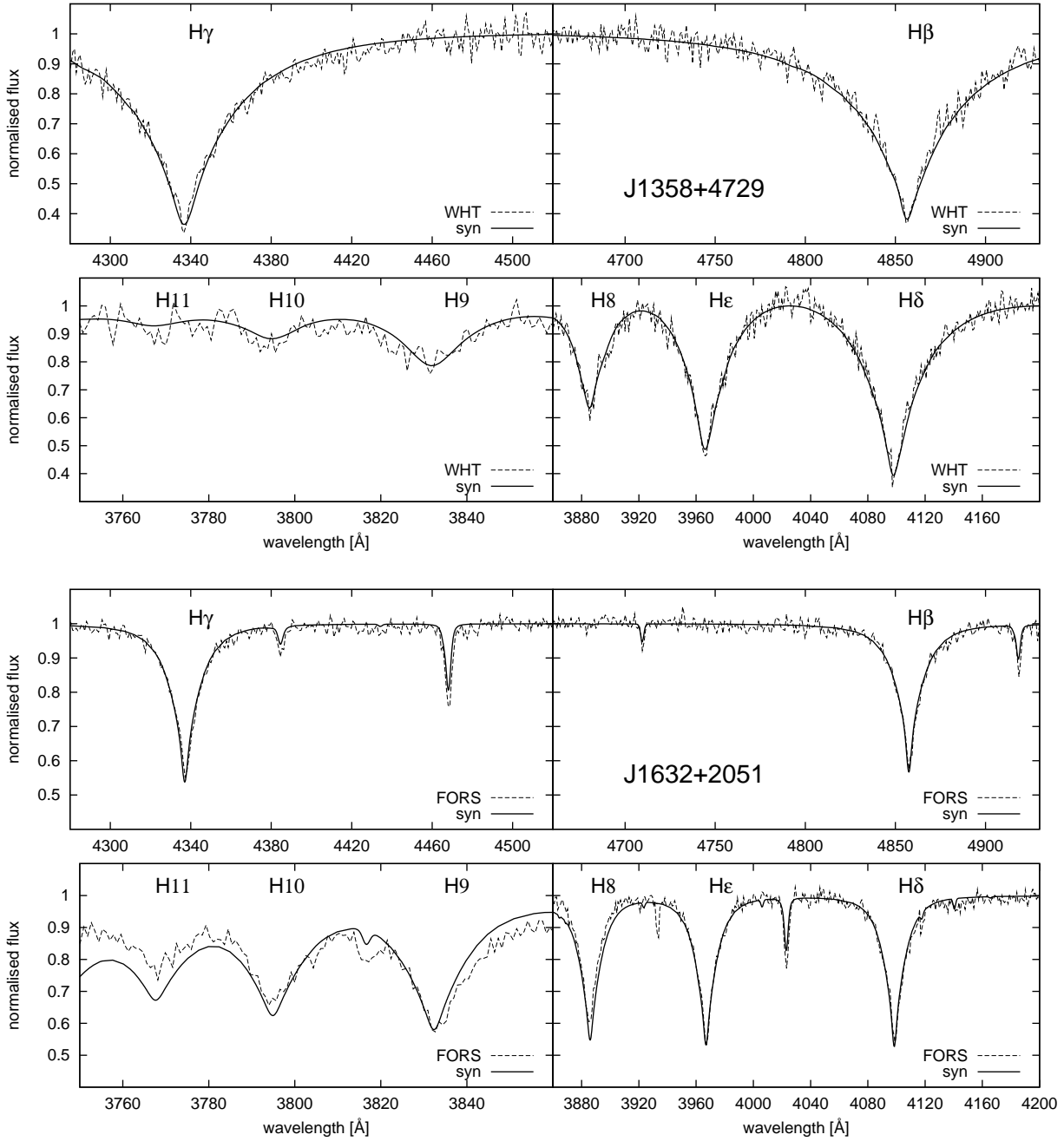


Figure A.13: Comparison between the synthetic model with the observed spectrum from the WHT for the DA J1358+4729 (top) and the sdB J1632+2051 (bottom). Note the overall good agreement except for the higher Balmer lines of J1632+2051. However this is a typical rectification artefact.

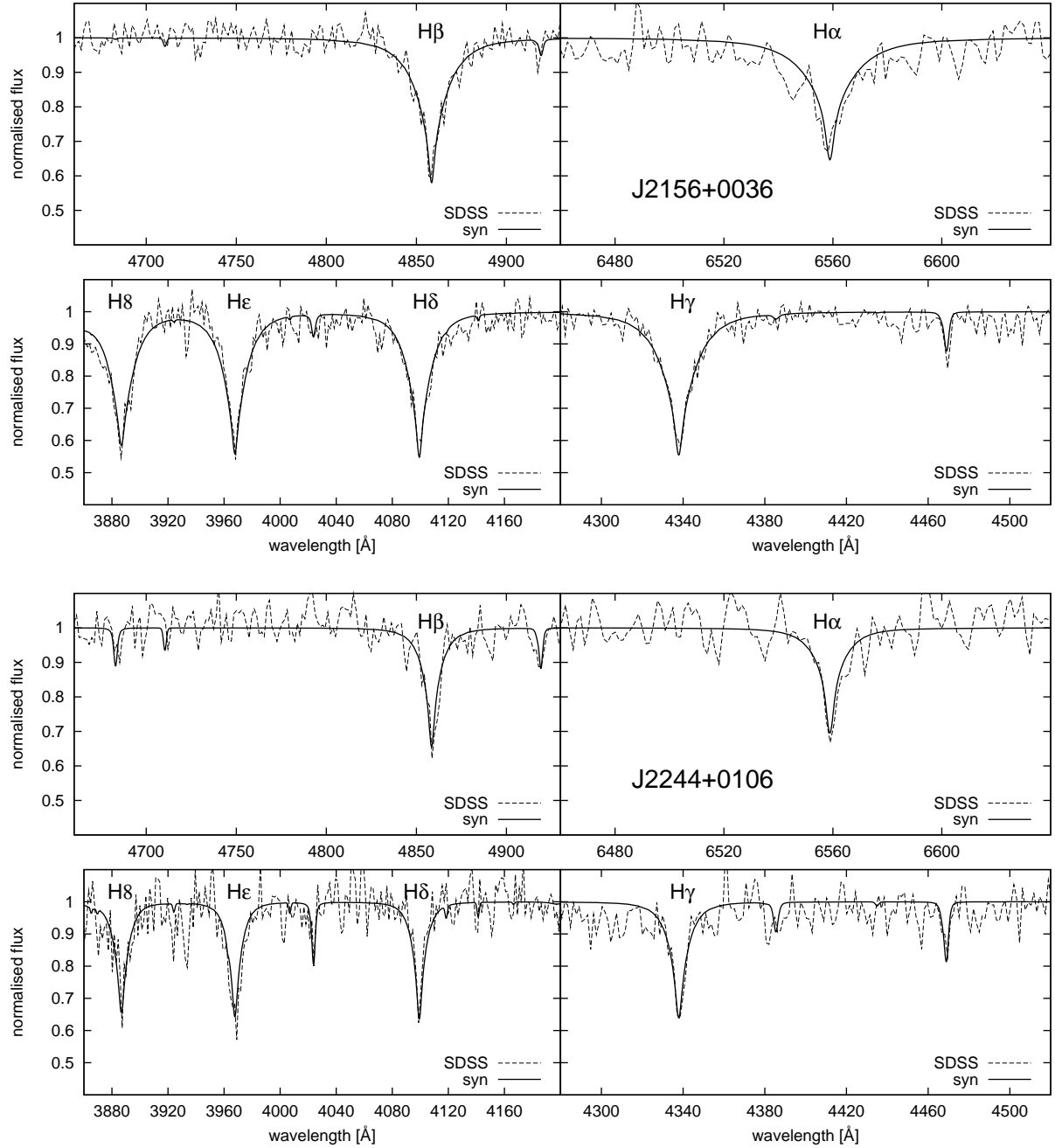


Figure A.14: Comparison between the synthetic model with the observed spectrum from the WHT for the sdBs J2156+0036 (top) and J2244+0106 (bottom). Note the overall good agreement.

Bibliography

- Abadi, M. G., Navarro, J. F., & Steinmetz, M. 2009, *ApJ*, 691, L63
- Abazajian, K. N., Adelman-McCarthy, J. K., Agüeros, M. A., et al. 2009, *ApJS*, 182, 543
- Adams, D. 1979, *The Hitchhiker's Guide to the Galaxy* (Pan Books)
- Adelman-McCarthy, J. K., Agüeros, M. A., Allam, S. S., et al. 2008, *ApJS*, 175, 297
- Allen, C. & Santillan, A. 1991, *Revista Mexicana de Astronomia y Astrofisica*, 22, 255
- Altmann, M., Edelmann, H., & de Boer, K. S. 2004, *A&A*, 414, 181
- Arp, H. C. 1955, *AJ*, 60, 317
- Battaglia, G., Helmi, A., Morrison, H., et al. 2005, *MNRAS*, 364, 433
- Becker, S. R. 1998, in *Astronomical Society of the Pacific Conference Series*, Vol. 131, *Properties of Hot Luminous Stars*, ed. I. Howarth, 137
- Belokurov, V., Zucker, D. B., Evans, N. W., et al. 2006, *ApJ*, 642, L137
- Bender, R., Kormendy, J., Bower, G., et al. 2005, *ApJ*, 631, 280
- Blaauw, A. 1961, *Bull. Astron. Inst. Netherlands*, 15, 265
- Bond, H. E. & Perry, C. L. 1971, *PASP*, 83, 638
- Bromley, B. C., Kenyon, S. J., Geller, M. J., et al. 2006, *ApJ*, 653, 1194
- Brown, T. M., Bowers, C. W., Kimble, R. A., Sweigart, A. V., & Ferguson, H. C. 2000, *ApJ*, 532, 308
- Brown, T. M., Ferguson, H. C., Davidsen, A. F., & Dorman, B. 1997, *ApJ*, 482, 685
- Brown, W. R., Geller, M. J., & Kenyon, S. J. 2009, *ApJ*, 690, 1639
- Brown, W. R., Geller, M. J., Kenyon, S. J., & Kurtz, M. J. 2005, *ApJ*, 622, L33
- Brown, W. R., Geller, M. J., Kenyon, S. J., & Kurtz, M. J. 2006a, *ApJ*, 640, L35

- Brown, W. R., Geller, M. J., Kenyon, S. J., & Kurtz, M. J. 2006b, *ApJ*, 647, 303
- Brown, W. R., Geller, M. J., Kenyon, S. J., Kurtz, M. J., & Bromley, B. C. 2007a, *ApJ*, 660, 311
- Brown, W. R., Geller, M. J., Kenyon, S. J., Kurtz, M. J., & Bromley, B. C. 2007b, *ApJ*, 671, 1708
- Buonanno, R., Corsi, C. E., Buzzoni, A., et al. 1994, *A&A*, 290, 69
- Burbidge, E. M. & Sandage, A. 1958, *ApJ*, 128, 174
- Buser, R. 2000, *Science*, 287, 69
- Busso, G., Moehler, S., Zoccali, M., Heber, U., & Yi, S. K. 2005, *ApJ*, 633, L29
- Butler, K. & Giddings, J. R. 1985, *Newsletter of Analysis of Astronomical Spectra*, Univ. London, 9
- Carlsberg-Meridian-Catalog. 2006, Copenhagen Univ. Obs., Inst. of Astr., Cambridge, UK, Real Inst. y Obs. de la Armada en San Fernando, 1304, 0
- Carney, B. W., Aguilar, L. A., Latham, D. W., & Laird, J. B. 2005, *AJ*, 129, 1886
- Carney, B. W., Latham, D. W., Laird, J. B., Grant, C. E., & Morse, J. A. 2001, *AJ*, 122, 3419
- Castelli, F. & Kurucz, R. L. 2003, in *IAU Symposium*, Vol. 210, *Modelling of Stellar Atmospheres*, ed. N. Piskunov, W. W. Weiss, & D. F. Gray, 20P
- Catelan, M. 2009, *Ap&SS*, 18
- Charpinet, S., van Grootel, V., Reese, D., et al. 2008, *A&A*, 489, 377
- Clewley, L., Warren, S. J., Hewett, P. C., et al. 2002, *MNRAS*, 337, 87
- Code, A. D. & Welch, G. A. 1979, *ApJ*, 228, 95
- Conlon, E. S., Dufton, P. L., Keenan, F. P., & Leonard, P. J. T. 1990, *A&A*, 236, 357
- Conlon, E. S., Dufton, P. L., Keenan, F. P., McCausland, R. J. H., & Holmgren, D. 1992, *ApJ*, 400, 273
- Copernicus, N. 1543, *De revolutionibus orbium coelestium*, ed. Copernicus, N.
- Costa, E., Méndez, R. A., Pedreros, M. H., et al. 2009, *AJ*, 137, 4339
- Cutri, R. M., Skrutskie, M. F., van Dyk, S., et al. 2003, *2MASS All Sky Catalog of point sources*.

- Davies, M. B. & King, A. 2005, *ApJ*, 624, L25
- D’Cruz, N. L., Dorman, B., Rood, R. T., & O’Connell, R. W. 1996, *ApJ*, 466, 359
- de la Fuente Marcos, R. & de la Fuente Marcos, C. 2008, *ApJ*, 685, L125
- De Marco, O., Shara, M. M., Zurek, D., et al. 2005, *ApJ*, 632, 894
- Dehnen, W. & Binney, J. J. 1998, *MNRAS*, 298, 387
- Demarque, P. & Virani, S. 2007, *A&A*, 461, 651
- Dinescu, D. I., Girard, T. M., & van Altena, W. F. 1999, *AJ*, 117, 1792
- Dorman, B. 1992, *ApJS*, 80, 701
- Dorman, B., Rood, R. T., & O’Connell, R. W. 1993, *ApJ*, 419, 596
- Drilling, J. S. 1994, in *Astronomical Society of the Pacific Conference Series*, Vol. 60, *The MK Process at 50 Years: A Powerful Tool for Astrophysical Insight*, ed. C. J. Corbally, R. O. Gray, & R. F. Garrison, 57
- Edelmann, H., Napiwotzki, R., Heber, U., Christlieb, N., & Reimers, D. 2005, *ApJ*, 634, L181
- Eisenhauer, F., Genzel, R., Alexander, T., et al. 2005, *ApJ*, 628, 246
- Fellhauer, M., Belokurov, V., Evans, N. W., et al. 2006, *ApJ*, 651, 167
- Ferraro, F. R., Beccari, G., Dalessandro, E., et al. 2009, *Nature*, 462, 1028
- Fuentes, C. I., Stanek, K. Z., Gaudi, B. S., et al. 2006, *ApJ*, 636, L37
- Galilei, G. 1610, *Sidereus nuncius*, ed. Galilei, G.
- Geier, S., Tillich, A., Heber, U., et al. 2010, *A&A*
- Ghez, A. M., Duchêne, G., Matthews, K., et al. 2003, *ApJ*, 586, L127
- Ghez, A. M., Salim, S., Hornstein, S. D., et al. 2005, *ApJ*, 620, 744
- Giddings, J. R. 1981, PhD thesis, , University of London
- Gnedin, O. Y., Gould, A., Miralda-Escudé, J., & Zentner, A. R. 2005, *ApJ*, 634, 344
- Goodman, J. & Paczynski, B. 2005, *ArXiv Astrophysics e-prints*
- Gould, A. & Quillen, A. C. 2003, *ApJ*, 592, 935
- Green, E. M., Fontaine, G., Hyde, E. A., For, B.-Q., & Chayer, P. 2008, in *Astronomical Society of the Pacific Conference Series*, Vol. 392, *Hot Subdwarf Stars and Related Objects*, ed. U. Heber, C. S. Jeffery, & R. Napiwotzki, 75

- Green, R. F., Schmidt, M., & Liebert, J. 1986, *ApJS*, 61, 305
- Greenstein, J. L. & Sargent, A. I. 1974, *ApJS*, 28, 157
- Gualandris, A. & Portegies Zwart, S. 2007, *MNRAS*, 376, L29
- Gualandris, A., Portegies Zwart, S., & Sipior, M. S. 2005, *MNRAS*, 363, 223
- Gvaramadze, V. V., Gualandris, A., & Portegies Zwart, S. 2009, *MNRAS*, 396, 570
- Hambly, N. C., MacGillivray, H. T., Read, M. A., et al. 2001, *MNRAS*, 326, 1279
- Han, Z., Podsiadlowski, P., Maxted, P. F. L., & Marsh, T. R. 2003, *MNRAS*, 341, 669
- Hanke, M. 2006, Projektarbeit, Elitestudiengang Uni Erlangen-Nürnberg
- Hansen, B. M. S. 2007, *ApJ*, 671, L133
- Hansen, B. M. S. & Milosavljević, M. 2003, *ApJ*, 593, L77
- Heber, U. 1986, *A&A*, 155, 33
- Heber, U., Edelmann, H., Napiwotzki, R., Altmann, M., & Scholz, R.-D. 2008a, *A&A*, 483, L21
- Heber, U., Hirsch, H., Ströer, A., et al. 2006, *Baltic Astronomy*, 15, 91
- Heber, U., Hirsch, H. A., Edelmann, H., et al. 2008b, in *Astronomical Society of the Pacific Conference Series*, Vol. 392, *Hot Subdwarf Stars and Related Objects*, ed. U. Heber, C. S. Jeffery, & R. Napiwotzki, 167
- Heber, U., Hunger, K., Jonas, G., & Kudritzki, R. P. 1984, *A&A*, 130, 119
- Heber, U., Reid, I. N., & Werner, K. 2000, *A&A*, 363, 198
- Hempel, M. & Holweger, H. 2003, *A&A*, 408, 1065
- Herschel, J. F. W. 1864, *Royal Society of London Philosophical Transactions Series I*, 154, 1
- Herschel, W. 1784, *Royal Society of London Philosophical Transactions Series I*, 74, 437
- Hills, J. G. 1988, *Nature*, 331, 687
- Hirsch, H. A., Heber, U., & O'Toole, S. J. 2008, in *Astronomical Society of the Pacific Conference Series*, Vol. 392, *Hot Subdwarf Stars and Related Objects*, ed. U. Heber, C. S. Jeffery, & R. Napiwotzki, 131
- Hirsch, H. A., Heber, U., O'Toole, S. J., & Bresolin, F. 2005, *A&A*, 444, L61
- Hoogerwerf, R., de Bruijne, J. H. J., & de Zeeuw, P. T. 2001, *A&A*, 365, 49

- House, F. & Kilkenney, D. 1978, *A&A*, 67, 421
- Huang, W., Gies, D. R., & McSwain, M. V. 2009, *ApJ*, 703, 81
- Humason, M. L. & Zwicky, F. 1947, *ApJ*, 105, 85
- Hwang, H. S., Lee, M. G., Park, H. S., et al. 2008, *ApJ*, 674, 869
- IAU. 1959, *AJ*, 64, 195
- Iben, I. J. & Tutukov, A. V. 1986, *ApJ*, 311, 753
- Irrgang, A., Przybilla, N., Heber, U., Fernanda Nieva, M., & Schuh, S. 2010, *ApJ*, 711, 138
- Johnson, D. R. H. & Soderblom, D. R. 1987, *AJ*, 93, 864
- Jordi, K., Grebel, E. K., & Ammon, K. 2006, *A&A*, 460, 339
- Kahn, F. D. & Woltjer, L. 1959, *ApJ*, 130, 705
- Kallivayalil, N., van der Marel, R. P., & Alcock, C. 2006, *ApJ*, 652, 1213
- Kapteyn, J. C. 1922, *ApJ*, 55, 302
- Kepler, J. 1609, *Astronomia nova.*, ed. Kepler, J.
- Kilkenney, D. 1989, *MNRAS*, 238, 955
- Kilkenney, D. 2007, *Communications in Asteroseismology*, 150, 234
- Kilkenney, D. & Busse, J. 1992, *MNRAS*, 258, 57
- Kilkenney, D., Fontaine, G., Green, E. M., & Schuh, S. 2010, *Information Bulletin on Variable Stars*, 5927, 1
- Kilkenney, D., Koen, C., O'Donoghue, D., & Stobie, R. S. 1997, *MNRAS*, 285, 640
- Kilkenney, D., Luvhimbi, E., O'Donoghue, D., et al. 1995, *MNRAS*, 276, 906
- Kilkenney, D. & Lydon, J. 1986, *MNRAS*, 218, 279
- Kilkenney, D. & Muller, S. 1989, *South African Astronomical Observatory Circular*, 13, 69
- Kilkenney, D., O'Donoghue, D., & Stobie, R. S. 1991, *MNRAS*, 248, 664
- Kilkenney, D. & Pauls, L. 1990, *MNRAS*, 244, 133
- Kilkenney, D. & van Wyk, F. 1990, *MNRAS*, 244, 727
- Kippenhahn, R. & Weigert, A. 1990, *Stellar Structure and Evolution*, ed. A. Kippenhahn, R. & Weigert

- Koester, D. 2002, *A&A Rev.*, 11, 33
- Koester, D., Napiwotzki, R., Christlieb, N., et al. 2001, *A&A*, 378, 556
- Kurucz, R. 1993, *ATLAS9 Stellar Atmosphere Programs CD-ROM No. 13*. Smithsonian Astrophysical Observatory
- Kurucz, R. L. 1996, in *Astronomical Society of the Pacific Conference Series*, Vol. 108, M.A.S.S., *Model Atmospheres and Spectrum Synthesis*, ed. S. J. Adelman, F. Kupka, & W. W. Weiss, 160
- Landau, L. D. & Lifschitz, E. M. 1972 (Verlag Harri Deutsch)
- Lang, K. R. 1999, *Astrophysical formulae*, ed. K. R. Lang
- Lawrence, A., Warren, S. J., Almaini, O., et al. 2007, *MNRAS*, 379, 1599
- Layden, A. C. 1998, in *Astronomical Society of the Pacific Conference Series*, Vol. 136, *Galactic Halos*, ed. D. Zaritsky, 14
- Lee, Y.-W., Demarque, P., & Zinn, R. 1990, *ApJ*, 350, 155
- Leonard, P. J. T. & Duncan, M. J. 1988, *AJ*, 96, 222
- Leonard, P. J. T. & Linnell, A. P. 1992, *AJ*, 103, 1928
- Li, Y. & White, S. D. M. 2008, *MNRAS*, 384, 1459
- Lisker, T., Heber, U., Napiwotzki, R., et al. 2005, *A&A*, 430, 223
- López-Morales, M. & Bonanos, A. Z. 2008, *ApJ*, 685, L47
- Lu, Y., Yu, Q., & Lin, D. N. C. 2007, *ApJ*, 666, L89
- Mathieu, R. D. & Geller, A. M. 2009, *Nature*, 462, 1032
- Mathys, G. 1987, *A&AS*, 71, 201
- Maxted, P. f. L., Heber, U., Marsh, T. R., & North, R. C. 2001, *MNRAS*, 326, 1391
- McMahon, R. G., Irwin, M. J., & Maddox, S. J. 2000, *VizieR Online Data Catalog*, 1267, 0
- Mengel, J. G., Norris, J., & Gross, P. G. 1976, *ApJ*, 204, 488
- Miyamoto, M. & Nagai, R. 1975, *PASJ*, 27, 533
- Moehler, S. 2001, *PASP*, 113, 1162
- Morales-Rueda, L., Maxted, P. F. L., Marsh, T. R., North, R. C., & Heber, U. 2003, *MNRAS*, 338, 752

- Munari, U., Sordo, R., Castelli, F., & Zwitter, T. 2005, *A&A*, 442, 1127
- Napiwotzki, R., Karl, C. A., Lisker, T., et al. 2004a, *Ap&SS*, 291, 321
- Napiwotzki, R., Yungelson, L., Nelemans, G., et al. 2004b, in *Astronomical Society of the Pacific Conference Series*, Vol. 318, *Spectroscopically and Spatially Resolving the Components of the Close Binary Stars*, ed. R. W. Hilditch, H. Hensberge, & K. Pavlovski, 402–410
- Navarro, J. F., Frenk, C. S., & White, S. D. M. 1996, *ApJ*, 462, 563
- Navarro, J. F., Frenk, C. S., & White, S. D. M. 1997, *ApJ*, 490, 493
- Nemec, J. M. 1991, *Nature*, 352, 286
- Nieva, M. F. & Przybilla, N. 2007, *A&A*, 467, 295
- Odenkirchen, M. & Brosche, P. 1992, *Astronomische Nachrichten*, 313, 69
- Odenkirchen, M., Grebel, E. K., Dehnen, W., et al. 2003, *AJ*, 126, 2385
- O’Leary, R. M. & Loeb, A. 2008, *MNRAS*, 383, 86
- Oort, J. H. 1977, *ARA&A*, 15, 295
- Oort, J. H. & Spitzer, L. J. 1955, *ApJ*, 121, 6
- Paczynski, B. 1990, *ApJ*, 348, 485
- Paltrinieri, B., Ferraro, F. R., Carretta, E., & Fusi Pecci, F. 1998, *MNRAS*, 293, 434
- Pauli, E., Napiwotzki, R., Altmann, M., et al. 2003, *A&A*, 400, 877
- Pauli, E., Napiwotzki, R., Heber, U., Altmann, M., & Odenkirchen, M. 2006, *A&A*, 447, 173
- Perryman, M. A. C., Lindegren, L., Kovalevsky, J., et al. 1997, *A&A*, 323, L49
- Peterson, R. C., Carney, B. W., & Latham, D. W. 1984, *ApJ*, 279, 237
- Philip, A. G. D. 2000, *News Letter of the Astronomical Society of New York*, 5, 5
- Pier, J. R. 1983, *ApJS*, 53, 791
- Piotto, G. 2003, in *Astronomical Society of the Pacific Conference Series*, Vol. 296, *New Horizons in Globular Cluster Astronomy*, ed. G. Piotto, G. Meylan, S. G. Djorgovski, & M. Riello, 263
- Preston, G. W. & Sneden, C. 2000, *AJ*, 120, 1014
- Przybilla, N. & Butler, K. 2001, *A&A*, 379, 955

- Przybilla, N. & Butler, K. 2004a, *ApJ*, 609, 1181
- Przybilla, N. & Butler, K. 2004b, *ApJ*, 610, L61
- Przybilla, N., Butler, K., Becker, S. R., & Kudritzki, R. P. 2001a, *A&A*, 369, 1009
- Przybilla, N., Butler, K., Becker, S. R., & Kudritzki, R. P. 2006, *A&A*, 445, 1099
- Przybilla, N., Butler, K., Becker, S. R., Kudritzki, R. P., & Venn, K. A. 2000, *A&A*, 359, 1085
- Przybilla, N., Butler, K., & Kudritzki, R. P. 2001b, *A&A*, 379, 936
- Przybilla, N., Nieva, M. F., Heber, U., & Butler, K. 2008a, *ApJ*, 684, L103
- Przybilla, N., Nieva, M. F., Heber, U., et al. 2008b, *A&A*, 480, L37
- Przybilla, N., Nieva, M. F., Tillich, A., et al. 2008c, *A&A*, 488, L51
- Przybilla, N., Tillich, A., Scholz, R.-D., & Heber, U. 2010, *ApJ* submitted
- Renzini, A. & Fusi Pecci, F. 1988, *ARA&A*, 26, 199
- Rousseuw, P. & Leroy, A. 1987, *Robust Regression & Outlier Detection* (Wiley)
- Rubin, V. C., Ford, W. K. J., & Thonnard, N. 1980, *ApJ*, 238, 471
- Rudolph, A. L., Fich, M., Bell, G. R., et al. 2006, *ApJS*, 162, 346
- Saffer, R. A., Bergeron, P., Koester, D., & Liebert, J. 1994, *ApJ*, 432, 351
- Saffer, R. A., Keenan, F. P., Hambly, N. C., Dufton, P. L., & Liebert, J. 1997, *ApJ*, 491, 172
- Sakamoto, T., Chiba, M., & Beers, T. C. 2003, *A&A*, 397, 899
- Salpeter, E. E. 1955, *ApJ*, 121, 161
- Sandage, A. R. 1953, *AJ*, 58, 61
- Schaller, G., Schaerer, D., Meynet, G., & Maeder, A. 1992, *A&AS*, 96, 269
- Schlegel, D. J., Finkbeiner, D. P., & Davis, M. 1998, *ApJ*, 500, 525
- Schödel, R., Eckart, A., Iserlohe, C., Genzel, R., & Ott, T. 2005, *ApJ*, 625, L111
- Schödel, R., Ott, T., Genzel, R., et al. 2002, *Nature*, 419, 694
- Shapley, H. 1922, *Nature*, 110, 545
- Sherwin, B. D., Loeb, A., & O'Leary, R. M. 2008, *MNRAS*, 386, 1179

- Sirko, E., Goodman, J., Knapp, G. R., et al. 2004, *AJ*, 127, 914
- Smith, M. C., Ruchti, G. R., Helmi, A., et al. 2007, *MNRAS*, 379, 755
- Steinmetz, M., Zwitter, T., Siebert, A., et al. 2006, *AJ*, 132, 1645
- Ströer, A., Heber, U., Lisker, T., Napiwotzki, R., & Dreizler, S. 2005, in *Astronomical Society of the Pacific Conference Series*, Vol. 334, 14th European Workshop on White Dwarfs, ed. D. Koester & S. Moehler, 309
- Stryker, L. L. 1993, *PASP*, 105, 1081
- Telting, J. H., Geier, S., Østensen, R. H., et al. 2008, *A&A*, 492, 815
- Telting, J. H. & Østensen, R. H. 2004, *A&A*, 419, 685
- Tillich, A., Geier, S., Heber, U., et al. 2009a, *Journal of Physics Conference Series*, 172
- Tillich, A., Geier, S., Heber, U., et al. 2010a, *Ap&SS*, 63
- Tillich, A., Geier, S., Heber, U., et al. 2010b, *Ap&SS*, ASTR1963
- Tillich, A., Geier, S., Heber, U., et al. 2010c, *A&A* in prep.
- Tillich, A., Heber, U., O’Toole, S. J., Østensen, R., & Schuh, S. 2007, *A&A*, 473, 219
- Tillich, A., Przybilla, N., Scholz, R., & Heber, U. 2009b, *A&A*, 507, L37
- Tillich, A., Przybilla, N., Scholz, R.-D., & Heber, U. 2010d, *A&A* submitted
- Tobin, W. & Kilkenny, D. 1981, *MNRAS*, 194, 937
- Trumpler, R. J. 1930, *PASP*, 42, 214
- Tutukov, A. V. & Fedorova, A. V. 2009, *Astronomy Reports*, 53, 839
- van Albada, T. S., Bahcall, J. N., Begeman, K., & Sanscisi, R. 1987, in *IAU Symposium*, Vol. 117, *Dark matter in the universe*, ed. J. Kormendy & G. R. Knapp, 58–67
- van Leeuwen, F. 2007, *A&A*, 474, 653
- Ventura, P., Caloi, V., D’Antona, F., et al. 2009, *ArXiv e-prints*
- Vučković, M., Aerts, C., Østensen, R., et al. 2007, *A&A*, 471, 605
- Werner, K. & Dreizler, S. 1999, *Journal of Computational and Applied Mathematics*, 109, 65
- Wilkinson, M. I. & Evans, N. W. 1999, *MNRAS*, 310, 645
- Xue, X. X., Rix, H. W., Zhao, G., et al. 2008, *ApJ*, 684, 1143

- Yanny, B., Newberg, H. J., Kent, S., et al. 2000, *ApJ*, 540, 825
- Yanny, B., Rockosi, C., Newberg, H. J., et al. 2009, *AJ*, 137, 4377
- Yi, S., Demarque, P., & Oemler, A. J. 1997, *ApJ*, 486, 201
- Yi, S. K. 2008, in *Astronomical Society of the Pacific Conference Series*, Vol. 392, *Hot Subdwarf Stars and Related Objects*, ed. U. Heber, C. S. Jeffery, & R. Napiwotzki, 3
- York, D. G., Adelman, J., Anderson, Jr., J. E., et al. 2000, *AJ*, 120, 1579
- Yu, Q. & Tremaine, S. 2003, *ApJ*, 599, 1129
- Zwicky, F. 1957, *Morphological astronomy*, ed. F. Zwicky

Acknowledgements

This dissertation is dedicated to my family. In particular I want to thank my wife Martina Tillich and my mother Anna Tillich. Thank you for always supporting me in every respect. Special thanks go to my friends from my hometown and from university, wherever they currently are.

This work was only possible because of the help, advice and collaboration of a lot of people, whom I wish to thank very much. I also wish to thank my PhD supervisor Uli Heber for his always open door and for supporting me with his experience and knowledge. Due to him and his faith in me, this project became reality.

I want to thank all the people of the Dr. Remeis-Sternwarte in Bamberg for the help and the good working environment. In general, I also want to thank the hot subdwarf and white dwarf communities for the great time I had at several meetings and other occasions. In addition to this it was a pleasure for me to learn from and collaborate with many people, who provided me with letters of reference, generously shared their wisdom and sometimes also their data with me. For this I want to thank Stephan Geier, Heiko Hirsch, Norbert Przybilla, Fernanda Nieva, Markus Firnstein, Horst Drechsel, Florian Schiller, Manfred Hanke, Stefan Neßlinger, Heinz Edelmann, Ralf Napiwotzki, Thomas Kupfer, Sebastian Müller, Andreas Irrgang, Jörn Wilms, Simon OToole, Roy Østensen, Sonja Schuh, Tony Lynas-Gray, Ralf-Dieter Scholz, Warren Brown, Artie Hatzes and in particular Dave Kilkenny for being referee of this thesis.

I am grateful for the help, support and assistance provided by the staff of the CAHA in Spain and the ESO at La Silla in Chile during my visits. I made extensive use of NASA's Astrophysics Data System Abstract Service (ADS), the Sloan Digital Sky Survey (SDSS), the Digitized Sky Survey (DSS), the UKIRT Infrared Deep Sky Survey (UKIDSS), the SIMBAD and VIZIER databases, operated at CDS Strasbourg in France, the NIST atomic spectra database and the LEO Dictionary.

This work was supported by the Deutsche Forschungsgemeinschaft (DFG) under grant HE1356/45-1. The travel to the Calar Alto observatory was also supported by the DFG under grant He1356/50-1.

Lebenslauf

Name: Franz Alfred Tillich

Geburt: 18. Mai 1981 in Arad/Rumänien

Staatsangehörigkeit: Deutsch

Grundschule: 09/1987 - 07/1991 Grundschule Röthenbacher Hauptstraße

Gymnasium: 09/1991 - 07/2000 Sigmund-Schuckert-Gymnasiums
Allgemeine Hochschulreife (Note: 1,7)

Wehrdienst: 07/2000 - 04/2001 Elektronikstaffel des Jagdbombergeschwaders 32

Universität: 10/2001 - 09/2006 Studium der Physik an der
Universität Erlangen-Nürnberg
Physikalisches Wahlpflichtfach:
Astro-, Kern-, und Teilchenphysik
Nicht-Physikalisches Wahlpflichtfach:
Allgemeine Elektrotechnik

09/2003 - 12/2003 Auslandssemester an der University of
Joensuu, Finnland

01/2006 - 09/2006 Diplomarbeit an der Dr. Remeis-Sternwarte Bamberg
Thema: Zeitaufgelste Spektroskopie des
multiperiodisch pulsierenden Sterns PG1605+072
Betreuer: Prof. Dr. Uli Heber

09/2006 Abschluß des Studiums:
Dipl. Phys. Univ. (Note: 1.62):

09/2006 - 04/2010 Doktorand an der Dr. Remeis-Sternwarte Bamberg
finanziert durch die Deutsche Forschungsgemeinschaft
Thema: Hyper-velocity stars
Betreuer: Prof. Dr. Uli Heber